

SEISMIC PERFORMANCE OF MULTISTOREY STEEL CONCENTRICALLY BRACED FRAMES EQUIPPED WITH FRICTION DAMPERS

Teză destinată obținerii
titlului științific de doctor inginer
la
Universitatea "Politehnica" din Timișoara
în domeniul Inginerie Civilă
de către

Ing. Norin Filip-Văcărescu

Conducător științific: prof.univ.dr.ing Dan Dubină
MC al Academiei Romane
Referenți științifici: prof.univ.dr. ing. Ahmed Elghazouli
prof.univ.dr.ing. Dan Crețu
conf.univ.dr.ing. Aurel Stratan

Ziua susținerii tezei: 20 Iulie 2011

Seriile Teze de doctorat ale UPT sunt:

- | | |
|------------------------|---|
| 1. Automatică | 7. Inginerie Electronică și Telecomunicații |
| 2. Chimie | 8. Inginerie Industrială |
| 3. Energetică | 9. Inginerie Mecanică |
| 4. Ingineria Chimică | 10. Știința Calculatoarelor |
| 5. Inginerie Civilă | 11. Știința și Ingineria Materialelor |
| 6. Inginerie Electrică | |

Universitatea „Politehnica” din Timișoara a inițiat seriile de mai sus în scopul diseminării expertizei, cunoștințelor și rezultatelor cercetărilor întreprinse în cadrul școlii doctorale a universității. Seriile conțin, potrivit H.B.Ex.S Nr. 14 / 14.07.2006, tezele de doctorat susținute în universitate începând cu 1 octombrie 2006.

Copyright © Editura Politehnica – Timișoara, 2006

Această publicație este supusă prevederilor legii dreptului de autor. Multiplicarea acestei publicații, în mod integral sau în parte, traducerea, tipărirea, reutilizarea ilustrațiilor, expunerea, radiodifuzarea, reproducerea pe microfilme sau în orice altă formă este permisă numai cu respectarea prevederilor Legii române a dreptului de autor în vigoare și permisiunea pentru utilizare obținută în scris din partea Universității „Politehnica” din Timișoara. Toate încălcările acestor drepturi vor fi penalizate potrivit Legii române a drepturilor de autor.

România, 300159 Timișoara, Bd. Republicii 9,
tel. 0256 403823, fax. 0256 403221
e-mail: editura@edipol.upt.ro

Acknowledgements

This thesis was developed during my activity within the Department of Steel Structures and Structural Mechanics CMMC, the Center of Excellence in the Mechanics of Materials and Safety of Structures CEMSIG, from the "Politehnica" University of Timișoara. The experimental program, and the entire research made in these four years was in the framework of two research grants: Grantul PNCDI II „Parteneriate”, contract nr. 31.042/2007, cu titlul “ Raspunsul seismic al cadrelor multietajate cu contravantuiri centrice echipate cu disipatori prin frecare ” in contextul cerintelor de dezvoltare durabila PROACTEX and COST C26 Urban Habitat Constructions under Catastrophic Events.

I would like to thank my coordinating professor Prof. dr. ing. Dan Dubina, MC of the Romanian Academy, for all his support and guidance. Prof. Dubina played without a doubt a crucial role in my growth as a researcher and as an engineer.

I would like to thank the distinguished guests Prof. Ahmed Elghazouli and Prof. Dan Crețu for accepting the invitation and finding the time to be part of the scientific committee.

I would also like to express special thanks to my master, colleague and friend, Assoc. Prof. Aurel Stratan for his patience, guidance and valuable advices throughout the research.

I would like to thank my fellow PhD students and young researchers Neagu Calin, Danku Gelu, Andrei Crisan, Sorin Bordea for their advices and comments. Their help with the experimental program was invaluable.

I would also like to thank my colleagues Assoc. Prof. Adrian Dogariu, Prof. Raul Zaharia, Assoc. Prof. Adrian Ciutina, Prof. Daniel Grecea, Assoc. Prof. Florea Dinu and Assoc. Prof. Viorel Ungureanu for their encouragement, support and help.

I would like to thank the laboratory staff Dan, Adi, Miloicu, for their help with the experimental program.

Last but surely not least I would like to thank my family for their love and continuous support throughout these difficult years. Without them this thesis would not have been possible.

Filip-Văcărescu, Norin

Titlul tezei: Seismic Performance of Multistorey Steel Concentrically Braced Frames Equipped with Friction Dampers

Teze de doctorat ale UPT, Seria 5, Nr. 73, Editura Politehnica, 2011, 199 pagini, 190 figuri, 126 tabele.

ISSN:1842-581X

ISBN (10): 978-606-554-309-6

Cuvinte cheie: seismic motion, braces, friction dampers, brace with damper assembly, performance base design, performance criteria, hysteretic behaviour

Rezumat,

In this paper the performance of concentrically braced frames with friction dampers in the bracing is analysed. For this purpose an experimental program was performed to determine the behaviour of the dampers and of the damper with brace assemble. Numerical analyses were performed on 2 types of concentrically braced frames were analysed using 2 sets of seismic motions recordings scaled to the design spectra. All the analyses were made with two distinct types of dampers placed in the braces and comparing the results with the corresponding structures without dampers. Base on the results of the numerical program a design methodology was proposed for each damper type and exemplified in relevant case studies.

Summary

In this paper the performance of concentrically braced frames with friction dampers in the bracing is analysed. Two types of concentrically braced frames were analysed: (i) simple CBF and (ii) dual CBF with 2 adjacent MRF. The structures considered were analysed using 2 sets of seismic motions recordings scaled to the design spectra. The two target spectra were scaled to the fundamental period of vibration of the analysed structure, so as to yield roughly the same design seismic forces. All the analyses were made with two distinct types of dampers placed in the braces and comparing the results with the corresponding structures without dampers. The paper is structured into 6 chapters with the following topics:

Chapter 2 presents a general overview on the characteristics of seismic motions and on current use of passive damping devices in civil engineering applications. It is shown that seismic motions with long period of vibration can be caused by soft soils and the forward directivity effect. It is pointed out that the nonlinear dynamic response of the structures can have significant variations depending on the period of vibration. This led to the choice of two types of seismic motions that were used in the analyses: (i) semi-artificial seismic motions characteristic for soft soil type (Bucharest, $T_c=1.6s$) and (ii) artificially generated seismic motions characteristic for stiff soil (Class B soil according to SREN1998-1 with $T_c=1.6s$). This chapter also includes an overview of passive damping devices and shows that the use of damping devices, in different configurations, is a modern and effective way of reducing seismic response of structures. It is pointed out that the behaviour of the damper prototype studied in this paper is different from the general current concept of passive damper. This fact correlated with current interest worldwide towards devices that reduce seismic actions and lack of studies in this field in our country provides the motivation of this thesis.

Chapter 3 presents the experimental program for damper prototypes studied in this paper. This chapter presents the experimental tests performed on the two dampers with capacities of 800kN and 1500 kN and of a brace with damper assembly under two different design concepts. A first concept states that the brace with damper are designed so that energy dissipation occurs in the device alone and the brace remains in elastic domain and a second design concept states that the brace will enter plastic domain and both brace and damper will contribute to final response of the assembly. As a result of the experimental tests the hysteretic behaviours of the dampers and of the brace with damper assembly were obtained.

Chapter 4 presents the numerical program performed to determine the performance of concentrically braced structures with dampers in the braces. Based on the results from the experimental program numerical models for the damper, brace and brace with damper assembly were calibrated. Nonlinear time-history analyses were made using two sets of seismic motions recordings scaled to their respective design spectra. Three performance levels were considered for each seismic motion corresponding to serviceability limit state (SLS), ultimate limit state (ULS) and collapse prevention (CP). Performance based evaluation was performed using acceptance criteria for plastic axial

deformation in the braces and plastic rotation for beams and columns according to FEMA356. Two types of concentrically braced frames were analysed: (i) simple CBF and (ii) dual CBF+MRF without dampers. The same structures were analysed equipped with SERB dampers and with "classic" friction damper in the braces.

Chapter 5 presents proposed design provisions for the design structures with SERB dampers and "classical" friction dampers. A design methodology is proposed for each type of damper and case studies were made following the proposed methodology. Both design methodologies proposed were applied for case studies on the structures with FD3 dampers and SERB dampers and the performance of the structures was evaluated using nonlinear TH analyses.

Chapter 6 presents the conclusions of the thesis and personal contributions of the author.

Table of Contents

1	INTRODUCTION.....	20
2	STATE OF ART.....	23
2.1	INTRODUCTION.....	23
2.2	CHARACTERISTICS OF SEISMIC MOTION.....	23
2.3	SEISMIC DESIGN	28
2.4	PASSIVE DAMPING DEVICES.....	29
2.4.1	<i>Steel Yielding Devices</i>	29
2.4.2	<i>Shape Memory Alloys (SMA)</i>	39
2.4.3	<i>Friction Dampers</i>	44
3	EXPERIMENTAL PROGRAM.....	49
3.1	INTRODUCTION.....	49
3.2	DESIGN PRINCIPLES.....	51
3.2.1	<i>Experimental Frame Design</i>	52
3.2.2	<i>Load Protocol</i>	54
3.2.3	<i>Measuring Instruments</i>	55
3.3	EXPERIMENTAL PROGRAM	59
3.3.1	<i>Experimental Tests on Damping Devices</i>	59
3.3.2	<i>Experimental Tests on Braces and on the Braces with Dampers Assembly</i>	61
3.4	CONCLUSIONS	78
3.4.1	<i>„Strong” brace with damper configuration</i>	79
3.4.2	<i>„Weak” brace with damper configuration</i>	79
4	NUMERICAL MODELING	82
4.1	INTRODUCTION.....	82
4.2	ELEMENT MODELING.....	82
4.2.1	<i>Numerical Model for the Brace</i>	82
4.2.2	<i>Numerical Model for the Damper</i>	84
4.2.3	<i>Numerical Model for the Brace with Damper</i>	86
4.3	CBF WITH AND WITHOUT DAMPER.....	87
4.3.1	<i>Geometry and Design</i>	87
4.3.2	<i>CBF Frame with and without Dampers</i>	89
4.4	DUAL FRAME WITH AND WITHOUT DAMPERS	112
4.4.1	<i>Geometry and Design</i>	112
4.4.2	<i>Numerical Analysis on Dual Frame with and without Dampers</i>	114
4.5	AN ALTERNATIVE TYPE OF FRICTION DAMPER DEVICE	142
4.5.1	<i>Element Model for FD3 Damper</i>	142
4.5.2	<i>Numerical Modelling on CBF with FD3 dampers for Soft Soil Type ($T_C=1.6s$)</i>	143
4.5.3	<i>Numerical Modelling on CBF with FD3 dampers for Stiff Soil Type ($T_C=0.5s$)</i>	148
4.5.4	<i>Numerical Modelling on Dual MRF+CBF with FD3 dampers using 7 Semi-artificial Seismic Motion Characteristic for Soft Soil Type ($T_C=1.6s$)</i>	150

4.5.5	<i>Numerical Modelling on Dual MRF+CBF with FD3 dampers for Stiff Soil Type ($T_c=0.5s$)</i>	157
4.6	CONCLUSION	159
4.6.1	<i>Structures with SERB Type Dampers in the Braces</i>	159
4.6.2	<i>Structures with FD3 Type Damper in the Braces</i>	161
5	DESIGN RECOMMENDATIONS	162
5.1	DESIGN PROVISIONS FOR STRUCTURES WITH FD3 TYPE DAMPERS	162
5.2	DESIGN PROVISIONS FOR STRUCTURES WITH SERB TYPE DAMPERS	166
5.3	CASE STUDIES	169
5.3.1	<i>Case Study for Structure with FD3 Damper</i>	169
5.3.2	<i>Case Study for Structure with SERB Damper</i>	171
5.3.3	<i>Evaluation of Seismic Performance</i>	173
5.4	DISCUSSION	182
6	CONCLUSIONS AND PERSONAL CONTRIBUTIONS	186
6.1	SUMMARY.....	186
6.2	PERSONAL CONTRIBUTIONS.....	188
	REFERENCES	191
	APPENDIX A:	194
	APPENDIX B:	196

LIST OF FIGURES

Fig. 1.1: Classification of steel frames: a,b,d) Centrally braced frames (CBF); c) Eccentrically braced frames (EBF); e) Moment resisting frames (MRF) [1].	20
Fig. 1.2. Conceptual diagram of damping devices [2].....	21
Fig. 2.1. The main factors that influence seismic motion in a given location (1 – source factors; 2 – seismic wave propagation; 3 – local factors; 4 – soil-structure interaction) [3].....	23
Fig. 2.2. Recorded seismic motions (Stratan A., 2003 [3]).....	24
Fig. 2.3. Elastic response spectra according to EC8 for type 1 earthquakes ($M_S > 5.5$) and type 2 earthquakes ($M_S \leq 5.5$), for type B soil [3]	25
Fig. 2.4. Main types of faults [4].....	25
Fig. 2.5. The effects of forward directivity on ground speed recordings, after Somerville et al., 1997, in Whittaker [8]	26
Fig. 2.6. Normalized acceleration spectra for different types of soil (Seed et al, 1976, in NEHRP 2000[9])	27
Fig. 2.7: Example of a frame with shear walls [12].....	29
Fig. 2.8. Stress distribution for shear panels with one or more stiffeners [13]	30
Fig. 2.9. Perforated panel for shear walls [14].....	30
Fig. 2.10. a) U.S. Federal Courthouse, Seattle and b) The Century, San Francisco [15]	31
Fig. 2.11: Canam-Manac Headquarters Expansion, St. George, Quebec [1]...	32
Fig. 2.12. The 35 storey office building in Kobe and nearby low rise office building [16]	32
Fig. 2.13. Sylmar Hospital, Los Angeles, CA— 6 floors [16].....	33
Fig. 2.14. Components of a buckling restrained brace [17]	34
Fig. 2.15: Example of BRB hysteretic behavior (courtesy of S.Bordea [18]) ..	34
Fig. 2.16 Cross-section types used for BRB's [17]	35
Fig. 2.17. Examples of structural configurations for BRB's: a) diagonals; b) Chevron brace; c) cross braces; c) V braces [17].....	35
Fig. 2.18. Toyota Stadium [19].....	36
Fig. 2.19. Nippon TV Headquarters (32+2 floors, 68 BRB's were used) [19]..	36
Fig. 2.20: Osaka International Convention Center (420 mil. US dollars project, 13+2 floors, 370 BRB's used) [19]	37
Fig. 2.21. Hewlett Packard building, Corvallis Campus, USA [19]	37
Fig. 2.22. UC Davis Plant and Environmental Science Facility [18].....	38
Fig. 2.23: Wallace F. Bennett Federal Building: a) before and b) after rehabilitation [20].....	39
Fig. 2.24. Shape memory effect [17]	40
Fig. 2.25. Typical superelastic stress-strain curve [21]	41
Fig. 2.26. Nitinol brace configuration [22]	41
Fig. 2.27. a) Use of SMA in connections for steel members; b) use of SMA for bridges [22].....	42
Fig. 2.28. San Feliciano Cathedral, Foligno, Italy [23].....	42
Fig. 2.29: a) San Giorgio bell tower, San Martino in Rio, Italia; b) SMA devices used for the retrofit [24]	43
Fig. 2.30: Basilica San Francesco [23]	43
Fig. 2.31. SMA devices installed on the roof of Basilica S.Francesco in Assisi [23].....	44
Fig. 2.32. Common hysteretic loops of friction dampers [25].....	45
Fig. 2.33. Boeing Commercial Airplane Factory, Everett, WA, USA: a) inside	

view; b) Pall Friction Dampers used [26]	46
Fig. 2.34. Moscone West Convention Center with Pall Dampers in the braces, San Francisco, USA [26].....	46
Fig. 2.35. Boeing Development Center, Cafeteria and Auditorium Buildings, Boeing Field, Seattle, WA, USA; a) general view of the building; b) Pall Friction Dampers used [26].....	47
Fig. 2.36. Ambulatory Care Center, Sharp Memorial Hospital, San Diego, California, USA with Pall Friction Dampers in chevron bracing system [26] ...	47
Fig. 2.37. Behavior of SERB damper compared to normal friction damper	48
Fig. 3.1. a) Hysteretic behaviour of SERB type friction damper prototype [27]; b) SERB type friction damper components [29]	50
Fig. 3.2. Serb damper SERB 194: a) damper geometry; b) hysteretic characteristic [27].....	50
Fig. 3.3. Experimental test configuration: a) Frame geometry; b) extracted experimental configuration	52
Fig. 3.4: Experimental test configuration of the brace specimen	53
Fig. 3.5: Pinned connection: a) of the brace and b) of the beam	53
Fig. 3.6: Experimental test stand with guidance frame: a) lateral view; b) front view	54
Fig. 3.7: Force controlled load protocol for single damper tests	54
Fig. 3.8. ECCS load protocol: a) e_y and F_y determination from monotonic tests; b) cyclic load protocol.....	55
Fig. 3.9. a) Measurement devices positioning scheme; b) Positioning of measuring devices on the CHS section brace test specimen	56
Fig. 3.10. a) Measurement devices positioning scheme; b) Positioning of measuring devices on the HEA brace test specimen without damper	57
Fig. 3.11. Measurement devices positioning scheme for brace with damper experimental tests	58
Fig. 3.12. Measurement devices positioning for the damper alone	58
Fig. 3.13. Measurement devices positioning scheme for HEA brace with damper experimental tests	59
Fig. 3.14. a) Load protocol for 800kN damper; b) Load protocol for 1500kN damper	60
Fig. 3.15. Experimental setup for damper tests.....	60
Fig. 3.16. Hysteretic behavior of SERB800 damper.....	61
Fig. 3.17. Hysteretic behavior of SERB1500 damper	61
Fig. 3.18. Experimental test setup for experimental tests on braces with and without dampers	62
Fig. 3.19. Experimental test setup for "strong " brace with damper configuration.....	63
Fig. 3.20. a) Longitudinal view of the experimental test setup for "strong " brace with damper configuration; b) damper connection	64
Fig. 3.21. Damper connection to brace and pinned base connection: a) lateral view; b) longitudinal view.....	64
Fig. 3.22: Force displacement curve obtained from BDE experimental tests ..	65
Fig. 3.23. Experimental test setup for CHS brace without damper	66
Fig. 3.24: Experimental test setup for CHS brace without damper: a) general view; b) base connection detail	66
Fig. 3.25.Failure of the connection between the CHS brace specimen and connection plates of the pinned support	67

Fig. 3.26: Buckling of CHS brace under monotonic compression load	67
Fig. 3.27. Force displacement curves for the CHS brace obtained from monotonic tests	68
Fig. 3.29. Determination of yield displacement e_y for CHS brace	68
Fig. 3.29. Buckling of the CHS brace at cyclic tests	69
Fig. 3.30. a) Plastic hinge formation at the middle of the CHS brace; b) Crack development near the connection of the CHS brace with the pinned base plates	70
Fig. 3.32: Force displacement curve recorded from cyclic tests on the CHS brace without damper	70
Fig. 3.32. Experimental test setup for CHS brace with damper specimen	71
Fig. 3.33: Cyclic behavior of CHS brace with damper	71
Fig. 3.34. Experimental test setup for monotonic tests on HEA100 brace.....	72
Fig. 3.35. Buckling of the HEA100 brace under monotonic compression load .	73
Fig. 3.36. Force displacement curves for the HEA100 brace obtained from monotonic tests	73
Fig. 3.37. Determination of yield displacement for HB-MT specimen using initial stiffness method	74
Fig. 3.38. Determination of yield displacement for HB-MT specimen using tangent stiffness method	74
Fig. 3.39. Buckling of the HEA100 brace at cyclic tests	75
Fig. 3.40. Force displacement curve recorded for cyclic tests on the HEA100 brace	76
Fig. 3.41. Experimental test setup for HEA100 brace with damper specimen .	77
Fig. 3.42. Damper connection to HEA brace and pinned base connection	77
Fig. 3.43: Hysteretic behavior of HEA100 brace with damper	78
Fig. 3.44: Comparison between „strong” brace with damper and a brace without damper behaviour	79
Fig. 3.45. Comparison between hysteretic behavior of the same brace with and without damper	80
Fig. 3.46. Comparison between hysteretic behavior of the same brace with and without damper at load level of up to $2xe_y$	80
Fig. 3.47. Comparison of force levels in the brace with and without damper up to $2e_y$	81
Fig. 4.1. Menegotto-Pinto steel model with Fillipou isotropic hardening [31] .	83
Fig. 4.2. Brace discretisation in: a) 4 elements; b) 2 elements	83
Fig. 4.3. Comparison between cyclic behaviors of brace from the numerical model with the one obtained experimentally	84
Fig. 4.4. Trial hysteretic models: a) Biliniar kinematic; b) Rambert-Osgood curve; c) Takeda; d) Richard-Abbot curve [32].....	85
Fig. 4.5. Link behaviors for damper model: a) Gap-Hook; b) Bilinear Symmetric	85
Fig. 4.6.a) Behavior of damper model; b) Comparison between the damper behavior of the model and the damper behavior obtained experimentally	86
Fig. 4.7. Comparison between numerical and experimental behavior of brace with damper.....	86
Fig. 4.8. Frame geometry: a) Plan layout; b) Selected frame	87
Fig. 4.9. Design spectra for Bucharest [1]	88
Fig. 4.10. Final geometry and sections of the designed frame.....	89
Fig. 4.11. Elastic spectra: a) Soft soil type $T_c=1.6s$; b) Stiff soil type $T_c=0.5s$	89

Fig. 4.12. Semi-artificial seismic motion characteristic for soft soil type (Bucharest $T_c=1.6s$)	90
Fig. 4.13. Artificially generated seismic motions characteristic for stiff soil (Type B $T_c=0.5s$)	90
Fig. 4.14. Maximum drift values for the structure with and without dampers	92
Fig. 4.15. Maximum drift at each storey at: a) SLS; b) ULS; c) CP for the structure with and without dampers	92
Fig. 4.16. Top displacement at: a) SLS; b) ULS; c) CP for the structure with and without dampers	93
Fig. 4.17. Permanent top displacement at: a) SLS; b) ULS; c) CP for the structure with and without dampers	93
Fig. 4.18. Plastic hinge formation for CBF: a) without dampers; b) with dampers at SLS	97
Fig. 4.19. Recorded top displacement in time for the CBF structure at SLS (soft soil).....	97
Fig. 4.20. Plastic hinge formation for CBF: a) without dampers; b) with dampers at ULS	98
Fig. 4.21. Recorded top displacement in time for the CBF structure at ULS (soft soil).....	99
Fig. 4.22. Plastic hinge formation in the structure with and without damper at CP (soft soil)	100
Fig. 4.23. Recorded top displacement in time for the CBF structure at CP (soft soil).....	101
Fig. 4.24. Maximum drift values for the structure with and without dampers (stiff soil)	102
Fig. 4.25. Maximum drift at each storey at: a) SLS; b) ULS; c) CP for the structure with and without dampers (stiff soil)	103
Fig. 4.26. Top displacement at: a) SLS; b) ULS; c) CP for the structure with and without dampers (stiff soil).....	103
Fig. 4.27. Permanent top displacement at: a) SLS; b) ULS; c) CP for the structure with and without dampers (stiff soil)	103
Fig. 4.28. Plastic hinge formation for CBF: a) without dampers; b) with dampers at SLS	107
Fig. 4.29. Recorded top displacement in time for the CBF structure at SLS (stiff soil).....	108
Fig. 4.30. Plastic hinge formation for CBF: a) without dampers; b) with dampers at ULS	108
Fig. 4.31. Recorded top displacement in time for the CBF structure at ULS (stiff soil).....	109
Fig. 4.32. Plastic hinge formation in the structure with and without damper at CP (soft soil)	110
Fig. 4.33. Recorded top displacement in time for the CBF structure at ULS (stiff soil).....	111
Fig. 4.34. Frame geometry of dual CBF+MRF frame	112
Fig. 4.35. Design spectra for Bucharest.....	113
Fig. 4.36. Section dimensions of the dual frame.....	114
Fig. 4.37. Maximum drift values for the dual structure with and without dampers	115
Fig. 4.38. Maximum drift at each storey at: a) SLS; b) ULS; c) CP for the dual structure with and without dampers	116

Fig. 4.39. Top displacement at: a) SLS; b) ULS; c) CP for the dual structure with and without dampers.....	116
Fig. 4.40. Permanent top displacement at: a) SLS; b) ULS; c) CP for the structure with and without dampers	116
Fig. 4.41. Plastic hinge formation for dual MRF+CBF structure: a) without dampers; b) with dampers at SLS	123
Fig. 4.42. Recorded top displacement in time for the dual MRF+CBF structure at SLS (soft soil).....	123
Fig. 4.43. Plastic hinge formation for dual MRF+CBF structure: a) without dampers; b) with dampers at ULS	124
Fig. 4.44. Recorded top displacement in time for the dual MRF+CBF structure at ULS (soft soil).....	125
Fig. 4.45. Plastic hinge formation in the structure with and without damper at CP (soft soil)	127
Fig. 4.46. Recorded top displacement in time for the dual MRF+CBF structure at CP (soft soil)	127
Fig. 4.47. Maximum drift values for the structure with and without dampers (stiff soil)	130
Fig. 4.48. Maximum drift at each storey at: a) SLS; b) ULS; c) CP for the structure with and without dampers (stiff soil)	130
Fig. 4.49. Top displacement at: a) SLS; b) ULS; c) CP for the structure with and without dampers (stiff soil).....	130
Fig. 4.50. Permanent top displacement at: a) SLS; b) ULS; c) CP for the structure with and without dampers (stiff soil)	131
Fig. 4.51. Plastic hinge formation for dual MRF+CBF structure: a) without dampers; b) with dampers at SLS	135
Fig. 4.52. Recorded top displacement in time for the dual MRF+CBF structure at SLS (stiff soil).....	136
Fig. 4.53. Plastic hinge formation for dual MRF+CBF structure: a) without dampers; b) with dampers at ULS	137
Fig. 4.54. Recorded top displacement in time for the dual MRF+CBF structure at ULS (stiff soil).....	137
Fig. 4.55. Plastic hinge formation in the structure with and without damper at CP (soft soil)	139
Fig. 4.56. Recorded top displacement in time for the dual MRF+CBF structure at CP (stiff soil)	139
4.57. a) Bilinear kinematic link behaviour used; b) Hysteretic behaviour of the FD3 numerical model	143
Fig. 4.58. Maximum drift values for the structure with FD3 and SERB dampers and without dampers	143
Fig. 4.59. Maximum drift at each storey at: a) SLS; b) ULS; c) CP for the structure with FD3 and SERB dampers and without dampers	144
Fig. 4.60. Top displacement at: a) SLS; b) ULS; c) CP for the structure with and without dampers	144
Fig. 4.61. Permanent top displacement at: a) SLS; b) ULS; c) CP for the structure with and without dampers	144
Fig. 4.62. Maximum drift values for the structure with and without dampers (stiff soil)	149
Fig. 4.63. Maximum drift at each storey at: a) SLS; b) ULS; c) CP for the structure with and without dampers (stiff soil)	149
Fig. 4.64. Top displacement at: a) SLS; b) ULS; c) CP for the structure with and	

without dampers (stiff soil)	149
Fig. 4.65. Permanent top displacement at: a) SLS; b) ULS; c) CP for the structure with and without dampers (stiff soil)	149
Fig. 4.66. Maximum drift values for the dual structure with and without dampers	150
Fig. 4.67. Maximum drift at each storey at: a) SLS; b) ULS; c) CP for the dual structure with and without dampers	150
Fig. 4.68. Top displacement at: a) SLS; b) ULS; c) CP for the dual structure with and without dampers.....	151
Fig. 4.69. Permanent top displacement at: a) SLS; b) ULS; c) CP for the dual structure with and without dampers	151
Fig. 4.70. Maximum drift values for the structure with and without dampers (stiff soil)	158
Fig. 4.71. Maximum drift at each storey at: a) SLS; b) ULS; c) CP for the dual structure with and without dampers (stiff soil)	158
Fig. 4.72. Top displacement at: a) SLS; b) ULS; c) CP for the structure with and without dampers (stiff soil)	158
Fig. 4.73. Permanent top displacement at: a) SLS; b) ULS; c) CP for the structure with and without dampers (stiff soil)	159
Fig. 5.1. Axial force component for beams in the case of V bracings with dampers	163
Fig. 5.2. Simplified damper behaviour: a) Example on experimental damper behaviour; b) simplified bilinear curve parameters.....	166
Fig. 5.3. Simplified damper behaviour at ULS	167
Fig. 5.4. Design spectra for Bucharest [1]	170
Fig. 5.5. Section dimensions for the CBF with FD3 dampers case study	171
Fig. 5.6. Section dimensions for the CBF with SERB dampers case study	173
Fig. 5.7. Maximum drift values for the structures with dampers (soft soil) ...	174
Fig. 5.8. Maximum drift values at each storey at: a) SLS; b) ULS and c) CP (soft soil)	174
Fig. 5.9. Top displacement: a) SLS; b) ULS and c) CP (soft soil)	174
Fig. 5.10. Permanent top displacement at a) SLS; b) ULS and c) CP (soft soil)	175
Fig. 5.11. Displacement time-history of top floor at: a) SLS; b) ULS and c) CP (soft soil)	176
Fig. 5.12. . Plastic hinge location at ULS: a) No damper; b) SERB damper; c) FD3 damper (soft soil)	176
Fig. 5.13. Plastic hinge location at CP a) No damper; b) SERB damper; c) FD3 damper (soft soil)	177
Fig. 5.14. Maximum drift values for the structures with dampers (stiff soil) ..	179
Fig. 5.15. Maximum drift values at each storey at: a) SLS; b) ULS and c) CP (stiff soil)	179
Fig. 5.16. Top displacement: a) SLS; b) ULS and c) CP (stiff soil)	179
Fig. 5.17. Permanent top displacement at a) SLS; b) ULS and c) CP (stiff soil)	180
Fig. 5.18. Displacement time-history of top floor at: a) SLS; b) ULS and c) CP (stiff soil)	181
Fig. 5.19. Plastic hinge location at CP: a) structure with FD3 damper; b) structure with SERB damper (stiff soil).....	181
Fig. 5.20. Comparison of maximum drift values for the 2 types of seismic	

motions used for: a) structures with SERB damper; b) structures with FD3 damper	183
Fig. 5.21. Comparison of top displacement of structures with SERB dampers for the 2 types of seismic motions used for: a) SLS; b) ULS and c) CP.....	184
Fig. 5.22. Comparison of top displacement of structures with FD3 dampers for the 2 types of seismic motions used for: a) SLS; b) ULS and c) CP.....	184
Fig. 5.23. Comparison of permanent top displacement of structures with SERB dampers for the 2 types of seismic motions used for: a) SLS; b) ULS and c) CP	184
Fig. 5.24. Comparison of permanent top displacement of structures with FD3 dampers for the 2 types of seismic motions used for: a) SLS; b) ULS and c) CP	185

LIST OF TABLES

Table 1.1. Examples of devices for structures isolated from seismic motion and and for structures with supplemental damping.....	22
Table 3.1. Hysteretic behavior of displacement dependent devices [17]	49
Table 3.2. Parameters for the SERB dampers tested experimentally	51
Table 3.3. Displacement transducers used and measured parameters for CHS section brace tests	56
Table 3.4. Displacement transducers used and measured parameters for HEA section brace tests without dampers.....	57
Table 3.5. Displacement transducers used and measured parameters for experimental tests on brace with damper assembly.....	58
Table 3.6. Displacement transducers used and measured parameters for experimental tests on HEA brace with damper assembly.....	59
Table 3.7. Experimental program for brace tests with and without dampers ..	62
Table 3.8. Cyclic displacement based load protocol determined for CHS brace tests	69
Table 3.9. Cyclic displacement based load protocol determined for HEA100 brace tests.....	75
Table 3.10. Energy per cycle for brace with and without damper.....	81
Table 4.1. Shape parameters for Menegotto-Pinto steel model with Fillipou isotropic hardening.....	83
Table 4.2. Parametric study to determine optimum number of elements and plastic hinge length	84
Table 4.3. Correspondence of seismic level to performance level	91
Table 4.4. Displacement at buckling and yield for compression and tension braces.....	91
Table 4.5. Mean values of axial plastic deformation for braces in compression at SLS.....	94
Table 4.6. Mean values of axial plastic deformation for braces in tension at SLS	94
Table 4.7. Mean values for plastic rotation at SLS for central beams (soft soil)	94
Table 4.8. Mean values of axial plastic deformation for braces in compression at ULS.....	94
Table 4.9. Mean values of axial plastic deformation for braces in tension at ULS	95
Table 4.10. Mean values for plastic rotation at ULS for central beams.....	95
Table 4.11. Mean values of axial plastic deformation for braces in compression at CP	96
Table 4.12. Mean values of axial plastic deformation for braces in tension at CP	96
Table 4.13. Mean values for plastic rotation at CP for central beams.....	96
Table 4.14. Axial plastic deformation values for compression braces at SLS (soft soil)	98
Table 4.15. Axial plastic deformation for braces in compression at ULS (soft soil).....	99
Table 4.16. Axial plastic deformation for braces in tension at ULS (soft soil) .	99
Table 4.17. Plastic rotation at ULS for central beams (soft soil)	100
Table 4.18. Axial plastic deformation for braces in compression at CP (soft soil)	

.....	101
Table 4.19. Axial plastic deformation for braces in tension at CP (soft soil) ..	101
Table 4.20. Plastic rotation at CP for central beams (soft soil)	102
Table 4.21. Mean values of axial plastic deformation for braces in compression at SLS (stiff soil).....	104
Table 4.22. Mean values of axial plastic deformation for braces in tension at SLS (stiff soil)	104
Table 4.23. Mean values for plastic rotation at SLS for central beams (stiff soil)	104
Table 4.24. Mean values of axial plastic deformation for braces in compression at ULS (stiff soil).....	105
Table 4.25. Mean values of axial plastic deformation for braces in tension at ULS (stiff soil)	105
Table 4.26. Mean values for plastic rotation at ULS for central beams (stiff soil)	105
Table 4.27. Mean values of axial plastic deformation for braces in compression at CP (stiff soil)	106
Table 4.28. Mean values of axial plastic deformation for braces in tension at CP (stiff soil)	106
Table 4.29. Mean values for plastic rotation at CP for central beams (stiff soil)	107
Table 4.30. Axial plastic deformation values for compression braces at SLS (stiff soil)	108
Table 4.31. Axial plastic deformation for braces in compression at ULS (stiff soil).....	109
Table 4.32. Axial plastic deformation for braces in tension at ULS (stiff soil)	109
Table 4.33. Plastic rotation at ULS for central beams (stiff soil)	110
Table 4.34. Axial plastic deformation for braces in compression at CP (stiff soil)	111
Table 4.35. Axial plastic deformation for braces in tension at CP (stiff soil) ..	111
Table 4.36. Plastic rotation at CP for central beams (stiff soil).....	112
Table 4.37. Displacement at buckling and yield for compression and tension braces.....	115
Table 4.38. Mean values of axial plastic deformation for braces in compression at SLS.....	117
Table 4.39. Mean values of axial plastic deformation for braces in tension at SLS	117
Table 4.40. Mean values for plastic rotation at SLS for central beams (soft soil)	117
Table 4.41. Mean values of axial plastic deformation for braces in compression at ULS.....	118
Table 4.42. Mean values of axial plastic deformation for braces in tension at ULS	118
Table 4.43. Mean values for plastic rotation at ULS for central beams	119
Table 4.44. Mean values for plastic rotation at ULS for MRF beams	119
Table 4.45. Mean values for plastic rotation at ULS for central columns	120
Table 4.46. Mean values of axial plastic deformation for braces in compression at CP	120
Table 4.47. Mean values of axial plastic deformation for braces in tension at CP	120
Table 4.48. Mean values for plastic rotation at CP for central beams.....	121

Table 4.49. Mean values for plastic rotation at CP for MRF beams	121
Table 4.50. Mean values for plastic rotation at CP for central columns	122
Table 4.51. Mean values for plastic rotation at CP for MRF columns	122
Table 4.52. Axial plastic deformation values for compression braces at SLS (soft soil)	124
Table 4.53. Axial plastic deformation for braces in compression at ULS (soft soil).....	125
Table 4.54. Axial plastic deformation for braces in tension at ULS (soft soil)	125
Table 4.55. Plastic rotation at ULS for central beams (soft soil)	126
Table 4.56. Plastic rotation at ULS for MRF beams (soft soil).....	126
Table 4.57. Plastic rotation at ULS for central columns (soft soil).....	126
Table 4.58. Axial plastic deformation for braces in compression at CP (soft soil)	128
Table 4.59. Axial plastic deformation for braces in tension at CP (soft soil) ..	128
Table 4.60. Plastic rotation at CP for central beams (soft soil)	128
Table 4.61. Plastic rotation at CP for MRF beams (soft soil).....	129
Table 4.62. Plastic rotation at CP for central columns (soft soil).....	129
Table 4.63. Plastic rotation at CP for MRF columns	129
Table 4.64. Mean values of axial plastic deformation for braces in compression at SLS (stiff soil).....	131
Table 4.65. Mean values of axial plastic deformation for braces in tension at SLS (stiff soil)	132
Table 4.66. Mean values for plastic rotation at SLS for central beams (stiff soil)	132
Table 4.67. Mean values of axial plastic deformation for braces in compression at ULS (stiff soil).....	132
Table 4.68. Mean values of axial plastic deformation for braces in tension at ULS (stiff soil)	132
Table 4.69. Mean values for plastic rotation at ULS for central beams (stiff soil)	133
Table 4.70. Mean values for plastic rotation at ULS for MRF beams (stiff soil)	133
Table 4.71. Mean values of axial plastic deformation for braces in compression at CP (stiff soil)	133
Table 4.72. Mean values of axial plastic deformation for braces in tension at CP (stiff soil)	134
Table 4.73. Mean values for plastic rotation at CP for central beams (stiff soil)	134
Table 4.74. Mean values for plastic rotation at CP for MRF beams	134
Table 4.75. Axial plastic deformation values for compression braces at SLS (soft soil)	136
Table 4.76. Axial plastic deformation for braces in compression at ULS (stiff soil).....	138
Table 4.77. Axial plastic deformation for braces in tension at ULS (stiff soil) ..	138
Table 4.78. Plastic rotation at ULS for central beams (stiff soil)	138
Table 4.79. Plastic rotation at ULS for MRF beams (stiff soil).....	138
Table 4.80. Axial plastic deformation for braces in compression at CP (stiff soil)	140
Table 4.81. Axial plastic deformation for braces in tension at CP (stiff soil) ..	140
Table 4.82. Plastic rotation at CP for central beams (stiff soil).....	140

Table 4.83. Plastic rotation at CP for MRF beams (stiff soil)	141
Table 4.84. Mean values of axial plastic deformation for braces in compression at SLS.....	145
Table 4.85. Mean values of axial plastic deformation for braces in tension at SLS	145
Table 4.86. Mean values for plastic rotation at SLS for central beams (soft soil)	145
Table 4.87. Mean values of axial plastic deformation for braces in compression at ULS.....	146
Table 4.88. Mean values of axial plastic deformation for braces in tension at ULS	146
Table 4.89. Mean values for plastic rotation at ULS for central beams.....	146
Table 4.90. Mean values of axial plastic deformation for braces in compression at CP	147
Table 4.91. Mean values of axial plastic deformation for braces in tension at CP	147
Table 4.92. Mean values for plastic rotation at CP for central beams.....	147
Table 4.93. Mean values for plastic rotation at CP for central columns	148
Table 4.94. Mean values of axial plastic deformation for braces in compression at SLS.....	152
Table 4.95. Mean values of axial plastic deformation for braces in tension at SLS	152
Table 4.96. Mean values for plastic rotation at SLS for central beams (soft soil)	152
Table 4.97. Mean values of axial plastic deformation for braces in compression at ULS.....	153
Table 4.98. Mean values of axial plastic deformation for braces in tension at ULS	153
Table 4.99. Mean values for plastic rotation at ULS for central beams.....	153
Table 4.100. Mean values for plastic rotation at ULS for MRF beams.....	154
Table 4.101. Mean values for plastic rotation at ULS for central columns.....	154
Table 4.102. Mean values of axial plastic deformation for braces in compression at CP.....	155
Table 4.103. Mean values of axial plastic deformation for braces in tension at CP.....	155
Table 4.104. Mean values for plastic rotation at CP for central beams.....	155
Table 4.105. Mean values for plastic rotation at CP for MRF beams.....	156
Table 4.106. Mean values for plastic rotation at CP for central columns.....	156
Table 4.107. Mean values for plastic rotation at CP for MRF columns	157
Table 5.1. Selection of damper slip load	170
Table 5.2. Maximum values of plastic deformation in compression braces at CP (soft soil)	177
Table 5.3. Maximum values of plastic deformation in tension braces at CP (soft soil).....	177
Table 5.4. Maximum values for plastic rotation at CP for central beams (soft soil).....	178
Table 5.5. Maximum values for plastic rotation at CP for central columns (stiff soil).....	178
Table 5.6. Maximum values for plastic rotation at CP for central beams (stiff soil).....	182
Table 5.7. Maximum values for plastic rotation at CP for central columns	182

1 Introduction

The static configuration of a building represents in all configurations a spatial system capable of transmitting to the foundations the effect of vertical loads, own weight, live load and also the effects of the horizontal forces that act on the structure from wind and seismic loading.

The effect of spatial interaction is assured by both the type of connection between the component elements, columns, beams, and bracings or by reinforced concrete diaphragms as well as by the floor slabs of each floor which form horizontal diaphragms and give high rigidity in their own plane. For an optimal design of these structures one must find a compromise between the strength, rigidity, ductility and architectural demands.

Steel frame structures generally fall into 3 main categories according to the way they resist to the action of lateral forces (Fig. 1.1):

- moment resisting frames (MRF)
- concentrically braced frames (CBF)
- eccentrically braced frames (EBF)

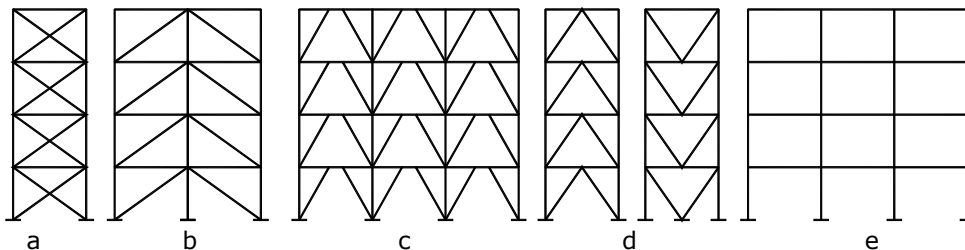


Fig. 1.1: Classification of steel frames: a,b,d) Centrally braced frames (CBF); c) Eccentrically braced frames (EBF); e) Moment resisting frames (MRF) [1]

For checking at ultimate limit states, the methodology of dimensioning of structures situated in seismic areas can lead to the following types of structural design concepts:

- dissipative structures
- structures isolated from seismic action
- structures with supplemental damping

Dissipative structures are designed to consume the energy induced by the seismic motion in the structure by allowing some specific elements to enter plastic domain. These dissipative elements act as fuses for the structure consuming energy, while the rest of the elements that are considered non-dissipative are designed to remain in elastic domain.

For structures isolated from seismic action and those with supplemental damping the structure is conceived as not to enter plastic domain by implementing devices which can absorb the seismic energy and can modify the period of vibration of the structure to more favorable values for global

behavior. These devices can be of three types:

- Seismic isolation devices
- Passive energy dissipation devices
- Active energy dissipation devices

Passive systems are designed to be used both for new structures and for seismic retrofit of existing structures. In general these devices function on principles such as friction between surfaces, yielding of components, and phase transformation of steel alloys, viscoelastic deformation of solids or fluids combined with the control of the flow of liquid.

Active/hybrid/semi-active control systems are an evolution of passive devices that have sensors and real time control and evaluation systems that modify partially or completely the properties of the damping devices during the recorded ground motion in order to obtain an optimal behavior of the structure. The concept on which these types of dampers function can be better observed in Fig. 1.2.

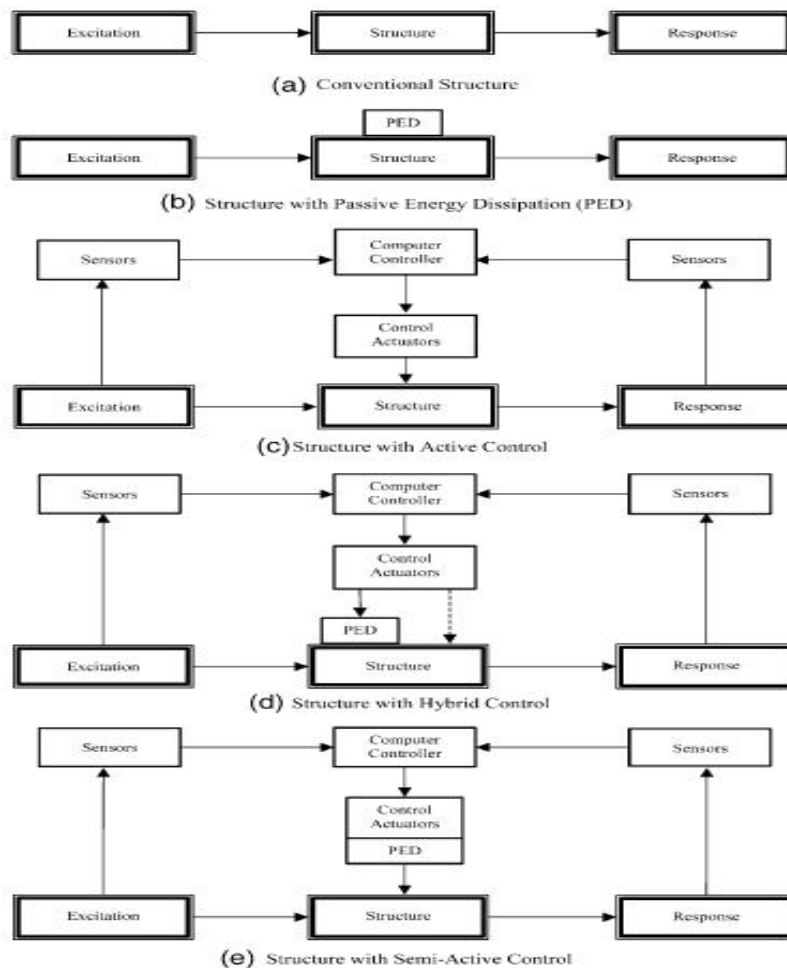


Fig. 1.2. Conceptual diagram of damping devices [2]

A few examples of devices corresponding to the three categories mentioned above can be found in Table 1.

Base isolation	Elastomeric isolators Lead rubber bearings Sliders
Passive	Shear walls Steel hysteretic dampers Buckling restrained braces Eccentrically braced frames with dissipative link element Friction dampers Fluid viscous dampers Magnetorheologic fluid dampers Tuned mass dampers Shape memory alloys
Active	Active bracing systems Active tuned mass dampers Systems with variable strength and stiffness „Smart“ materials

Table 1. Examples of devices for structures isolated from seismic motion and for structures with supplemental damping

The use of different types of damping devices to reduce the seismic response of a structure is a modern and innovative approach to design of structures. This field of research is still young and is being developed continuously throughout the world. Extensive research programs are in motion that address the many difficult issues that need to be addressed in the design and retrofit of structures with damping devices or seismic isolators. Although structural design including dampers and isolators is still largely based on experimental tests there, as the number of structures designed with these new devices increases, there is a growing need to determine design procedures that can address multiple design cases. This paper presents the analyses of the behavior of a distinct type of friction damper both experimentally and numerically. Based on the experimental data numerical models are developed to evaluate the performance of concentrically braced frames equipped with such devices in the braces leading to the proposal of design guidelines for new structures that incorporate such devices.

2 State of art

2.1 Introduction

Seismic design of structures is a continuously growing field in civil engineering. The interest and exponential growth of this field was and is fuelled by the effects of some important earthquakes in history such as Loma Pieta (1989), Northridge (1994) and Hyogoken-Nanbu (1995). These earthquakes first revealed the existing flaws in structural design. Important economic losses led to the firm resolution that design must go beyond prevention of structural collapse and also reduce structural and non-structural damage for frequent low intensity earthquakes. Seismic recordings of these earthquakes also brought to light new aspects of the characteristics of seismic motions related to directivity effect of near-field earthquakes, frequency content, soil structure interaction and soil type influence. A proper identification of seismic motion characteristics can be crucial in the design stage of a structure. In the quest to reduce seismic response of structures and to limit damage induced by frequent low intensity seismic motion innovative technologies were developed that use a variety of devices that function on various mechanical principles. These devices are introduced in different structural configurations both for new structures and for seismic retrofit of existing structures. This chapter presents some of the characteristics of seismic actions that have an important effect on the design and creates a general view on the use of damping devices in modern structures, in particular passive damping devices.

2.2 Characteristics of seismic motion

The main factors that influence seismic motion in a given location can be classified in 4 categories: (1) source factors, (2) seismic wave propagation, (3) local factors, (4) soil-structure interaction (Fig. 2.1). The differences between the characteristics of earthquakes and the complex interaction between the factors that influence the final characteristics of a seismic recording can lead to significant variation of the recordings. In Fig. 2.2 several accelerograms of seismic events are presented using the same scale for time and acceleration. Significant differences can be observed in terms of acceleration, duration and general aspect of the accelerogram.

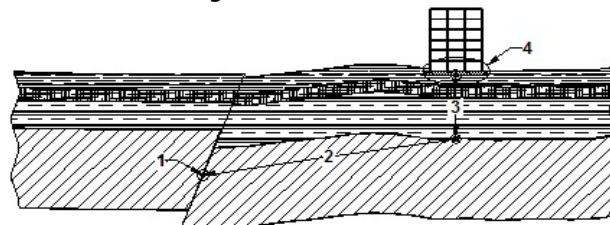


Fig. 2.1. The main factors that influence seismic motion in a given location (1 – source factors; 2 – seismic wave propagation; 3 – local factors; 4 – soil-structure interaction) [3]

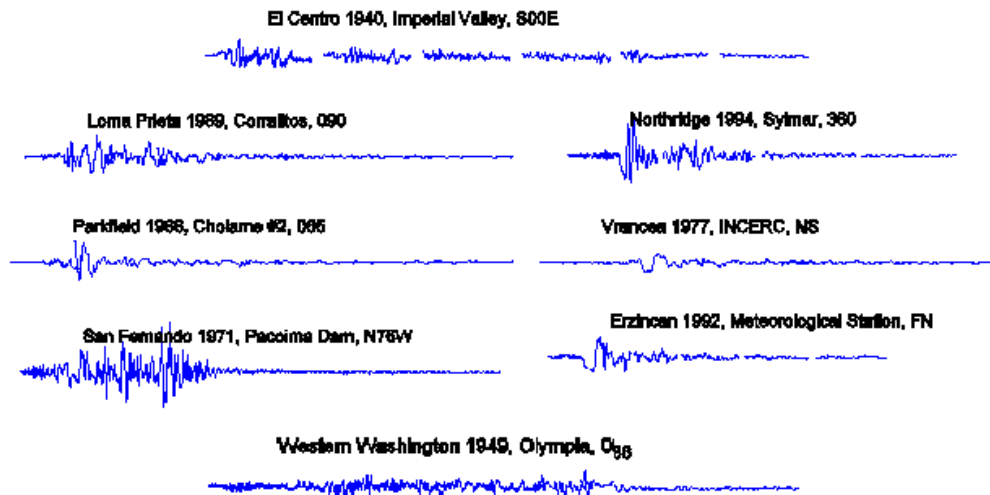


Fig. 2.2. Recorded seismic motions (Stratan A., 2003 [3])

Most earthquakes take place as a result of tectonic activities. There are 3 generally recognized tectonic regimes (Oros, 2002 [4], Stewart et al., 2001 [5]):

- active tectonic plates boundaries (inter-plate earthquakes)
- tectonic plates interior (intra-plate earthquakes)
- oceanic rifts

Earthquakes that are generated at the active boundaries of tectonic (inter-plate earthquakes) are capable of producing seismic events of considerable magnitude characterized by high ground accelerations, long periods of motion and high intensity that can influence large areas (hundreds of km). Because high frequencies decrease faster with distance than low frequencies, a far-field earthquake will contain more energy in the low frequency domain. As a consequence larger far-field earthquakes can have more devastating effects on structures with long periods of vibration than smaller near-field earthquakes. As examples of inter-plate source earthquakes we can mention here: California (SUA), Japan, Turkey and Romania (Vrancea subcrustal seismic zone).

As opposed to inter-plate earthquakes, intra-plate earthquakes are generated by geological faults inside tectonic plates. These faults are generally smaller than those associated with tectonic plate boundaries resulting in earthquakes with smaller magnitudes, duration and affected areas. Therefore seismic hazard associated to a location affected by intra-plate earthquakes is associated in general to medium magnitude local events (Chandler et al., 1992 [6]). Intra-plate earthquakes are present in Australia, eastern part of North America, Europe, and Banat (RO) etc.

In a simplified approach the differences between the characteristics of inter-plate and intra-plate earthquakes can be reduced to the difference between high magnitude earthquakes and medium magnitude earthquakes respectively. The difference between high magnitude earthquakes (with magnitude of

surface waves $M_S > 5.5$) and medium magnitude ones ($M_S \leq 5.5$) can be observed based on the response spectra specified in Eurocode 8, 2003 [7] (Fig. 2.3, Class B soil). Far-field earthquakes with high magnitude (Type1) are characterized by smaller spectral amplitudes in the short period zone (spectral zone with constant acceleration) and larger spectral amplitudes for medium and long periods in comparison to near-field earthquakes with medium and small magnitude (Type2).

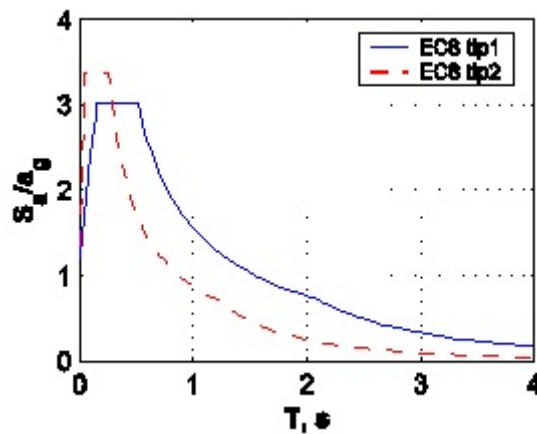


Fig. 2.3. Elastic response spectra according to EC8 for type 1 earthquakes ($M_S > 5.5$) and type 2 earthquakes ($M_S \leq 5.5$), for type B soil [3]

Depending on the geometry of the seismic source 4 types of faults can be distinguished (Oros, 2002[4], Fig. 2.4):

- Reverse fault. The slip takes place vertically with the superposition of one tectonic block over the other.
- Normal faults.
- Strike-slip faults. The slip takes place in horizontal direction.
- Oblique slip faults. Slip is a combination of both directions and inclination. These are the most common faults in nature.

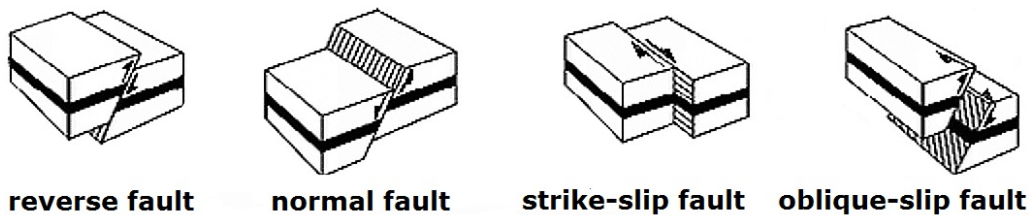


Fig. 2.4. Main types of faults [4]

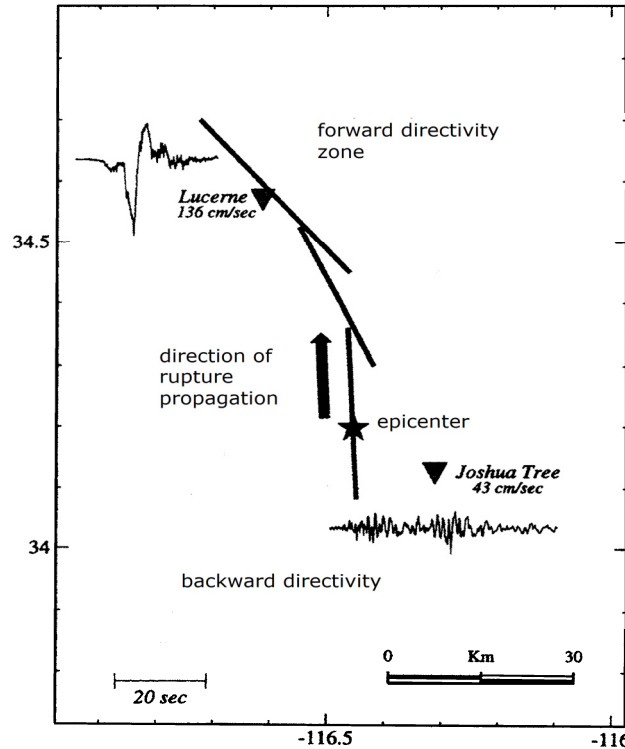


Fig. 2.5. The effects of forward directivity on ground speed recordings, after Somerville et al., 1997, in Whittaker [8]

The type of fault influences the model of radiation of the seismic source (Kim, 1987, in Oros, 2002[4]). For example peak values of displacements and accelerations calculated for reverse and normal faults are increased by a factor of 2.5 and 3, respectively, compared with the ones calculated for strike slip faults.

For near-field earthquakes having a distance to fault of up to 20-60 km, the azimuth of the location with respect to the source affects the characteristics of the seismic motions considerably. The forward directivity effect takes place when the rupture of a fault and the slip propagate towards the location (Stewart et al., 2001 [5]). Because the speed of rupture is close to the speed of seismic shear waves (S), there is an energy build up near the rupture front. Seismic motion reaches this type of location has the shape of a pulse (the effect of the shockwave), characterized by short duration and large amplitudes in the domain of long and medium periods. This phenomenon occurs for the seismic wave component normal to the fault. When the location is near the epicenter and the rupture front propagates from the location, seismic waves are more distributed in time. This effect is called backward directivity and is characterized by longer duration of the motion and reduced values of amplitudes. The effects of forward directivity (a single pulse with long period and reduced duration) and backward directivity (a complex movement with smaller amplitudes and longer duration) on ground velocity recordings are

presented in Fig. 2.5 for the Landers earthquake, California, 1992. The directivity effect can be observed for both strike-slip faults and vertical faults (normal and reverse). In both cases the motion pulse caused by forward directivity is perpendicular to the fault.

Another important factor that influences the seismic motion is the type of soil through which the seismic waves propagate. Studies by Idriss et al. indicate a strong connection between the amplitude of seismic motion and the amplification of peak ground acceleration (PGA) by soft soil layers. The amplification is maximum (between 1.5 and 4.0) for small amplitudes of maximum acceleration at rock base (0.05 - 0.1 g) and tends to decrease as the earthquake intensity increases (factors of around 1.0 for $PGA_{rock} = 0.4g$). This effect is attributed to the nonlinear response of the soft soil layer to high intensities of seismic motions. The influence of the type of soil on the shape of the response spectra is presented in Fig. 2.6, according to statistic studies by Seed et al. on a set of 104 seismic recording from the USA, Japan and Turkey.

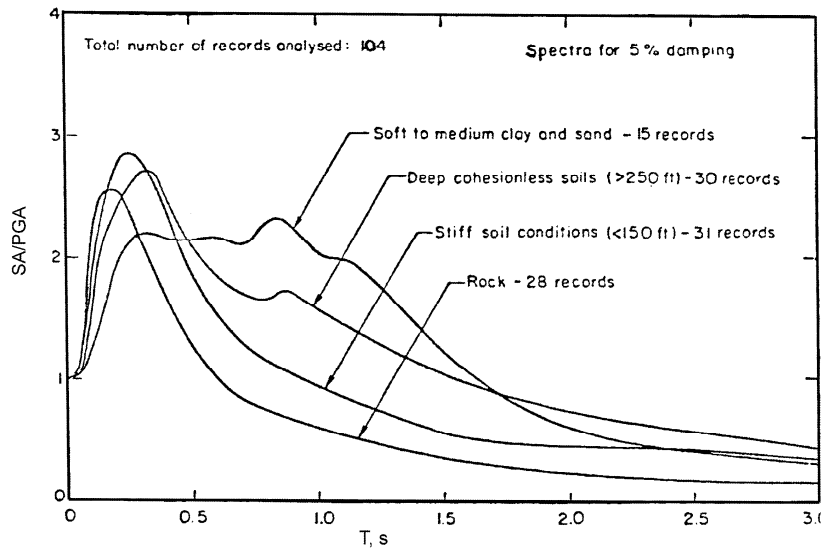


Fig. 2.6. Normalized acceleration spectra for different types of soil
(Seed et al, 1976, in NEHRP 2000[9])

A considerable amplification of spectral quantities can be observed for long and medium periods (> 1.0 sec) in the case of soft soils. In most cases the maximum increase in the response takes place for periods close to the predominant period of vibration of the soft soil. The key parameters that govern the increase or decrease of the ground motion are: layer thickness, modulus of elasticity, damping and speed of shear waves in soft soil layers, soil/rock impedance, layer types and the properties of the soil layer at the interface between the soft soil and base rock layer.

2.3 Seismic Design

Current design of structures in seismic zones is made with elastic methods of analysis with the seismic hazard defined by acceleration response spectra determined for a certain period of recurrence. The elastic response of a structure to seismic action is completely defined by the acceleration response spectra. When the need arises to investigate nonlinear dynamic response of a structure, seismic recordings (acceleration recordings) that completely define a seismic motion (amplitude, frequency content and duration) are used.

In general design codes impose a minimum number of seismic recordings to be used that vary between 3 and 7. Eurocode 8 [7] specifies a number of minimum 3 seismic recordings and FEMA 356 [10] contains the following recommendations:

- In the case when 3 seismic recordings are used maximum values of recorded response parameters will be used (forces, displacements, etc.)
- In the case when 7 seismic recordings are used, mean values of recorded response parameters can be used.

The accelerograms selected for the nonlinear dynamic analysis of a structure must completely characterize possible seismic motions in a given location. Selection of seismic recordings with magnitude close to the target magnitude is important as it strongly affects the frequency content and duration of the motion (Stewart et al., 2001 [5]).

Usually seismic recordings of historical events are preferred, but it is not uncommon that these recordings do not exist for certain locations. In such cases artificially generated recordings scaled on the target spectra can be used. The nonlinear response of the structure is affected considerably by the ratio between fundamental period of vibration of the structure and corner period of seismic motion. In particular studies on the behaviour of CBF frames showed that higher ductility than those predicted by design for structures with periods larger than 1.5s. The influence of soil conditions is also evident in the increased variability in the response observed for CBF structures on soft soils compared with the corresponding results for moderately stiff to stiff soil conditions (Elghazouli et al.). Studies by Elghazouli et al. [11] showed that ductility estimates on stiffer soils exhibited a coefficient of variation (COV) of approx. 0.3 for CB structures with periods longer than 0.3 s, whereas the COV increased to >0.6 in the case of soft soil conditions and further studies on the demand imposed on relatively low-period CB frames, particularly in the case of soft soil conditions are recommended. The strong variance in behaviour of CBF frames depending on soil type lead to the choice of seismic recordings for the study herein. In order to evaluate the nonlinear dynamic response of structures to seismic recordings with substantial differences in corner period two sets of seismic motions were considered: 7 semi-artificial seismic motion characteristic for soft soil type (Vrancea seismic zone, with $T_C=1.6s$) and 7 artificially generated seismic motions characteristic for stiff soil (Class B soil according to Eurocode 8 [7] with $T_C=0.5s$).

2.4 Passive damping devices

2.4.1 Steel Yielding Devices

2.4.1.1 *Steel Shear Walls*

Steel shear walls have been accepted worldwide as being an efficient method of energy dissipation induced in the structure by seismic loads. Conceptually a shear wall is a vertical panel connected to neighboring beams and columns. (Fig. 2.7).

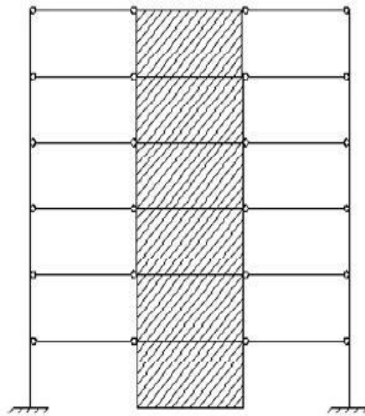


Fig. 2.7: Example of a frame with shear walls [12]

The design concept of shear walls can be roughly divided into two steps. For the first structural applications of shear walls in Japan and United States the shear panels were designed with a considerable number of stiffeners and thickness to prevent local and global buckling from shear forces that appear even under low lateral excitations and to increase their shear resistance. Numerous studies were conducted on shear panels since then which indicated a good behavior of simple, unstiffened, thin steel panels mostly because of their high inelastic deformation capacity. In current practice most of the shear walls used are made from thinner steel panels without stiffeners. The design concept allows local buckling of the panel under shear and diagonal tension zones are formed that dissipate energy through successive yield under cyclic loads. Stress distribution for shear panels with one or more stiffeners is presented in Fig. 2.8.

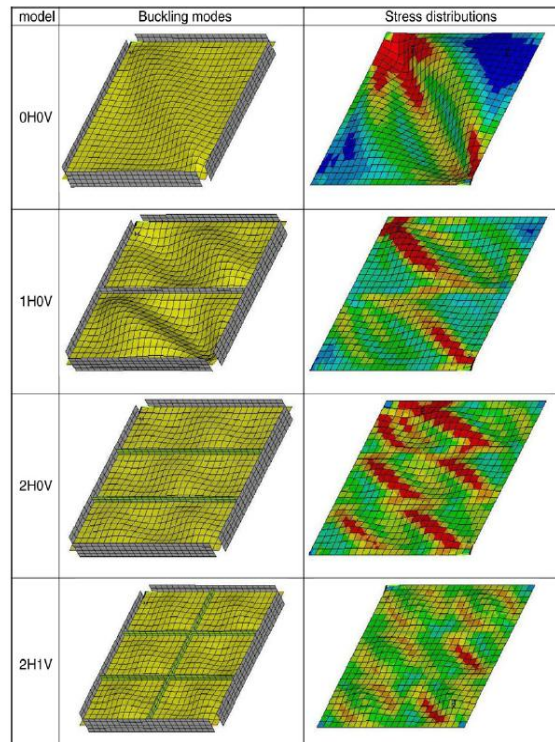


Fig. 2.8. Stress distribution for shear panels with one or more stiffeners [13]

Current research efforts are channeled towards the use of different types of materials for the shear panels (cold formed steel, aluminum, low yield steel) and the possibility of reducing the resistance of the shear wall by using panels with perforations (Bruneau et al., 2005 [14]) (Fig. 2.9).



Fig. 2.9. Perforated panel for shear walls [14]

Most of the design provisions for steel shear walls can be found in documents from United States and Canada. NEHRP „Recommended Provisions for Seismic Regulations for New Buildings and Other Structures“ (Building Seismic Safety Council 2004), „Seismic Provisions for Structural Steel Buildings“ (AISC, 2004) and FEMA450 include design recommendations for steel shear walls. Canadian standard CAN/CSA S16-01 „Limit States Design of Steel Structures“ (CSA, 2001) included design specifications for shear walls since 1994.

Examples of application of steel shear walls in buildings:

Steel shear walls have been used in the USA and Japan for over three decades. A few examples of buildings for which the main lateral load resisting system is made with shear walls are:

- United States Federal Courthouse, Seattle, WA— 23 floors (350')(Fig. 2.10a)
- Sylmar Hospital, Los Angeles, CA— 6 floors (Fig. 2.13)
- Canam-Manac Headquarters Expansion, St. George, Quebec— 6 floors (Fig. 2.11)
- Hyatt Regency Hotel , Reunion, Dallas, TX— 50 floors (562')
- The Century, San Francisco, CA— 46- floors (465'; the project was cancelled after the completion of design and permit)(Fig. 2.10b)
- Nippon Steel Building, Tokyo, Japan— 20 floors
- Shinjuku Nomura Building, Tokyo, Japan— 51 floors (693')
- Kobe Office Building, Kobe, Japan— 35 floors (425')



a



b

Fig. 2.10. a) U.S. Federal Courthouse, Seattle and b) The Century, San Francisco [15]



Fig. 2.11: Canam-Manac Headquarters Expansion, St. George, Quebec [1]

The behavior of structures with shear walls could be observed during real seismic events. One of the key structures equipped with shear walls was the 35 storey office building in Kobe, Japan, that survived the 1995 Kobe earthquake. Japanese researchers (Fujitani et.al., 1996, in Astaneh-Asl, A., (2001) [16]) studied the seismic performance of this particular building. Their studies showed that damage in the structure was limited to local buckling of shear panels at the 26 th floor with a permanent drift of 225 mm in north direction and 35mm in west direction. In comparison the low rise building without shear walls adjacent to the 35 storey one suffered severe damage with the formation of a soft storey mechanism that led to the destruction of the upmost 3 floors (Fig. 2.12).

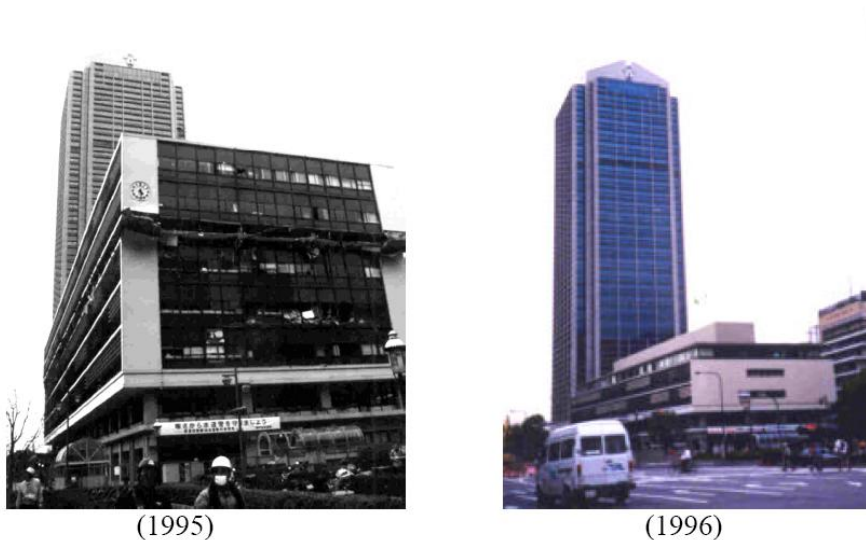


Fig. 2.12. The 35 storey office building in Kobe and nearby low rise office building [16]

In seismic zones in the USA such as California shear walls were used for seismic rehabilitation of existing building such as Sylmar County Hospital, Los Angeles (Fig. 2.13). The structure has a steel frame with reinforced

concrete shear walls at the first 2 storey and steel shear walls disposed on perimeter frames for the next 4 floors. This structure survived 2 major earthquakes Whittier in 1987 and Northridge in 1994.



Fig. 2.13. Sylmar Hospital, Los Angeles, CA— 6 floors [16]

2.4.1.2 Buckling Restrained Braces (BRB-)

Buckling restrained braces (BRB) are an energy dissipation system based on the limitation of local buckling of braces and was originally designed for seismic rehabilitation of structures but their use later extended to new structures. This type of braces appeared as a solution to low ductility of the classic bracing system by preventing local buckling in the compressed braces. Their behavior is characterized by symmetric behavior in tension and compression. BRB's first appeared in Japan in the 1980s and starting from 1988 a number of approximately 300 buildings were equipped with this type of braces manufactured by Nippon Steel Corporation. In the United States, following experimental investigations from 1999 at Berkley University, CA, this system was used for rehabilitation of UC Davis Plant and found an increasing growth in applications for structures in the years that followed. This rapid development of this system was sustained by intensive research programs in the USA, Japan, Taiwan and more recently Europe.

The main concept of this system is to prevent the buckling of a steel core that is introduced in a steel casing (steel) tube filled with concrete. Between the steel core and the concrete a slip surface is provided to ensure that axial loads are taken entirely by the steel core. This slip surface is essential to the mechanism on which these braces function and can be made from different materials, carefully selected to ensure a satisfactory slip between the steel and the concrete. The purpose of the concrete filling is to prevent the local buckling of the steel core and, together with the steel casing to prevent the global buckling of the brace resulting in a stable hysteretic behavior. (Fig. 2.14).

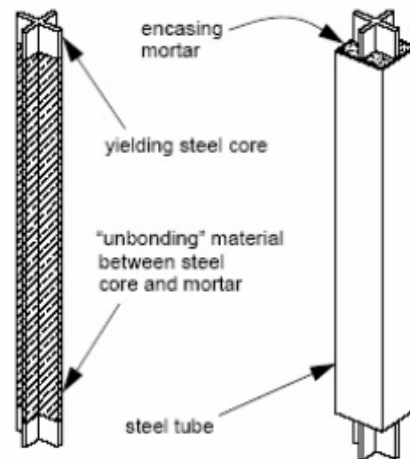


Fig. 2.14. Components of a buckling restrained brace [17]

In comparison to normal brace behavior BRB's have a stable hysteretic behavior with symmetrical tension and compression cycles and have the possibility to undergo numerous inelastic cycles with negligible degradation and without failure (Fig. 2.15).

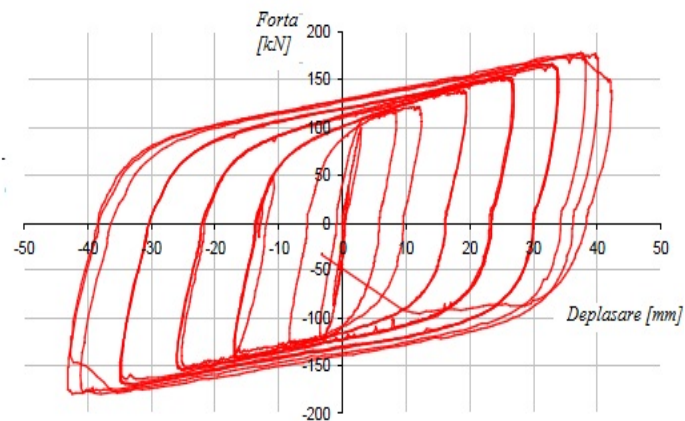


Fig. 2.15: Example of BRB hysteretic behavior (courtesy of S.Bordea [18])

A few examples of cross section types generally used for BRB's are presented in Fig. 2.16.

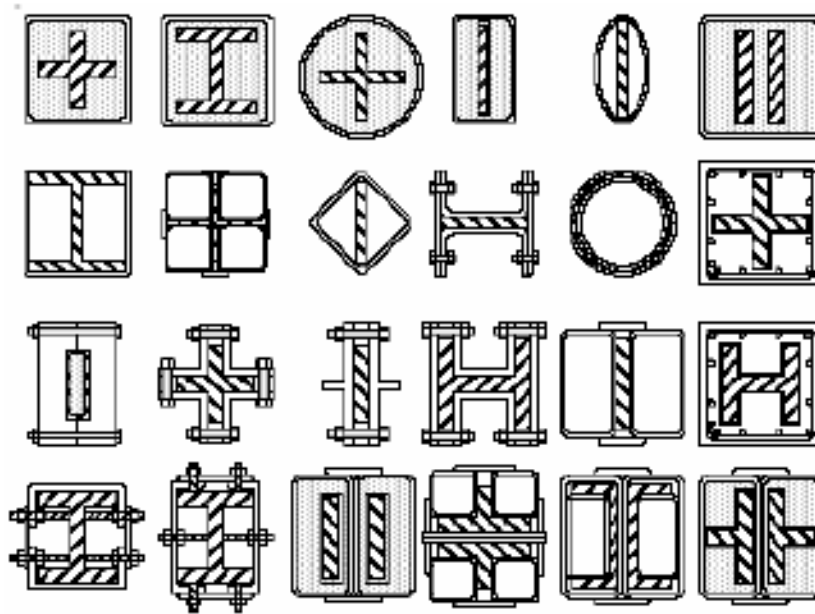


Fig. 2.16 Cross-section types used for BRB's [17]

Buckling restrained braces are generally used in structural configuration as V and X braces, or diagonals. (Fig. 2.17).

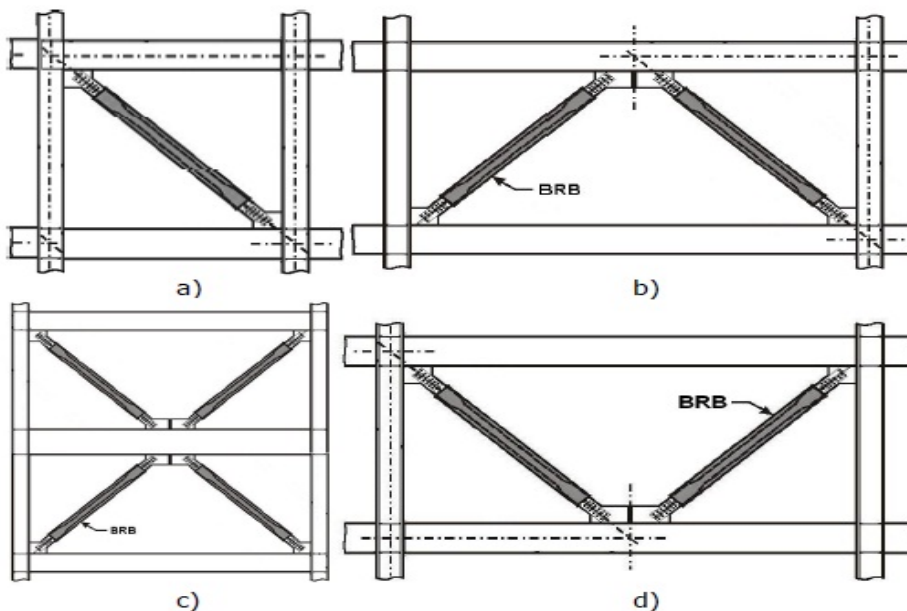


Fig. 2.17. Examples of structural configurations for BRB's: a) diagonals; b) Chevron brace; c) cross braces; c) V braces [17]

In the following figures a few relevant examples of buildings with BRB systems are presented.

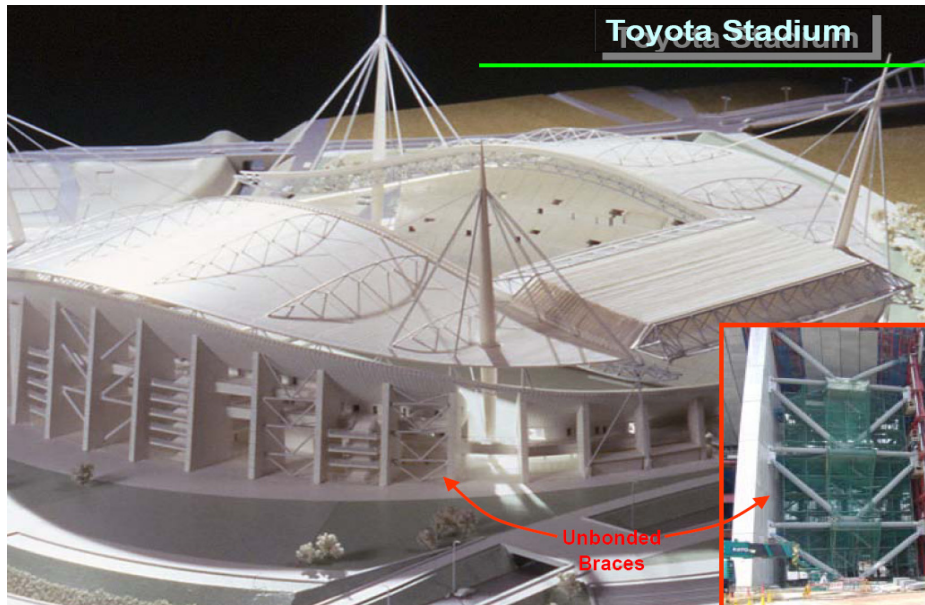


Fig. 2.18. Toyota Stadium [19]



Fig. 2.19. Nippon TV Headquarters (32+2 floors, 68 BRB's were used) [19]



Fig. 2.20: Osaka International Convention Center (420 mil. US dollars project, 13+2 floors, 370 BRB's used) [19]



Fig. 2.21. Hewlett Packard building, Corvallis Campus, USA [19]

Buckling restrained braces were successfully used in Japan for over 200 buildings since 1987. ARUP San Francisco started the implementation of BRB's in the US for UC Davis Plant and Environmental Science Facility in 1999-2000(Fig. 2.22).



Fig. 2.22. UC Davis Plant and Environmental Science Facility [18]

A good example of seismic rehabilitation of existing buildings is the Wallace F. Bennett Federal Building, Salt Lake City, Utah (Fig. 2.23)



a.



b.

Fig. 2.23: Wallace F. Bennett Federal Building: a) before and b) after rehabilitation [20]

2.4.2 Shape Memory Alloys (SMA)

The properties of shape memory alloys were first observed in 1932 but it was only in 1962 when phase transformation of NiTi alloys was observed and studies to determine possible applications of the alloys were started. In civil engineering research efforts on applications of these alloys for energy dissipation were intensified in later years. Numerical and experimental tests

estimated an energy dissipation capacity of up to 35% (Graesser and Cozzarelli, 1991, in Castellano et al. [21]). Studies followed that investigated the use of shape memory alloys for seismic isolation devices and dampers (for example damping devices made from SMA wires wrapped around a cylindrical core Krumme et al. 1995, Clark et al. 1995, in Castellano et al.[21]).

The term shape memory alloy applies to a class of steel material with the capacity to "remember" their shape before deformation and to be able to recover that shape through heating even after having suffered severe deformations (Fig. 2.24). The basis of this recovery lays in the reversible transformation between 2 crystalline phases of the material called Martensite and Austenite. This phase transformation takes place under heating or cooling of the material with temperature values that vary in a specific range. The hysteretic behavior of this type of material is of interest for civil engineering application due to the possibility of manufacturing devices that can sustain theoretically an infinite number of cycles.

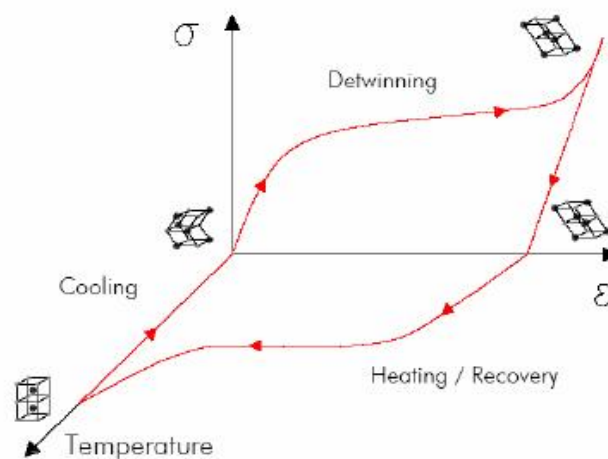


Fig. 2.24. Shape memory effect [17]

Another typical property for SMAs is their superelasticity effect (Fig. 2.25). A superelastic alloy under load has a linear elastic behavior up to a certain stress threshold (σ_1) where phase transformation from Austenite to Martensite starts, creating a stress plateau that lasts until the entire microstructure becomes martensitic. Upon unloading the material undergoes reverse transformation because applied stress is what makes Martensite stable in superelastic range. The term "superelasticity" derives from this effect that causes the material to recover an enormous amount of deformation (almost 10 times that recovered for conventional steel).

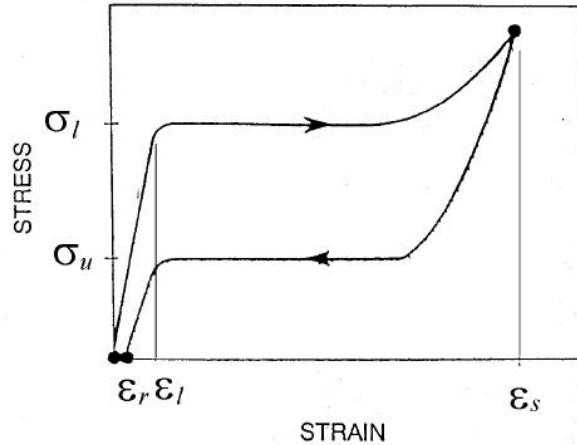


Fig. 2.25. Typical superelastic stress-strain curve [21]

Superelastic alloys used in structural applications are usually NiTi based alloys and a few Cu based alloys (CuZn and CuAl). Another advantage of SMAs is their high resistance to corrosion (even higher than stainless steel for NiTi alloys). Unfortunately no design recommendations exist at the moment because different alloys for SMAs have very different properties and design is mainly based on experimental investigations.

Studies conducted by Clark et al. (from Song G. et al.[22]) on damping devices made from SMA cables wrapped around 2 cylindrical supports installed in a 2 span frame (Fig. 2.26) showed that these devices have a good versatility, simple functioning mechanism, good self centering capabilities and overall good energy dissipation.

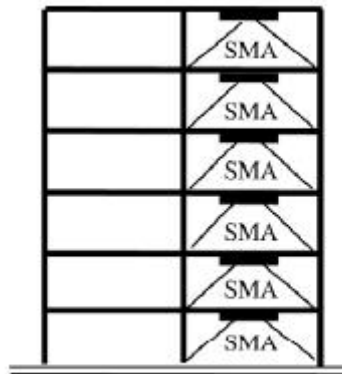


Fig. 2.26. Nitinol brace configuration [22]

Other applications of damping devices made with SMA were studied for application at suspension bridges or simple supported bridges (Fig. 2.27b) or as connection members for steel structures (Fig. 2.27a).

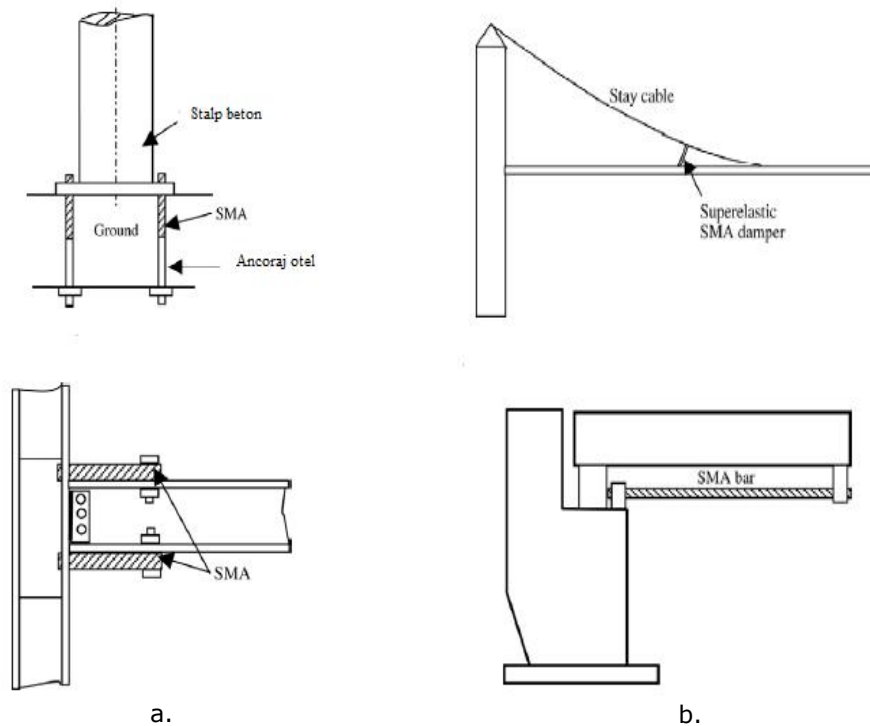


Fig. 2.27. a) Use of SMA in connections for steel members; b) use of SMA for bridges [22]

This material also has large applicability in seismic rehabilitation of existing buildings. An example of structure retrofitted with SMA devices is S. Feliciano in Foligno Cathedral, Italy. 9 SMA devices were used to connect the roofing with the facade of the structure (Fig. 2.28).



Fig. 2.28. San Feliciano Cathedral, Foligno, Italy [23]

Other examples of structures with SMA are the retrofit of S.Georgio bell tower in S.Martino in Rio, Italy with 4 SMA devices placed in paralel with the tower ties (Fig. 2.29) and Basilica San Francesco in Assisi (Fig. 2.30), retrofitted with 47 SMA devices placed at roof levels (Fig. 2.31).



a.



b.

Fig. 2.29: a) San Georgio bell tower, San Martino in Rio, Italia; b) SMA devices used for the retrofit [24]



Fig. 2.30: Basilica San Francesco [23]



Fig. 2.31. SMA devices installed on the roof of Basilica S.Francesco in Assisi [23]

2.4.3 Friction Dampers

Friction provides an excellent mechanism for energy dissipation and has been used for many years in the automotive industry (brakes). This type of dampers are made of ordinary materials and simple mechanical configurations and provide a relatively solution for structures with dampers. A variety of friction dampers is available worldwide with different materials for the contact surface that provides friction resistance. Friction dampers are usually found placed in the bracing systems and provide stable rectangular shaped hysteretic loops capable of dissipating large quantities of energy with negligible degradation (Fig. 2.32).

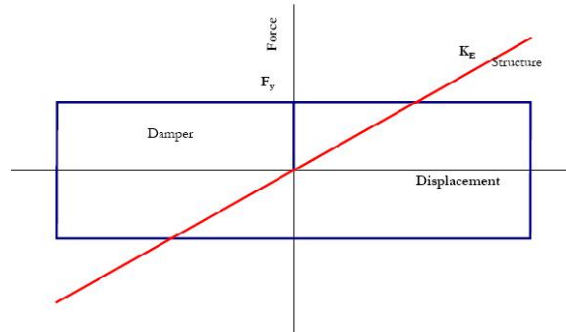


Fig. 2.32. Common hysteretic loops of friction dampers [25]

The behavior of friction dampers is similar to an ideal elastic plastic behavior. Such dampers, like Pall friction dampers and Sumimoto friction dampers, can be installed in the braces and are designed to slip at a given optimal load before the yielding of any structural members. The main parameters for this type of friction dampers are the (i) slip force and (ii) initial stiffness of the damper. In conjunction with an elastic plastic behavior the slip force of the damper can be equated to the yield force of this type of idealized behavior. This type of dampers provides appropriate stiffness in conjunction with supplemental damping to reduce the seismic response of the structure ([26]). Friction dampers are finding increasing application worldwide. For example Pall Friction Dampers were used for the seismic protection of more than 80 important buildings in Canada, USA, China and India. A few examples of these structures are:

- Boeing Commercial Airplane Factory, Everett, WA, USA: Pall friction dampers with capacity up to 200,000 lb. (900kN) and stroke up to 15 inch (380 mm) (Fig. 2.33)
- Moscone West Convention Center, San Francisco, USA: Pall Friction Dampers up to 500,000 lb. (2250 kN) capacity and 9 inch (230 mm) stroke (Fig. 2.34)
- Boeing Development Center, Cafeteria and Auditorium Buildings, Boeing Field, Seattle, WA, USA: 350 Pall friction Dampers of 100-500 kip slip load and up to 10 inches stroke (Fig. 2.35)
- Ambulatory Care Center, Sharp Memorial Hospital, San Diego, California, USA: Pall Friction Dampers in chevron braces (Fig. 2.36)
- Concordia University Library Building, Montreal, Canada
- Justice Headquarters, Ottawa, Canada
- Canadian Space Agency Headquarters, St-Hubert, Canada



Fig. 2.33. Boeing Commercial Airplane Factory, Everett, WA, USA: a) inside view; b) Pall Friction Dampers used [26]



Fig. 2.34. Moscone West Convention Center with Pall Dampers in the braces, San Francisco, USA [26]



Fig. 2.35. Boeing Development Center, Cafeteria and Auditorium Buildings, Boeing Field, Seattle, WA, USA; a) general view of the building; b) Pall Friction Dampers used [26]



Fig. 2.36. Ambulatory Care Center, Sharp Memorial Hospital, San Diego, California, USA with Pall Friction Dampers in chevron bracing system [26]

The damper studied herein is also a friction damper but has a completely different behavior concept. The damper studied is a strain hardening friction damper with 2 distinct zones. A starting zone with low stiffness conceived to ensure structural flexibility and to increase the period of vibration of the structure to more favorable values ($T > T_C$) for low values of seismic action and a second zone with increased stiffness conceived to limit displacements for high values of seismic action (Fig. 2.37).

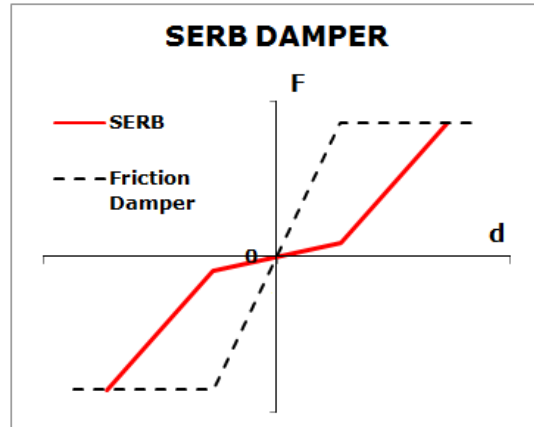


Fig. 2.37. Behavior of SERB damper compared to normal friction damper

This different concept of friction damper compared to "classical" friction dampers in conjunction with the lack of studies on damping devices to reduce seismic response of buildings in our country provides the motivation for of this study.

3 Experimental Program

3.1 Introduction

A general classification of passive dampers is done according to their behaviour as follows:

(i) Velocity dependent devices

These devices are dependent of the velocity of application of the load. They modify their hysteretic behaviour according to velocity. As an example we can mention here fluid viscous dampers and fluid spring dampers.

(ii) Displacement dependent devices

In the category enter devices with non-linear behaviour such as: steel hysteretic dampers, shape memory alloy devices, and with linear behaviour such as: elastomeric viscoelastic devices. As an example the hysteretic behaviour of some of these dampers is presented in Table 2.

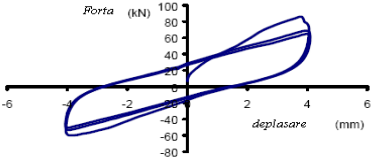
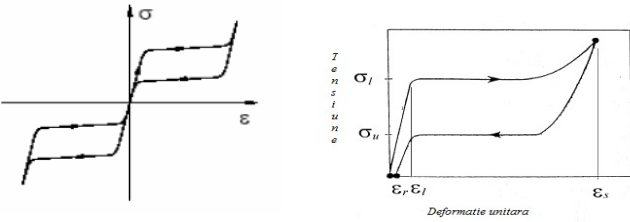
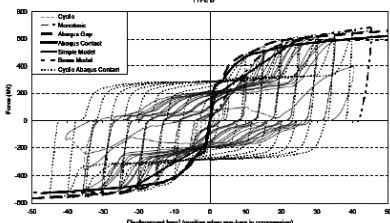
Viscoelastic elastomeric dampers	
Shape memory alloys	
Steel yielding devices (PIN+INERD)	

Table 2. Hysteretic behavior of displacement dependent devices [17]

In this category we can include the damper studied herein. The damper used in this research is a strain hardening friction damper of SERB type manufactured in Romania with the hysteretic behaviour described in Fig. 3.1a.



Fig. 3.1. a) Hysteretic behaviour of SERB type friction damper prototype [27]; b) SERB type friction damper components [29]

The damper dissipates energy through the elongation of a set of prestressed circular steel coils around a central steel core (Fig. 3.1b). The damper is characterised by 4 main parameters:

- Slip
- Stiffness of strengthening branch
- Maximum force
- Maximum stroke

This mechanical telescopic device ensures an increase in flexibility of the structure and allows energy dissipation even at small displacements avoiding the formation of plastic hinges. Damper geometry and hysteretic characteristic are presented in Fig. 3.2:

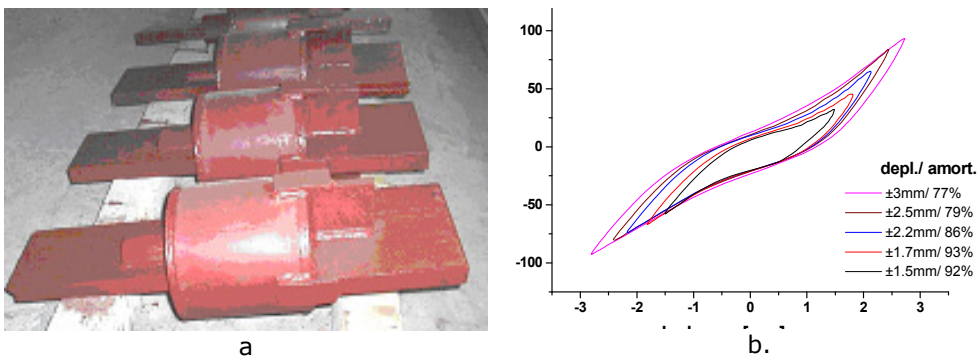


Fig. 3.2. Serb damper SERB 194: a) damper geometry; b) hysteretic characteristic [27]

Two dampers were tested experimentally with the parameters described in Table 3

Parameters	SERB1	SERB2
Slip [mm]	2	2
Stiffness [kN/m]	2×10^5	2×10^5
Max. force [kN]	1000	1500
Max. stroke [mm]	+/- 15	+/- 20

Table 3. Parameters for the SERB dampers tested experimentally

The aim of the experimental program was to determine experimentally the behaviour of the dampers and the combined behaviour of the brace with damper assembly in two distinct design concepts.

3.2 Design Principles

For braced structural systems the seismic design concept translates in designing the braces to dissipate the energy induced by the earthquake through the formation of plastic hinges protecting the elements that are considered non-dissipative from degradation. This concept leads to the introduction of the behaviour factor q that reduces the design seismic forces. Introducing damping devices in the structure leads to an increase in energy dissipation capacity of the structure. For these structures the energy dissipation devices represent „sacrificial” elements that assume the role of energy consumers entirely by plastic deformations that occur in the devices. The device prototype that is being analysed here presents a particular pseudo-elastic behaviour. This device does not have elements that yield. Instead, it consumes energy through friction from the elongation and compression of a set of steel rings around a steel core. The structures equipped with this particular type of dampers can be designed using two different concepts. A first concept is to design the braces to remain in elastic domain controlling the response of the structure solely through the friction dampers. In this case the structure has no ductile elements and is designed with a behaviour factor corresponding to low dissipative structures of $1 < q < 2$ and benefits from the reduction of design seismic forces due to the increase in global damping. However, introducing supplemental damping in the structure leads to a much smaller reduction of design seismic loads compared to the reduction that comes from using a higher behaviour factor value that corresponds to a dissipative design approach in which the brace itself is the main energy consuming element. For example an increase of damping in the structure to 15% critical damping leads to a reduction of the loads with only 35%. Furthermore these types of dampers have a brittle failure that must be avoided in all configurations. All the above mentioned lead to a second design concept in which the damper has sufficient over strength compared to the brace to assure that the brace has deformation in the plastic domain and is the weaker element in the configuration. This concept should benefit in theory from both the energy dissipation capacity of the brace and the supplemental damping from the device, and the failure will occur in the brace and not in the device. For seismic motion levels

corresponding to ultimate limit state the brace is the „active“ element according to the dissipative design concept and for service limit state the damper is the „active“ element ensuring that the brace remains in elastic domain and providing an overall damping increase. According to P100/2006 [1] the relative story drift criteria for SLS is $0.008h$, where h is the story height. For the structure analysed here this translates in a drift value of 28mm which leads to a displacement of 20mm in the brace. The damping devices were selected to satisfy this displacement criteria corresponding to SLS. Both design concepts presented above will be used in the configuration of the experimental tests that will be presented further on.

3.2.1 Experimental Frame Design

The experimental configuration was designed starting from the general geometry presented in Fig. 3.3a. The experimental model consists of half of the beam and one of the central braces in a triangular configuration, hinged at both ends (Fig. 3.3b).

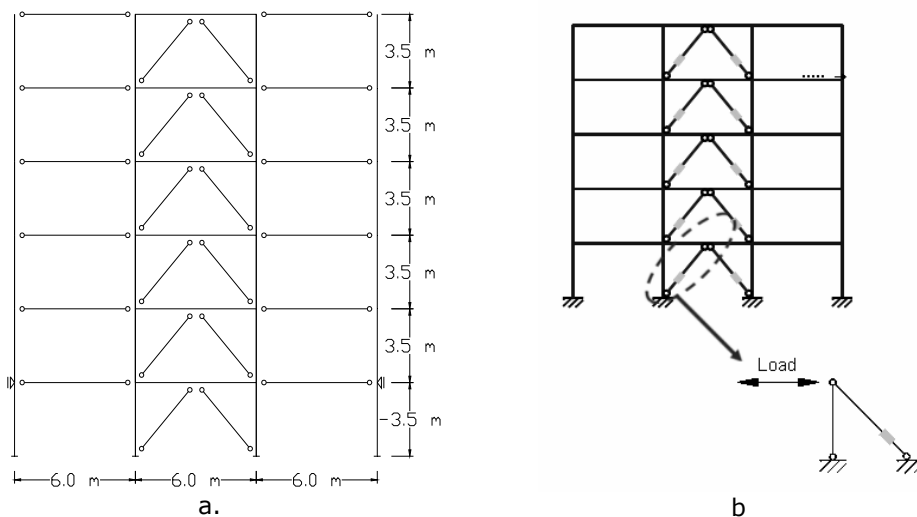


Fig. 3.3. Experimental test configuration: a) Frame geometry; b) extracted experimental configuration

The experimental tests were in the CEMSIG laboratory of the Department of Steel Structures and Structural Mechanics of Politehnica University, Timisoara. The brace and beam assembly were rotated 90 degrees from their positioning in the frame to facilitate load application on the brace. All the elements of the assembly are pinned (Fig. 3.5). Load application was done through a 1000kN hydraulic QUIRI actuator with electronic command which was fixed on the pre-existent experimental test frame (Fig. 3.4).

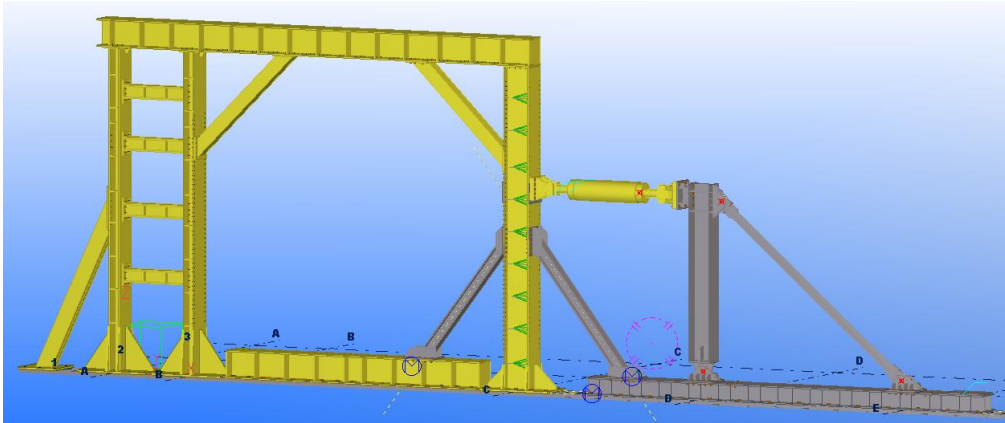
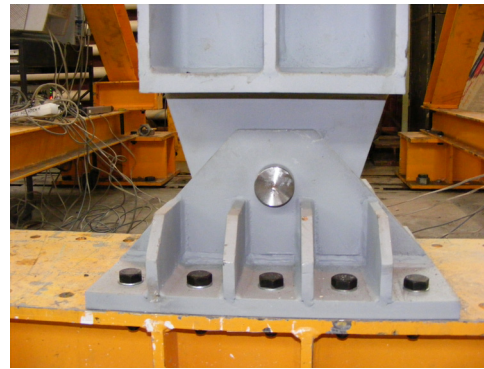


Fig. 3.4: Experimental test configuration of the brace specimen



a.



b.

Fig. 3.5: Pinned connection: a) of the brace and b) of the beam

In addition to the initial configuration presented above a secondary frame was constructed around the specimen to prevent out of plane deformation. Two profiles were attached to the front and back of the vertical beam element that ensure a 4 point contact with the two guidance beams to prevent any out of plane displacements (Fig. 3.6).

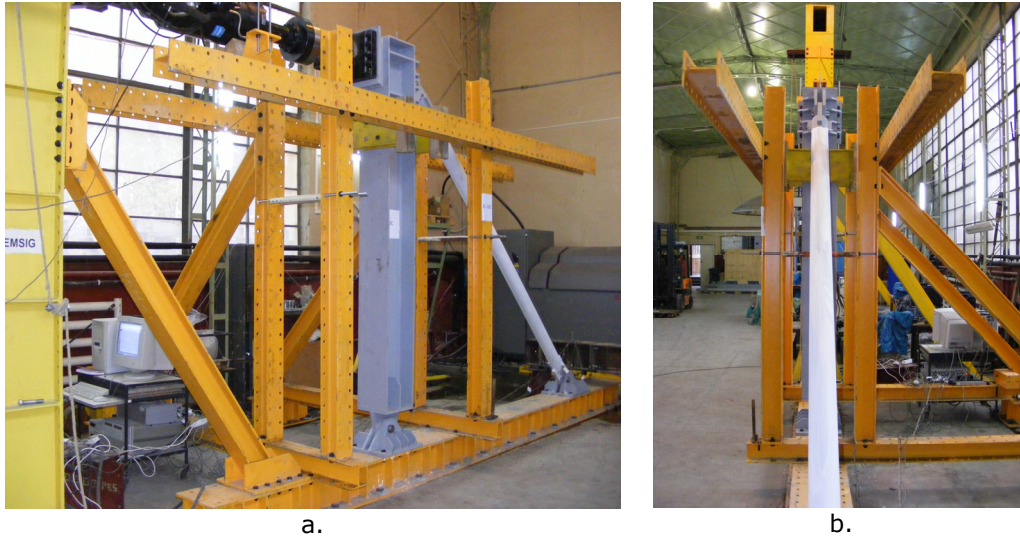


Fig. 3.6: Experimental test stand with guidance frame: a) lateral view; b) front view

3.2.2 Load Protocol

For the experimental tests on the single dampers a cyclic load protocol was used having as reference the maximum force capacity of the two devices. The tests were made using a force controlled load protocol with 3 cycles at each load step of 0.2, 0.4, 0.6, 0.8 and 1 times maximum device force capacity (Fig. 3.7).

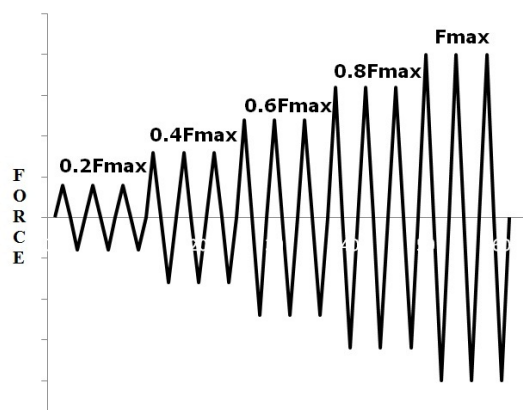


Fig. 3.7: Force controlled load protocol for single damper tests

This load protocol was also used for experimental tests on brace with damper configuration in the “strong” brace design concept that will be explained later in this chapter.

For the rest of the experimental tests on the brace with damper specimens a

load protocol recommended by European Convention for Constructional Steelworks (ECCS, 1985 [28]). The protocol consists of a monotonic test to determine the force-displacement relationship of the specimen. Yield displacement e_y and yield force F_y at the intersection of the initial stiffness α_y and a tangent to the F-e curve with 10% slope (Fig. 3.8). With the determined values of e_y the displacement based cyclic load protocol is constructed with one cycle at each elastic step of $0.25e_y$, $0.5e_y$, $0.75e_y$, $1e_y$ and 3 cycles at each load step multiple of $2e_y$ ($2e_y$, $4e_y$, $6e_y$, $8e_y$, etc.) (Fig. 3.8b).

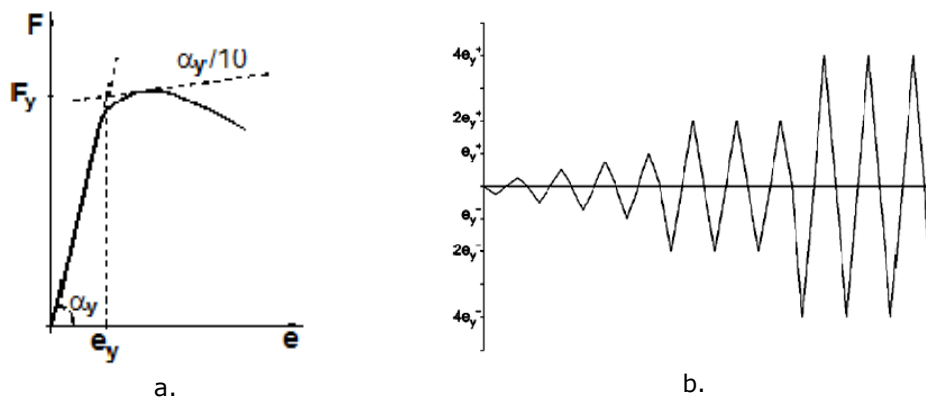


Fig. 3.8. ECCS load protocol: a) e_y and F_y determination from monotonic tests; b) cyclic load protocol

3.2.3 Measuring Instruments

The experimental tests on the two dampers with 1000kN and 1500kN capacity were made in the INSTRON universal testing machine in the CEMSIG laboratory. Data acquisition was done directly through the control and acquisition station of the machine itself without any other additional measuring instruments. Monitored parameters were total force in the damper and damper stroke.

For the experimental tests on single brace and brace with damper configurations recorded parameters were: total applied force, total displacement of the specimen, relative displacement between certain predetermined points relevant for each type of test. Total applied force acquisition was done directly through the control station of the hydraulic QUIRI force actuators with 1000kN capacity. Force actuator control is done exclusively through MTS control software.

All displacements were recorded with 2 types of displacement transducers:

- Position transducers with restoring spring (PTRS), TRS series from NOVOTechnik with 5V and 10V output signal. This type of position transducer is made of a central body and a actuating shaft with restoring spring that slides in the central body. The devices have a 50mm and 100mm measuring capacity with an error of 0.002mm.
- Cable-extension transducers (CET) CELESCO PT100 series.

The positioning of these position transducers varied throughout the

experimental program to satisfy the specific needs of each specimen. It can be mentioned here that each displacement was measured with a pair of transducers placed at opposite sides of the specimen. The value of the monitored displacement is then computed as the mean value of the two transducer recordings. The positioning of the displacement measuring devices for each specimen type is presented in the following section.

3.2.3.1 Measurements for Experimental Tests on Single Brace without Dampers

Measured parameters in the experimental tests on single brace without dampers were: applied force, total displacement, relative displacement between brace ends and base slip (Fig. 3.9 a and b). For the experimental tests on circular hollow section braces position transducers with restoring spring with 10V and 5V capacity were used exclusively.

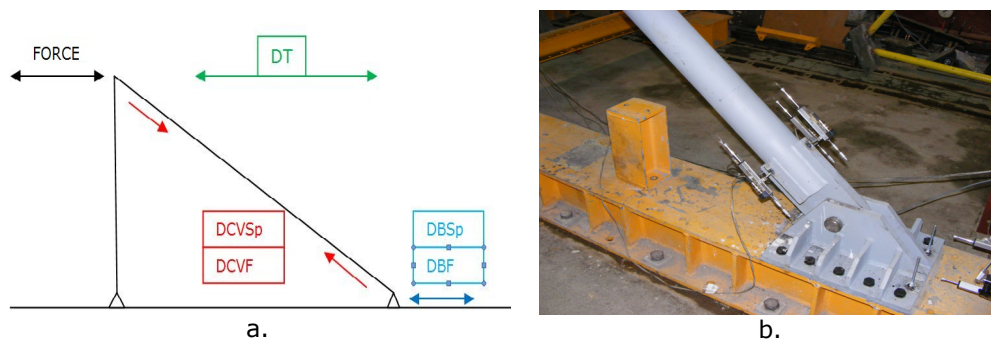


Fig. 3.9. a) Measurement devices positioning scheme; b) Positioning of measuring devices on the CHS section brace test specimen

The position transducers used for these experimental tests are presented in Table 4.

MEASURING DEVICE	TYPE	MEASURED PARAMETERS
DCVSp	PTRS 10V	Relative brace displacement
DCVF	PTRS 10V	Relative brace displacement
DBF	PTRS 5V	Horizontal base slip
DBSp	PTRS 5V	Horizontal base slip
DT	PTRS 10V	Total displacement

Table 4. Displacement transducers used and measured parameters for CHS section brace tests

The initial configuration of position transducers was preserved for the HEA brace tests (Fig. 3.10) replacing some PTRS transducers with CET transducers. Two additional transducers were positioned to measure the deflection at the middle of the brace (**Error! Reference source not found.**).

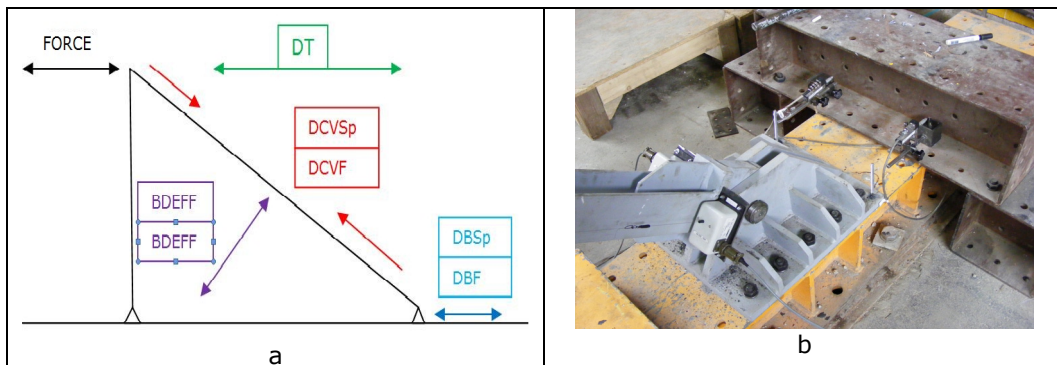


Fig. 3.10. a) Measurement devices positioning scheme; b) Positioning of measuring devices on the HEA brace test specimen without damper

The position transducers used for experimental tests on HEA brace without dampers are presented in Table 5.

MEASURING DEVICE	TYPE	MEASURED PARAMETERS
DCVSp	CET	Relative brace displacement
DCVF	CET	Relative brace displacement
DBF	PTRS 5V	Horizontal base slip
DBSp	PTRS 5V	Horizontal base slip
DT	PTRS 10V	Total displacement
BDEFF	CET	Brace deflection
BDEFB	CET	Brace deflection

Table 5. Displacement transducers used and measured parameters for HEA section brace tests without dampers

3.2.3.2 Measurements for Experimental Tests on Single Brace With Dampers

Two position transducers that measure the displacement of the damper alone and two position transducers that measure the displacement of the brace with damper assembly were introduced for the experimental tests on single brace with dampers. Measured parameters were: applied force, total displacement at top, relative displacement between brace ends, displacement of the damper alone and displacement of brace with damper assembly (Fig. 3.11). Because the connection between the damper and the other elements was done with bolted end plates two additional position transducers were introduced for the damper to measure the displacement of the damper together with the bolted connection to be able to correct potential errors introduced by slip in the connection (Fig. 3.12).

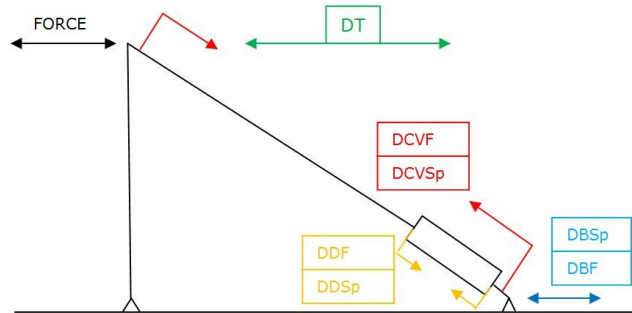


Fig. 3.11. Measurement devices positioning scheme for brace with damper experimental tests



Fig. 3.12. Measurement devices positioning for the damper alone

The position transducers used for experimental tests on brace with damper assembly are presented in Table 6.

MEASURING DEVICE	TYPE	MEASURED PARAMETERS
DCVSp	PTRS 10V	Relative brace displacement
DCVF	PTRS 10V	Relative brace displacement
DBF	PTRS 5V	Horizontal base slip
DBSp	PTRS 5V	Horizontal base slip
DT	PTRS 10V	Total displacement
DDF	PTRS 10V	Damper displacement
DDSp	PTRS 10V	Damper displacement
DDJJ	PTRS 10V	Damper with connection displacement
DDJS	PTRS 10V	Damper with connection displacement

Table 6. Displacement transducers used and measured parameters for experimental tests on brace with damper assembly

Two additional transducers were positioned to measure the deflection at the middle of the brace for the experimental tests on HEA brace with damper assembly (Fig. 3.13).

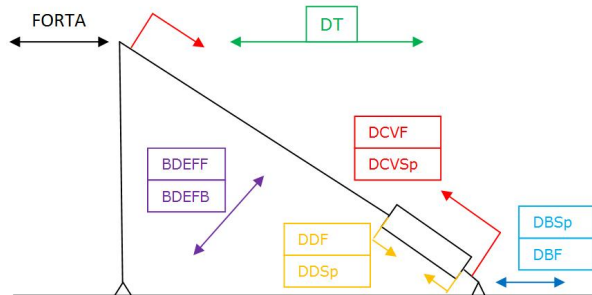


Fig. 3.13. Measurement devices positioning scheme for HEA brace with damper experimental tests

The position transducers used for experimental tests on HEA brace with damper assembly are presented in Table 7.

MEASURING DEVICE	TYPE	MEASURED PARAMETERS
DCVSp	CET	Relative brace displacement
DCVF	CET	Relative brace displacement
DBF	PTRS 5V	Horizontal base slip
DBSp	PTRS 5V	Horizontal base slip
DT	PTRS 10V	Total displacement
DDF	PTRS 10V	Damper displacement
DDSp	PTRS 10V	Damper displacement
DDJJ	PTRS 10V	Damper with connection displacement
DDJS	PTRS 10V	Damper with connection displacement
BDEFF	CET	Brace deflection
BDEFB	CET	Brace deflection

Table 7. Displacement transducers used and measured parameters for experimental tests on HEA brace with damper assembly

3.3 Experimental Program

The experimental program was divided in two main stages:

1. Experimental tests on damping devices
2. Experimental tests on braces and on the braces with dampers assembly.

3.3.1 Experimental Tests on Damping Devices

Experimental tests were made on two dampers with capacities of 800kN and 1500 kN to validate their hysteretic behaviour and to ensure that the devices function in the desired parameters having a symmetric behaviour in tension and compression with stable hysteretic loops. The experimental tests on dampers were made in the INSTRON universal testing machine in the CMMC laboratory (Fig. 3.15). A force based cyclic load protocol was used scaled to maximum device force capacity (Fig. 3.14). Three cycles were made at each load step with a final load step of $0.8F_{max}$.

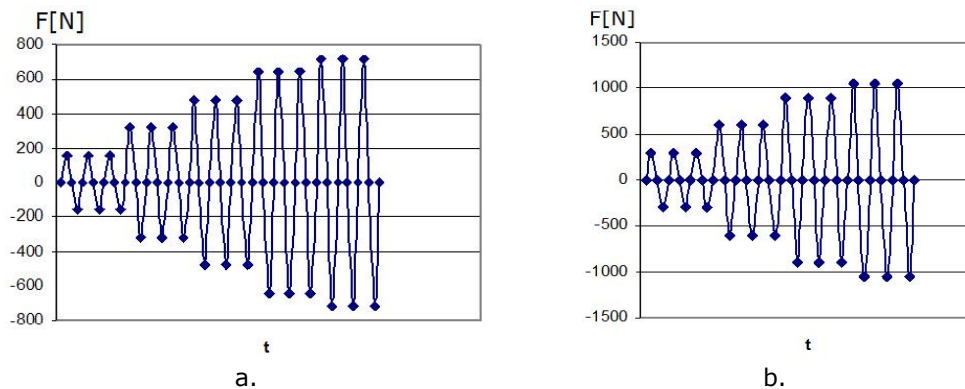


Fig. 3.14. a) Load protocol for 800kN damper; b) Load protocol for 1500kN damper

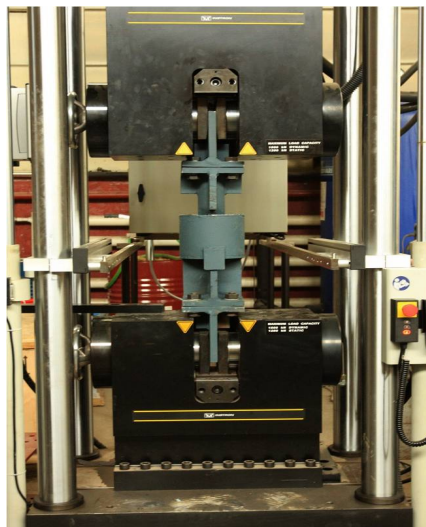


Fig. 3.15. Experimental setup for damper tests

The hysteretic behaviours of the SERB800 damper and SERB1500 damper obtained experimentally are presented in Fig. 3.16 and Fig. 3.17 respectively.

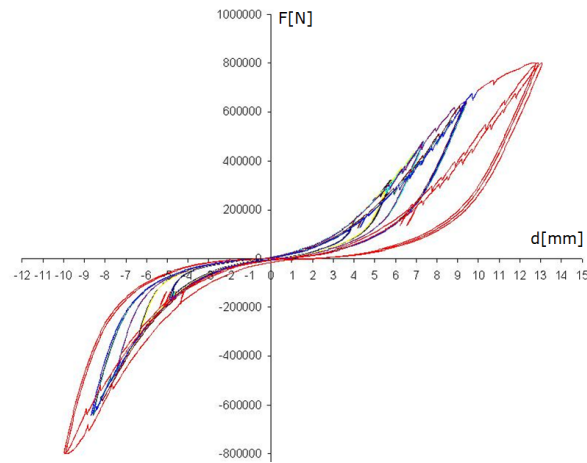


Fig. 3.16. Hysteretic behavior of SERB800 damper

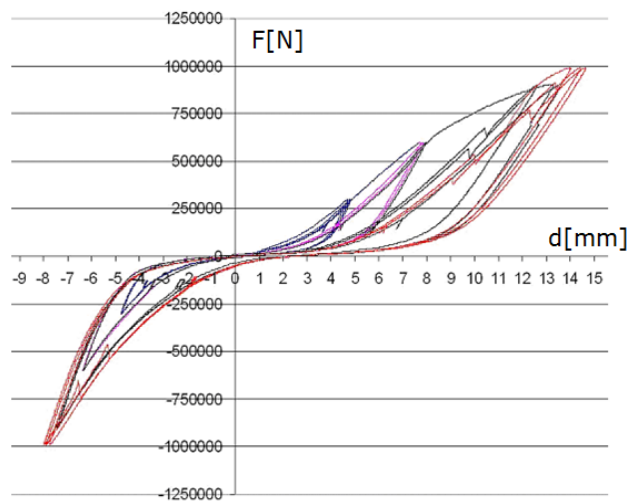


Fig. 3.17. Hysteretic behavior of SERB1500 damper

Both devices had a similar behaviour with stable hysteretic behaviour in tension and compression. The translation of the loops that can be observed in the tension part was caused by the slip in the connection elements between the devices and the clamping plates of the testing machine. The connection was redesigned for the experimental tests on brace with damper assembly to ensure no slip.

3.3.2 Experimental Tests on Braces and on the Braces with Dampers Assembly

The experimental setup is made up of half a beam with a brace setup rotated

by 90 degrees from their original positioning in the frame. All elements of the experimental setup are pinned at both ends. The brace both with and without damper is the interchangeable element of the experimental test setup and represents the object of the study (Fig. 3.18).

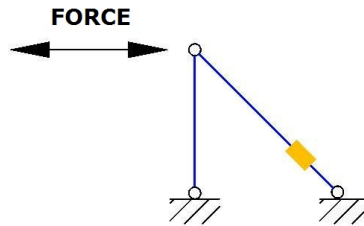


Fig. 3.18. Experimental test setup for experimental tests on braces with and without dampers

Two different design concepts are used in the experimental program. The first concept states that the brace with damper are designed so that energy dissipation occurs in the device alone and the brace remains in elastic domain. This concept is achieved by ensuring that the brace has sufficient overstrength in comparison with the damper. The second design concept states that the brace will enter plastic domain and both brace and damper will contribute to final response of the assembly. This design concept was achieved by ensuring the overstrength of the damper compared to buckling capacity of brace. The cross sections used for the brace reflect these two design concepts as follows:

- „Strong” brace concept: HEA240
- „Weak” brace concept: circular hollow section D133x5 and HEA100 profile.

The experimental program is detailed in Table 8:

No	Brace	Specimen	Damper	Test type	No.	Measured parameters
1.	HEA 240	BDE-C	YES	Cyclic	2	-relative displacement of the brace -total displacement -applied force -damper displacement
2.	CHS D133,t=5	B-MT B-MC	NO	Monotonic	2	
3.	CHS D133,t=5	B-C	NO	Cyclic	2	
4.	CHS D133,t=5	BDY	YES	Cyclic	2	
5.	CHS D133,t=5	BDY	YES	Cyclic	2	
6.	HEA100	HB-MT HB-MC	NO	Monotonic	2	
7.	HEA100	HB-C	NO	Cyclic	1	
8.	HEA100	HBDY-C1	YES	Cyclic	1	
9.	HEA100	HBDY-C2	YES	Cyclic	1	

Table 8. Experimental program for brace tests with and without dampers

3.3.2.1 „Strong“ Brace with Dampers (BDE)

For this set of experimental tests the brace was design with sufficient overstrength to ensure it remains in elastic domain. The aim of these tests was to validate the behaviour of the brace with damper assembly in this design concept. The loading protocol used for these tests was identical to the one used for the single damper tests having as reference damper force capacity. The connection between the brace and the damper and between damper and pinned base connection was done with bolted end plates using 4M22 12.9 bolts at each connection (Fig. 3.20b and Fig. 3.21). The experimental test setup is presented in Fig. 3.19 and Fig. 3.20a.



Fig. 3.19. Experimental test setup for "strong " brace with damper configuration

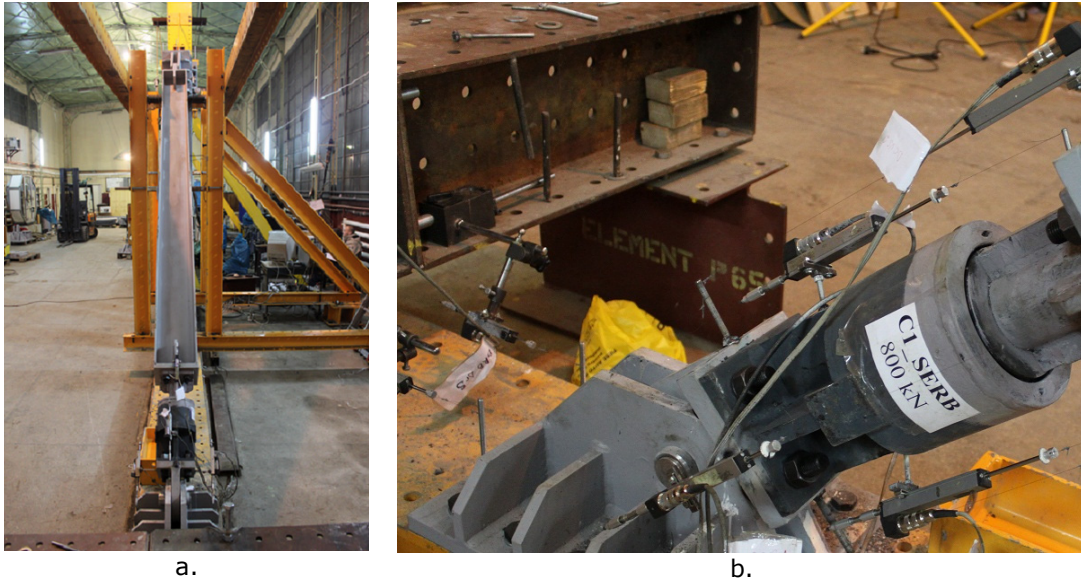


Fig. 3.20. a) Longitudinal view of the experimental test setup for "strong" brace with damper configuration; b) damper connection



Fig. 3.21. Damper connection to brace and pinned base connection: a) lateral view; b) longitudinal view

Recorded force displacement relationship for the HEA240 brace with 800kN damper is presented in Fig. 3.22.

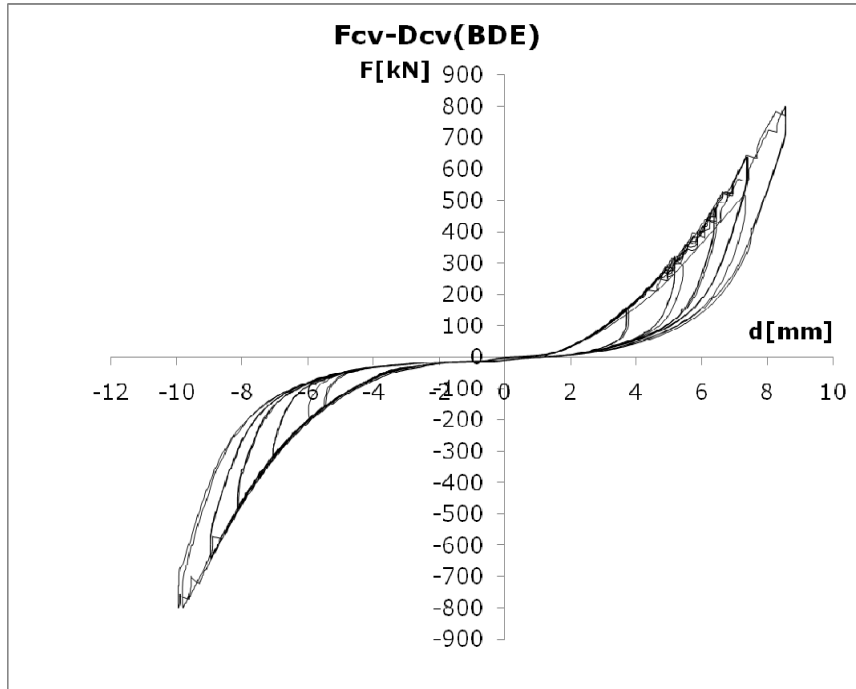


Fig. 3.22: Force displacement curve obtained from BDE experimental tests

The total response of the system is governed by the damper behaviour having a symmetrical behaviour in tension and compression without strength and stiffness degradation. The brace remained in elastic domain for the entire duration of the test. No slip was recorded in the damper connections. The test was stopped when the damper reached its maximum capacity.

3.3.2.2 "Weak" Brace Design Concept. Circular Hollow Section Brace (CHS) without Damper

All braces without dampers were first tested monotonically to determine yield displacement and yield force needed to establish the ECCS cyclic load protocol that was later used for cyclic tests. The experimental test setup had the same general configuration for all tests (Fig. 3.23 and Fig. 3.24a,b)



Fig. 3.23. Experimental test setup for CHS brace without damper



a.



b.

Fig. 3.24: Experimental test setup for CHS brace without damper: a) general view; b) base connection detail

At the monotonic tension tests the specimen failed after reaching the yield plateau. Failure was localised in the connection between the CHS brace and connection plates of the pinned support (Fig. 3.25). Because failure occurred after the specimen yielded the results were considered satisfactory.



Fig. 3.25. Failure of the connection between the CHS brace specimen and connection plates of the pinned support

The monotonic tensile tests were followed by monotonic compression tests in the same test setup configuration. The brace buckled in the mid section (Fig. 3.26) and the test was stopped when the compression force fell below 30% of maximum compression force reached.



Fig. 3.26: Buckling of CHS brace under monotonic compression load

Force displacement curves for the CHS brace obtained from monotonic tests are presented in Fig. 3.27.

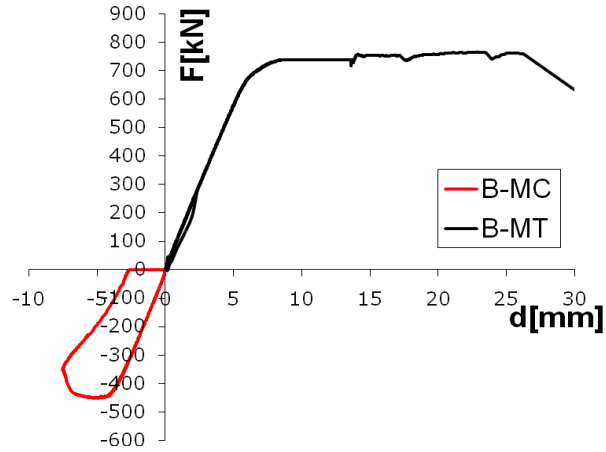


Fig. 3.27. Force displacement curves for the CHS brace obtained from monotonic tests

Based on the monotonic test results yield displacement e_y was computed using initial stiffness method (Fig. 3.28).

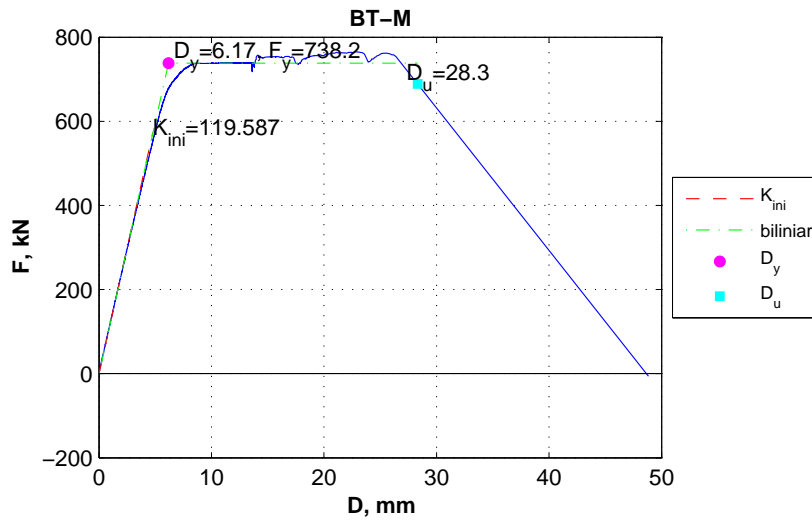


Fig. 3.28. Determination of yield displacement e_y for CHS brace

The ECCS cyclic load protocol was computed using the yield displacement determined ($e_y=6.2\text{mm}$) resulting the following load step values of the displacement (Table 9):

No. of cycles	Load step	Displ. ($e_y = 6.2 \text{ mm}$) [mm]
1	$0.25 \times e_y$	1.55
1	$0.5 \times e_y$	3.1
1	$0.75 \times e_y$	4.62
1	$1 \times e_y$	6.2
3	$2 \times e_y$	12.4
3	$4 \times e_y$	24.8
3	$6 \times e_y$	37.2
3	$8 \times e_y$	49.6
3	$10 \times e_y$	62

Table 9. Cyclic displacement based load protocol determined for CHS brace tests

The cyclic load protocol detailed above was used for the cyclic tests on CHS brace without damper that followed. At tension load cycles the brace exhibited a strength decay of approximately 20% for the second and third cycle at each load step. Buckling of the brace occurred for compression cycles (Fig. 3.29) with the formation of a plastic hinge in the middle of the brace (Fig. 3.30a). The first buckling of the brace was recorded at a force level of approximately $0.7F_y$ (F_y =yield force of the brace) and the values of the buckling force dropped continuously for the successive compression cycles that followed. Failure of the specimen occurred in the connection with the pinned base at a load level of $8x e_y$ (Fig. 3.30b).



Fig. 3.29. Buckling of the CHS brace at cyclic tests



Fig. 3.30. a) Plastic hinge formation at the middle of the CHS brace; b) Crack development near the connection of the CHS brace with the pinned base plates

The force displacement curve recorded from cyclic tests on the CHS brace without damper are presented in Fig. 3.31.

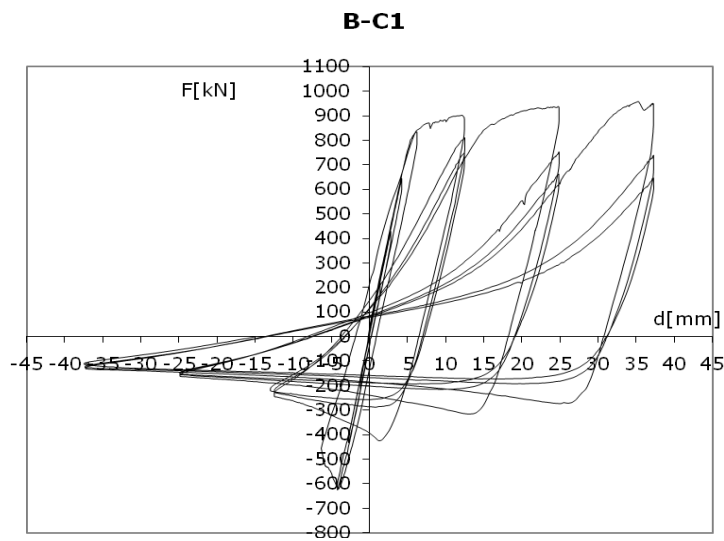


Fig. 3.31: Force displacement curve recorded from cyclic tests on the CHS brace without damper

3.3.2.3 "Weak" Brace Design Concept. Circular Hollow Section Brace with Damper

For experimental tests setup of CHS brace with damper the device was connected to the brace in the same way as for the HEA240 brace using bolted

end plates connections (Fig. 3.32). Only cyclic tests were performed for the CHS brace with damper specimen using the load protocol determined for the same brace without damper ($e_y=6.2\text{mm}$) as explained in the previous sub-chapter

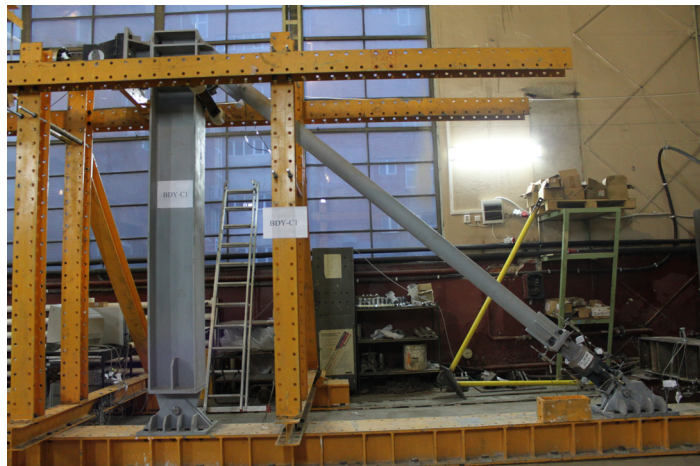


Fig. 3.32. Experimental test setup for CHS brace with damper specimen

The first test was done using the 800kN damper which unfortunately broke due to a manufacturing flaw. The steel lid of the damper body broke when the maximum stroke of the device was reached and the test was stopped at that point. The experimental tests on brace with damper specimens that followed were made with the 1500kN damper. The cyclic behaviour of the CHS brace with this damper is presented in Fig. 3.33.

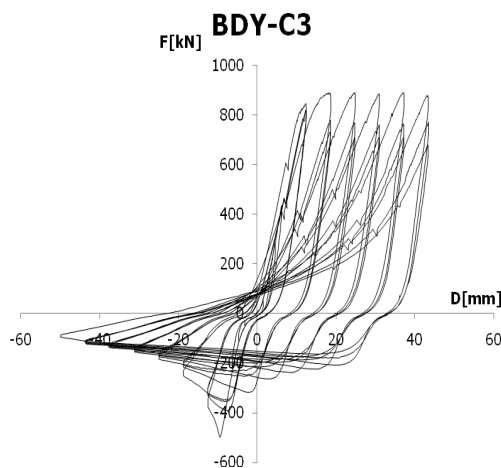


Fig. 3.33: Cyclic behavior of CHS brace with damper

For both braces with and without dampers at tension load cycles the brace

exhibited a strength decay of approximately 20% for the second and third cycle at each load step. The brace exhibited a significant stiffness degradation for each successive tension cycles. The brace buckles in compression forming a plastic hinge in the middle. The first buckling of the brace was recorded at a force level of approximately $0.7F_y$ (F_y =yield force of the brace) and the values of the buckling force dropped continuously for the successive compression cycles that followed. Failure of the specimen occurred in the connection with the pinned base at a load level of $8x e_y$. The influence of the damper behaviour on the global behaviour of the assembly is important up to a load level of $2x e_y$. The results will be discussed comparatively at the end of this chapter.

3.3.2.4 "Weak" Brace Design Concept. HEA100 Brace without Damper

The experimental tests on HEA100 braces followed the same test procedure as the experimental tests on CHS braces. The braces were first subjected to monotonic tests to determine yield force and yield displacement needed for cyclic load protocol. The experimental test setup was identical with the one used for CHS braces (Fig. 3.34). The braces were positioned with their weak axis in the plane of the test frame to ensure that buckling occurs in the vertical direction.



Fig. 3.34. Experimental test setup for monotonic tests on HEA100 brace

For the case of tension monotonic tests the brace yielded along its entire length and the test was stopped when the brace reached strengthening domain, before the failure of the brace. In compression the brace buckled in the mid-span and the test was stopped when the values of the compression force dropped with more than 30% of maximum compression force reached (Fig. 3.35).



Fig. 3.35. Buckling of the HEA100 brace under monotonic compression load

Force displacement curves for the HEA100 brace obtained from monotonic tests are presented in Fig. 3.36.

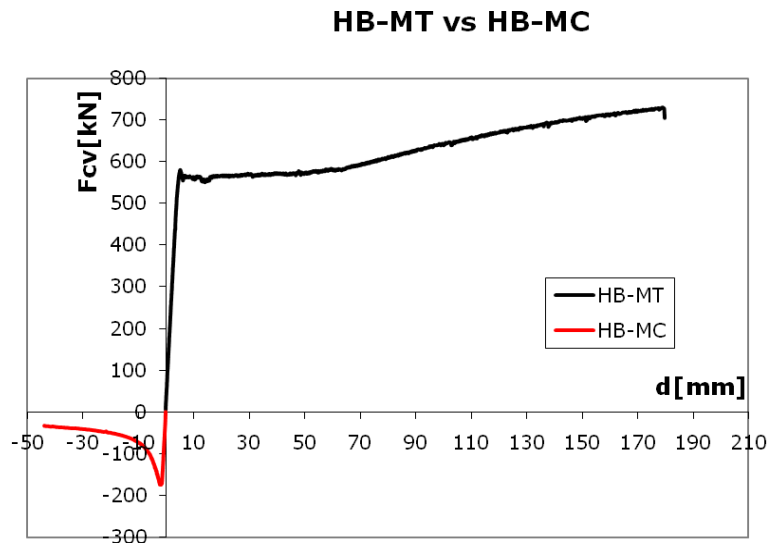


Fig. 3.36. Force displacement curves for the HEA100 brace obtained from monotonic tests

Two methods were used to determine yield displacement for the HEA100 brace. Both the initial stiffness method (Fig. 3.37) and tangent stiffness method (Fig. 3.38) led to similar values of yield displacement of $e_y=4\text{mm}$.

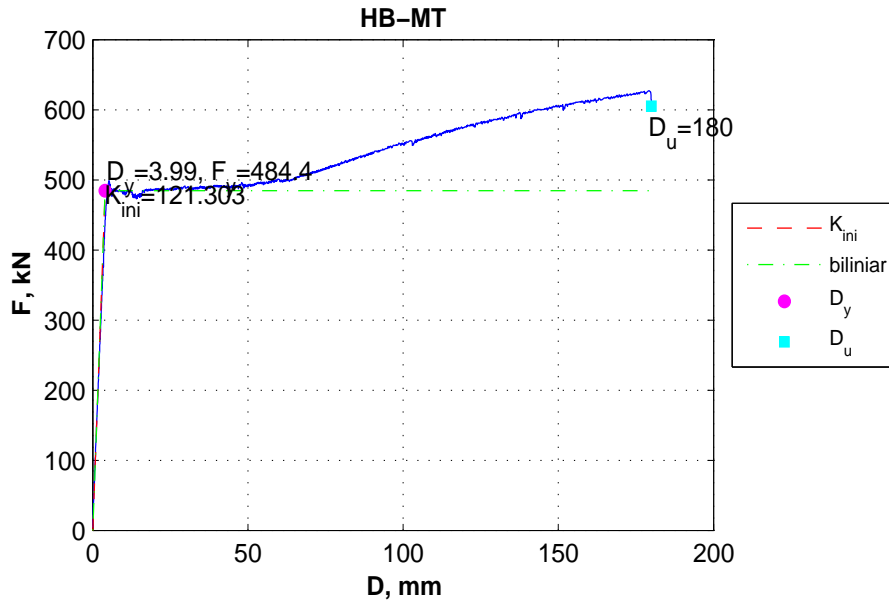


Fig. 3.37. Determination of yield displacement for HB-MT specimen using initial stiffness method

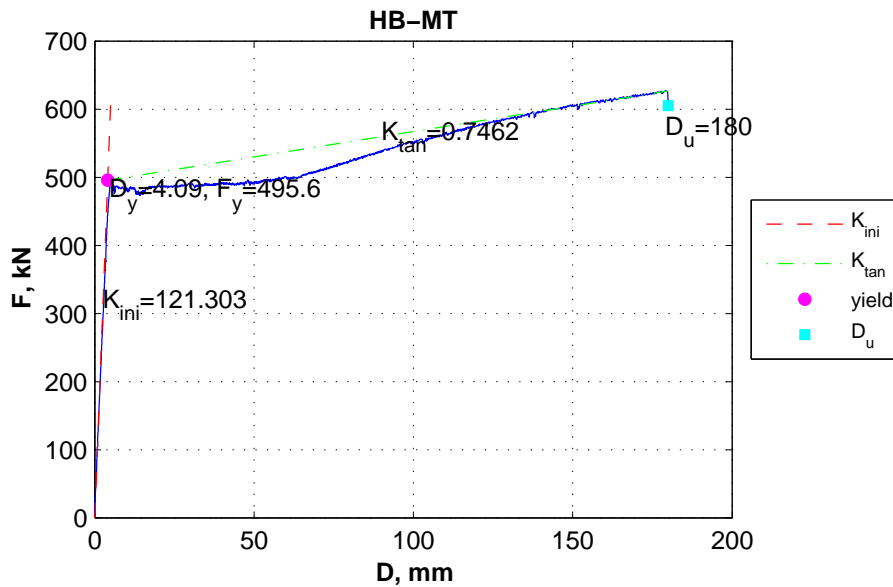


Fig. 3.38. Determination of yield displacement for HB-MT specimen using tangent stiffness method

For the yield displacement of 4mm the following load steps of the ECCS cyclic

load protocol were computed (Table 10):

No. of Cycles	Load Step ($e_y=4\text{mm}$)	Displ. [mm]
1	$0.25 \times e_y$	1
1	$0.5 \times e_y$	2
1	$0.75 \times e_y$	3
1	$1 \times e_y$	4
3	$2 \times e_y$	8
3	$4 \times e_y$	16
3	$6 \times e_y$	24
3	$8 \times e_y$	32
3	$10 \times e_y$	40

Table 10. Cyclic displacement based load protocol determined for HEA100 brace tests

The behaviour of the HEA brace under cyclic load was very similar with the behaviour recorded for the CHS brace. At tension load cycles the brace exhibited a strength decay of approximately 20% for the second and third cycle at each load step. The brace exhibited a significant stiffness degradation for each successive tension cycles. Buckling of the brace occurred for compression cycles (Fig. 3.39) with the formation of a plastic hinge in the middle of the brace. The first buckling of the brace was recorded at a force level of approximately $0.7F_y$ (F_y =yield force of the brace) and the values of the buckling force dropped continuously for the successive compression cycles that followed. The test was stopped when the values of the compression force dropped with more than 50% of maximum compression force reached.



Fig. 3.39. Buckling of the HEA100 brace at cyclic tests

The force displacement curve recorded for cyclic tests on the HEA100 brace without damper are presented in Fig. 3.40.

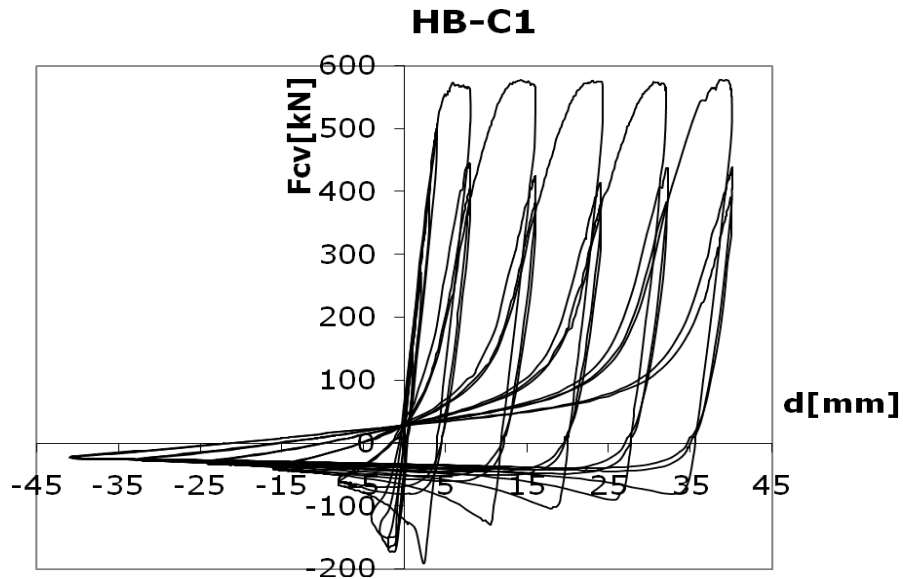


Fig. 3.40. Force displacement curve recorded for cyclic tests on the HEA100 brace

3.3.2.5 "Weak" Brace Design Concept. HEA100 Brace with Damper

The two experimental tests that followed were cyclic tests on HEA100 brace with damper assembly using the same test setup as for the previous tests (Fig. 3.41) and the cyclic load protocol determined for $e_y=4\text{mm}$. Damper connection with the other elements was made with bolted end plates (Fig. 3.42).



Fig. 3.41. Experimental test setup for HEA100 brace with damper specimen



Fig. 3.42. Damper connection to HEA brace and pinned base connection

The recorded behaviour of the HEA brace with damper assembly under cyclic loading is presented in Fig. 3.43.

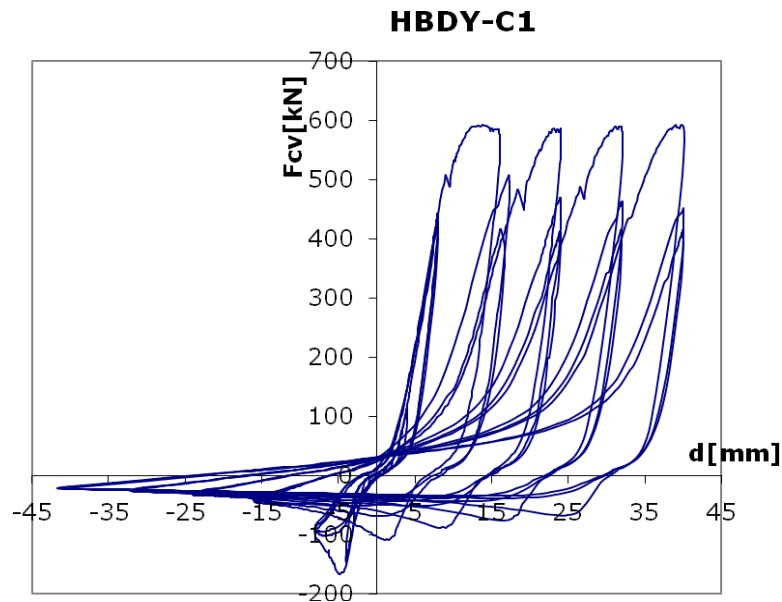


Fig. 3.43: Hysteretic behavior of HEA100 brace with damper

The damper behavior has the highest influence on the global behavior of the brace with damper assembly up to load levels of $2x_{e_y}$. Up to this level the brace remains in elastic domain and the global behaviour is governed by the damper behaviour. After this load level is exceeded the behavior of the brace is similar to that of the brace without damper with strength and stiffness degradation at each successive tension cycles and buckling of the brace in compression. The test was stopped when the values of the compression force dropped with more than 50% of maximum compression force reached.

3.4 Conclusions

Experimental tests were performed on single dampers to determine the hysteretic behaviour of the dampers experimentally and to validate the behaviour provided initially by the manufacturer and on the brace with dampers assembly to determine the combined behaviour of the two elements in two distinct design concepts.

In order to analyze the influence of the damper on the global behavior of the brace the hysteretic behavior of the brace without damper is taken as reference curve. The behavior of the brace with damper obtained for the two design concepts of „weak“ and „strong“ brace is therefore compared with the hysteretic behavior of the brace without damper.

3.4.1 „Strong” brace with damper configuration

The behavior of the brace with dampers taken as reference is considered that recorded for double T section profile of the brace (HB-C) mainly following two parameters: recorded total force in the brace and total displacement of the brace. This is compared to the behaviour recorded for the system comprised of „strong” brace (HEA240) with damper (BDE) (Fig. 3.44).

In this design concept the global behaviour of the system of brace and damper is completely governed by the constitutive law of the damper and its properties. The system does not suffer any degradation in terms of strength and stiffness these being strictly dependent on the damper properties. The system will continue to take on load until the maximum capacity of the device is reached, with the brace remaining in elastic range. This high load carrying capacity without strength and stiffness degradation represents the advantage of this type of design concept but can also lead to an increase of the load levels in the beams and columns of the braced frame due to the pseudo-elastic behaviour of the damper. Furthermore failure of this type of system is a brittle one due to failure of the device and must be avoided.

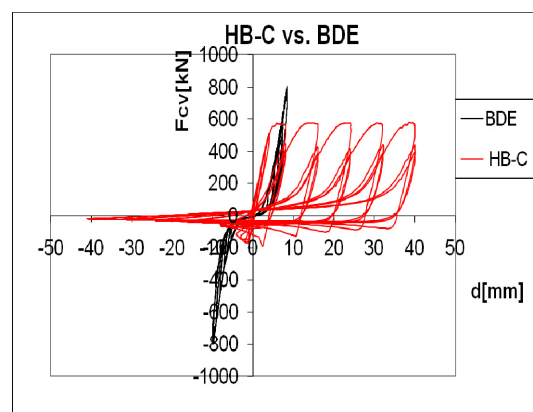


Fig. 3.44: Comparison between „strong” brace with damper and a brace without damper behaviour

3.4.2 „Weak” brace with damper configuration

In this design concept the brace is allowed to have plastic deformation and the global behaviour of the damper brace system is a mixed one. The weak element in this configuration is the brace which will ultimately fail. The behaviour of this system is presented in Fig. 3.45 in comparison with the behaviour of the same brace, under the same load protocol but without damper.

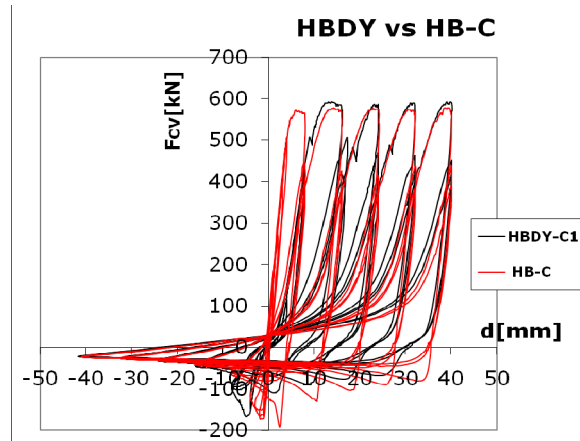


Fig. 3.45. Comparison between hysteretic behavior of the same brace with and without damper

In both configurations the force level drops significantly after the first cycle at each load step and the next two cycles of the same deformation step. The brace with damper has a higher flexibility and yields at the same load step but at a displacement of approximately 50% higher. For this system up to a level of $2e_y$ the global behavior is governed by the behavior of the damper and by the behaviour of the simple brace at higher load steps. The difference between these two systems can be observed more closely up to a level of two times yield deformation e_y (Fig. 3.46).

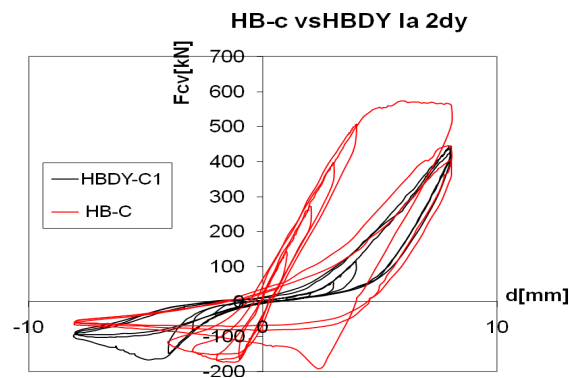


Fig. 3.46. Comparison between hysteretic behavior of the same brace with and without damper at load level of up to $2xe_y$

Up to this level the behaviour is that given by the damper parameters. At tension cycles the brace remains in elastic domain and the load level in the system is significantly smaller than that of the brace without damper with a higher overall flexibility. For compression cycles the brace with damper buckles at the same load level as the one without damper but has a higher deformation capacity due to the damper properties. The experimental results are in

agreement with the two design concepts considered. For the starting load levels of up to $2e_y$ the brace remains in elastic domain and has a lower level of energy dissipation (Table 11) but there is a significant decrease in load level due to the damper and also an increase in flexibility (Fig. 3.47). After this level the hysteretic behaviour of the system is very similar to that of the brace without damper, with energy dissipation due to the formation of a plastic hinge in the brace.

ENERGY PER CYCLE[kJ]			
HB-C		HBDY-C1	
CYCLE	E	LEVEL	E
1	100.47	0.25 e_y	155.2
2	232.62	0.5 e_y	
3	398.85	0.75 e_y	
4	732.71	e_y	189.4
5	3448	1x2 e_y	968.4
6	1841	2x2 e_y	909.88
7	1469	3x2 e_y	943.89
8	6218	1x4 e_y	8762.5
9	3129	2x4 e_y	3716.2
10	2693	3x4 e_y	2735.7
11	7433.5	1x6 e_y	6639
12	4064.6	2x6 e_y	4374
13	3688.4	3x6 e_y	3716.7
14	8235	1x8 e_y	8013
15	5228.5	2x8 e_y	5356.7
16	4682.3	3x8 e_y	4701.6
17	9248.1	1x10 e_y	9137.6
18	5986	2x10 e_y	6067.1
19	5498.1	3x10 e_y	5591

Table 11. Energy per cycle for brace with and without damper

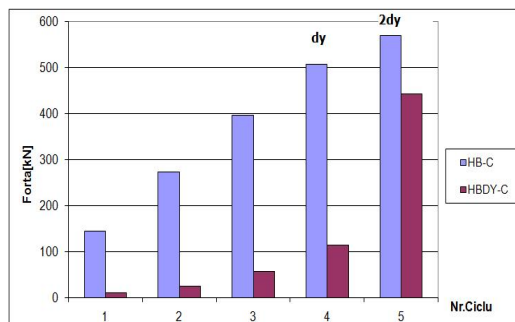


Fig. 3.47. Comparison of force levels in the brace with and without damper up to $2e_y$

Failure in this design concept is represented by the failure of the brace in compression. As a conclusion it is expected that this type of damper could improve the behaviour of rigid structures that are sensitive to formation of plastic hinges at levels corresponding to service limit state. The efficiency of this type of damper for a multistorey steel structure will be determined from numerical analyses using the behaviour of the damper and the behaviour of the damper with brace assembly obtained experimentally.

4 Numerical Modelling

4.1 Introduction

Experimental tests have been performed for two series of brace members equipped with strain hardening friction dampers: 1st series with the brace designed to avoid buckling; 2nd series with the brace designed as dissipative member, which limits the strength demands on columns and beams, and contributes to the energy-dissipation capacity of the system through yielding and buckling. The equivalent brace-damper model experimentally calibrated has been applied in numerical simulation of multi-storey steel frames in order to determine their performance in comparison with conventional concentric braced systems. This chapter presents the calibration of a numerical model for the brace and damper assembly as well as numerical simulations on several multi-storey steel frames. A performance based evaluation of the structures is presented as well as the resulted conclusions.

The numerical modelling can be split mainly in two independent parts or stages. The first stage consists of numerical simulation of the behaviour of the two elements, the brace and the damper separately, but most importantly their behaviour as a whole. The second stage consists of a series of numerical simulation on the full frame with and without dampers in the braces. Numerical time-history analyses were conducted using a set of semi-artificial seismic motions scaled to the design spectra. The final stage consists of performance base evaluation of the structure with this type of damping devices and the comparison with other types of damping devices used for seismic protection.

4.2 Element Modelling

4.2.1 Numerical Model for the Brace

Using as reference the experimental behaviour of the HEA100 brace a numerical model that could model with sufficient accuracy the cyclic behaviour of the brace was developed. The main issue that arises with brace modelling is the accurate modelling of brace behaviour at buckling. For the numerical simulation SEISMOSTRUCT version 5.5 Build 10 software was used, a finite element package that uses fibre formulation. The buckling behaviour of brace was modelled using geometric imperfections computed according to EN1993 1-1 [30]. The brace element was divided into segments with each point having

corresponding values of the imperfections computed based on a parabolic shape of the deflection with the value of the imperfection computed at midpoint of the element $e_0=26.54$ mm. The material model used for the steel was Menegotto-Pinto steel model with Fillipou isotropic hardening (Fillipou et.al (1980)) with parameters obtained experimentally from tensile tests on steel samples from the brace() and calibrated parameters shown in Table 12.

A1	A2	A3	A4
17	0.1	0.025	8

Table 12. Shape parameters for Menegotto-Pinto steel model with Fillipou isotropic hardening

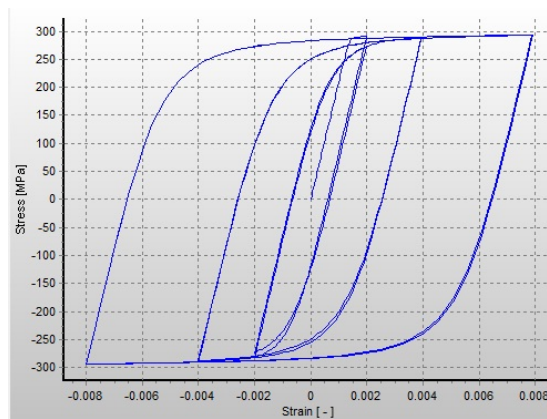


Fig. 4.1. Menegotto-Pinto steel model with Fillipou isotropic hardening [31]

A parametric study was conducted to determine the optimum number of elements in which the brace is to be divided and the value of the imperfections to be adopted comparing the cyclic behaviour of the brace with the behaviour obtained from experimental tests. The brace was divided in 2 and 4 elements (Fig. 4.2.) and for each of the two models 4 values of the imperfections were considered: e_0 , $e_0/2$, $e_0/3$, $e_0/4$ and length of the plastic hinge of 16.66%, 20% and 25% (Table 13).

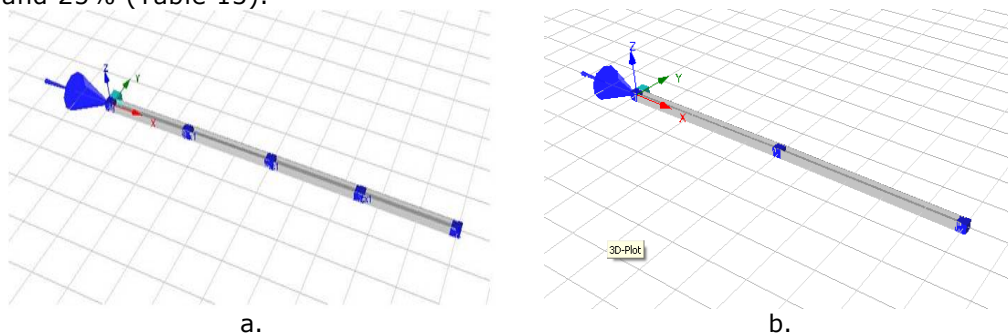


Fig. 4.2. Brace discretisation in: a) 4 elements; b) 2 elements

No. of elements	Imperfection values				Plastic hinge length
	e_0	$e_0/2$	$e_0/3$	$e_0/4$	
2	e_0	$e_0/2$	$e_0/3$	$e_0/4$	16.66%
4	e_0	$e_0/2$	$e_0/3$	$e_0/4$	
2	e_0	$e_0/2$	$e_0/3$	$e_0/4$	20%
4	e_0	$e_0/2$	$e_0/3$	$e_0/4$	
2	e_0	$e_0/2$	$e_0/3$	$e_0/4$	25%
4	e_0	$e_0/2$	$e_0/3$	$e_0/4$	

Table 13. Parametric study to determine optimum number of elements and plastic hinge length

The best results were obtained for the 2 element brace with a value of imperfection at midpoint of $e_0/2$ and plastic hinge length of 20%. The behaviour of this brace model is presented in Fig. 4.3. in comparison with the behaviour of the same brace obtained experimentally. Parametric studies conducted by Landolfo et.al.2010 [31] also recommended the use of 2 element division for modelling cyclic behaviour of brace.

HB-C experimental vs. numerical

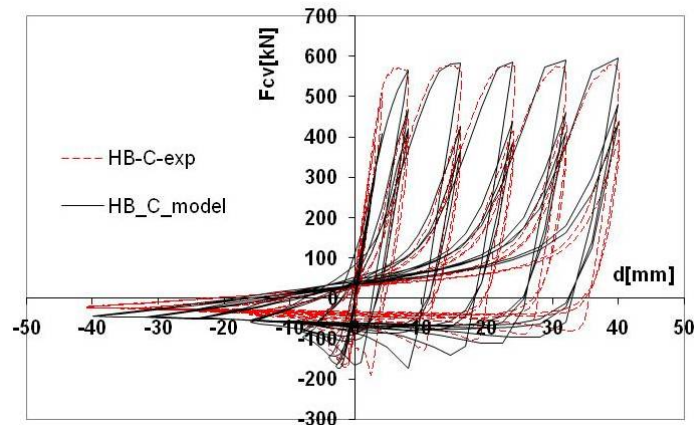


Fig. 4.3. Comparison between cyclic behaviours of brace from the numerical model with the one obtained experimentally

4.2.2 Numerical Model for the Damper

The main issues with modelling the behaviour of the damper are the pinching effect of hysteretic curve, strength stiffening and lack of degradation of the loops. For modelling of damping devices SEISMOSTRUCT software offers the use of link elements that have the possibility of defining different hysteretic behaviour for each of the 6 degrees of freedom. Several hysteretic behaviours were tested in an attempt to model the behaviour of the SERB damper. These behaviours were defined for the degree of freedom corresponding to axial deformation having a linear elastic behaviour defined for

the other 5 with sufficient stiffness to ensure their restraint. Some of the trial hysteretic behaviour models are presented in Fig. 4.4.

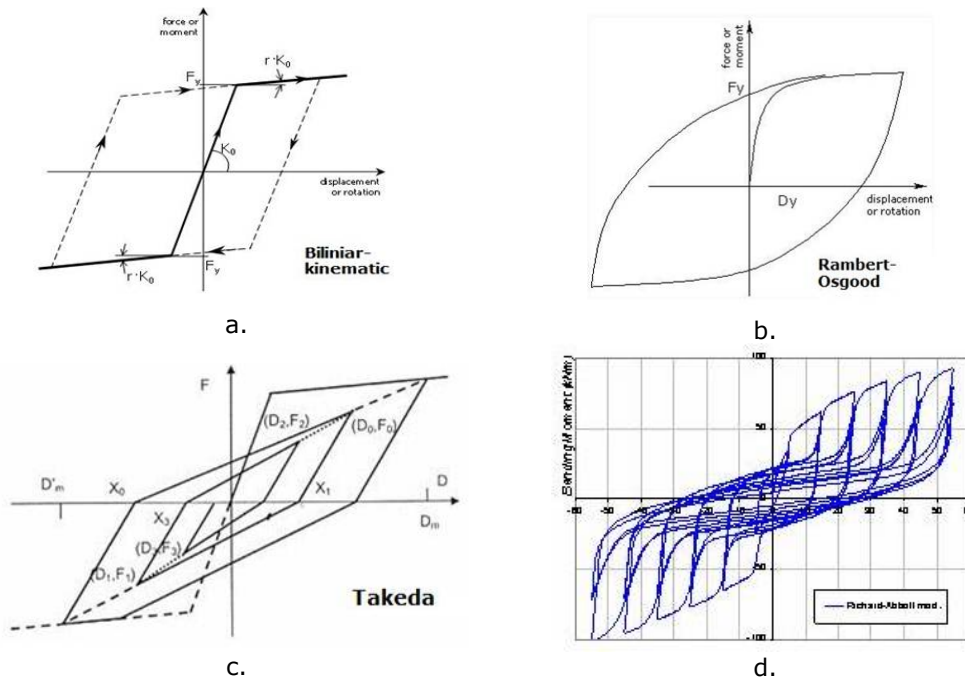


Fig. 4.4. Trial hysteretic models: a) Bilinear kinematic; b) Rambert-Osgood curve; c) Takeda; d) Richard-Abbot curve [32]

A conclusion of these trials was that to model the behaviour of the SERB damper a combination of two link elements was needed. The final damper model was constructed using a two link elements working in parallel namely a bilinear symmetric behaviour type link (Fig. 4.5.b) combined with a gap-hook element that is employed to model the pinching of the curve (Fig. 4.5.a).

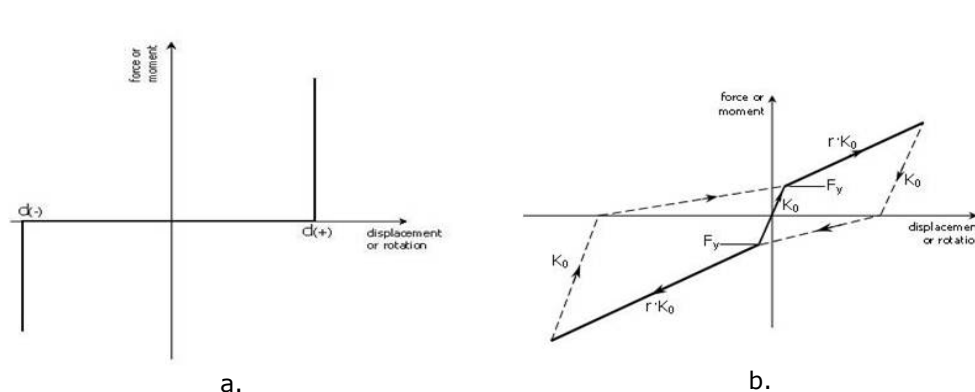


Fig. 4.5. Link behaviours for damper model: a) Gap-Hook; b) Bilinear Symmetric

The combined behaviour of the two hysteretic behaviours presented above is shown in (Fig. 4.6.a.). The damper model was compared with the behaviour obtained experimentally (Fig. 4.6.b.).

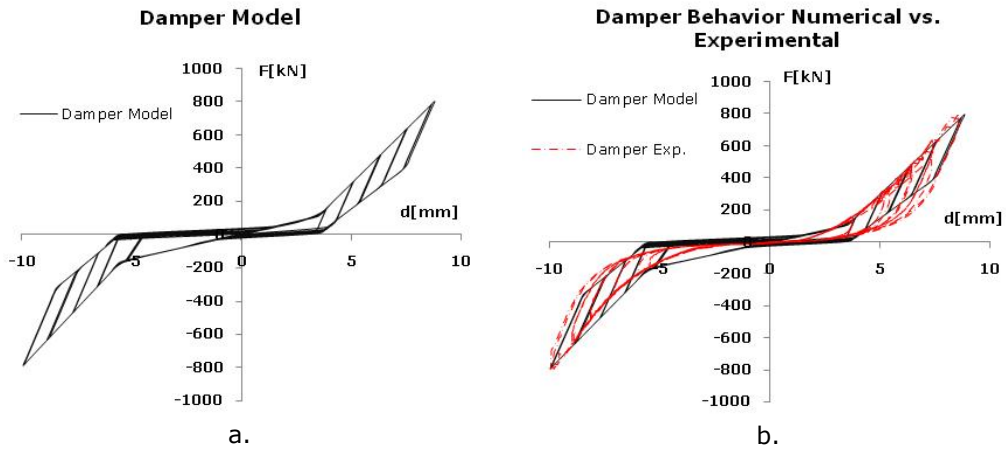


Fig. 4.6.a) Behaviour of damper model; b) Comparison between the damper behaviour of the model and the damper behaviour obtained experimentally

4.2.3 Numerical Model for the Brace with Damper

The numerical model of the brace with damper is obtained combining the models for the brace and for the damper. The results from the numerical model were compared to the experimental results HBDY-C1 (Fig. 4.7.).

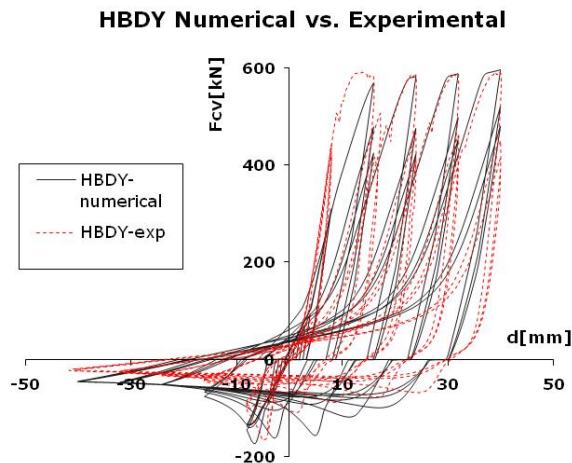


Fig. 4.7. Comparison between numerical and experimental behaviour of brace with damper

The numerical model presents the same global behaviour as the one obtained

from experimental data with a damper governed behaviour up to $2\epsilon_y$ and a brace governed behaviour afterwards, reaching the same peak values of force for each tension cycle and with sufficiently accurate modelling of sliding of the damper at zero force point transition. This two models for the brace and for the damper as presented above are employed in the overall assessment of the behaviour of the full frame.

4.3 CBF with and without damper

4.3.1 Geometry and Design

The structure analysed is a 5 storey plane frame with a underground level extracted from a 3x3 layout (Fig. 4.8a) with 3 spans of 6 m with chevron bracing in the mid-span and a storey height of 3.5m (Fig. 4.8b). The frame was design according to EC3 and EC8 with some special considerations from the Romanian seismic design code P100/2006 considering the design spectra for Bucharest with a corner period of $T_C=1.6s$ and peak ground acceleration $a_g=0.24g$.

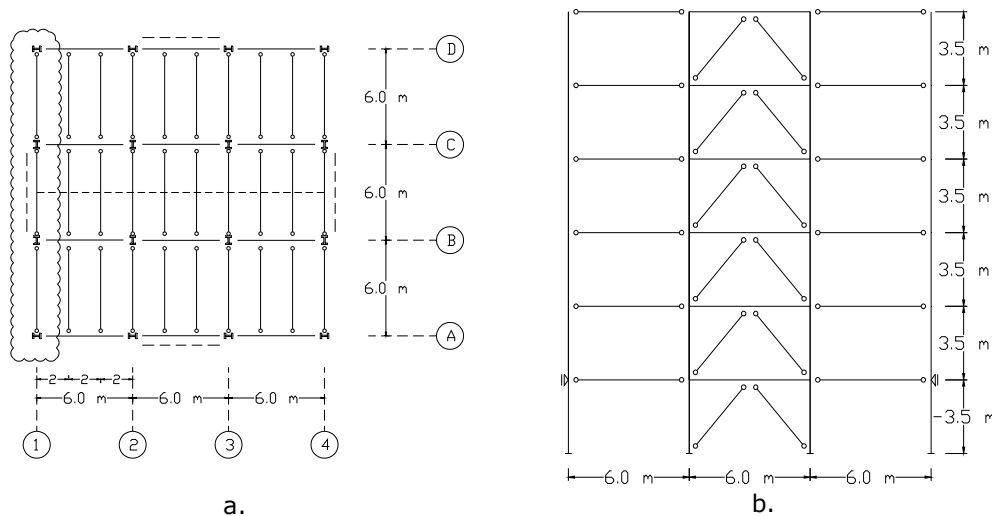


Fig. 4.8. Frame geometry: a) Plan layout; b) Selected frame

Loads considered:

- Permanent load: $p = 10.75kN / m$ from bay, $P = 60kN$ from secondary beams;
- Live load: $q = 3kN / m$ from bay, $Q = 36kN$ from secondary beams;
- Seismic load: design spectra for Bucharest with a corner period of $T_C=1.6s$ (Fig. 4.9) with behaviour factor $q = 2.5$ (high ductility class) and $\Omega \leq q = 2.5$.

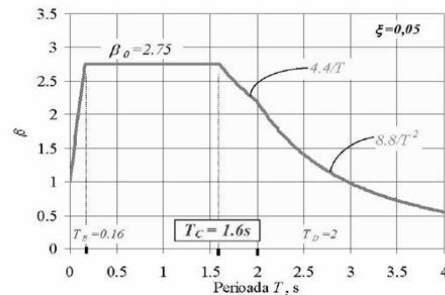


Fig. 4.9. Design spectra for Bucharest [1]

The computed mass at each level for spectral and modal analysis is $m = 113.3t$ for levels 1 through 4 and $m = 106.7t$ for the top level.

Load combinations:

- ULS base: $1.35G + 1.5Q$
- SLS base: $1.0G + 1.0Q$
- ULS special-dissipative elements: $1.0G + E + 0.4Q$
- ULS special-non-dissipative elements: $1.0G + \Omega E + 0.4Q$
- SLS special: $1.0G + q \cdot vE + 0.4Q$

Global imperfections were added as equivalent horizontal loads $H = \phi V$ added to all load cases with the values $H = 1.981kN$ for levels 1 through 4 and $H = 1.815kN$ for the top level. In addition $P\Delta$ effects were modelled with the help of a lean-on column connected with rigid diaphragm at each level loaded with the corresponding area of the secondary frame $V = 864kN$.

Damping was considered 2% for the frame and was modelled as stiffness proportional using tangent stiffness and introduced by the means of a stiffness matrix multiplier coefficient α_K computed as:

$$\alpha_K = \frac{T \cdot \xi}{\pi}$$

where:

T = first period of vibration of the structure

ξ = equivalent viscous damping (2%)

Rigid body diaphragm constraint type was considered for the nodes corresponding to each level of the structure and including the corresponding node of the lean-on column.

Final computed section dimensions of the frame are presented in Fig. 4.10.

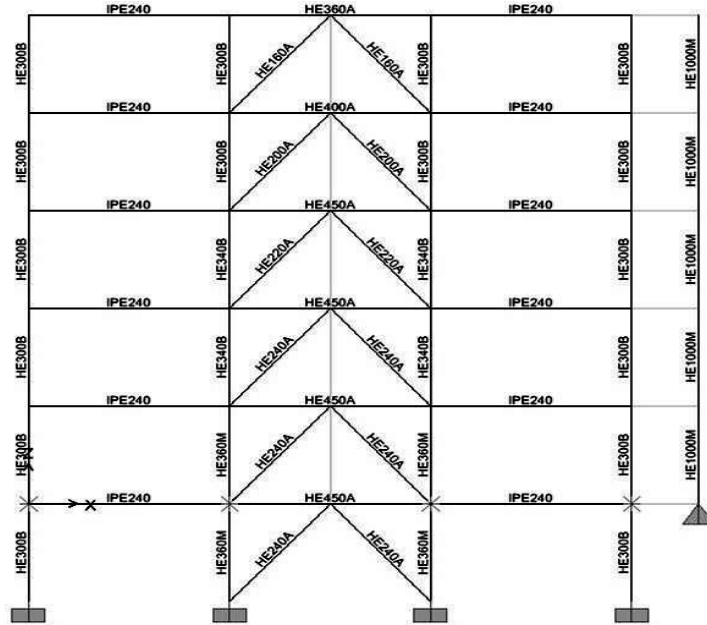


Fig. 4.10. Final geometry and sections of the designed frame

4.3.2 CBF Frame with and without Dampers

Time-history analyses are conducted using two sets of seismic motions recordings scaled to the design spectra as follows: 7 semi-artificial seismic motion characteristic for soft soil type (Bucharest)(Fig. 4.12) and 7 artificially generated seismic motions characteristic for stiff soil (Class B soil according to SREN1998-1[])(Fig. 4.13) both with and without dampers. The two target spectra were scaled to the fundamental period of vibration of the analysed structure, so as to yield roughly the same design seismic forces(Fig. 4.11).

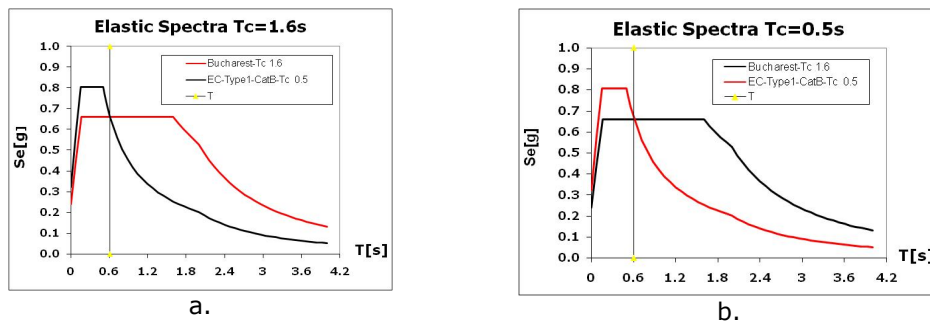


Fig. 4.11. Elastic spectra: a) Soft soil type $T_c=1.6s$; b) Stiff soil type $T_c=0.5s$

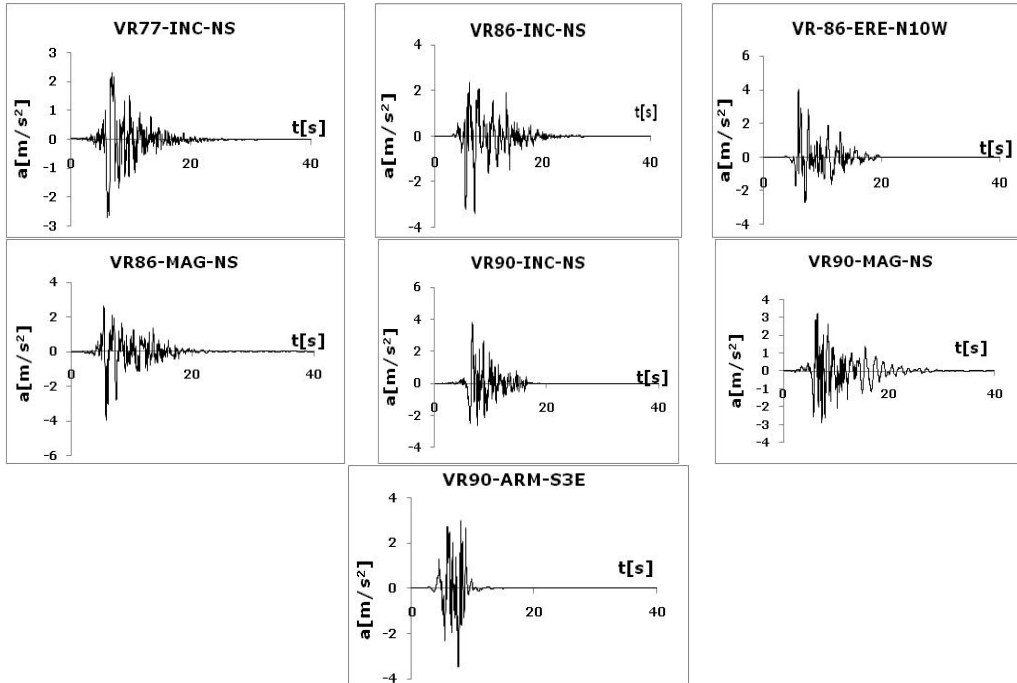


Fig. 4.12. Semi-artificial seismic motion characteristic for soft soil type (Bucharest $T_c=1.6s$)

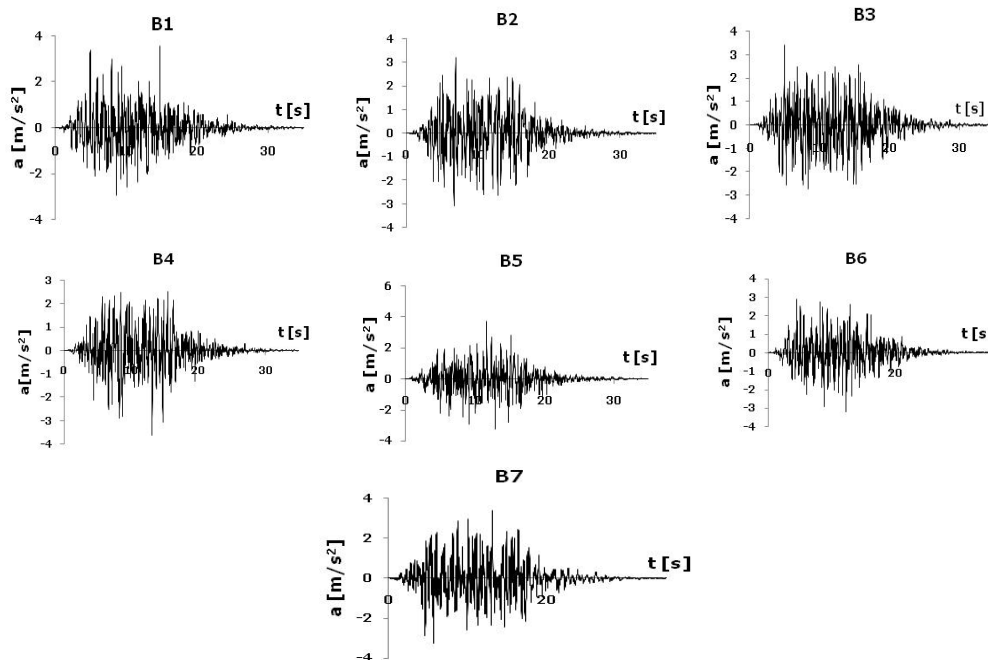


Fig. 4.13. Artificially generated seismic motions characteristic for stiff soil (Type B $T_c=0.5s$)

Three performance levels were considered for each seismic motion having an acceleration multiplier of 0.5 (30 years return period), 1.0 (100 years return period), 1.5(475 years return period) corresponding to serviceability limit state (SLS), ultimate limit state (ULS) and collapse prevention (CP):

- SLS → $a_{g,SLS} = 0.5 \cdot a_{g,ULS}$
- ULS $a_{g,ULS}$
- CP → $a_{g,CP} = 1.5 \cdot a_{g,ULS}$

Each level of seismic action corresponds to a performance level as shown in Table 14.

Seismic Action	a_g	Performance Level
Serviceability Limit State (SLS)	$0.5 \cdot a_{g,ULS}$	Immediate Occupancy (IO)
Ultimate Limit State (ULS)	$a_{g,ULS}$	Life Safety (LS)
Collapse Prevention (CP)	$1.5 \cdot a_{g,ULS}$	Collapse Prevention (CP)

Table 14. Correspondence of seismic level to performance level

Performance based evaluation was performed using acceptance criteria for plastic axial deformation in the braces and plastic rotation for beams and columns according to FEMA356 [10].

4.3.2.1 TH Analysis of CBF Structure for Soft Soil Type ($T_C=1.6s$)

Performance criteria followed was (i) plastic axial deformation in braces and (ii) plastic rotation for beams and column.

- (i) Plastic axial deformation in the braces with displacement at yield Δ_y and at buckling Δ_c computed from individual single brace models using pushover analysis as follows (Table 15):

Brace	Compression Δ_c [mm]	Tension Δ_y [mm]
HEA240	4.49	5.747
HEA220	3.965	5.71
HEA200	3.578	5.64
HEA160	2.76	5.57

Table 15. Displacement at buckling and yield for compression and tension braces

- (ii) Plastic rotation for beams and columns having rotation at yield θ_y computed as:

- Columns:

$$\theta_y = \frac{Z \cdot F_{ye} \cdot I_C}{6EI_C} \left(1 - \frac{P}{P_{ye}} \right) [10];$$

- Central beams (computed as columns):

$$\theta_y = \frac{Z \cdot F_{ye} \cdot l_B}{6EI_B} \left(1 - \frac{P}{P_{ye}} \right) \quad [10].$$

where:

Z = Plastic section modulus (W_{pl})

F_{ye} = expected yield strength of material

l_C, l_B = element length for column and beam respectively

P = axial force at instant of calculation

P_{ye} = expected axial yield force of member

E = modulus of elasticity

I_C, I_B = moment of inertia for column and beam respectively.

Maximum drift levels (Fig. 4.14), maximum drift at each storey (Fig. 4.15) and top displacement for the structure (Fig. 4.16) without dampers are presented as mean values of semi-artificial values for all 7 seismic motions at levels corresponding to SLS, ULS and CP in comparison with the same values recorded for the structure with dampers in the braces.

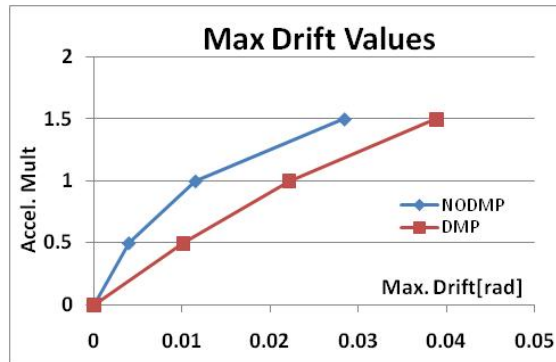


Fig. 4.14. Maximum drift values for the structure with and without dampers

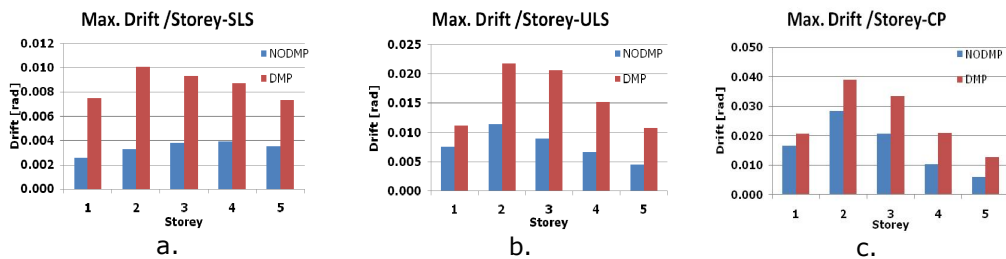


Fig. 4.15. Maximum drift at each storey at: a) SLS; b) ULS; c) CP for the structure with and without dampers

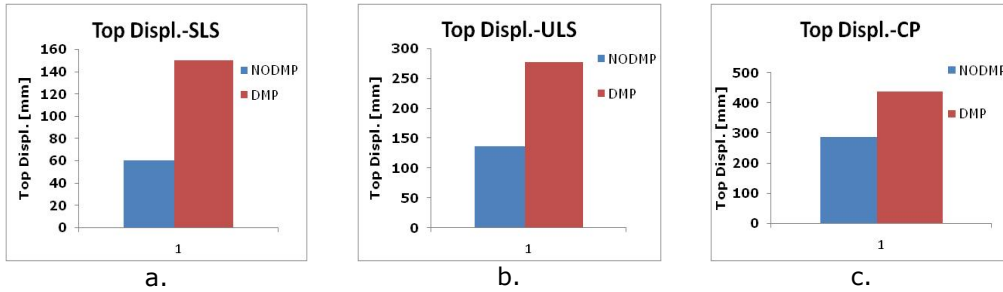


Fig. 4.16. Top displacement at: a) SLS; b) ULS; c) CP for the structure with and without dampers

At the end of each seismic recording used the structure was left to vibrate freely for 10s. Recorded values of permanent displacement at top of the structure are presented as mean values for all 7 recordings in Fig. 4.17.

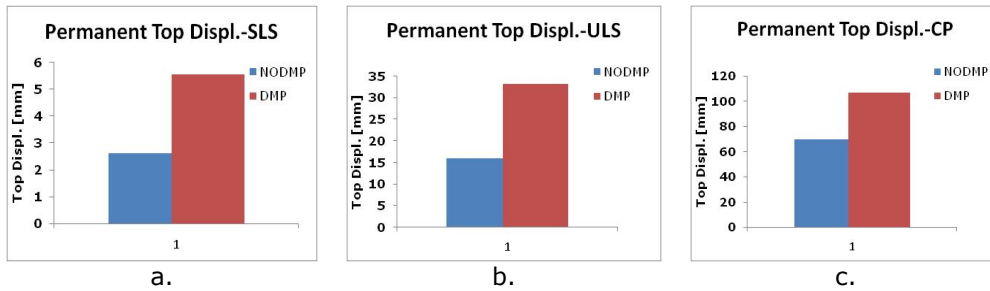


Fig. 4.17. Permanent top displacement at: a) SLS; b) ULS; c) CP for the structure with and without dampers

For all 7 semi-artificial seismic motion characteristic for soft soil type used the results showed that for all performance levels the building with dampers exhibited a significant increase in drift for all 5 storeys and higher values of permanent displacement at the top of the structure. Values of plastic axial deformations and plastic are presented here as mean value for all 7 seismic recordings at (i)SLS with $a_{g,SLS} = 0.5 \cdot a_{g,ULS}$ (Table 16, Table 17, Table 18), (ii)ULS with $a_{g,ULS}$ (Table 19, Table 20, Table 21) and (iii)CP with $a_{g,CP} = 1.5 \cdot a_{g,ULS}$ (Table 22, Table 23, Table 24).

(i) SLS with $a_{g,SLS} = 0.5 \cdot a_{g,ULS}$ characteristic for soft soil type ($T_C=1.6s$)

BRACE Compr.	Plastic deformation demand-SLS, mm		Plastic deformation capacity, mm
	NODMP	DMP	
LOC.	NODMP	DMP	IO
BR1L	-	-	1.1225
BR1R	-	-	1.1225
BR2L	0.206	1.000	1.1225
BR2R	0.347	0.751	1.1225

BR3L	0.360	0.779	0.99125
BR3R	0.272	0.424	0.99125
BR4L	0.299	0.768	0.8945
BR4R	0.156	0.372	0.8945
BR5L	0.103	0.584	0.692
BR5R	0.069	0.197	0.692
BR(storey no.)R- right brace for selected storey			
BR(storey no.)L- left brace for selected storey			

Table 16. Mean values of axial plastic deformation for braces in compression at SLS

BRACE Tension	Plastic deformation demand-SLS , mm		Plastic deformation capacity, mm
	LOC.	NODMP	
No plastic deformation			
BR(storey no.)R- right brace for selected storey			
BR(storey no.)L- left brace for selected storey			

Table 17. Mean values of axial plastic deformation for braces in tension at SLS

BEAM	NODMP		DMP	
	LOC.	Plastic rotation demand-ULS, rad	Plastic rotation capacity, rad LS	Plastic rotation demand-ULS, rad
No plastic rotation in elements				
CB(storey no.)a- central beam for selected storey at end a				
CB(storey no.)b- central beam for selected storey at end b				

Table 18. Mean values for plastic rotation at SLS for central beams (soft soil)

(ii) ULS with $a_{g,ULS}$ characteristic for soft soil type ($T_c=1.6s$)

BRACE Compr.	Plastic deformation demand-ULS , mm		Plastic deformation capacity, mm
	LOC.	NODMP	
BR1L	1.605	1.029	22.45
BR1R	1.764	0.875	22.45
BR2L	2.004	3.234	22.45
BR2R	1.674	2.807	22.45
BR3L	1.403	2.250	19.825
BR3R	1.202	1.036	19.825
BR4L	0.991	1.767	17.89
BR4R	0.696	0.959	17.89
BR5L	0.443	1.728	13.84
BR5R	0.478	1.295	13.84
BR(storey no.)R- right brace for selected storey			
BR(storey no.)L- left brace for selected storey			

Table 19. Mean values of axial plastic deformation for braces in compression at ULS

BRACE Tension. LOC.	Plastic deformation demand- ULS , mm		Plastic deformation capacity, mm
	NODMP	DMP	LS
BR1L	0.284	-	40.2283
BR1R	0.960	-	40.2283
BR2L	3.238	3.998	40.2283
BR2R	3.829	4.569	40.2283
BR3L	0.142	6.330	39.97
BR3R	0.330	6.119	39.97
BR4L	0.039	1.316	39.48
BR4R	0.050	1.946	39.48
BR5L	-	0.037	39.039
BR5R	-	0.259	39.039
BR(storey no.)R- right brace for selected storey			
BR(storey no.)L- left brace for selected storey			

Table 20. Mean values of axial plastic deformation for braces in tension at ULS

BEAM LOC.	NODMP		DMP	
	Plastic rotation demand- ULS, rad	Plastic rotation capacity, rad LS	Plastic rotation demand-ULS, rad	Plastic rotation capacity, rad LS
CB1a	0.00120	VARIES	0.00406	VARIES
CB2a	0.00063	VARIES	0.00759	VARIES
CB3a	-	VARIES	0.00423	VARIES
CB4a	-	VARIES	0.00175	VARIES
CB5a	-	VARIES	-	VARIES
CB1b	0.00127	VARIES	0.00257	VARIES
CB2b	0.00099	VARIES	0.00605	VARIES
CB3b	-	VARIES	0.00220	VARIES
CB4b	-	VARIES	0.00066	VARIES
CB5b	-	VARIES	-	VARIES
CB(storey no.)a- central beam for selected storey at end a				
CB(storey no.)b- central beam for selected storey at end b				

Table 21. Mean values for plastic rotation at ULS for central beams

(iii) CP with $a_{g,CP} = 1.5 \cdot a_{g,ULS}$ characteristic for soft soil type ($T_C=1.6s$)

BRACE Compr. LOC.	Plastic deformation demand-CP , mm		Plastic deformation capacity, mm
	NODMP	DMP	CP
BR1L	2.883	2.763	31.43
BR1R	2.546	2.763	31.43
BR2L	2.727	3.788	31.43
BR2R	2.927	3.176	31.43
BR3L	1.620	2.658	27.755
BR3R	1.639	1.868	27.755
BR4L	1.477	2.413	25.046
BR4R	1.361	1.665	25.046

BR5L	0.767	2.100	19.376
BR5R	0.722	1.357	19.376
BR(storey no.)R- right brace for selected storey			
BR(storey no.)L- left brace for selected storey			

Table 22. Mean values of axial plastic deformation for braces in compression at CP

BRACE Tension.	Plastic deformation demand-CP , mm		Plastic deformation capacity, mm
	NODMP	DMP	CP
BR1L	6.506	2.908	51.7221
BR1R	5.856	1.852	51.7221
BR2L	18.453	14.358	51.7221
BR2R	17.474	13.911	51.7221
BR3L	0.554	18.632	51.39
BR3R	0.476	18.541	51.39
BR4L	0.112	6.253	50.76
BR4R	0.268	5.701	50.76
BR5L	0.000	0.577	50.193
BR5R	0.000	0.812	50.193
BR(storey no.)R- right brace for selected storey			
BR(storey no.)L- left brace for selected storey			

Table 23. Mean values of axial plastic deformation for braces in tension at CP

BEAM LOC.	NODMP		DMP	
	Plastic rotation demand-CP, rad	Plastic rotation capacity, rad CP	Plastic rotation demand-CP, rad	Plastic rotation capacity, rad CP
CB1a	0.01517	VARIES	0.02205	VARIES
CB2a	0.01259	VARIES	0.02247	VARIES
CB3a	0.00188	VARIES	0.01017	VARIES
CB4a	-	VARIES	0.00306	VARIES
CB5a	-	VARIES	-	VARIES
CB1b	0.01423	VARIES	0.01975	VARIES
CB2b	0.01111	VARIES	0.02088	VARIES
CB3b	0.00161	VARIES	0.00719	VARIES
CB4b	-	VARIES	0.00318	VARIES
CB5b	-	VARIES	-	VARIES
CB(storey no.)a- central beam for selected storey at end a				
CB(storey no.)b- central beam for selected storey at end b				

Table 24. Mean values for plastic rotation at CP for central beams

At all levels of seismic motion the structure with dampers has a higher number of plastic hinges in elements with significant increase in values of plastic axial deformations and rotations than the structure without dampers. In the following paragraph a relevant example for the 7 seismic motions characteristic to soft soil will be presented and discussed in detail. The CBF structure will be presented comparatively with and without dampers at (i). SLS with $a_{g,SLS} = 0.5 \cdot a_{g,ULS}$, (ii) ULS with $a_{g,ULS}$ and (iii) CP with $a_{g,CP} = 1.5 \cdot a_{g,ULS}$.

(i) SLS with $a_{g,SLS} = 0.5 \cdot a_{g,ULS}$ characteristic for soft soil type ($T_C=1.6s$)

Plastic hinge formation in the structure with and without damper is presented in Fig. 4.18.

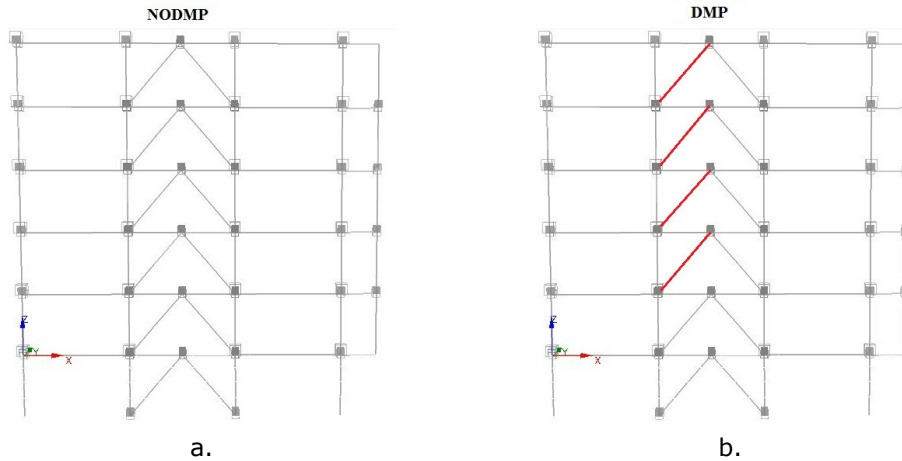


Fig. 4.18. Plastic hinge formation for CBF: a) without dampers; b) with dampers at SLS

For this performance level the building without dampers does not form any plastic hinges in elements while the building fitted with dampers forms plastic hinges in the bracing with values of plastic deformation that already exceed the acceptance criteria for immediate occupancy (IO) from FEMA356 [10] (Table 25). Values of permanent top displacement are higher for the frame with dampers as shown in Fig. 4.19.

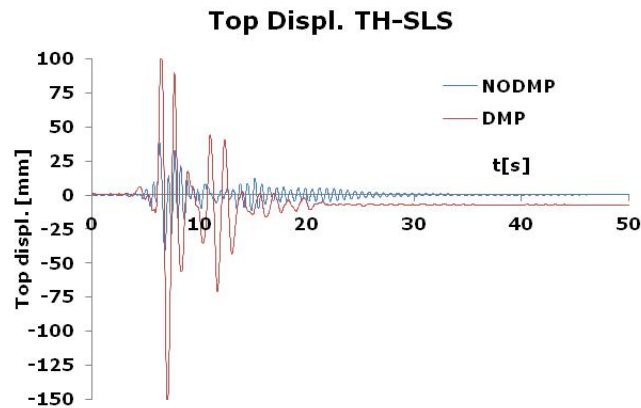


Fig. 4.19. Recorded top displacement in time for the CBF structure at SLS (soft soil)

BRACE Compr.	Plastic deformation demand- SLS, mm		Plastic deformation capacity, mm
	NODMP	DMP	IO
BR2L	-	3.012	1.1225
BR3L	-	1.736	0.99125
BR4L	-	1.061	0.8945
BR5L	-	0.216	0.692
BR(storey no.)R- right brace for selected storey			
BR(storey no.)L- left brace for selected storey			

Table 25. Axial plastic deformation values for compression braces at SLS (soft soil)

(ii) ULS with $a_{g,ULS}$ characteristic for soft soil type ($T_C=1.6s$)

Plastic hinge formation in the structure with and without damper is presented in Fig. 4.20.

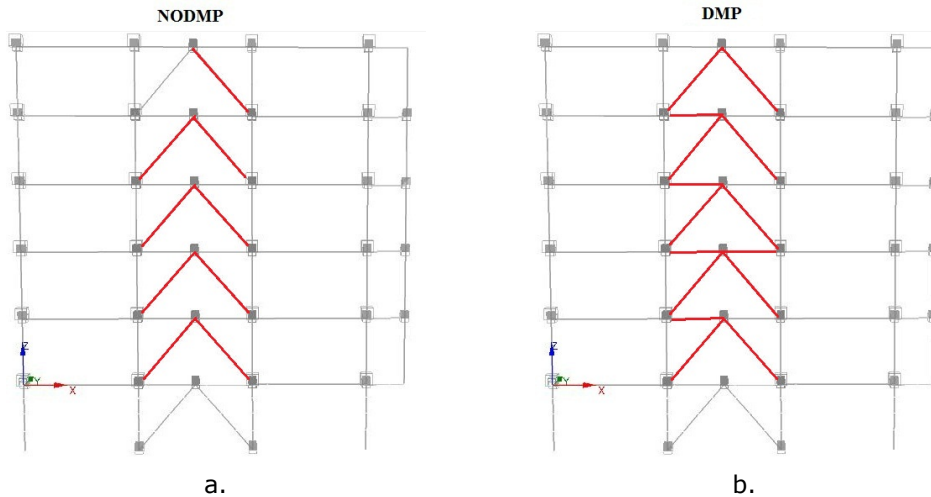


Fig. 4.20. Plastic hinge formation for CBF: a) without dampers; b) with dampers at ULS

At ULS both frames with and without dampers form plastic hinges in braces. At this level the structure with dampers has a higher number of plastic hinges in elements and a higher value of plastic deformation/rotation in elements and a higher value of permanent top displacement (Fig. 4.21) than the structure without dampers. Plastic rotations occur only for the central beams of the frame with dampers. All plastic deformations and rotations satisfy the acceptance criteria corresponding to life safety (LS) from FEMA 356 [10]. Specific values of axial plastic deformation recorded for braces in tension, compression and plastic rotation of central beams are presented in Table 26, Table 27, Table 28 respectively.

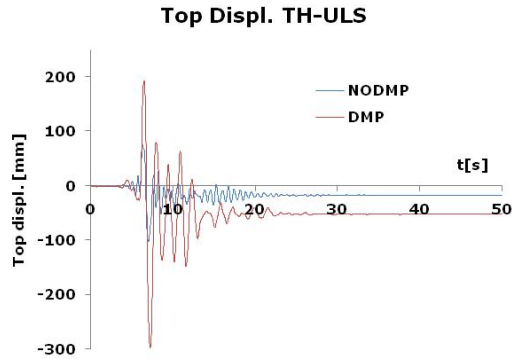


Fig. 4.21. Recorded top displacement in time for the CBF structure at ULS (soft soil)

BRACE Compr.	Plastic deformation demand- ULS , mm		Plastic deformation capacity, mm
	NODMP	DMP	
LOC.			LS
BR1L	2.623	2.054	22.45
BR1R	1.473	0.749	22.45
BR2L	3.137	4.688	22.45
BR2R	1.974	3.614	22.45
BR3L	1.626	3.603	19.825
BR3R	1.106	1.980	19.825
BR4L	0.639	2.636	17.89
BR4R	0.825	1.803	17.89
BR5L	-	1.101	13.84
BR5R	0.419	1.979	13.84
BR(storey no.)R- right brace for selected storey			
BR(storey no.)L- left brace for selected storey			

Table 26. Axial plastic deformation for braces in compression at ULS (soft soil)

BRACE Tension.	Plastic deformation demand- ULS , mm		Plastic deformation capacity, mm
	NODMP	DMP	
LOC.			LS
BR1R	2.070	-	40.2283
BR2R	4.470	7.935	40.2283
BR3R	-	11.900	39.97
BR4R	-	3.729	39.48
BR(storey no.)R- right brace for selected storey			
BR(storey no.)L- left brace for selected storey			

Table 27. Axial plastic deformation for braces in tension at ULS (soft soil)

BEAM	NODMP		DMP	
	Plastic rotation demand-ULS, rad	Plastic rotation capacity, rad LS	Plastic rotation demand-ULS, rad	Plastic rotation capacity, rad LS
CB1a	-	-	0.0128	0.0154
CB2a	-	-	0.0142	0.0161
CB3a	-	-	0.00651	0.0155
CB4a	-	-	0.00135	0.0181
CB2b	-	-	0.00832	0.0152
CB(storey no.)a- central beam for selected storey at end a				
CB(storey no.)b- central beam for selected storey at end b				

Table 28. Plastic rotation at ULS for central beams (soft soil)

(iii) CP with $a_{g,CP} = 1.5 \cdot a_{g,ULS}$ characteristic for soft soil type ($T_c=1.6s$)

Plastic hinge formation in the structure with and without damper is presented in Fig. 4.22.

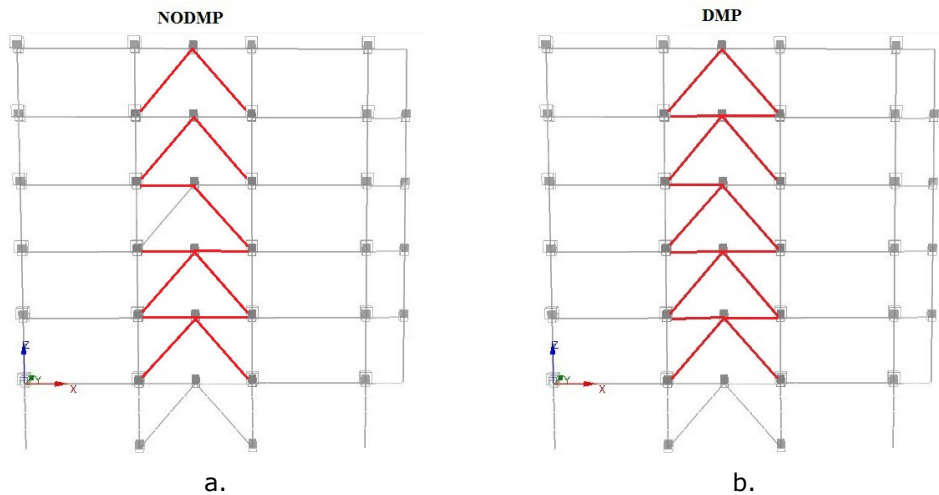


Fig. 4.22. Plastic hinge formation in the structure with and without damper at CP (soft soil)

At CP both frames with and without dampers form plastic hinges in braces and central beams. Similar to previous levels of seismic motion the structure with dampers has a higher number of plastic hinges in elements, a higher value of plastic deformation/rotation in elements and higher values of permanent top displacement (Fig. 4.23) than the structure without dampers. Plastic rotations for the central beams no longer satisfy the acceptance criteria corresponding to collapse prevention (CP) from FEMA 356 [10]. Specific values of axial plastic deformation recorded for braces in tension, compression and plastic rotation of central beams are presented in Table 29, Table 30 and Table 31 respectively.

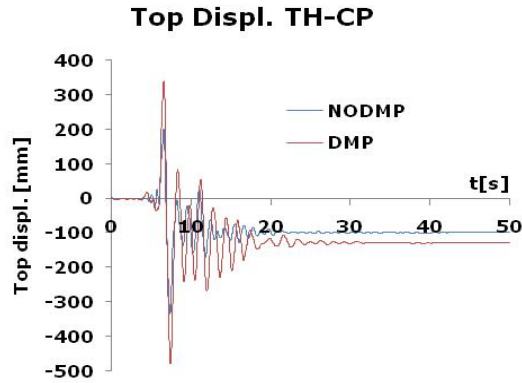


Fig. 4.23. Recorded top displacement in time for the CBF structure at CP (soft soil)

BRACE Compr.	Plastic deformation demand-CP , mm		Plastic deformation capacity, mm
	NODMP	DMP	
LOC.			CP
BR1L	1.932	3.291	31.43
BR1R	3.082	2.462	31.43
BR2L	-	-	31.43
BR2R	3.470	4.387	31.43
BR3L	-	-	27.755
BR3R	2.164	2.480	27.755
BR4L	1.536	2.601	25.046
BR4R	1.680	2.925	25.046
BR5L	0.443	1.351	19.376
BR5R	0.849	3.213	19.376
BR(storey no.)R- right brace for selected storey			
BR(storey no.)L- left brace for selected storey			

Table 29. Axial plastic deformation for braces in compression at CP (soft soil)

BRACE Tension.	Plastic deformation demand-CP , mm		Plastic deformation capacity, mm
	NODMP	DMP	
LOC.			CP
BR1L	5.415	-	51.7221
BR1R	4.933	3.632	51.7221
BR2L	21.360	18.997	51.7221
BR2R	26.107	17.781	51.7221
BR3L	-	16.662	51.39
BR3R	0.419	29.069	51.39
BR4L	-	0.221	50.76
BR4R	-	8.202	50.76
BR5L	-	-	50.193
BR5R	-	-	50.193
BR(storey no.)R- right brace for selected storey			
BR(storey no.)L- left brace for selected storey			

Table 30. Axial plastic deformation for braces in tension at CP (soft soil)

BEAM LOC.	NODMP		DMP	
	Plastic rotation demand-CP, rad	Plastic rotation capacity, rad CP	Plastic rotation demand-CP, rad	Plastic rotation capacity, rad CP
CB1a	0.0307	0.0241	0.0375	0.0237
CB2a	0.0229	0.0241	0.0323	0.0241
CB3a	0.00525	0.0234	0.0150	0.0237
CB4a	-	-	0.00213	0.0269
CB1b	0.0157	0.0224	0.0212	0.0225
CB2b	0.0116	0.0225	0.0202	0.0223
CB4b	-	-	0.00222	0.0266
CB(storey no.)a- central beam for selected storey at end a				
CB(storey no.)b- central beam for selected storey at end b				

Table 31. Plastic rotation at CP for central beams (soft soil)

The first set of numerical analyses showed that the frame equipped with dampers increases the flexibility of the structure, forming plastic hinges at SLS with a higher number of plastic hinges with higher values of plastic deformation/rotation in braces and beams respectively that no longer satisfy the performance criteria and generally a worse global behaviour. The conclusion is that this particular type of damper is not efficient in reducing the seismic response of a building for earthquakes characterized by a high value of corner period $T_c=1.6s$ (soft soil) in this design concept.

4.3.2.2 TH Analysis of CBF Structure for Stiff Soil Type ($T_c=0.5s$)

Maximum drift levels (Fig. 4.24), maximum drift at each storey (Fig. 4.25) and top displacement for the structure (Fig. 4.26) without dampers are presented as mean values of recorded values for all 7 seismic motions at levels corresponding to SLS, ULS and CP in comparison with the same values recorded for the structure with dampers in the braces.

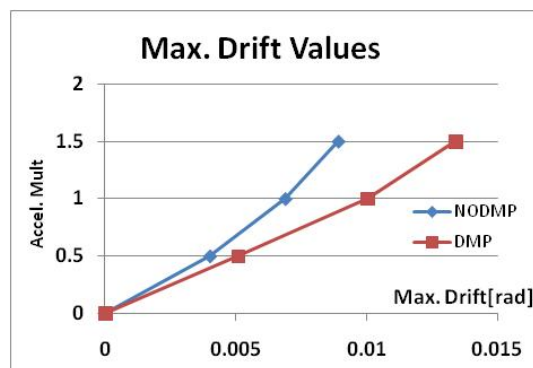


Fig. 4.24. Maximum drift values for the structure with and without dampers (stiff soil)

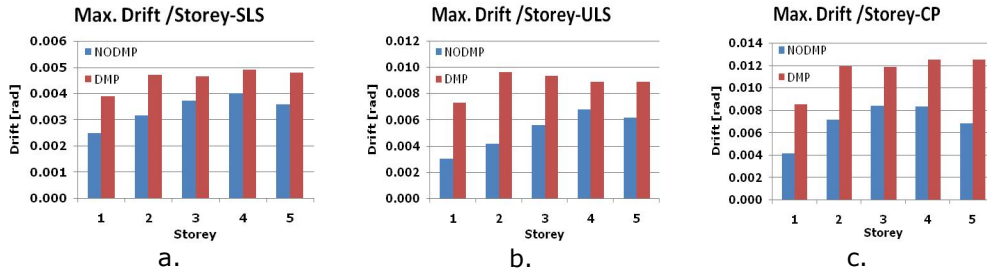


Fig. 4.25. Maximum drift at each storey at: a) SLS; b) ULS; c) CP for the structure with and without dampers (stiff soil)

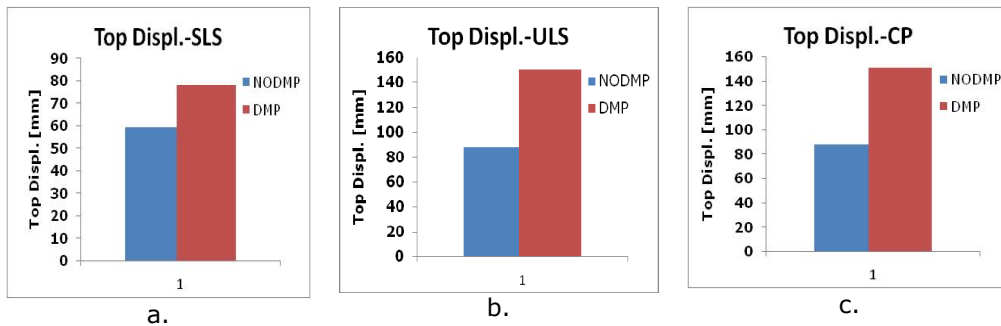


Fig. 4.26. Top displacement at: a) SLS; b) ULS; c) CP for the structure with and without dampers (stiff soil)

At the end of each seismic recording used the structure was left to vibrate freely for 10s. Recorded values of permanent displacement at top of the structure are presented as mean values for all 7 recordings in Fig. 4.27.

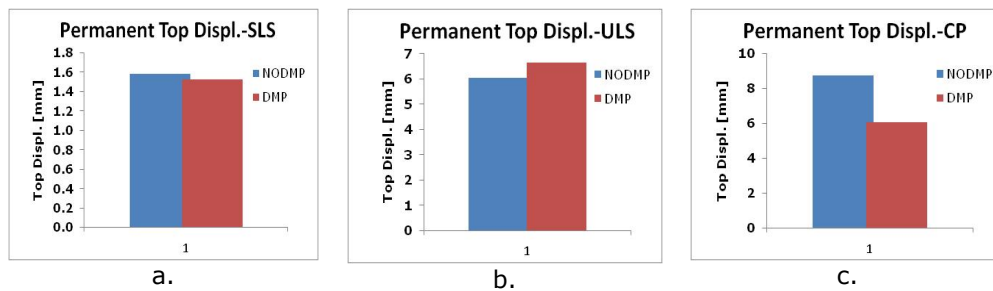


Fig. 4.27. Permanent top displacement at: a) SLS; b) ULS; c) CP for the structure with and without dampers (stiff soil)

For all 7 seismic motions characteristic for stiff soil type used the results showed that for all performance levels the building with dampers exhibited an increase in drift for all 5 storeys. The structure with dampers has lower values of permanent displacement at the top of the structure at SLS and CP. Values of plastic axial deformations and plastic rotations are presented here as mean

value for all 7 seismic recordings at (i) SLS with $a_{g,SLS} = 0.5 \cdot a_{g,ULS}$ (Table 32, Table 33, Table 34), (ii) ULS with $a_{g,ULS}$ (Table 35, Table 36, Table 37) and (iii) CP with $a_{g,CP} = 1.5 \cdot a_{g,ULS}$ (Table 38, Table 39, Table 40).

(i) SLS with $a_{g,SLS} = 0.5 \cdot a_{g,ULS}$ characteristic for stiff soil type ($T_C=0.5s$)

BRACE Compr.	Plastic deformation demand- SLS , mm		Plastic deformation capacity, mm
	NODMP	DMP	IO
LOC.			
BR1L	-	-	1.1225
BR1R	-	-	1.1225
BR2L	-	-	1.1225
BR2R	-	-	1.1225
BR3L	0.215	-	0.99125
BR3R	0.040	-	0.99125
BR4L	0.321	-	0.8945
BR4R	0.065	-	0.8945
BR5L	0.158	0.036	0.692
BR5R	0.001	0.057	0.692
BR(storey no.)R- right brace for selected storey			
BR(storey no.)L- left brace for selected storey			

Table 32. Mean values of axial plastic deformation for braces in compression at SLS (stiff soil)

BRACE Tension	Plastic deformation demand- SLS , mm		Plastic deformation capacity, mm
	NODMP	DMP	IO
LOC.			
No plastic axial deformation			
BR(storey no.)R- right brace for selected storey			
BR(storey no.)L- left brace for selected storey			

Table 33. Mean values of axial plastic deformation for braces in tension at SLS (stiff soil)

BEAM	NODMP		DMP	
	Plastic rotation demand- ULS, rad	Plastic rotation capacity, rad LS	Plastic rotation demand-ULS, rad	Plastic rotation capacity, rad LS
LOC.				
No plastic rotation in elements				
CB(storey no.)a- central beam for selected storey at end a				
CB(storey no.)b- central beam for selected storey at end b				

Table 34. Mean values for plastic rotation at SLS for central beams (stiff soil)

(ii) ULS with $a_{g,ULS}$ characteristic for stiff soil type ($T_C=0.5s$)

BRACE Compr.	Plastic deformation demand- ULS , mm		Plastic deformation capacity, mm
	NODMP	DMP	
LOC.			LS
BR1L	0.073	-	22.45
BR1R	0.381	-	22.45
BR2L	0.710	0.526	22.45
BR2R	0.915	0.970	22.45
BR3L	1.113	0.317	19.825
BR3R	1.218	0.823	19.825
BR4L	1.109	0.809	17.89
BR4R	0.807	1.198	17.89
BR5L	0.561	0.978	13.84
BR5R	0.413	1.312	13.84
BR(storey no.)R- right brace for selected storey			
BR(storey no.)L- left brace for selected storey			

Table 35. Mean values of axial plastic deformation for braces in compression at ULS (stiff soil)

BRACE Tension.	Plastic deformation demand- ULS , mm		Plastic deformation capacity, mm
	NODMP	DMP	
LOC.			LS
BR1L	-	-	40.2283
BR1R	-	-	40.2283
BR2L	-	-	40.2283
BR2R	-	-	40.2283
BR3L	0.086	-	39.97
BR3R	0.022	0.035	39.97
BR4L	-	-	39.48
BR4R	-	0.154	39.48
BR5L	-	0.024	39.039
BR5R	-	0.018	39.039
BR(storey no.)R- right brace for selected storey			
BR(storey no.)L- left brace for selected storey			

Table 36. Mean values of axial plastic deformation for braces in tension at ULS (stiff soil)

BEAM	NODMP		DMP	
	Plastic rotation demand- ULS, rad	Plastic rotation capacity, rad LS	Plastic rotation demand-ULS, rad	Plastic rotation capacity, rad LS
LOC.				
No plastic rotation				
CB(storey no.)a- central beam for selected storey at end a				
CB(storey no.)b- central beam for selected storey at end b				

Table 37. Mean values for plastic rotation at ULS for central beams (stiff soil)

(iii) CP with $a_{g,CP} = 1.5 \cdot a_{g,ULS}$ characteristic for stiff soil type ($T_C=0.5s$)

BRACE Compr.	Plastic deformation demand-CP , mm		Plastic deformation capacity, mm
	LOC.	DMP	
BR1L	0.772	-	31.43
BR1R	0.763	0.058	31.43
BR2L	1.550	1.809	31.43
BR2R	1.419	2.977	31.43
BR3L	1.505	1.827	27.755
BR3R	1.558	2.199	27.755
BR4L	1.259	1.521	25.046
BR4R	1.632	1.648	25.046
BR5L	0.981	1.555	19.376
BR5R	0.965	1.544	19.376
BR(storey no.)R- right brace for selected storey			
BR(storey no.)L- left brace for selected storey			

Table 38. Mean values of axial plastic deformation for braces in compression at CP (stiff soil)

BRACE Tension.	Plastic deformation demand-CP , mm		Plastic deformation capacity, mm
	LOC.	DMP	
BR1L	0.049	-	51.7221
BR1R	-	-	51.7221
BR2L	0.715	0.351	51.7221
BR2R	1.284	1.435	51.7221
BR3L	0.168	0.954	51.39
BR3R	0.293	2.221	51.39
BR4L	0.076	1.554	50.76
BR4R	0.122	3.398	50.76
BR5L	-	1.084	50.193
BR5R	-	1.610	50.193
BR(storey no.)R- right brace for selected storey			
BR(storey no.)L- left brace for selected storey			

Table 39. Mean values of axial plastic deformation for braces in tension at CP (stiff soil)

BEAM LOC.	NODMP		DMP	
	Plastic rotation demand-CP, rad	Plastic rotation capacity, rad CP	Plastic rotation demand-CP, rad	Plastic rotation capacity, rad CP
CB1a	-	VARIABLES	-	VARIABLES
CB2a	0.00008	VARIABLES	-	VARIABLES
CB3a	-	VARIABLES	0.00051	VARIABLES
CB4a	-	VARIABLES	-	VARIABLES
CB5a	-	VARIABLES	-	VARIABLES
CB1b	-	VARIABLES	-	VARIABLES
CB2b	-	VARIABLES	0.00059	VARIABLES
CB3b	-	VARIABLES	0.00051	VARIABLES
CB4b	0.00010	VARIABLES	0.00111	VARIABLES
CB5b	-	VARIABLES	-	VARIABLES

CB(storey no.)a- central beam for selected storey at end a
 CB(storey no.)b- central beam for selected storey at end b

Table 40. Mean values for plastic rotation at CP for central beams (stiff soil)

At SLS the structure with dampers avoids almost completely the formation of plastic hinges in braces. At ULS the structure with dampers has lower values of axial plastic deformation in braces in compression but with slightly higher values for the braces in tension. At CP the structure with dampers has higher values of plastic deformation/rotation in elements. All plastic deformations/rotations satisfy the acceptance criteria at all levels. In the following paragraph a relevant example for the 7 seismic motions characteristic to stiff soil will be presented and discussed in detail. The CBF structure will be presented comparatively with and without dampers at (i). SLS with $a_{g,SLS} = 0.5 \cdot a_{g,ULS}$, (ii) ULS with $a_{g,ULS}$ and (iii) CP with $a_{g,CP} = 1.5 \cdot a_{g,ULS}$.

(i) SLS with $a_{g,SLS} = 0.5 \cdot a_{g,ULS}$ characteristic for stiff soil type ($T_c=0.5s$)

Plastic hinge formation in the structure with and without damper is presented in Fig. 4.28.

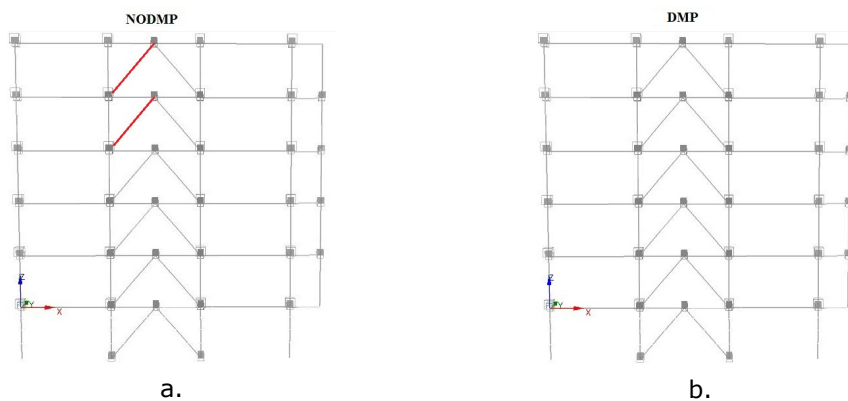


Fig. 4.28. Plastic hinge formation for CBF: a) without dampers; b) with dampers at SLS

For this level of seismic action the building with dampers does not form any

plastic hinges in braces while the building without dampers forms plastic hinges in the bracing with values of plastic deformation that satisfy the acceptance criteria for immediate occupancy (IO) from FEMA356 [10] (Table 41). The values of permanent top displacement are very close with values slightly higher for the structure with dampers (Fig. 4.34).

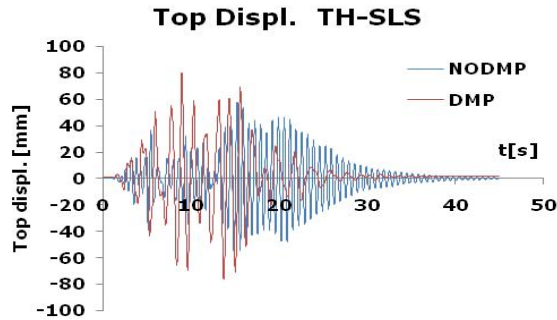


Fig. 4.29. Recorded top displacement in time for the CBF structure at SLS (stiff soil)

BRACE Compr. LOC.	Plastic deformation demand- SLS , mm		Plastic deformation capacity, mm
	NODMP	DMP	IO
BR4L	0.080	-	1.1225
BR5L	0.124	-	0.99125
BR(storey no.)R- right brace for selected storey			
BR(storey no.)L- left brace for selected storey			

Table 41. Axial plastic deformation values for compression braces at SLS (stiff soil)

(ii) ULS with $a_{g,ULS}$ characteristic for stiff soil type ($T_C=0.5s$)

Plastic hinge formation in the structure with and without damper is presented in Fig. 4.30.

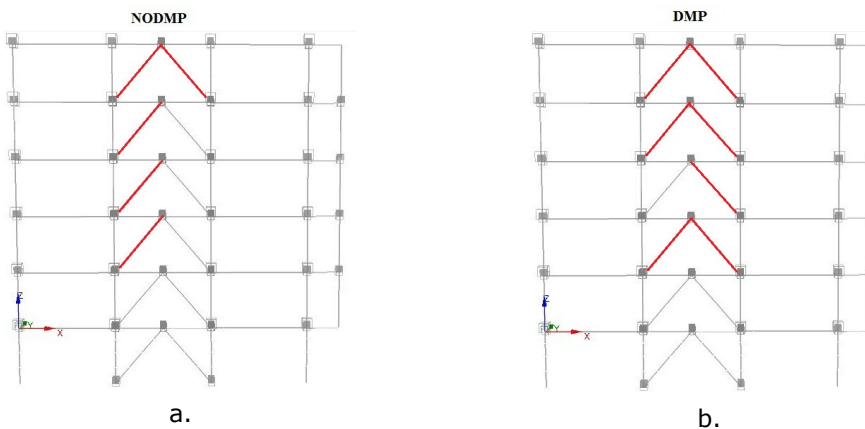


Fig. 4.30. Plastic hinge formation for CBF: a) without dampers; b) with dampers at ULS

At ULS both frames with and without dampers form plastic hinges in braces. At this level the structures have a similar behaviour with similar values of plastic deformation/rotation in elements. No plastic rotations of the central beams are recorded for either structure. All plastic deformations satisfy the acceptance criteria corresponding to life safety (LS) from FEMA 356 [10]. The structure with dampers has lower values of permanent top displacement than the structure without dampers (Fig. 4.36). Specific values of axial plastic deformation recorded for braces in tension, compression and plastic rotation of central beams are presented in Table 42, Table 43 and Table 44 respectively.

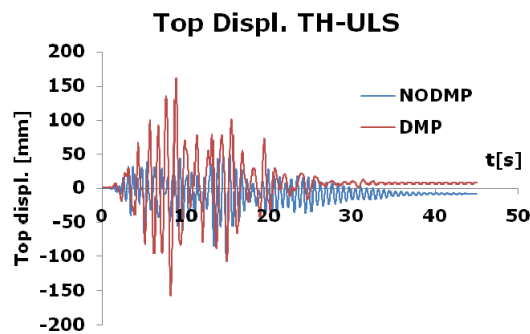


Fig. 4.31. Recorded top displacement in time for the CBF structure at ULS (stiff soil)

BRACE Compr.	Plastic deformation demand- ULS , mm		Plastic deformation capacity, mm LS
	NODMP	DMP	
LOC.			
BR2L	1.403	0.464	22.45
BR2R	-	2.032	22.45
BR3L	1.887	-	19.825
BR3R	-	1.147	19.825
BR4L	1.984	1.122	17.89
BR4R	-	1.006	17.89
BR5L	1.293	1.046	13.84
BR5R	0.033	1.218	13.84
BR(storey no.)R- right brace for selected storey			
BR(storey no.)L- left brace for selected storey			

Table 42. Axial plastic deformation for braces in compression at ULS (stiff soil)

BRACE Tension.	Plastic deformation demand- ULS , mm		Plastic deformation capacity, mm LS
	NODMP	DMP	
LOC.			
BR3L	0.142	-	39.97
BR5R	-	0.508	39.039
BR(storey no.)R- right brace for selected storey			
BR(storey no.)L- left brace for selected storey			

Table 43. Axial plastic deformation for braces in tension at ULS (stiff soil)

BEAM	NODMP		DMP	
LOC.	Plastic rotation demand-ULS, rad	Plastic rotation capacity, rad LS	Plastic rotation demand-ULS, rad	Plastic rotation capacity, rad LS
No plastic rotation				
CB(storey no.)a- central beam for selected storey				
CB(storey no.)b- central beam for selected storey				

Table 44. Plastic rotation at ULS for central beams (stiff soil)

(iii) CP with $a_{g,CP} = 1.5 \cdot a_{g,ULS}$ characteristic for stiff soil type ($T_c=0.5s$)

Plastic hinge formation in the structure with and without damper is presented in Fig. 4.32.

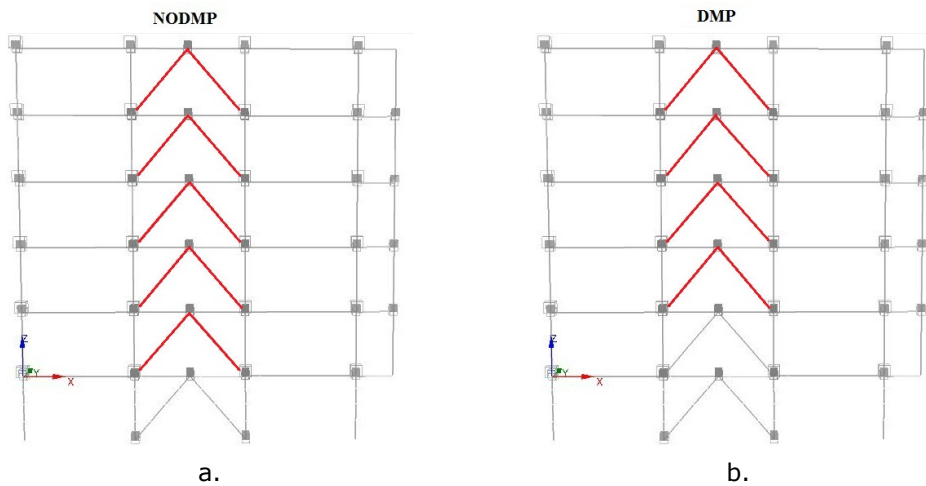


Fig. 4.32. Plastic hinge formation in the structure with and without damper at CP (soft soil)

At CP both frames with and without dampers form plastic hinges in braces and central beams. Structure with dampers has lower values of plastic axial deformation for compression braces and slightly higher for tension braces than the structure without dampers. No plastic rotations of the central beams are recorded for either structure with slightly lower values of permanent top displacement for the structure with dampers (Fig. 4.38). All plastic deformations satisfy the acceptance criteria corresponding to collapse prevention (CP) from FEMA 356 [10]. Specific values of axial plastic deformation recorded for braces in tension, compression and plastic rotation of central beams are presented in Table 45, Table 46 and Table 47 respectively.

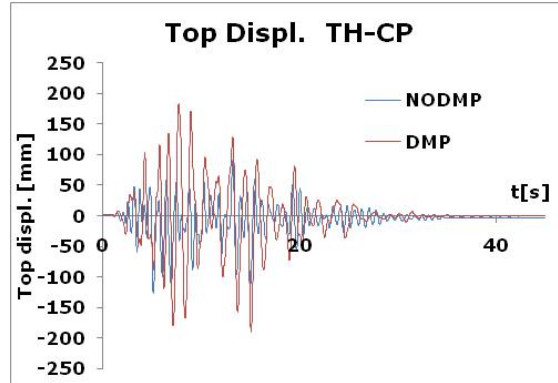


Fig. 4.33. Recorded top displacement in time for the CBF structure at ULS (stiff soil)

BRACE Compr.	Plastic deformation demand-CP , mm		Plastic deformation capacity, mm
	NODMP	DMP	
BR1L	2.182	-	31.43
BR1R	0.427	-	31.43
BR2L	3.343	1.091	31.43
BR2R	-	2.263	31.43
BR3L	2.764	2.306	27.755
BR3R	0.487	2.054	27.755
BR4L	2.592	2.112	25.046
BR4R	0.874	1.843	25.046
BR5L	2.037	1.666	19.376
BR5R	0.844	2.196	19.376
BR(storey no.)R- right brace for selected storey			
BR(storey no.)L- left brace for selected storey			

Table 45. Axial plastic deformation for braces in compression at CP (stiff soil)

BRACE Tension.	Plastic deformation demand-CP , mm		Plastic deformation capacity, mm
	NODMP	DMP	
BR1L	0.346	-	51.7221
BR1R	-	-	51.7221
BR2L	3.486	-	51.7221
BR2R	0.741	-	51.7221
BR3L	1.019	3.756	51.39
BR3R	-	2.495	51.39
BR4L	0.530	4.723	50.76
BR4R	-	5.829	50.76
BR5L	-	2.706	50.193
BR5R	-	4.722	50.193
BR(storey no.)R- right brace for selected storey			
BR(storey no.)L- left brace for selected storey			

Table 46. Axial plastic deformation for braces in tension at CP (stiff soil)

BEAM	NODMP		DMP	
LOC.	Plastic rotation demand-CP, rad	Plastic rotation capacity, rad CP	Plastic rotation demand-CP, rad	Plastic rotation capacity, rad CP
No plastic rotation				
CB(storey no.)a- central beam for selected storey				
CB(storey no.)b- central beam for selected storey				

Table 47. Plastic rotation at CP for central beams (stiff soil)

The second set of numerical analyses showed that the frame equipped with dampers has a better performance avoiding the formation of plastic hinges at SLS and reducing the values of permanent displacement and reducing the number of plastic hinges in elements. The conclusion is that this particular type of damper is efficient in reducing the seismic response of a building for earthquakes characterized by short corner period $T_c=0.5s$ (stiff soil).

4.4 Dual Frame with and without Dampers

4.4.1 Geometry and Design

The dual frame has the same geometry in plan and elevation with the CBF frame presented in 4.3.1. It consists of 3 equal spans of 6m with a storey height of 3.5m having a centrally braced frame (CBF) in the mid-span and two moment resisting frames (MRF) in the first and third spans (Fig. 4.34). The frame was design according to EC3[30] and EC8[7] with some special considerations from the Romanian seismic design code P100/2006[1] considering the design spectra for Bucharest with a corner period of $T_c=1.6s$ and peak ground acceleration $a_g=0.24g$.

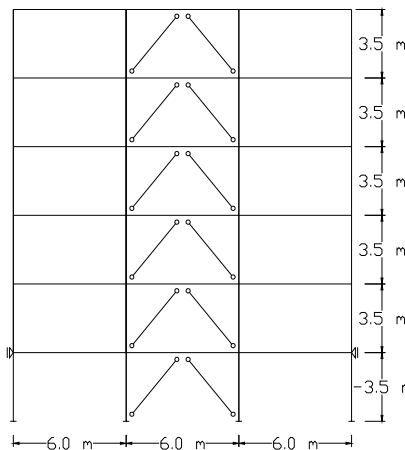


Fig. 4.34. Frame geometry of dual CBF+MRF frame

Considered loads were the same as the ones considered for the CBF frame:

- Permanent load: $p = 10.75 \text{ kN/m}$ from bay, $P = 60 \text{ kN}$ from secondary beams;
- Live load: $q = 3 \text{ kN/m}$ from bay, $Q = 36 \text{ kN}$ from secondary beams;
- Seismic load: design spectra for Bucharest with a corner period of $T_C = 1.6 \text{ s}$ (Fig. 4.40) with behaviour factor $q = 3$ (high ductility class) and $\Omega \leq q = 3$.

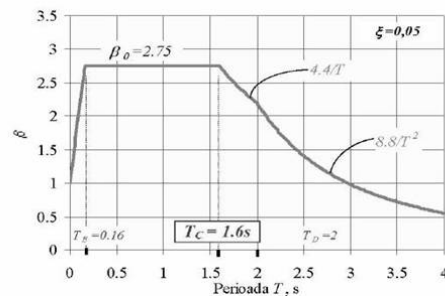


Fig. 4.35. Design spectra for Bucharest

The computed mass at each level for spectral and modal analysis is $m = 113.3t$ for levels 1 through 4 and $m = 106.7t$ for the top level.

Load combinations:

- ULS base: $1.35G + 1.5Q$
- SLS base: $1.0G + 1.0Q$
- ULS special-dissipative elements: $1.0G + E + 0.4Q$
- ULS special-non-dissipative elements: $1.0G + \Omega E + 0.4Q$
- SLS special: $1.0G + q \cdot vE + 0.4Q$

Global imperfections were added as equivalent horizontal loads $H = \phi V$ added to all load cases with the values $H = 1.981 \text{ kN}$ for levels 1 through 4 and $H = 1.815 \text{ kN}$ for the top level. In addition $P\Delta$ effects were modelled with the help of a lean-on column connected with rigid diaphragm at each level loaded with the corresponding area of the secondary frame $V = 864 \text{ kN}$. In addition MRF frames were designed to ensure 25% lateral load carrying capacity. The same 2% damping was considered as for the previous frame.

The final section dimensions are presented in Fig. 4.36.

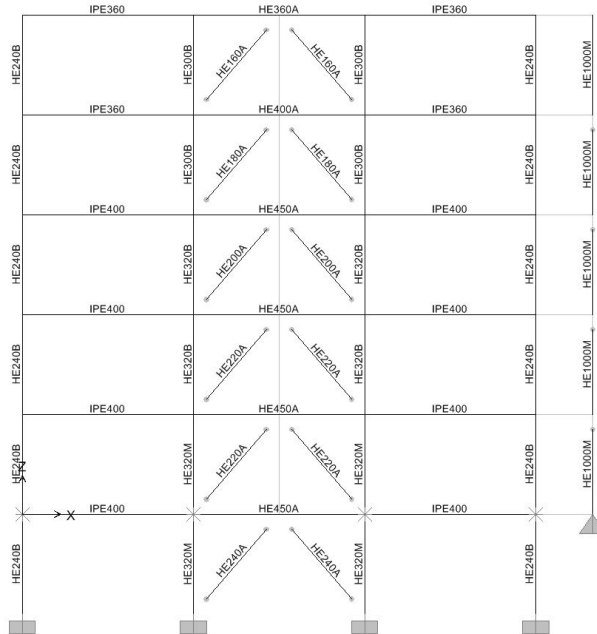


Fig. 4.36. Section dimensions of the dual frame

4.4.2 Numerical Analysis on Dual Frame with and without Dampers

The analysis procedure is identical to the one used for the CBF consisting of nonlinear dynamic analysis using the same two sets of 7 seismic motions scaled on the response spectra for soft soil ($T_C=1.6s$) and stiff soil ($T_C=0.5s$) presented in 4.3.2. Three performance levels were considered for each seismic motion having an acceleration multiplier of 0.5, 1.0, 1.5 corresponding to serviceability limit state (SLS), ultimate limit state (ULS) and collapse prevention (CP):

- SLS $\rightarrow a_{g,SLS} = 0.5 \cdot a_{g,ULS}$
- ULS $a_{g,ULS}$
- CP $\rightarrow a_{g,CP} = 1.5 \cdot a_{g,ULS}$

4.4.2.1 TH Analysis of Dual CBF+MRF Structure for Soft Soil Type ($T_C=1.6s$)

Performance criteria followed was (i) plastic axial deformation in braces and (ii) plastic rotation for beams and column.

- (i) Plastic axial deformation in the braces with displacement at yield Δ_y and at buckling Δ_c computed from individual single brace models using pushover analysis as follows (Table 48):

Brace	Compression Δ_c [mm]	Tension Δ_y [mm]
HEA220	3.965	5.71
HEA200	3.578	5.64
HEA180	3.207	5.585
HEA160	2.76	5.57

Table 48. Displacement at buckling and yield for compression and tension braces

(ii) Plastic rotation for beams and columns having rotation at yield θ_y computed as:

- Columns:

$$\theta_y = \frac{Z \cdot F_{ye} \cdot l_c}{6EI_c} \left(1 - \frac{P}{P_{ye}} \right) \quad [10];$$

- Central beams (computed as columns):

$$\theta_y = \frac{Z \cdot F_{ye} \cdot l_B}{6EI_B} \left(1 - \frac{P}{P_{ye}} \right) \quad [10];$$

- MRF beams:

$$\theta_y = \frac{Z \cdot F_{ye} \cdot l_B}{6EI_B} \quad [10].$$

where:

Z = Plastic section modulus (W_{pl})

F_{ye} = expected yield strength of material

l_c, l_B = element length for column and beam respectively

P = axial force at instant of calculation

P_{ye} = expected axial yield force of member

E = modulus of elasticity

I_c, I_B = moment of inertia for column and beam respectively.

Maximum drift levels (Fig. 4.37), maximum drift at each storey (Fig. 4.38) and top displacement for the structure (Fig. 4.39) without dampers are presented as mean values of recorded values for all 7 seismic motions at levels corresponding to SLS, ULS and CP in comparison with the same values recorded for the structure with dampers in the braces.

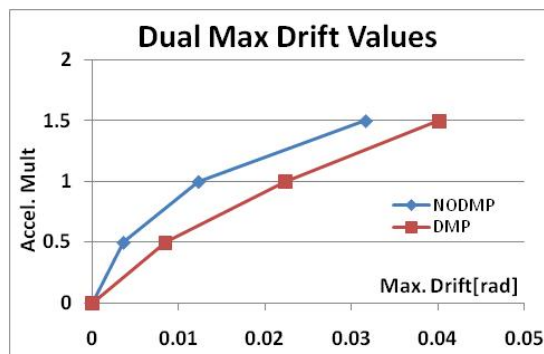


Fig. 4.37. Maximum drift values for the dual structure with and without dampers

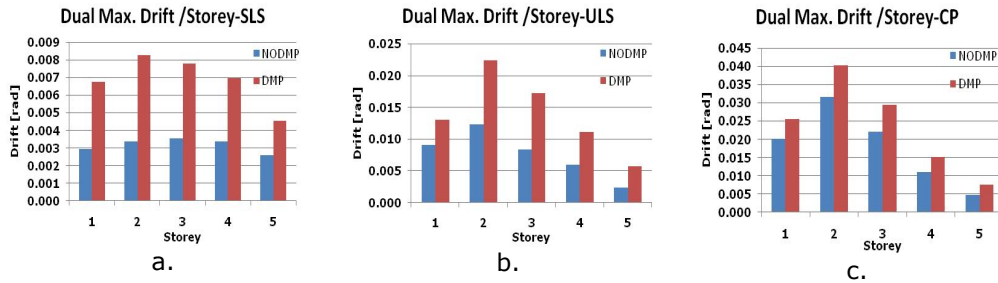


Fig. 4.38. Maximum drift at each storey at: a) SLS; b) ULS; c) CP for the dual structure with and without dampers

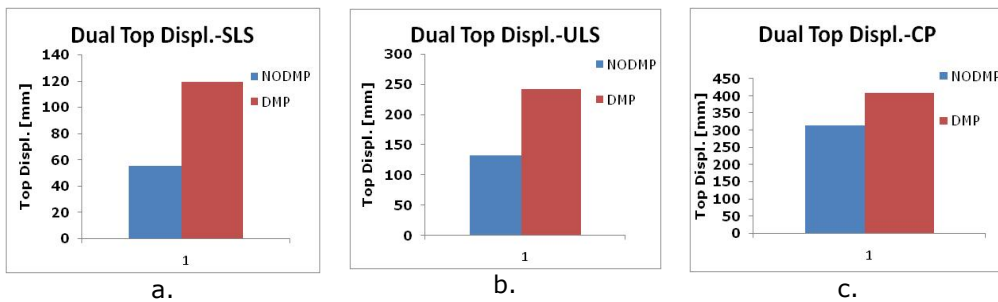


Fig. 4.39. Top displacement at: a) SLS; b) ULS; c) CP for the dual structure with and without dampers

At the end of each seismic recording used the structure was left to vibrate freely for 10s. Recorded values of permanent displacement at top of the structure are presented as mean values for all 7 recordings in Fig. 4.40.

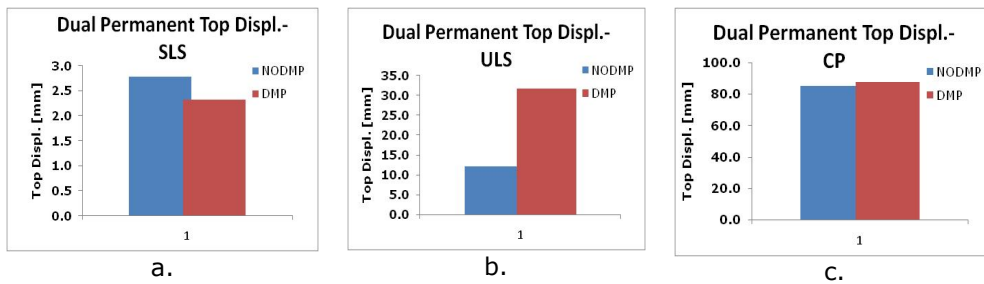


Fig. 4.40. Permanent top displacement at: a) SLS; b) ULS; c) CP for the structure with and without dampers

The behaviour recorded for the dual frame was similar to that of the simple CBF. For all 7 recorded seismic motion characteristic for soft soil type used the results showed that for all performance levels the building with dampers exhibited a significant increase in drift for all 5 storeys and higher values of permanent displacement at the top of the structure at ULS and CP. Values of

plastic axial deformations and plastic rotations for all recordings are presented here as mean value for all 7 seismic recordings at (i)SLS with $a_{g,SLS} = 0.5 \cdot a_{g,ULS}$ (Table 49, Table 50, Table 51), (ii)ULS with $a_{g,ULS}$ (Table 52, Table 53, Table 54, Table 55, Table 56) and (iii)CP with $a_{g,CP} = 1.5 \cdot a_{g,ULS}$ (Table 57, Table 58, Table 59, Table 60, Table 61, Table 62).

(i) SLS with $a_{g,SLS} = 0.5 \cdot a_{g,ULS}$ characteristic for soft soil type ($T_C=1.6s$)

BRACE Compr.	Plastic deformation demand- SLS , mm		Plastic deformation capacity, mm
	NODMP	DMP	
LOC.			IO
BR1L	0.269	0.096	0.99125
BR1R	0.371	0.072	0.99125
BR2L	0.329	0.838	0.99125
BR2R	0.432	0.735	0.99125
BR3L	0.498	0.657	0.8945
BR3R	0.360	0.378	0.8945
BR4L	0.337	0.783	0.80175
BR4R	0.220	0.096	0.80175
BR5L	-	0.114	0.692
BR5R	-	-	0.692
BR(storey no.)R- right brace for selected storey			
BR(storey no.)L- left brace for selected storey			

Table 49. Mean values of axial plastic deformation for braces in compression at SLS

BRACE Tension	Plastic deformation demand- SLS , mm		Plastic deformation capacity, mm
	NODMP	DMP	
LOC.			IO
No plastic deformation			
BR(storey no.)R- right brace for selected storey			
BR(storey no.)L- left brace for selected storey			

Table 50. Mean values of axial plastic deformation for braces in tension at SLS

BEAM	NODMP		DMP	
	Plastic rotation demand- ULS, rad	Plastic rotation capacity, rad LS	Plastic rotation demand-ULS, rad	Plastic rotation capacity, rad LS
LOC.				
No plastic rotation in elements				
CB(storey no.)a- central beam for selected storey at end a				
CB(storey no.)b- central beam for selected storey at end b				

Table 51. Mean values for plastic rotation at SLS for central beams (soft soil)

(ii) ULS with $a_{g,ULS}$ characteristic for soft soil type ($T_C=1.6s$)

BRACE Compr.	Plastic deformation demand- ULS , mm		Plastic deformation capacity, mm
	NODMP	DMP	
LOC.			LS
BR1L	1.953	1.586	19.825
BR1R	1.825	1.485	19.825
BR2L	1.687	2.374	19.825
BR2R	1.464	2.126	19.825
BR3L	1.282	1.838	17.89
BR3R	1.093	1.084	17.89
BR4L	0.985	1.751	16.035
BR4R	0.508	1.247	16.035
BR5L	0.114	0.877	13.84
BR5R	0.126	0.380	13.84
BR(storey no.)R- right brace for selected storey			
BR(storey no.)L- left brace for selected storey			

Table 52. Mean values of axial plastic deformation for braces in compression at ULS

BRACE Tension.	Plastic deformation demand- ULS , mm		Plastic deformation capacity, mm
	NODMP	DMP	
LOC.			LS
BR1L	1.764	0.638	39.991
BR1R	3.859	1.046	39.991
BR2L	3.639	4.862	39.991
BR2R	6.713	6.135	39.991
BR3L	0.003	3.344	39.48
BR3R	0.038	5.978	39.48
BR4L	-	0.812	39.095
BR4R	-	0.892	39.095
BR5L	-	-	39.039
BR5R	-	-	39.039
BR(storey no.)R- right brace for selected storey			
BR(storey no.)L- left brace for selected storey			

Table 53. Mean values of axial plastic deformation for braces in tension at ULS

BEAM	NODMP		DMP	
LOC.	Plastic rotation demand-ULS, rad	Plastic rotation capacity, rad LS	Plastic rotation demand-ULS, rad	Plastic rotation capacity, rad LS
CB1a	0.00040	VARIES	0.00470	VARIES
CB2a	-	VARIES	0.00076	VARIES
CB3a	-	VARIES	-	VARIES
CB4a	-	VARIES	-	VARIES
CB5a	-	VARIES	-	VARIES
CB1b	0.00105	VARIES	0.00264	VARIES
CB2b	-	VARIES	0.00066	VARIES
CB3b	-	VARIES	-	VARIES
CB4b	-	VARIES	-	VARIES
CB5b	-	VARIES	-	VARIES
CB(storey no.)a- central beam for selected storey at end a				
CB(storey no.)b- central beam for selected storey at end b				

Table 54. Mean values for plastic rotation at ULS for central beams

BEAM MRF	NODMP		DMP	
LOC.	Plastic rotation demand-ULS, rad	Plastic rotation capacity, rad LS	Plastic rotation demand-ULS, rad	Plastic rotation capacity, rad LS
B1L	0.00088	0.0191	0.00678	0.0191
B2L	0.00050	0.0191	0.01004	0.0191
B3L	-	0.0191	0.00098	0.0191
B4L	-	0.0211	0.00009	0.0211
B5L	-	0.0211	-	0.0211
B1R	0.00277	0.0191	0.00853	0.0191
B2R	0.00124	0.0191	0.01156	0.0191
B3R	-	0.0191	0.00266	0.0191
B4R	-	0.0211	0.00017	0.0211
B5R	-	0.0211	-	0.0211
B(storey no.)L- left MRF frame beam for selected storey				
B(storey no.)R- right MRF frame beam for selected storey				

Table 55. Mean values for plastic rotation at ULS for MRF beams

COLUMN	NODMP		DMP	
LOC.	Plastic rotation demand-ULS, rad	Plastic rotation capacity, rad LS	Plastic rotation demand-ULS, rad	Plastic rotation capacity, rad LS
CC1L	-	VARIES	-	VARIES
CC2L	-	VARIES	0.00336	VARIES
CC3L	-	VARIES	0.00446	VARIES
CC4L	-	VARIES	-	VARIES

CC5L	-	VARIES	-	VARIES
CC1R	-	VARIES	0.00207	VARIES
CC2R	-	VARIES	-	VARIES
CC3R	-	VARIES	-	VARIES
CC4R	-	VARIES	-	VARIES
CC5R	-	VARIES	-	VARIES
CC(storey no.)L- left central column for selected storey				
CC(storey no.)R- right central column for selected storey				

Table 56. Mean values for plastic rotation at ULS for central columns

(iii) CP with $a_{g,CP} = 1.5 \cdot a_{g,ULS}$ characteristic for soft soil type ($T_C = 1.6s$)

BRACE Compr.	Plastic deformation demand-CP , mm		Plastic deformation capacity, mm
	NODMP	DMP	
LOC.			CP
BR1L	2.100	2.192	27.755
BR1R	2.390	2.339	27.755
BR2L	1.966	2.961	27.755
BR2R	2.324	2.236	27.755
BR3L	1.422	1.784	25.046
BR3R	1.547	1.772	25.046
BR4L	1.585	2.253	22.449
BR4R	1.133	1.341	22.449
BR5L	0.286	1.354	19.376
BR5R	0.329	0.774	19.376
BR(storey no.)R- right brace for selected storey			
BR(storey no.)L- left brace for selected storey			

Table 57. Mean values of axial plastic deformation for braces in compression at CP

BRACE Tension.	Plastic deformation demand-CP , mm		Plastic deformation capacity, mm
	NODMP	DMP	
LOC.			CP
BR1L	11.927	6.883	51.417
BR1R	10.895	4.433	51.417
BR2L	19.780	18.833	51.417
BR2R	19.766	18.171	51.417
BR3L	0.184	15.371	50.76
BR3R	0.211	14.920	50.76
BR4L	0.000	2.455	50.265
BR4R	0.036	2.043	50.265
BR5L	-	-	50.193
BR5R	-	0.032	50.193
BR(storey no.)R- right brace for selected storey			
BR(storey no.)L- left brace for selected storey			

Table 58. Mean values of axial plastic deformation for braces in tension at CP

BEAM	NODMP		DMP	
LOC.	Plastic rotation demand-CP, rad	Plastic rotation capacity, rad CP	Plastic rotation demand-CP, rad	Plastic rotation capacity, rad CP
CB1a	0.01159	VARIES	0.01991	VARIES
CB2a	0.00643	VARIES	0.01379	VARIES
CB3a	-	VARIES	-	VARIES
CB4a	-	VARIES	-	VARIES
CB5a	-	VARIES	-	VARIES
CB1b	0.01557	VARIES	0.01383	VARIES
CB2b	0.00757	VARIES	0.01371	VARIES
CB3b	-	VARIES	0.00308	VARIES
CB4b	-	VARIES	0.00051	VARIES
CB5b	-	VARIES	-	VARIES
CB(storey no.)a- central beam for selected storey				
CB(storey no.)b- central beam for selected storey				

Table 59. Mean values for plastic rotation at CP for central beams

BEAM MRF	NODMP		DMP	
LOC.	Plastic rotation demand-CP, rad	Plastic rotation capacity, rad CP	Plastic rotation demand-CP, rad	Plastic rotation capacity, rad CP
B1L	0.01845	0.0286	0.02583	0.0286
B2L	0.02308	0.0286	0.03366	0.0286
B3L	0.00396	0.0286	0.00995	0.0286
B4L	-	0.0317	0.00074	0.0317
B5L	-	0.0317	-	0.0317
B1R	0.01806	0.0286	0.02418	0.0286
B2R	0.02236	0.0286	0.03357	0.0286
B3R	0.00451	0.0286	0.00841	0.0286
B4R	-	0.0317	0.00134	0.0317
B5R	-	0.0317	-	0.0317
B(storey no.)L- left MRF frame beam for selected storey				
B(storey no.)R- right MRF frame beam for selected storey				

Table 60. Mean values for plastic rotation at CP for MRF beams

COLUMN	NODMP		DMP	
LOC.	Plastic rotation demand-CP, rad	Plastic rotation capacity, rad CP	Plastic rotation demand-CP, rad	Plastic rotation capacity, rad CP
CC1L	0.00696	VARIES	0.00711	VARIES
CC2L	0.00832	VARIES	0.02922	VARIES
CC3L	0.01601	VARIES	0.01973	VARIES
CC4L	0.00013	VARIES	0.00101	VARIES
CC5L	-	VARIES	-	VARIES
CC1R	0.00202	VARIES	0.01482	VARIES

CC2R	0.01541	VARIES	0.02492	VARIES
CC3R	0.01317	VARIES	0.01727	VARIES
CC4R	-	VARIES	0.00157	VARIES
CC5R	-	VARIES	-	VARIES
CC(storey no.)L- left central column for selected storey				
CC(storey no.)R- right central column for selected storey				

Table 61. Mean values for plastic rotation at CP for central columns

COLUMN	NODMP		DMP	
	Plastic rotation demand-CP, rad	Plastic rotation capacity, rad CP	Plastic rotation demand-CP, rad	Plastic rotation capacity, rad CP
C1L	0.00648	VARIES	0.00734	VARIES
C2L	-	VARIES	-	VARIES
C3L	-	VARIES	-	VARIES
C4L	-	VARIES	-	VARIES
C5L	-	VARIES	-	VARIES
C1R	0.00540	VARIES	0.00709	VARIES
C2R	-	VARIES	-	VARIES
C3R	-	VARIES	-	VARIES
C4R	-	VARIES	-	VARIES
C5R	-	VARIES	-	VARIES
C(storey no.)L- left MRF column for selected storey				
C(storey no.)R- right MRF column for selected storey				

Table 62. Mean values for plastic rotation at CP for MRF columns

At all levels of seismic motion the structure with dampers has a higher number of plastic hinges in elements with significant increase in values of plastic axial deformations and rotations than the structure without dampers. At SLS the structure with dampers already forms plastic hinges in braces that do not satisfy the criteria for IO. At ULS the structure with dampers forms plastic hinges in central beams that are considered non-dissipative elements. At CP the behaviour of the two structures with and without dampers is similar and is considered unsatisfactory due to the formation of plastic hinges in several central columns with values that do not satisfy the acceptance criteria. In the following paragraph a relevant example for the 7 seismic motions characteristic to soft soil will be presented and discussed in detail.. The dual MRF+CBF structure will be presented comparatively with and without dampers at (i). SLS with $a_{g,SLS} = 0.5 \cdot a_{g,ULS}$, (ii) ULS with $a_{g,ULS}$ and (iii) CP with $a_{g,CP} = 1.5 \cdot a_{g,ULS}$.

(i) SLS with $a_{g,SLS} = 0.5 \cdot a_{g,ULS}$ characteristic for soft soil type ($T_C=1.6s$)

Plastic hinge formation in the structure with and without damper is presented in Fig. 4.41.

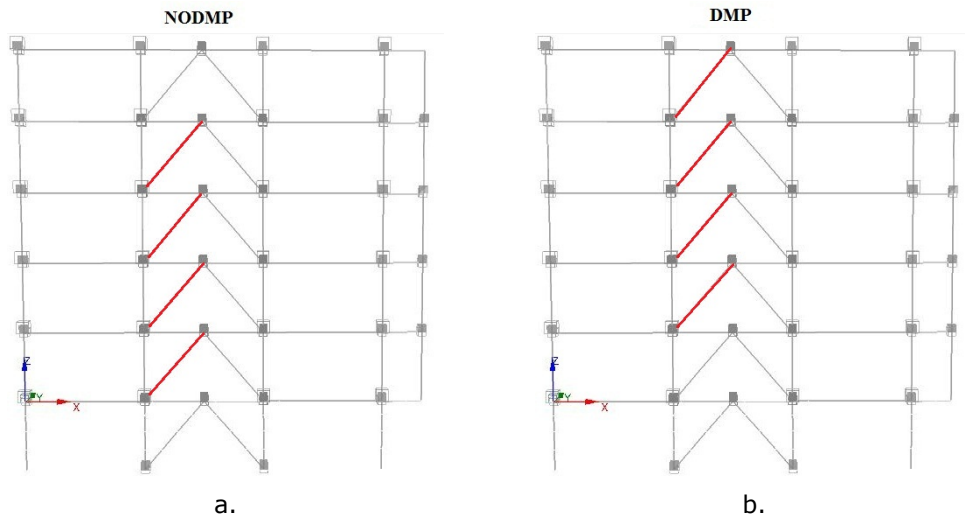


Fig. 4.41. Plastic hinge formation for dual MRF+CBF structure: a) without dampers; b) with dampers at SLS

For this performance level both structures form plastic hinges in braces under compression with the values of axial plastic deformation in the case of the structure with dampers exceeding the acceptance criteria for immediate occupancy (IO) from FEMA356 [10] (Table 63). The structure with dampers has a higher value of permanent displacement at the top of the structure compared to the structure without dampers (Fig. 4.42).

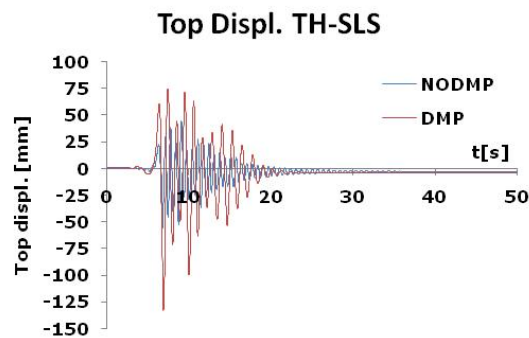


Fig. 4.42. Recorded top displacement in time for the dual MRF+CBF structure at SLS (soft soil)

BRACE Compr. LOC.	Plastic deformation demand- SLS , mm		Plastic deformation capacity, mm
	NODMP	DMP	IO
BR1L	0.901	-	0.991
BR1R	-	-	0.991
BR2L	0.861	1.625	0.991
BR2R	-	-	0.991
BR3L	0.690	1.470	0.894
BR3R	-	-	0.894
BR4L	0.363	1.765	0.801
BR4R	-	-	0.801
BR5L	-	0.577	0.692
BR5R	-	-	0.692
BR(storey no.)R- right brace for selected storey			
BR(storey no.)L- left brace for selected storey			

Table 63. Axial plastic deformation values for compression braces at SLS (soft soil)

No plastic axial deformation is recorded in tension braces at this level.

(ii) ULS with $a_{g,ULS}$ characteristic for soft soil type ($T_C=1.6s$)

Plastic hinge formation in the structure with and without damper is presented in Fig. 4.43.

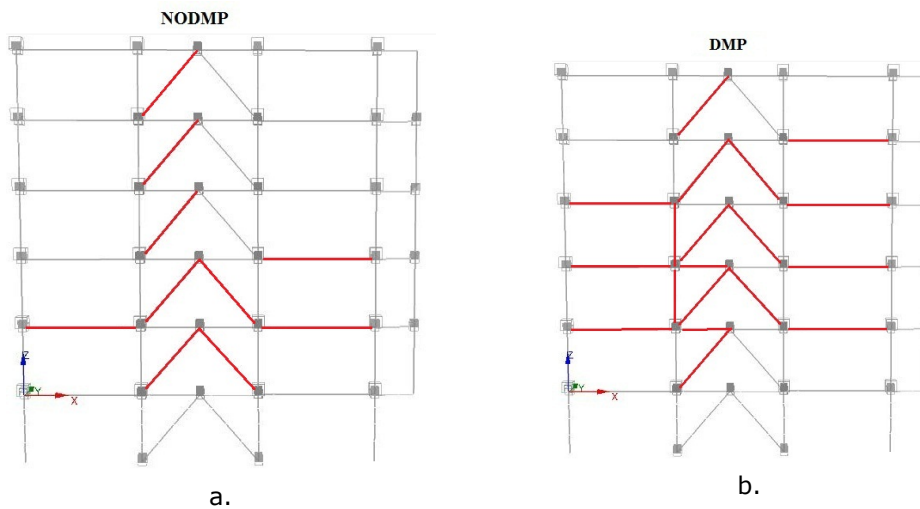


Fig. 4.43. Plastic hinge formation for dual MRF+CBF structure: a) without dampers; b) with dampers at ULS

At ULS both frames with and without dampers form plastic hinges in braces. At this level the structure with dampers has a higher number of plastic hinges in elements and a higher value of plastic deformation/rotation in elements than the structure without dampers. Plastic rotations for the central beams and columns are recorded only for the frame with dampers. All plastic axial deformations and plastic rotations for central beams and MRF beams satisfy the acceptance criteria corresponding to life safety (LS) from FEMA 356[10]. In addition the structure with dampers has a significantly higher value of

permanent displacement at the top of the structure compared to the structure without dampers (Fig. 4.44). Specific values of axial plastic deformation recorded for braces in tension, compression and plastic rotation of central beams and MRF beams are presented in Table 64, Table 65, Table 66 and Table 67 respectively. The performance of the structure with dampers is considered unsatisfactory due to the formation of plastic hinges in central columns that no longer satisfy the acceptance criteria (Table 68).

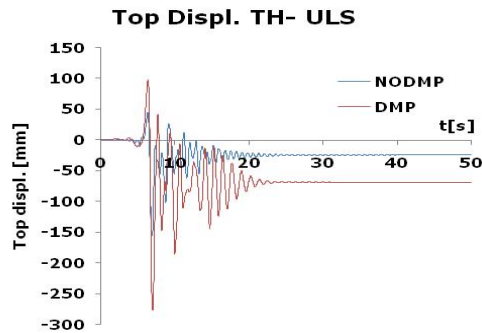


Fig. 4.44. Recorded top displacement in time for the dual MRF+CBF structure at ULS (soft soil)

BRACE Compr.	Plastic deformation demand- ULS , mm		Plastic deformation capacity, mm
	NODMP	DMP	
LOC.			LS
BR1L	2.378	2.985	19.825
BR1R	0.545	-	19.825
BR2L	2.503	3.352	19.825
BR2R	-	-	19.825
BR3L	1.904	2.304	17.89
BR3R	-	-	17.89
BR4L	1.912	2.375	16.035
BR4R	-	-	16.035
BR5L	0.709	2.681	13.84
BR5R	-	-	13.84
BR(storey no.)R- right brace for selected storey			
BR(storey no.)L- left brace for selected storey			

Table 64. Axial plastic deformation for braces in compression at ULS (soft soil)

BRACE Tension	Plastic deformation demand- ULS , mm		Plastic deformation capacity, mm
	NODMP	DMP	
LOC.			LS
BR1R	5.747	-	39.991
BR2R	13.723	13.262	39.991
BR3R	-	12.120	39.48
BR4R	-	1.176	39.095
BR(storey no.)R- right brace for selected storey			
BR(storey no.)L- left brace for selected storey			

Table 65. Axial plastic deformation for braces in tension at ULS (soft soil)

BEAM	NODMP		DMP	
LOC.	Plastic rotation demand-ULS, rad	Plastic rotation capacity, rad LS	Plastic rotation demand-ULS, rad	Plastic rotation capacity, rad LS
CB1a	-	-	0.00942	0.0154
CB2a	-	-	0.00181	0.0153
CB(storey no.)a- central beam for selected storey at end a				
CB(storey no.)b- central beam for selected storey at end b				

Table 66. Plastic rotation at ULS for central beams (soft soil)

BEAM MRF	NODMP		DMP	
LOC.	Plastic rotation demand-ULS, rad	Plastic rotation capacity, rad LS	Plastic rotation demand-ULS, rad	Plastic rotation capacity, rad LS
B1L	0.0006	0.0191	0.00692	0.0191
B2L		0.0191	0.0125	0.0191
B3L		0.0191	0.00129	0.0191
B4L		0.0211		0.0211
B5L		0.0211		0.0211
B1R	0.00644	0.0191	0.0116	0.0191
B2R	0.00355	0.0191	0.0160	0.0191
B3R		0.0191	0.0048	0.0191
B4R		0.0211	0.0011	0.0211
B5R		0.0211		0.0211
B(storey no.)L- left MRF frame beam for selected storey				
B(storey no.)R- right MRF frame beam for selected storey				

Table 67. Plastic rotation at ULS for MRF beams (soft soil)

COLUMN	NODMP		DMP	
LOC.	Plastic rotation demand-ULS, rad	Plastic rotation capacity, rad ULS	Plastic rotation demand-ULS, rad	Plastic rotation capacity, rad ULS
CC2L	-	-	0.0235	0.00253
CC3L	-	-	0.0165	0.00288
CC(storey no.)L- left central column for selected storey				
CC(storey no.)R- right central column for selected storey				

Table 68. Plastic rotation at ULS for central columns (soft soil)

(iii) CP with $a_{g,CP} = 1.5 \cdot a_{g,ULS}$ characteristic for soft soil type ($T_c=1.6s$)

Plastic hinge formation in the structure with and without damper is presented in Fig. 4.45.

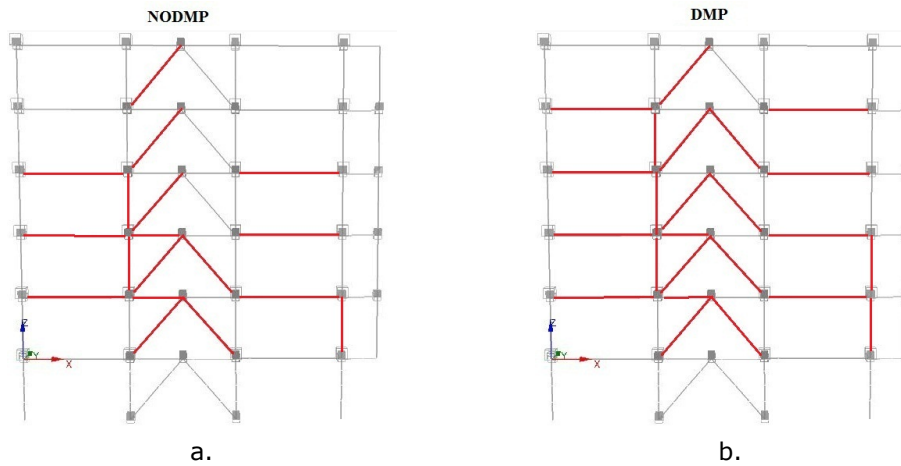


Fig. 4.45. Plastic hinge formation in the structure with and without damper at CP (soft soil)

At CP both frames with and without dampers form plastic hinges in braces, central beams, MRF beams and central columns. Similar to previous levels of seismic motion the structure with dampers has a higher number of plastic hinges in elements and a higher value of plastic deformation/rotation in elements than the structure without dampers. Plastic rotations for the central beams, MRF beams of the structure with dampers no longer satisfy the acceptance criteria corresponding to collapse prevention (CP) from FEMA 356[10]. The structure with dampers has a higher value of permanent displacement at the top of the structure compared to the structure without dampers (Fig. 4.46). Specific values of axial plastic deformation recorded for braces in tension, compression and plastic rotation of central beams and MRF beams are presented in Table 69, Table 70, Table 71 and Table 72 respectively. The performance of the structure with dampers is considered unsatisfactory due to the formation of plastic hinges in central columns and MRF columns that no longer satisfy the acceptance criteria (Table 73 and Table 74 respectively).

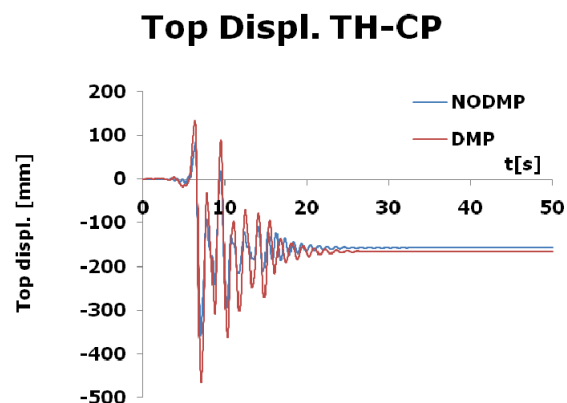


Fig. 4.46. Recorded top displacement in time for the dual MRF+CBF structure at CP (soft soil)

BRACE Compr.	Plastic deformation demand-CP , mm		Plastic deformation capacity, mm
	LOC.	NODMP	
BR1L	4.232	3.823	27.755
BR1R	1.896	1.706	27.755
BR2L	4.199	4.508	27.755
BR2R	1.564	2.057	27.755
BR3L	2.920	2.859	25.046
BR3R	-	0.247	25.046
BR4L	2.309	3.152	22.449
BR4R	-	-	22.449
BR5L	0.957	3.028	19.376
BR5R	-	-	19.376
BR(storey no.)R- right brace for selected storey			
BR(storey no.)L- left brace for selected storey			

Table 69. Axial plastic deformation for braces in compression at CP (soft soil)

BRACE Tension.	Plastic deformation demand-CP , mm		Plastic deformation capacity, mm
	LOC.	NODMP	
BR1L	0.911	-	51.417
BR1R	18.781	8.814	51.417
BR2L	0.248	-	51.417
BR2R	40.481	36.387	51.417
BR3L	0.858	-	50.76
BR3R	-	36.149	50.76
BR4R	-	5.297	50.265
BR5R	-	0.221	50.193
BR(storey no.)R- right brace for selected storey			
BR(storey no.)L- left brace for selected storey			

Table 70. Axial plastic deformation for braces in tension at CP (soft soil)

BEAM	NODMP		DMP		
	LOC.	Plastic rotation demand- CP, rad	Plastic rotation capacity, rad CP	Plastic rotation demand-CP, rad	Plastic rotation capacity, rad CP
CB1a		0.0140	0.0227	0.0271	0.0227
CB2a		0.0159	0.0224	0.0225	0.0224
CB(storey no.)a- central beam for selected storey at end a					
CB(storey no.)b- central beam for selected storey at end b					

Table 71. Plastic rotation at CP for central beams (soft soil)

BEAM MRF	NODMP		DMP	
	Plastic rotation demand-CP, rad	Plastic rotation capacity, rad CP	Plastic rotation demand-CP, rad	Plastic rotation capacity, rad CP
B1L	0.0192	0.0286	0.0208	0.0286
B2L	0.0241	0.0286	0.0338	0.0286
B3L	0.0022	0.0286	0.0116	0.0286
B4L		0.0317	0.0023	0.0317
B5L		0.0317		0.0317
B1R	0.0269	0.0286	0.0286	0.0286
B2R	0.0280	0.0286	0.0365	0.0286
B3R	0.0053	0.0286	0.0136	0.0286
B4R		0.0317	0.0032	0.0317
B5R		0.0317		0.0317
B(storey no.)L- left MRF frame beam for selected storey				
B(storey no.)R- right MRF frame beam for selected storey				

Table 72. Plastic rotation at CP for MRF beams (soft soil)

COLUMN	NODMP		DMP	
	Plastic rotation demand-CP, rad	Plastic rotation capacity, rad CP	Plastic rotation demand-CP, rad	Plastic rotation capacity, rad CP
CC2L	0.0448	0.00377	0.0529	0.00387
CC3L	0.0325	0.00446	0.0426	0.00455
CC4L	-	-	0.0070	0.00507
CC(storey no.)L- left central column for selected storey				
CC(storey no.)R- right central column for selected storey				

Table 73. Plastic rotation at CP for central columns (soft soil)

COLUMN	NODMP		DMP	
	Plastic rotation demand-CP, rad	Plastic rotation capacity, rad CP	Plastic rotation demand-CP, rad	Plastic rotation capacity, rad CP
C1R	0.0145	0.00725	0.0153	0.00722
C2R	-	-	0.0022	0.0269
C(storey no.)L- left MRF column for selected storey				
C(storey no.)R- right MRF column for selected storey				

Table 74. Plastic rotation at CP for MRF columns

The results obtained for the dual frame were very similar to those obtained for the CBF frame under the same seismic motion. This set of numerical analyses showed that the frame equipped with dampers increases the flexibility of the structure, forming plastic hinges even at SLS with a higher number of plastic hinges with higher values of plastic deformation/rotation in braces and beams respectively that no longer satisfy the performance criteria and generally a worse global behaviour. Values of permanent top displacement are higher for the structure with dampers. The conclusion is that this particular type of

damper is not efficient in reducing the seismic response of a building for earthquakes characterized by a high value of corner period $T_c=1.6s$ (soft soil).

4.4.2.2 TH Analysis of Dual CBF+MRF Structure for Stiff Soil Type ($T_c=0.5s$)

Maximum drift levels (Fig. 4.47), maximum drift at each storey (Fig. 4.48) and top displacement for the structure (Fig. 4.49) without dampers are presented as mean values of recorded values for all 7 seismic motions at levels corresponding to SLS, ULS and CP in comparison with the same values recorded for the structure with dampers in the braces.

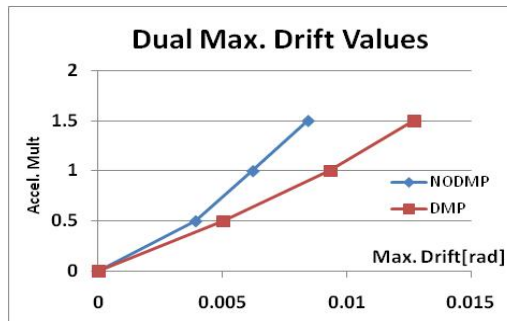


Fig. 4.47. Maximum drift values for the structure with and without dampers (stiff soil)

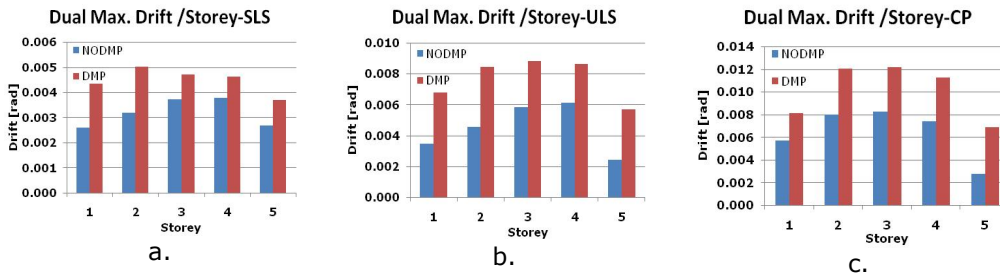


Fig. 4.48. Maximum drift at each storey at: a) SLS; b) ULS; c) CP for the structure with and without dampers (stiff soil)

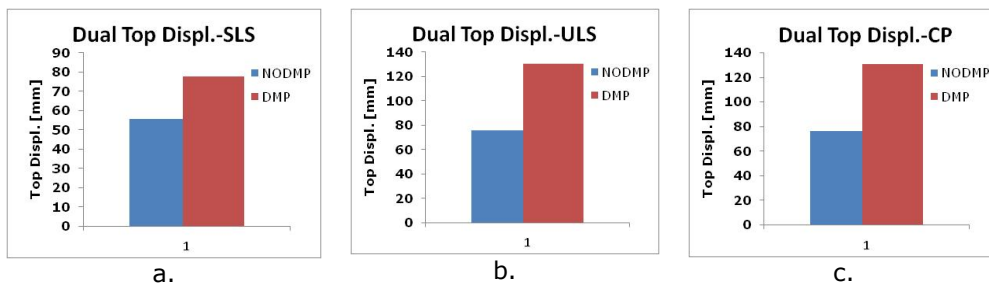


Fig. 4.49. Top displacement at: a) SLS; b) ULS; c) CP for the structure with and without dampers (stiff soil)

At the end of each seismic recording used the structure was left to vibrate freely for 10s. Recorded values of permanent displacement at top of the structure are presented as mean values for all 7 recordings in Fig. 4.50.

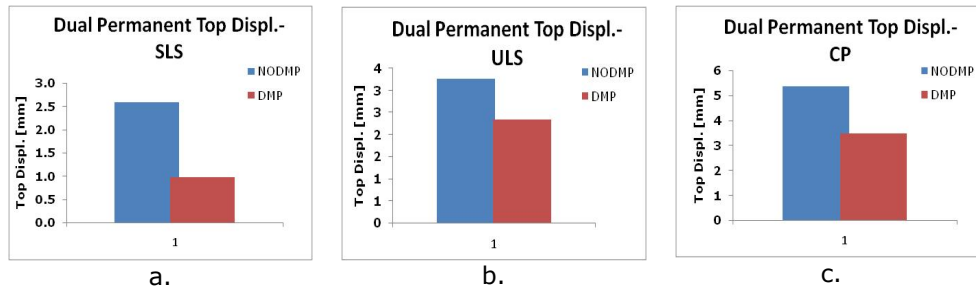


Fig. 4.50. Permanent top displacement at: a) SLS; b) ULS; c) CP for the structure with and without dampers (stiff soil)

For all 7 seismic motions characteristic for stiff soil type used the results showed that for all performance levels the building with dampers exhibited a increase in drift for all 5 storeys. The structure with dampers has lower values of permanent displacement at the top of the structure at all levels of seismic action. Values of plastic axial deformations and plastic rotations are presented here as mean value for all 7 seismic recordings at (i) SLS with $a_{g,SLS} = 0.5 \cdot a_{g,ULS}$ (Table 75, Table 76, Table 77), (ii) ULS with $a_{g,ULS}$ (Table 78, Table 79, Table 80, Table 81) and (iii) CP with $a_{g,CP} = 1.5 \cdot a_{g,ULS}$ (Table 82, Table 83, Table 84, Table 85).

(i) SLS with $a_{g,SLS} = 0.5 \cdot a_{g,ULS}$ characteristic for stiff soil type ($T_C=0.5s$)

BRACE Compr.	Plastic deformation demand-SLS, mm		Plastic deformation capacity, mm
	NODMP	DMP	
LOC.			IO
BR1L	0.094	-	0.99125
BR1R	0.133	-	0.99125
BR2L	0.191	-	0.99125
BR2R	0.332	-	0.99125
BR3L	0.380	-	0.8945
BR3R	0.569	-	0.8945
BR4L	0.295	-	0.80175
BR4R	0.301	-	0.80175
BR5L	-	-	0.692
BR5R	-	-	0.692
BR(storey no.)R- right brace for selected storey			
BR(storey no.)L- left brace for selected storey			

Table 75. Mean values of axial plastic deformation for braces in compression at SLS (stiff soil)

BRACE Tension	Plastic deformation demand-SLS , mm		Plastic deformation capacity, mm
	LOC.	NODMP	DMP
			IO
No plastic axial deformation			
BR(storey no.)R- right brace for selected storey			
BR(storey no.)L- left brace for selected storey			

Table 76. Mean values of axial plastic deformation for braces in tension at SLS (stiff soil)

BEAM	NODMP		DMP	
	LOC.	Plastic rotation demand-ULS, rad	Plastic rotation capacity, rad LS	Plastic rotation demand-ULS, rad
				Plastic rotation capacity, rad LS
No plastic rotation in elements				
CB(storey no.)a- central beam for selected storey at end a				
CB(storey no.)b- central beam for selected storey at end b				

Table 77. Mean values for plastic rotation at SLS for central beams (stiff soil)

(ii) ULS with $a_{g,ULS}$ characteristic for stiff soil type ($T_C=0.5s$)

BRACE Compr.	Plastic deformation demand-ULS , mm		Plastic deformation capacity, mm
	LOC.	NODMP	DMP
			LS
BR1L	0.602	-	19.825
BR1R	0.805	-	19.825
BR2L	0.998	0.608	19.825
BR2R	1.210	1.329	19.825
BR3L	1.273	0.633	17.89
BR3R	1.259	1.294	17.89
BR4L	1.178	0.949	16.035
BR4R	0.586	1.380	16.035
BR5L	0.064	0.530	13.84
BR5R	0.017	0.615	13.84
BR(storey no.)R- right brace for selected storey			
BR(storey no.)L- left brace for selected storey			

Table 78. Mean values of axial plastic deformation for braces in compression at ULS (stiff soil)

BRACE Tension.	Plastic deformation demand-ULS , mm		Plastic deformation capacity, mm
	LOC.	NODMP	DMP
			LS
BR1L	-	-	39.991
BR1R	-	-	39.991
BR2L	0.102	-	39.991
BR2R	-	0.060	39.991
BR3L	-	0.235	39.48
BR3R	-	0.142	39.48
BR4L	-	0.317	39.095
BR4R	-	0.370	39.095
BR5L	-	-	39.039
BR5R	-	-	39.039
BR(storey no.)R- right brace for selected storey			
BR(storey no.)L- left brace for selected storey			

Table 79. Mean values of axial plastic deformation for braces in tension at ULS (stiff soil)

BEAM	NODMP		DMP	
LOC.	Plastic rotation demand-ULS, rad	Plastic rotation capacity, rad LS	Plastic rotation demand-ULS, rad	Plastic rotation capacity, rad LS
No plastic rotation				
CB(storey no.)a- central beam for selected storey at end a				
CB(storey no.)b- central beam for selected storey at end b				

Table 80. Mean values for plastic rotation at ULS for central beams (stiff soil)

BEAM MRF	NODMP		DMP	
LOC.	Plastic rotation demand-ULS, rad	Plastic rotation capacity, rad LS	Plastic rotation demand-ULS, rad	Plastic rotation capacity, rad LS
No plastic rotation				
B(storey no.)L- left MRF frame beam for selected storey				
B(storey no.)R- right MRF frame beam for selected storey				

Table 81. Mean values for plastic rotation at ULS for MRF beams (stiff soil)

(iii) CP with $a_{g,CP} = 1.5 \cdot a_{g,ULS}$ characteristic for stiff soil type ($T_C=0.5s$)

BRACE Compr.	Plastic deformation demand-CP, mm		Plastic deformation capacity, mm CP
	NODMP	DMP	
BR1L	1.580	0.583	27.755
BR1R	1.207	0.833	27.755
BR2L	1.715	1.830	27.755
BR2R	1.337	2.346	27.755
BR3L	0.933	1.383	25.046
BR3R	1.231	1.703	25.046
BR4L	0.854	1.253	22.449
BR4R	1.177	1.736	22.449
BR5L	0.162	0.776	19.376
BR5R	0.379	1.211	19.376
BR(storey no.)R- right brace for selected storey			
BR(storey no.)L- left brace for selected storey			

Table 82. Mean values of axial plastic deformation for braces in compression at CP (stiff soil)

BRACE Tension.	Plastic deformation demand-CP , mm		Plastic deformation capacity, mm
	NODMP	DMP	
LOC.			CP
BR1L	0.268	-	51.7221
BR1R	1.345	-	51.7221
BR2L	3.260	1.840	51.7221
BR2R	4.052	3.226	51.7221
BR3L	-	3.094	51.39
BR3R	0.056	4.028	51.39
BR4L	-	1.501	50.76
BR4R	-	2.847	50.76
BR5L	-	0.085	50.193
BR5R	-	-	50.193
BR(storey no.)R- right brace for selected storey			
BR(storey no.)L- left brace for selected storey			

Table 83. Mean values of axial plastic deformation for braces in tension at CP (stiff soil)

BEAM	NODMP		DMP	
	Plastic rotation demand-CP, rad	Plastic rotation capacity, rad CP	Plastic rotation demand-CP, rad	Plastic rotation capacity, rad CP
LOC.				
No plastic rotation				
CB(storey no.)a- central beam for selected storey at end a				
CB(storey no.)b- central beam for selected storey at end b				

Table 84. Mean values for plastic rotation at CP for central beams (stiff soil)

BEAM MRF	NODMP		DMP	
	Plastic rotation demand-CP, rad	Plastic rotation capacity, rad CP	Plastic rotation demand-CP, rad	Plastic rotation capacity, rad CP
LOC.				
B1L	-	-	0.00265	0.0286
B2L	-	-	0.00274	0.0286
B3L	-	-	0.00193	0.0286
B4L	-	-	0.00197	0.0317
B5L	-	-	-	0.0317
B1R	-	-	0.00435	0.0286
B2R	-	-	0.00252	0.0286
B3R	-	-	0.00231	0.0286
B4R	-	-	-	0.0317
B5R	-	-	-	0.0317
B(storey no.)L- left MRF frame beam for selected storey				
B(storey no.)R- right MRF frame beam for selected storey				

Table 85. Mean values for plastic rotation at CP for MRF beams

At SLS the using dampers in the bracings prevents the formation of plastic hinges in braces. At ULS the structure with dampers has lower values of axial

plastic deformation in braces in compression but with slightly higher values for the braces in tension. At CP the structure with dampers has higher values of plastic deformation/rotation in elements. Plastic hinges appear in MRF braces only for the structure with dampers and no plastic hinges are formed in central beams at any level. The structure with dampers behaves better at all levels of seismic action for this type of seismic recording. All plastic deformations/rotations satisfy the acceptance criteria at all levels. In the following paragraph a relevant example for the 7 seismic motions characteristic to stiff soil will be presented and discussed in detail. The dual MRF+CBF structure will be presented comparatively with and without dampers at (i). SLS with $a_{g,SLS} = 0.5 \cdot a_{g,ULS}$, (ii) ULS with $a_{g,ULS}$ and (iii) CP with $a_{g,CP} = 1.5 \cdot a_{g,ULS}$.

(i) SLS with $a_{g,SLS} = 0.5 \cdot a_{g,ULS}$ characteristic for stiff soil type ($T_C = 0.5s$)

Plastic hinge formation in the structure with and without damper is presented in Fig. 4.51.

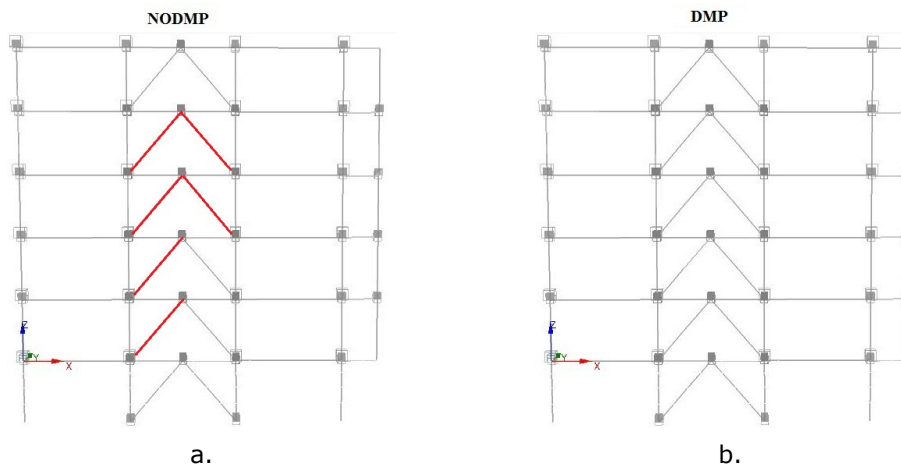


Fig. 4.51. Plastic hinge formation for dual MRF+CBF structure: a) without dampers; b) with dampers at SLS

For this performance level, only the structure without dampers forms plastic hinges in braces under compression with the values of axial plastic deformation that satisfy the acceptance criteria for immediate occupancy (IO) from FEMA356[10] (Table 86). The structure with dampers has significantly lower value of permanent displacement at the top of the structure compared to the structure without dampers (Fig. 4.52).

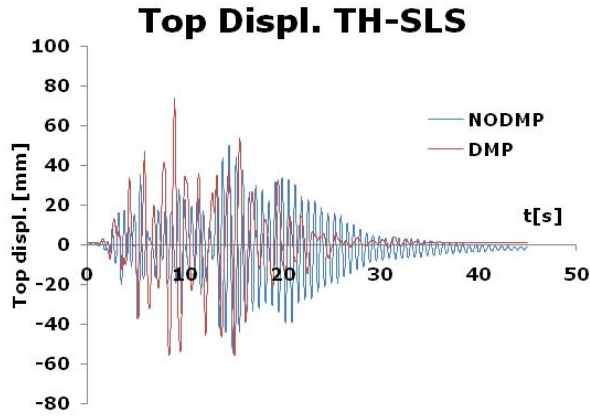


Fig. 4.52. Recorded top displacement in time for the dual MRF+CBF structure at SLS (stiff soil)

BRACE Compr.	Plastic deformation demand- SLS , mm		Plastic deformation capacity, mm
	NODMP	DMP	
BR1L	0.655	-	0.991
BR1R	-	-	0.991
BR2L	0.889	-	0.991
BR2R	-	-	0.991
BR3L	0.727	-	0.894
BR3R	0.303	-	0.894
BR4L	0.147	-	0.801
BR4R	0.156	-	0.801
BR5L	-	-	0.692
BR5R	-	-	0.692
BR(storey no.)R- right brace for selected storey			
BR(storey no.)L- left brace for selected storey			

Table 86. Axial plastic deformation values for compression braces at SLS (soft soil)

No plastic axial deformation is recorded in tension braces at this level.

(ii) ULS with $a_{g,ULS}$ characteristic for soft soil type ($T_C=1.6s$)

Plastic hinge formation in the structure with and without damper is presented in Fig. 4.53.

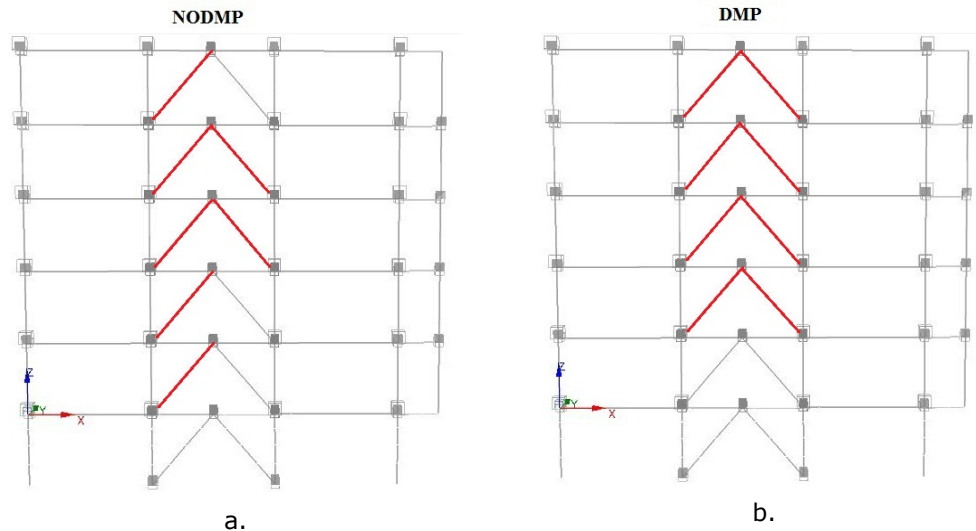


Fig. 4.53. Plastic hinge formation for dual MRF+CBF structure: a) without dampers; b) with dampers at ULS

At ULS both frames with and without dampers form plastic hinges in braces. At this level the structures have a similar behaviour with similar values of plastic deformation/rotation in elements. No plastic rotations of the central beams or of the MRF beams are recorded for either structure. All plastic deformations satisfy the acceptance criteria corresponding to life safety (LS) from FEMA 356[10]. The structure with dampers has lower values of permanent top displacement than the structure without dampers (Fig. 4.54). Specific values of axial plastic deformation recorded for braces in tension, compression and plastic rotation of central beams and MRF beams are presented in Table 87, Table 88, Table 89 and Table 90 respectively.

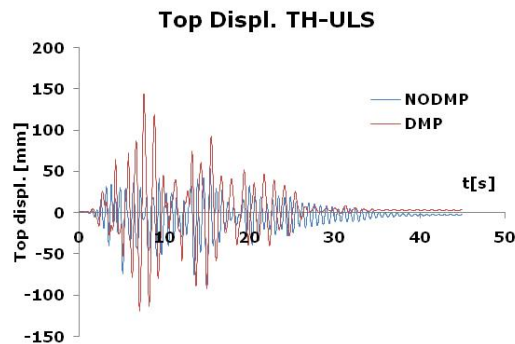


Fig. 4.54. Recorded top displacement in time for the dual MRF+CBF structure at ULS (stiff soil)

BRACE Compr.	Plastic deformation demand- ULS , mm		Plastic deformation capacity, mm
	NODMP	DMP	
LOC.			LS
BR1L	0.878	-	19.825
BR1R	-	-	19.825
BR2L	1.621	0.693	19.825
BR2R	-	1.461	19.825
BR3L	1.796	0.941	17.89
BR3R	0.455	1.726	17.89
BR4L	1.744	0.638	16.035
BR4R	0.453	1.967	16.035
BR5L	0.654	0.292	13.84
BR5R	-	0.726	13.84
BR(storey no.)R- right brace for selected storey			
BR(storey no.)L- left brace for selected storey			

Table 87. Axial plastic deformation for braces in compression at ULS (stiff soil)

BRACE Tension	Plastic deformation demand- ULS , mm		Plastic deformation capacity, mm
	NODMP	DMP	
LOC.			LS
BR2L	0.711	-	39.991
BR(storey no.)R- right brace for selected storey			
BR(storey no.)L- left brace for selected storey			

Table 88. Axial plastic deformation for braces in tension at ULS (stiff soil)

BEAM LOC.	NODMP		DMP	
	Plastic rotation demand- ULS, rad	Plastic rotation capacity, rad LS	Plastic rotation demand-ULS, rad	Plastic rotation capacity, rad LS
No plastic rotation				
CB(storey no.)a- central beam for selected storey at end a				
CB(storey no.)b- central beam for selected storey at end b				

Table 89. Plastic rotation at ULS for central beams (stiff soil)

BEAM MRF LOC.	NODMP		DMP	
	Plastic rotation demand- ULS, rad	Plastic rotation capacity, rad LS	Plastic rotation demand-ULS, rad	Plastic rotation capacity, rad LS
No plastic rotation				
B(storey no.)L- left MRF frame beam for selected storey				
B(storey no.)R- right MRF frame beam for selected storey				

Table 90. Plastic rotation at ULS for MRF beams (stiff soil)

No plastic hinges recorded in any columns.

(iii) CP with $a_{g,CP} = 1.5 \cdot a_{g,ULS}$ characteristic for soft soil type ($T_c=1.6s$)

Plastic hinge formation in the structure with and without damper is presented

in Fig. 4.55.

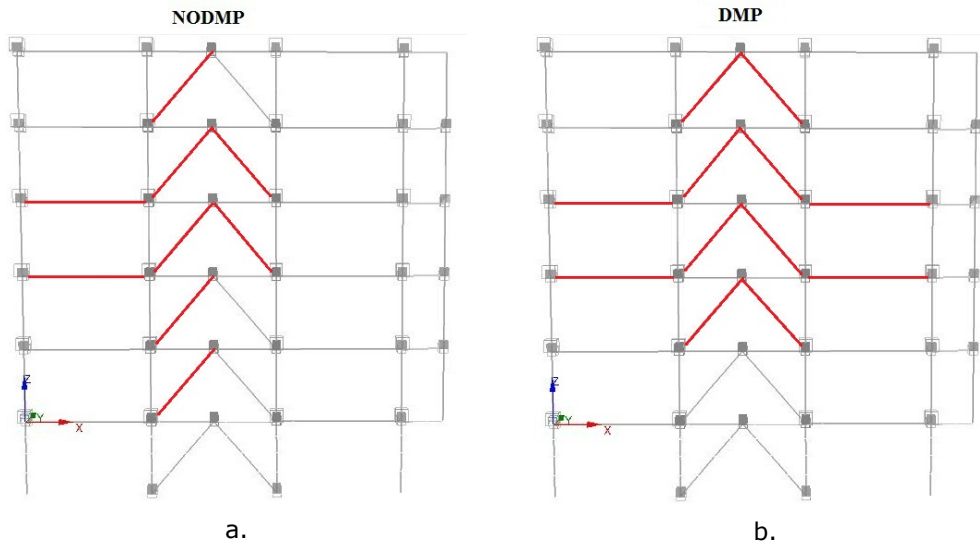


Fig. 4.55. Plastic hinge formation in the structure with and without damper at CP (soft soil)

At CP both frames with and without dampers form plastic hinges in braces. Structure with dampers has lower values of plastic axial deformation for compression braces and slightly higher for tension braces than the structure without dampers. No plastic rotations of the central beams are recorded for either structure with lower values of permanent top displacement for the structure with dampers (Fig. 4.56). Plastic hinges in MRF beams occur only for the frame with dampers. All plastic deformations satisfy the acceptance criteria corresponding to collapse prevention (CP) from FEMA 356[10]. Specific values of axial plastic deformation recorded for braces in tension, compression and plastic rotation of central beams and MRF beams are presented in Table 91, Table 92, Table 93 and Table 94 respectively.

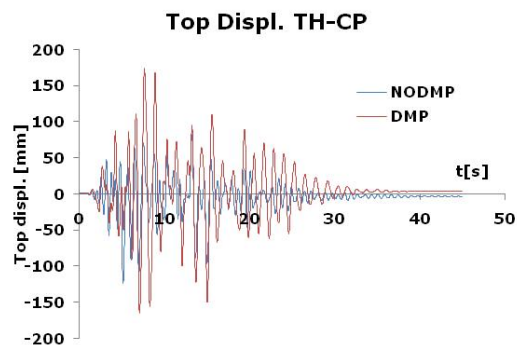


Fig. 4.56. Recorded top displacement in time for the dual MRF+CBF structure at CP (stiff soil)

BRACE Compr.	Plastic deformation demand-CP , mm		Plastic deformation capacity, mm
	LOC.	NODMP	
			CP
BR1L	1.972	-	27.755
BR1R	0.949	-	27.755
BR2L	2.046	2.633	27.755
BR2R	0.853	2.155	27.755
BR3L	1.185	2.246	25.046
BR3R	0.254	1.831	25.046
BR4L	0.632	2.007	22.449
BR4R	-	0.706	22.449
BR5L	0.648	0.832	19.376
BR5R	-	1.827	19.376
BR(storey no.)R- right brace for selected storey			
BR(storey no.)L- left brace for selected storey			

Table 91. Axial plastic deformation for braces in compression at CP (stiff soil)

BRACE Tension.	Plastic deformation demand-CP , mm		Plastic deformation capacity, mm
	LOC.	NODMP	
			CP
BR1L	1.649	-	51.417
BR1R	1.081	-	51.417
BR2L	5.739	3.933	51.417
BR2R	2.745	1.057	51.417
BR3L	-	6.539	50.76
BR3R	-	2.976	50.76
BR4L	-	4.257	50.265
BR4R	-	5.122	50.193
BR(storey no.)R- right brace for selected storey			
BR(storey no.)L- left brace for selected storey			

Table 92. Axial plastic deformation for braces in tension at CP (stiff soil)

BEAM	NODMP		DMP	
	LOC.	Plastic rotation demand- CP, rad	Plastic rotation capacity, rad CP	Plastic rotation demand-CP, rad
No plastic rotation				
CB(storey no.)a- central beam for selected storey at end a				
CB(storey no.)b- central beam for selected storey at end b				

Table 93. Plastic rotation at CP for central beams (stiff soil)

BEAM MRF	NODMP		DMP	
	Plastic rotation demand-CP, rad	Plastic rotation capacity, rad CP	Plastic rotation demand-CP, rad	Plastic rotation capacity, rad CP
B2L	0.0241	0.0286	0.00394	0.0286
B3L	0.0022	0.0286	0.00188	0.0286
B2R	-	0.0286	0.00165	0.0286
B3R	-	0.0286	0.00193	0.0286
B(storey no.)L- left MRF frame beam for selected storey				
B(storey no.)R- right MRF frame beam for selected storey				

Table 94. Plastic rotation at CP for MRF beams (stiff soil)

No plastic hinges were recorded in any columns.

The results obtained for the dual frame were very similar to those obtained for the CBF frame under the same seismic motion. This set of numerical analyses showed that equipping the dampers in the braces prevents the formation of plastic hinges in elements at seismic action levels corresponding to SLS and reducing permanent displacement at all levels of seismic action. For this type of seismic motions characteristic to stiff soil no plastic hinges were formed in non-dissipative elements such as central beams and columns. All values of axial plastic deformation and plastic rotation of MRF beams satisfy the acceptance criteria for all performance levels. The conclusion is that this particular type of damper is efficient in reducing the seismic response of a building by avoiding formation of plastic hinges in the braces at SLS and reducing the permanent displacement of the structure for earthquakes characterized by short corner period $T_c=0.5s$ (stiff soil).

The results obtained from numerical analysis of the two frames, the CBF and the dual MRF+CBF frame are very similar and lead to the same conclusions. In the case of earthquakes characterised by long corner period $T_c=1.6s$ (soft soil) introducing this type of damper in the braces has a defavorable effect on the behaviour of the structures at all levels of seismic action. One of the main concepts of this type of dampers is that it should increase the period of vibration of the structure to values higher than that of the corner period T_c . For earthquake with long corner period like those characteristic to Vrancea region in our country this does not occur. The structure with dampers has a higher number of plastic hinges that appear even at levels corresponding to SLS and do not satisfy the acceptance criteria at the corresponding performance level. Plastic hinges for in elements considered non-dissipative such as central beams and columns and the values of permanent displacement are significantly higher for the structure with dampers. However, this particular type of damper is efficient in reducing the seismic response of a building by avoiding formation of plastic hinges in the braces at SLS and reducing the permanent displacement of the structure for earthquakes characterized by short corner period $T_c=0.5s$ (stiff soil).

4.5 An Alternative Type of Friction Damper Device

To further broaden the view on the effects the introduction of a damper such as the one studied in this paper has on the seismic performance of the structure another set of numerical analysis is proposed using an already known type of friction damper. The “classical” friction damper possesses large rectangular hysteretic loops similar to an ideal elasto plastic behaviour. These friction dampers have stable hysteretic loops and have the capacity to dissipate large amounts of seismic energy. Such dampers, like Pall friction dampers, can be installed in the braces and are designed to slip at a given optimal load before the yielding of any structural members. The main parameters for this type of friction dampers are the (i) slip force and (ii) initial stiffness of the damper. In conjunction with an elasto plastic behaviour the slip force of the damper can be equated to the yield force of this type of idealised behaviour. For this case study the friction dampers were designed starting from the two structures (CBF and dual MRF+CBF) without dampers designed and were added in the model in the same position as the SERB dampers with the same stiffness as them. The slip force for each damper was determined as:

$$N_{FD3} = N_{b,Rd}$$

where

- N_{FD3} = slip force of FD3 damper;
- $N_{b,Rd}$ = bucking capacity of the corresponding brace where damper is installed.

The design principle used in this approach was that the structure will remain in elastic domain with seismic energy being consumed in the devices only. For this purpose after the determination of the slip forces for these dampers the braces were “upgraded” to ensure they remain in elastic domain. No other changes were made for the elements of the two frames discussed. This third set of numerical analyses can be summarised as:

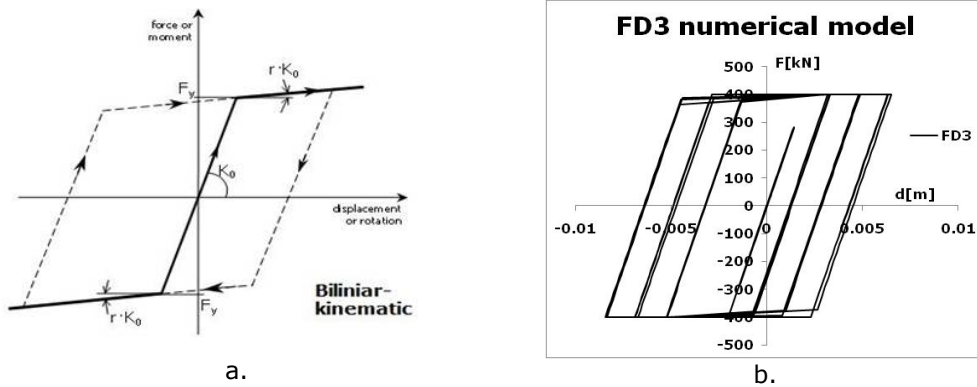
- (i) Numerical analyses on CBF
 - 7 semi-artificial seismic motion characteristic for soft soil type (Bucharest, $T_C=1.6s$)
 - 7 artificially generated seismic motions characteristic for stiff soil (Class B soil according to EN1998-1[7], $T_C=0.5s$)
- (ii) Numerical analyses on dual MRF+CBF frames
 - 7 semi-artificial seismic motion characteristic for soft soil type (Bucharest, $T_C=1.6s$)
 - 7 artificially generated seismic motions characteristic for stiff soil (Class B soil according to EN1998-1[7], $T_C=0.5s$)

For the purpose of simplicity the “classical” friction damper with rectangular hysteretic loops used in this third set on numerical simulations will be referred to from here on as FD3.

4.5.1 Element Model for FD3 Damper

Having a behaviour similar to the ideal elasto plastic behaviour these dampers were modelled as link elements having a bilinear kinematic behaviour defined for the degree of freedom corresponding to axial deformation(4.57a). The

parameters for the kinematic behaviour were: (i) stiffness $k=200000\text{kN/m}$, (ii) slip force $N_{FD3} = N_{b,Rd}$ and (iii) hardening ratio $r=0.00001$. This link model used lead to the desired rectangular shape hysteretic behaviour desired for the FD3 damper(4.57b).



4.57. a) Bilinear kinematic link behaviour used; b) Hysteretic behaviour of the FD3 numerical model

Numerical TH analyses were made for the two sets of seismic motion on each of the two types of structures using this model for the FD3 damper. All results will be presented in comparison with the structure without dampers and the structure with SERB type damper.

4.5.2 Numerical Modelling on CBF with FD3 dampers for Soft Soil Type ($T_C=1.6\text{s}$)

Maximum drift levels (Fig. 4.58), maximum drift at each storey (Fig. 4.59) and top displacement for the structure (Fig. 4.60) with FD3 dampers are presented as mean values of recorded values for all 7 seismic motions at levels corresponding to SLS, ULS and CP in comparison with the same values recorded for the structure with SERB dampers and the structure without dampers in the braces.

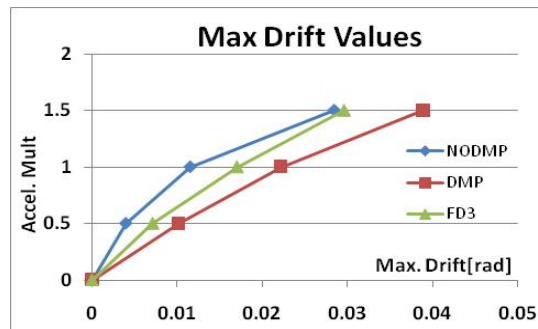


Fig. 4.58. Maximum drift values for the structure with FD3 and SERB dampers and without dampers

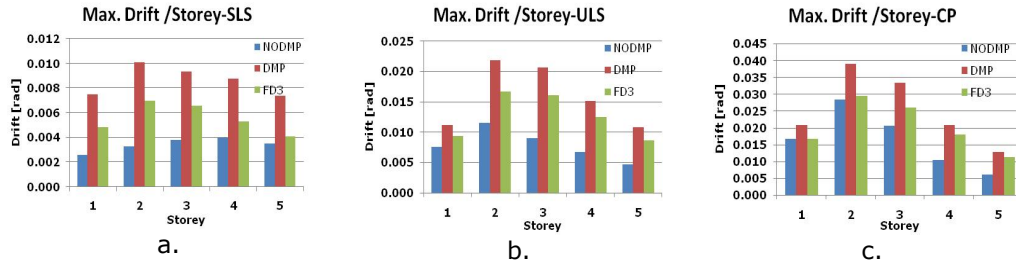


Fig. 4.59. Maximum drift at each storey at: a) SLS; b) ULS; c) CP for the structure with FD3 and SERB dampers and without dampers

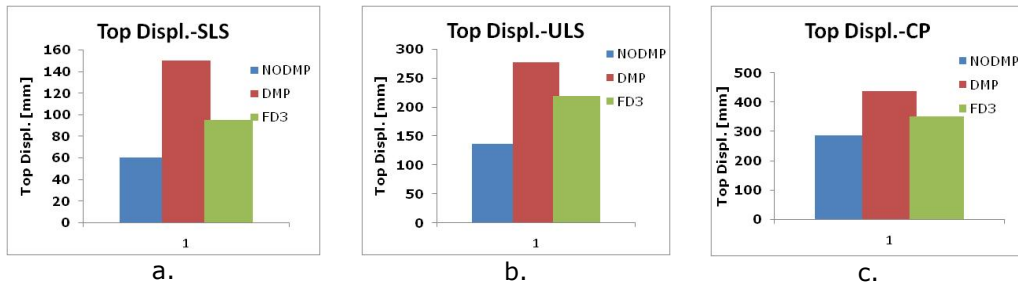


Fig. 4.60. Top displacement at: a) SLS; b) ULS; c) CP for the structure with and without dampers

At the end of each seismic recording used the structure was left to vibrate freely for 10s. Recorded values of permanent displacement at top of the structure are presented as mean values for all 7 recordings in Fig. 4.61.

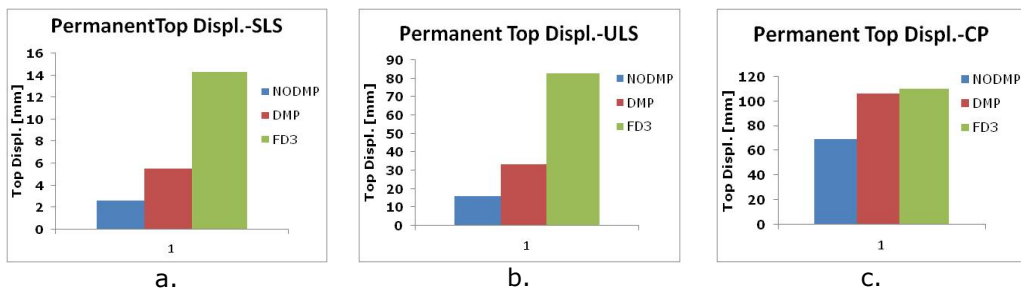


Fig. 4.61. Permanent top displacement at: a) SLS; b) ULS; c) CP for the structure with and without dampers

For all 7 semi-artificial seismic motion characteristic for soft soil type used the results showed that for all performance levels the building with FD3 dampers had higher values of drift then the structure without dampers but lower values then those recorded with the SERB damper. Permanent displacement at the top of the structure increased significantly for the structure with FD3 dampers at SLS and ULS. At CP these values were very close to the values recorded for the

structure with SERB dampers but still higher than for the structure without dampers. Values of plastic axial deformations and plastic rotations are presented here as mean value for all 7 seismic recordings at (i)SLS with $a_{g,SLS} = 0.5 \cdot a_{g,ULS}$ (Table 95, Table 96, Table 97), (ii)ULS with $a_{g,ULS}$ (Table 98, Table 99, Table 100) and (iii)CP with $a_{g,CP} = 1.5 \cdot a_{g,ULS}$ (Table 101, Table 102, Table 103, Table 104).

(i) SLS with $a_{g,SLS} = 0.5 \cdot a_{g,ULS}$ characteristic for soft soil type ($T_c=1.6s$)

BRACE Compr.	Plastic deformation demand-SLS , mm			Plastic deformation capacity, mm
	LOC.	NODMP	DMP	
			FD3	IO
BR1L	-	-	NO PLASTIC DEFORMATION	1.1225
BR1R	-	-		1.1225
BR2L	0.206	1.000		1.1225
BR2R	0.347	0.751		1.1225
BR3L	0.360	0.779		0.99125
BR3R	0.272	0.424		0.99125
BR4L	0.299	0.768		0.8945
BR4R	0.156	0.372		0.8945
BR5L	0.103	0.584		0.692
BR5R	0.069	0.197		0.692
				BR(storey no.)R- right brace for selected storey
				BR(storey no.)L- left brace for selected storey

Table 95. Mean values of axial plastic deformation for braces in compression at SLS

BRACE Tension	Plastic deformation demand-SLS , mm		Plastic deformation capacity, mm
	LOC.	NODMP	
			IO
No plastic deformation			
BR(storey no.)R- right brace for selected storey			
BR(storey no.)L- left brace for selected storey			

Table 96. Mean values of axial plastic deformation for braces in tension at SLS

BEAM	NODMP		DMP	
	LOC.	Plastic rotation demand-ULS, rad	Plastic rotation capacity, rad LS	Plastic rotation demand-ULS, rad
No plastic rotation in elements				
CB(storey no.)a- central beam for selected storey at end a				
CB(storey no.)b- central beam for selected storey at end b				

Table 97. Mean values for plastic rotation at SLS for central beams (soft soil)

(ii) ULS with $a_{g,ULS}$ characteristic for soft soil type ($T_c=1.6s$)

BRACE Compr.	Plastic deformation demand-ULS , mm			FD3	Plastic deformation capacity, mm
	LOC.	NODMP	DMP		
BR1L	1.605	1.029	NO PLASTIC DEFORMATION	22.45	
BR1R	1.764	0.875		22.45	
BR2L	2.004	3.234		22.45	
BR2R	1.674	2.807		22.45	
BR3L	1.403	2.250		19.825	
BR3R	1.202	1.036		19.825	
BR4L	0.991	1.767		17.89	
BR4R	0.696	0.959		17.89	
BR5L	0.443	1.728		13.84	
BR5R	0.478	1.295		13.84	
BR(storey no.)R- right brace for selected storey					
BR(storey no.)L- left brace for selected storey					

Table 98. Mean values of axial plastic deformation for braces in compression at ULS

BRACE Tension.	Plastic deformation demand-ULS , mm			FD3	Plastic deformation capacity, mm
	LOC.	NODMP	DMP		
BR1L	0.284	-	NO PLASTIC DEFORMATION	40.2283	
BR1R	0.960	-		40.2283	
BR2L	3.238	3.998		40.2283	
BR2R	3.829	4.569		40.2283	
BR3L	0.142	6.330		39.97	
BR3R	0.330	6.119		39.97	
BR4L	0.039	1.316		39.48	
BR4R	0.050	1.946		39.48	
BR5L	-	0.037		39.039	
BR5R	-	0.259		39.039	
BR(storey no.)R- right brace for selected storey					
BR(storey no.)L- left brace for selected storey					

Table 99. Mean values of axial plastic deformation for braces in tension at ULS

BEAM	NODMP		DMP		FD3
	LOC.	Plastic rotation demand-ULS, rad	Plastic rotation capacity, rad LS	Plastic rotation demand-ULS, rad	
CB1a	0.00120	VARIES	0.00406	VARIES	NO PLASTIC DEFORMATION
CB2a	0.00063	VARIES	0.00759	VARIES	
CB3a	-	VARIES	0.00423	VARIES	
CB4a	-	VARIES	0.00175	VARIES	
CB5a	-	VARIES	-	VARIES	
CB1b	0.00127	VARIES	0.00257	VARIES	
CB2b	0.00099	VARIES	0.00605	VARIES	
CB3b	-	VARIES	0.00220	VARIES	
CB4b	-	VARIES	0.00066	VARIES	
CB5b	-	VARIES	-	VARIES	
CB(storey no.)a- central beam for selected storey at end a					
CB(storey no.)b- central beam for selected storey at end b					

Table 100. Mean values for plastic rotation at ULS for central beams

(iii) CP with $a_{g,CP} = 1.5 \cdot a_{g,ULS}$ characteristic for soft soil type ($T_C=1.6s$)

BRACE Compr.	Plastic deformation demand-CP , mm			Plastic deformation capacity, mm
	LOC.	NODMP	DMP	
BR1L	2.883	2.763	NO PLASTIC DEFORMATION	31.43
BR1R	2.546	2.763		31.43
BR2L	2.727	3.788		31.43
BR2R	2.927	3.176		31.43
BR3L	1.620	2.658		27.755
BR3R	1.639	1.868		27.755
BR4L	1.477	2.413		25.046
BR4R	1.361	1.665		25.046
BR5L	0.767	2.100		19.376
BR5R	0.722	1.357		19.376
BR(storey no.)R- right brace for selected storey				
BR(storey no.)L- left brace for selected storey				

Table 101. Mean values of axial plastic deformation for braces in compression at CP

BRACE Tension.	Plastic deformation demand-CP , mm			Plastic deformation capacity, mm
	LOC.	NODMP	DMP	
BR1L	6.506	2.908	NO PLASTIC DEFORMATION	51.7221
BR1R	5.856	1.852		51.7221
BR2L	18.453	14.358		51.7221
BR2R	17.474	13.911		51.7221
BR3L	0.554	18.632		51.39
BR3R	0.476	18.541		51.39
BR4L	0.112	6.253		50.76
BR4R	0.268	5.701		50.76
BR5L	0.000	0.577		50.193
BR5R	0.000	0.812		50.193
BR(storey no.)R- right brace for selected storey				
BR(storey no.)L- left brace for selected storey				

Table 102. Mean values of axial plastic deformation for braces in tension at CP

BEAM	NODMP		DMP		FD3		
	LOC.	Plastic rotation demand-CP, rad	Plastic rotation capacity, rad CP	Plastic rotation demand-CP, rad	Plastic rotation capacity, rad CP	Plastic rotation demand-CP, rad	Plastic rotation capacity, rad CP
CB1a		0.01517	VARIES	0.02205	VARIES	0.00267	VARIES
CB2a		0.01259	VARIES	0.02247	VARIES	0.00728	VARIES
CB3a		0.00188	VARIES	0.01017	VARIES		VARIES
CB4a		-	VARIES	0.00306	VARIES		VARIES
CB5a		-	VARIES	-	VARIES		VARIES
CB1b		0.01423	VARIES	0.01975	VARIES	0.00283	VARIES
CB2b		0.01111	VARIES	0.02088	VARIES	0.00720	VARIES
CB3b		0.00161	VARIES	0.00719	VARIES		VARIES
CB4b		-	VARIES	0.00318	VARIES		VARIES
CB5b		-	VARIES	-	VARIES		VARIES
CB(storey no.)a- central beam for selected storey at end a							
CB(storey no.)b- central beam for selected storey at end b							

Table 103. Mean values for plastic rotation at CP for central beams

COLUMN	NODMP		DMP		FD3	
LOC.	Plastic rotation demand-CP, rad	Plastic rotation capacity, rad CP	Plastic rotation demand-CP, rad	Plastic rotation capacity, rad CP	Plastic rotation demand-CP, rad	Plastic rotation capacity, rad CP
CC1L	NO PLASTIC ROTATION	VARIES	NO PLASTIC ROTATION	VARIES		VARIES
CC2L		VARIES		VARIES	0.00123	VARIES
CC3L		VARIES		VARIES	0.00065	VARIES
CC4L		VARIES		VARIES		VARIES
CC5L		VARIES		VARIES		VARIES
CC1R		VARIES		VARIES		VARIES
CC2R		VARIES		VARIES	0.00176	VARIES
CC3R		VARIES		VARIES	0.00052	VARIES
CC4R		VARIES		VARIES		VARIES
CC5R		VARIES		VARIES		VARIES
CC(storey no.)L- left central column for selected storey						
CC(storey no.)R- right central column for selected storey						

Table 104. Mean values for plastic rotation at CP for central columns

For the 7 seismic motions characteristic to soft soil type the CBF structure with FD3 damper has a better performance at SLS and ULS. No plastic hinges form in any element for this type of damper. At levels corresponding to CP the structure with FD3 dampers forms plastic hinges the central beams of the first 2 storeys. The main difference is the formation of plastic hinges in central columns that remain undamaged for the structure without dampers and that with SERB damper.

4.5.3 Numerical Modelling on CBF with FD3 dampers for Stiff Soil Type ($T_c=0.5s$)

Maximum drift levels (Fig. 4.62), maximum drift at each storey (Fig. 4.63) and top displacement for the structure (Fig. 4.64) with FD3 dampers are presented as mean values of recorded values for all 7 seismic motions at levels corresponding to SLS, ULS and CP in comparison with the same values recorded for the structure with SERB dampers and the structure without dampers in the braces.

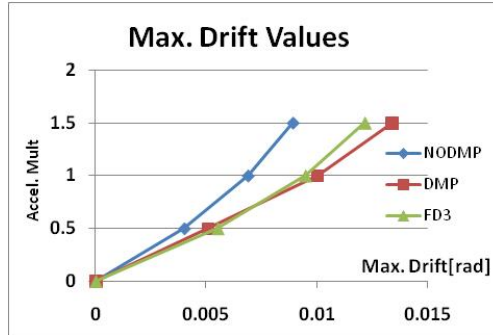


Fig. 4.62. Maximum drift values for the structure with and without dampers (stiff soil)

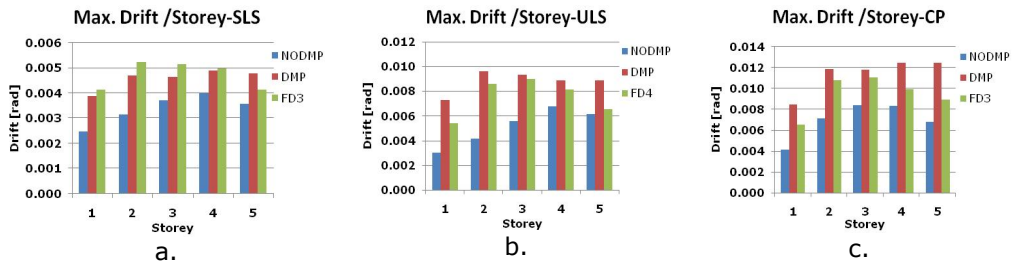


Fig. 4.63. Maximum drift at each storey at: a) SLS; b) ULS; c) CP for the structure with and without dampers (stiff soil)

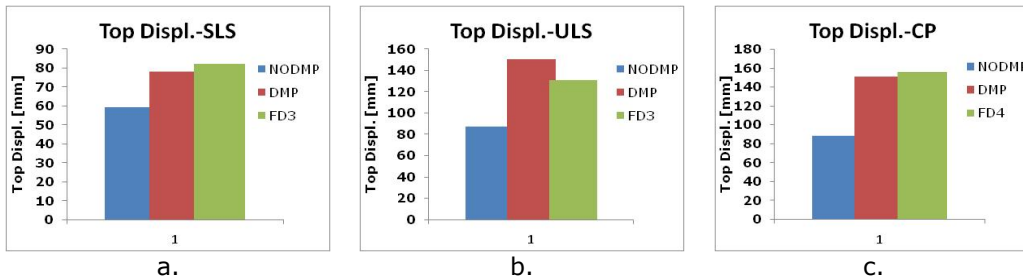


Fig. 4.64. Top displacement at: a) SLS; b) ULS; c) CP for the structure with and without dampers (stiff soil)

At the end of each seismic recording used the structure was left to vibrate freely for 10s. Recorded values of permanent displacement at top of the structure are presented as mean values for all 7 recordings in Fig. 4.65.

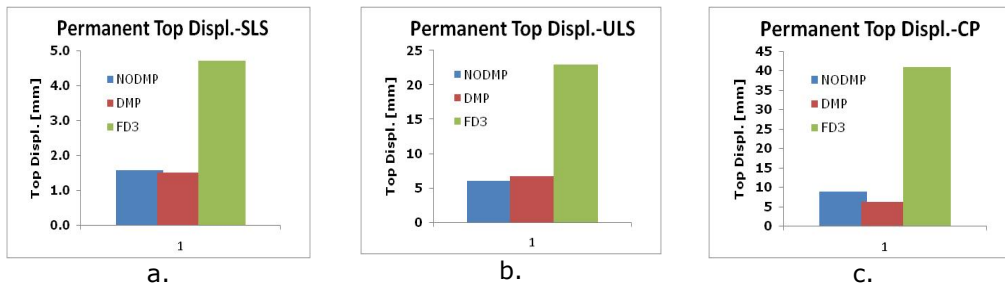


Fig. 4.65. Permanent top displacement at: a) SLS; b) ULS; c) CP (stiff soil)

For the 7 seismic motions characteristic for stiff soil type used the results showed that for all performance levels the building with FD3 dampers had a huge increase in values of permanent displacement compared with the structure without dampers and the structure with SERB dampers. At SLS drift values for the structure with FD3 dampers are the highest of the 3 compared structures. At ULS and CP, similar with the results obtained for the soft soil the FD3 damped structure has drift values between those recorded for the structure without dampers and that with SERB dampers. For seismic motions characteristic to stiff soil the structure with FD3 dampers does not form plastic hinges in any elements at any level of the seismic action.

4.5.4 Numerical Modelling on Dual MRF+CBF with FD3 dampers using 7 Semi-artificial Seismic Motion Characteristic for Soft Soil Type ($T_C=1.6s$)

Maximum drift levels (Fig. 4.66), maximum drift at each storey (Fig. 4.67) and top displacement for the structure (Fig. 4.68) with FD3 dampers are presented as mean values of recorded values for all 7 seismic motions at levels corresponding to SLS, ULS and CP in comparison with the same values recorded for the structure with SERB dampers and the structure without dampers in the braces.

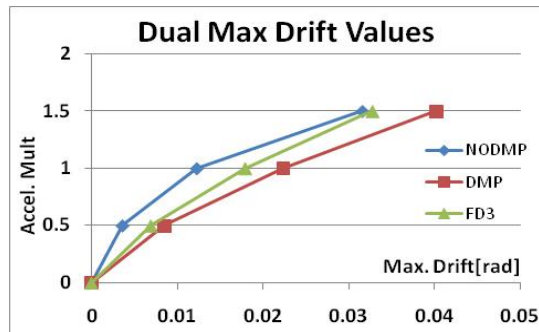


Fig. 4.66. Maximum drift values for the dual structure with and without dampers

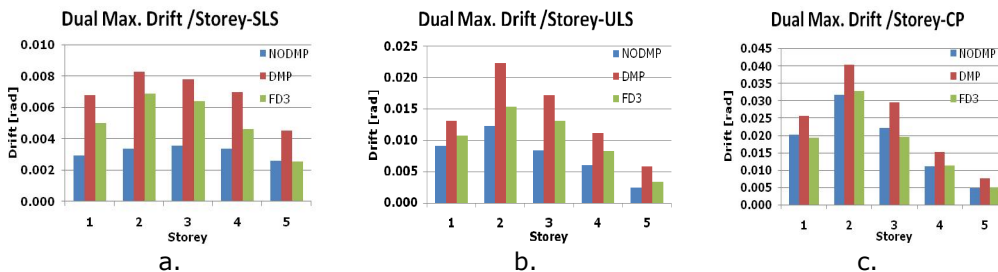


Fig. 4.67. Maximum drift at each storey at: a) SLS; b) ULS; c) CP for the dual structure with and without dampers

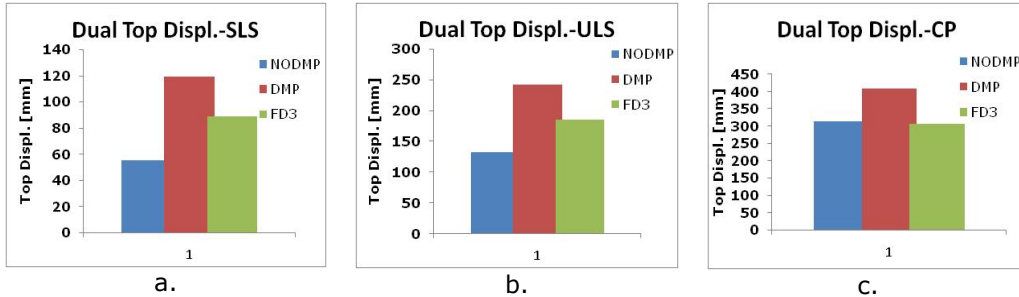


Fig. 4.68. Top displacement at: a) SLS; b) ULS; c) CP for the dual structure with and without dampers

At the end of each seismic recording used the structure was left to vibrate freely for 10s. Recorded values of permanent displacement at top of the structure are presented as mean values for all 7 recordings in Fig. 4.69.

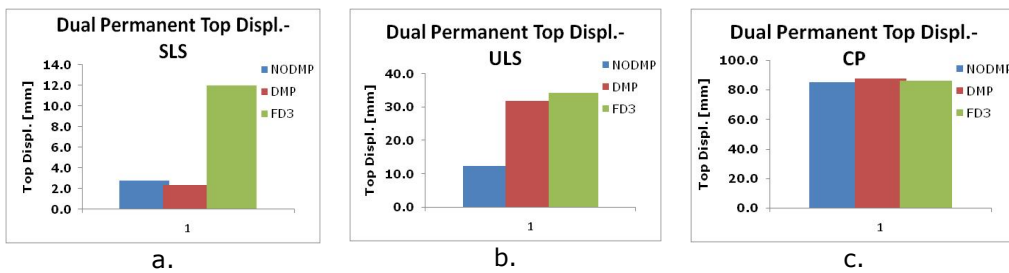


Fig. 4.69. Permanent top displacement at: a) SLS; b) ULS; c) CP for the dual structure with and without dampers

The behaviour recorded for the dual frame was similar to that of the simple CBF. For the 7 semi-artificial seismic motion characteristic for soft soil type used the structure with FD3 dampers has maximum drift values between the ones recorded for the structure without dampers and the structure with SERB dampers. It is noted here that at CP the structure with FD3 dampers has the lowest values of drift for most storeys. This is also valid for the case of recorded top displacement at levels corresponding to SLS and ULS. At CP the dual structure with FD3 dampers has slightly lower values of top displacement than the other 2 types of dual structures. Permanent displacement is approximately four times higher at SLS for this type of damper at SLS, only slightly higher at ULS and around the same values for CP. Values of plastic axial deformations and plastic rotations for all recordings can be found in Annex A1 and they are presented here as mean value for all 7 seismic recordings at (i)SLS with $a_{g,SLS} = 0.5 \cdot a_{g,ULS}$ (Table 105, Table 106, Table 107), (ii)ULS with $a_{g,ULS}$ (Table 108, Table 109, Table 110, Table 111, Table 112) and (iii)CP with $a_{g,CP} = 1.5 \cdot a_{g,ULS}$ (Table 113, Table 114, Table 115, Table 116, Table 117, Table 118).

(i) SLS with $a_{g,SLS} = 0.5 \cdot a_{g,ULS}$ characteristic for soft soil type ($T_C=1.6s$)

BRACE Compr.	Plastic deformation demand-SLS , mm			Plastic deformation capacity, mm
LOC.	NODMP	DMP	FD3	IO
BR1L	0.269	0.096	NO PLASTIC DEFORMATION	0.99125
BR1R	0.371	0.072		0.99125
BR2L	0.329	0.838		0.99125
BR2R	0.432	0.735		0.99125
BR3L	0.498	0.657		0.8945
BR3R	0.360	0.378		0.8945
BR4L	0.337	0.783		0.80175
BR4R	0.220	0.096		0.80175
BR5L	-	0.114		0.692
BR5R	-	-		0.692
BR(storey no.)R- right brace for selected storey				
BR(storey no.)L- left brace for selected storey				

Table 105. Mean values of axial plastic deformation for braces in compression at SLS

BRACE Tension	Plastic deformation demand-SLS , mm			Plastic deformation capacity, mm
LOC.	NODMP	DMP	FD3	IO
No plastic deformation				
BR(storey no.)R- right brace for selected storey				
BR(storey no.)L- left brace for selected storey				

Table 106. Mean values of axial plastic deformation for braces in tension at SLS

BEAM	NODMP		DMP		FD3
LOC.	Plastic rotation demand- SLS, rad	Plastic rotation capacity, rad LS	Plastic rotation demand- SLS, rad	Plastic rotation capacity, rad LS	Plastic rotation demand- SLS, rad
No plastic rotation in elements					
CB(storey no.)a- central beam for selected storey at end a					
CB(storey no.)b- central beam for selected storey at end b					

Table 107. Mean values for plastic rotation at SLS for central beams (soft soil)

(ii) ULS with $a_{g,ULS}$ characteristic for soft soil type ($T_C=1.6s$)

BRACE Compr.	Plastic deformation demand-ULS , mm			Plastic deformation capacity, mm
	LOC.	NODMP	DMP	
BR1L	1.953	1.586	NO PLASTIC DEFORMATION	19.825
BR1R	1.825	1.485		19.825
BR2L	1.687	2.374		19.825
BR2R	1.464	2.126		19.825
BR3L	1.282	1.838		17.89
BR3R	1.093	1.084		17.89
BR4L	0.985	1.751		16.035
BR4R	0.508	1.247		16.035
BR5L	0.114	0.877		13.84
BR5R	0.126	0.380		13.84
BR(storey no.)R- right brace for selected storey				
BR(storey no.)L- left brace for selected storey				

Table 108. Mean values of axial plastic deformation for braces in compression at ULS

BRACE Tension.	Plastic deformation demand-ULS , mm			Plastic deformation capacity, mm
	LOC.	NODMP	DMP	
BR1L	1.764	0.638	NO PLASTIC DEFORMATION	39.991
BR1R	3.859	1.046		39.991
BR2L	3.639	4.862		39.991
BR2R	6.713	6.135		39.991
BR3L	0.003	3.344		39.48
BR3R	0.038	5.978		39.48
BR4L	-	0.812		39.095
BR4R	-	0.892		39.095
BR5L	-	-		39.039
BR5R	-	-		39.039
BR(storey no.)R- right brace for selected storey				
BR(storey no.)L- left brace for selected storey				

Table 109. Mean values of axial plastic deformation for braces in tension at ULS

BEAM LOC.	NODMP		DMP		FD3
	Plastic rotation demand-ULS, rad	Plastic rotation capacity, rad LS	Plastic rotation demand-ULS, rad	Plastic rotation capacity, rad LS	
CB1a	0.00040	VARIES	0.00470	VARIES	NO PLASTIC ROTATION
CB2a	-	VARIES	0.00076	VARIES	
CB3a	-	VARIES	-	VARIES	
CB4a	-	VARIES	-	VARIES	
CB5a	-	VARIES	-	VARIES	
CB1b	0.00105	VARIES	0.00264	VARIES	
CB2b	-	VARIES	0.00066	VARIES	
CB3b	-	VARIES	-	VARIES	
CB4b	-	VARIES	-	VARIES	
CB5b	-	VARIES	-	VARIES	
CB(storey no.)a- central beam for selected storey at end a					
CB(storey no.)b- central beam for selected storey at end b					

Table 110. Mean values for plastic rotation at ULS for central beams

BEAM MRF	NODMP		DMP		FD3	
LOC.	Plastic rotation demand-ULS, rad	Plastic rotation capacity, rad LS	Plastic rotation demand-ULS, rad	Plastic rotation capacity, rad LS	Plastic rotation demand-ULS, rad	Plastic rotation capacity, rad LS
B1L	0.00088	0.0191	0.00678	0.0191	0.00366	0.0191
B2L	0.00050	0.0191	0.01004	0.0191	0.00253	0.0191
B3L	-	0.0191	0.00098	0.0191	0.00022	0.0191
B4L	-	0.0211	0.00009	0.0211	-	0.0211
B5L	-	0.0211	-	0.0211	-	0.0211
B1R	0.00277	0.0191	0.00853	0.0191	0.00389	0.0191
B2R	0.00124	0.0191	0.01156	0.0191	0.00257	0.0191
B3R	-	0.0191	0.00266	0.0191	0.00101	0.0191
B4R	-	0.0211	0.00017	0.0211	-	0.0211
B5R	-	0.0211	-	0.0211	-	0.0211
B(storey no.)L- left MRF frame beam for selected storey						
B(storey no.)R- right MRF frame beam for selected storey						

Table 111. Mean values for plastic rotation at ULS for MRF beams

COLUMN	NODMP		DMP		FD3
LOC.	Plastic rotation demand-ULS, rad	Plastic rotation capacity, rad LS	Plastic rotation demand-ULS, rad	Plastic rotation capacity, rad LS	Plastic rotation demand-ULS, rad
CC1L	-	VARIES	-	VARIES	NO PLASTIC ROTATION
CC2L	-	VARIES	0.00336	VARIES	
CC3L	-	VARIES	0.00446	VARIES	
CC4L	-	VARIES	-	VARIES	
CC5L	-	VARIES	-	VARIES	
CC1R	-	VARIES	0.00207	VARIES	
CC2R	-	VARIES	-	VARIES	
CC3R	-	VARIES	-	VARIES	
CC4R	-	VARIES	-	VARIES	
CC5R	-	VARIES	-	VARIES	
CC(storey no.)L- left central column for selected storey					
CC(storey no.)R- right central column for selected storey					

Table 112. Mean values for plastic rotation at ULS for central columns

(iii) CP with $a_{g,CP} = 1.5 \cdot a_{g,ULS}$ characteristic for soft soil type ($T_C = 1.6s$)

BRACE Compr.	Plastic deformation demand-CP , mm			FD3 NO PLASTIC DEFORMATION	Plastic deformation capacity, mm CP
	LOC.	NODMP	DMP		
BR1L	2.100	2.192		27.755	
BR1R	2.390	2.339		27.755	
BR2L	1.966	2.961		27.755	
BR2R	2.324	2.236		27.755	
BR3L	1.422	1.784		25.046	
BR3R	1.547	1.772		25.046	
BR4L	1.585	2.253		22.449	
BR4R	1.133	1.341		22.449	
BR5L	0.286	1.354		19.376	
BR5R	0.329	0.774		19.376	
BR(storey no.)R- right brace for selected storey					
BR(storey no.)L- left brace for selected storey					

Table 113. Mean values of axial plastic deformation for braces in compression at CP

BRACE Tension.	Plastic deformation demand-CP , mm			FD3 NO PLASTIC DEFORMATION	Plastic deformation capacity, mm CP
	LOC.	NODMP	DMP		
BR1L	11.927	6.883		51.417	
BR1R	10.895	4.433		51.417	
BR2L	19.780	18.833		51.417	
BR2R	19.766	18.171		51.417	
BR3L	0.184	15.371		50.76	
BR3R	0.211	14.920		50.76	
BR4L	0.000	2.455		50.265	
BR4R	0.036	2.043		50.265	
BR5L	-	-		50.193	
BR5R	-	0.032		50.193	
BR(storey no.)R- right brace for selected storey					
BR(storey no.)L- left brace for selected storey					

Table 114. Mean values of axial plastic deformation for braces in tension at CP

BEAM LOC.	NODMP		DMP		FD3	
	Plastic rotation demand-CP, rad	Plastic rotation capacity, rad CP	Plastic rotation demand-CP, rad	Plastic rotation capacity, rad CP	Plastic rotation demand-CP, rad	Plastic rotation capacity, rad CP
CB1a	0.01159	VARIES	0.01991	VARIES	0.00556	VARIES
CB2a	0.00643	VARIES	0.01379	VARIES	-	VARIES
CB3a	-	VARIES	-	VARIES	-	VARIES
CB4a	-	VARIES	-	VARIES	-	VARIES
CB5a	-	VARIES	-	VARIES	-	VARIES
CB1b	0.01557	VARIES	0.01383	VARIES	0.00331	VARIES
CB2b	0.00757	VARIES	0.01371	VARIES	-	VARIES
CB3b	-	VARIES	0.00308	VARIES	-	VARIES
CB4b	-	VARIES	0.00051	VARIES	-	VARIES
CB5b	-	VARIES	-	VARIES	-	VARIES
CB(storey no.)a- central beam for selected storey						
CB(storey no.)b- central beam for selected storey						

Table 115. Mean values for plastic rotation at CP for central beams

BEAM MRF	NODMP		DMP		FD3	
LOC.	Plastic rotation demand- CP, rad	Plastic rotation capacity, rad CP	Plastic rotation demand- CP, rad	Plastic rotation capacity, rad CP	Plastic rotation demand- CP, rad	Plastic rotation capacity, rad CP
B1L	0.01845	0.0286	0.02583	0.0286	0.0156	0.0286
B2L	0.02308	0.0286	0.03366	0.0286	0.0139	0.0286
B3L	0.00396	0.0286	0.00995	0.0286	0.0035	0.0286
B4L	-	0.0317	0.00074	0.0317	-	0.0317
B5L	-	0.0317		0.0317	-	0.0317
B1R	0.01806	0.0286	0.02418	0.0286	0.0161	0.0286
B2R	0.02236	0.0286	0.03357	0.0286	0.0143	0.0286
B3R	0.00451	0.0286	0.00841	0.0286	0.0035	0.0286
B4R	-	0.0317	0.00134	0.0317	-	0.0317
B5R	-	0.0317		0.0317	-	0.0317
B(storey no.)L- left MRF frame beam for selected storey						
B(storey no.)R- right MRF frame beam for selected storey						

Table 116. Mean values for plastic rotation at CP for MRF beams

COLUMN	NODMP		DMP		FD3	
LOC.	Plastic rotation demand- CP, rad	Plastic rotation capacity, rad CP	Plastic rotation demand- CP, rad	Plastic rotation capacity, rad CP	Plastic rotation demand- CP, rad	Plastic rotation capacity, rad CP
CC1L	0.00696	VARIES	0.00711	VARIES	0.00170	VARIES
CC2L	0.00832	VARIES	0.02922	VARIES	0.00801	VARIES
CC3L	0.01601	VARIES	0.01973	VARIES	0.00055	VARIES
CC4L	0.00013	VARIES	0.00101	VARIES	-	VARIES
CC5L	-	VARIES	-	VARIES	-	VARIES
CC1R	0.00202	VARIES	0.01482	VARIES	0.00493	VARIES
CC2R	0.01541	VARIES	0.02492	VARIES	0.00862	VARIES
CC3R	0.01317	VARIES	0.01727	VARIES	0.00128	VARIES
CC4R	-	VARIES	0.00157	VARIES	-	VARIES
CC5R	-	VARIES	-	VARIES	-	VARIES
CC(storey no.)L- left central column for selected storey						
CC(storey no.)R- right central column for selected storey						

Table 117. Mean values for plastic rotation at CP for central columns

COLUMN	NODMP		DMP		FD3	
LOC.	Plastic rotation demand-CP, rad	Plastic rotation capacity, rad CP	Plastic rotation demand-CP, rad	Plastic rotation capacity, rad CP	Plastic rotation demand-CP, rad	Plastic rotation capacity, rad CP
C1L	0.00648	VARIES	0.00734	VARIES	-	
C2L	-	VARIES	-	VARIES	0.00301	
C3L	-	VARIES	-	VARIES	0.00083	
C4L	-	VARIES	-	VARIES	-	
C5L	-	VARIES	-	VARIES	-	
C1R	0.00540	VARIES	0.00709	VARIES	0.00380	
C2R	-	VARIES	-	VARIES	0.00194	
C3R	-	VARIES	-	VARIES	-	
C4R	-	VARIES	-	VARIES	-	
C5R	-	VARIES	-	VARIES	-	
C(storey no.)L- left MRF column for selected storey						
C(storey no.)R- right MRF column for selected storey						

Table 118. Mean values for plastic rotation at CP for MRF columns

At levels of seismic motion corresponding to SLS and ULS the structure with FD3 dampers has no plastic hinges in braces central beams or any column. The only elements that form plastic hinges at ULS are the beams from the MRF with values of plastic rotation higher than the ones for the structure without dampers but lower than the ones recorded for the SERB damper. AT CP the structure with FD3 dampers forms plastic hinges in central beams and both central columns and columns of the MRF. Values of the plastic rotations for central columns is however lower than the ones recorded for the other dual structures but still exceed the acceptance criteria for some cases.

4.5.5 Numerical Modelling on Dual MRF+CBF with FD3 dampers for Stiff Soil Type ($T_c=0.5s$)

Maximum drift levels (Fig. 4.70), maximum drift at each storey (Fig. 4.71) and top displacement for the structure (Fig. 4.72) without dampers are presented as mean values of recorded values for all 7 seismic motions at levels corresponding to SLS, ULS and CP in comparison with the same values recorded for the structure with SERB dampers and the structure with no dampers in the braces.

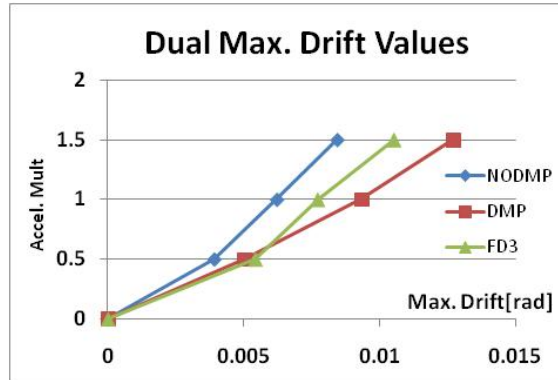


Fig. 4.70. Maximum drift values for the structure with and without dampers (stiff soil)

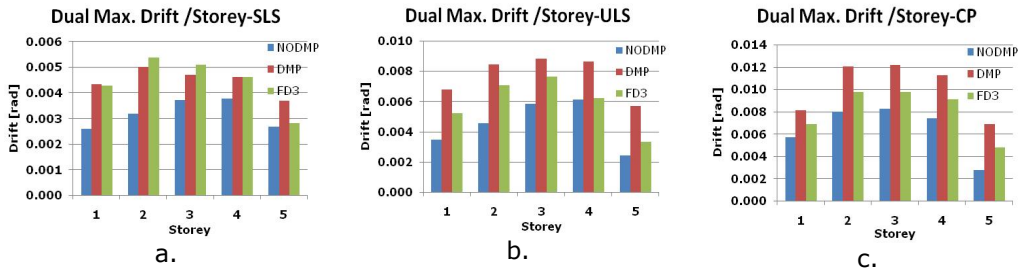


Fig. 4.71. Maximum drift at each storey at: a) SLS; b) ULS; c) CP for the dual structure with and without dampers (stiff soil)

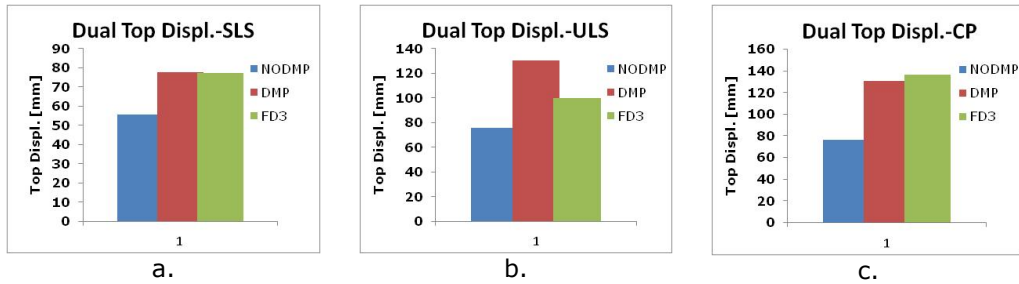


Fig. 4.72. Top displacement at: a) SLS; b) ULS; c) CP for the structure with and without dampers (stiff soil)

At the end of each seismic recording used the structure was left to vibrate freely for 10s. Recorded values of permanent displacement at top of the structure are presented as mean values for all 7 recordings in Fig. 4.73.

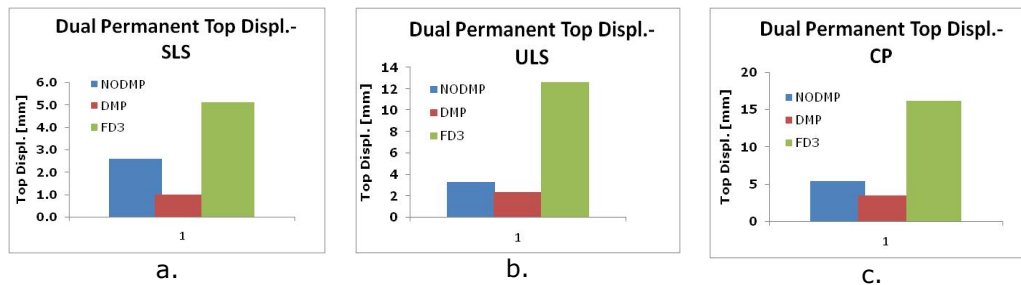


Fig. 4.73. Permanent top displacement at: a) SLS; b) ULS; c) CP for the structure with and without dampers (stiff soil)

Drift values for the structure with FD3 dampers are higher than the ones for the structure with SERB dampers and the structure without dampers but only at levels corresponding to SLS. At ULS and CP drift values are in-between the ones for the structure with no dampers and the structure with SERB dampers. Top displacement is similar as that recorded for the other type of damper at SLS and CP and has smaller values than the other type of damper at ULS. Permanent displacement is significantly higher at all levels for the FD3 damper. For seismic motions characteristic to stiff soil the structure with FD3 dampers does not form plastic hinges in any elements at any level of the seismic action.

4.6 Conclusions

Based on the results of the experimental program a numerical model was developed for the damper analysed in this paper and for the brace with damper assembly. In addition a numerical model for a second type of friction damper with rectangular hysteretic loops was implemented in the numerical model of the structure. Two types of structures were designed and modelled: (i) a concentrically braced structure with braces in the midspan and 2 adjacent MRF frames with beams considered pinned at both ends and (ii) a dual frame structure with concentric bracing in the midspan and two adjacent MRF frames, both types with the same dimensions in plan and elevation and the same considered loads. Numerical time-history analysis were made on these two frames using 2 sets of seismic motions scaled on the elastic response spectra: (i) 7 seismic motions characteristic for soft soil type with $T_c=1.6s$ and (ii) 7 seismic motions characteristic for stiff soil type with $T_c=0.5s$. Each of the two structures was analysed in 3 configurations: (i) "normal" structure without any dampers in the braces, (ii) structures with SERB type dampers in the braces and (iii) structures with FD3 type dampers in the braces. The obtained results are discussed comparing the performance the structures with each types of dampers to the structures without any dampers.

4.6.1 Structures with SERB Type Dampers in the Braces

Both CBF and dual MRF+CBF structures with SERB dampers had a similar

behaviour. The structures with dampers were more flexible in all cases with drift levels and values of maximum top displacement higher than the ones of the structures without dampers at all performance levels under both types of seismic motions. Values of permanent displacement differ from one type of seismic motion used to the other as follows: for seismic motions characteristic to soft soil type both CBF and dual MRF+CBF structures with dampers have higher values of permanent displacement than the ones without dampers and for seismic motions characteristic to stiff soil type the introduction of the damper in the braces lead to a reduction of permanent drift values for both structures.

Plastic hinge formation in elements and the values of plastic axial deformations and plastic rotations were similar for the two structures but are different for each type of seismic motion as follows:

- At SLS with $a_{g,SLS} = 0.5 \cdot a_{g,ULS}$ plastic hinges appear exclusively in the braces. For soft soil ($T_C=1.6s$) the structure with SERB dampers has a higher number of plastic hinges in the braces than the structure without dampers with higher values of plastic axial deformations that in some cases no longer satisfy the acceptance criteria for the corresponding performance level (IO). For stiff soil ($T_C=0.5s$) the damper avoids almost completely the formation of plastic hinges in braces keeping the structures in elastic domain.
- At ULS with $a_{g,ULS}$ the two structures continue to have a similar behaviour. For soft soil ($T_C=1.6s$) the structures with dampers behave worse than the "undamped" ones. Plastic hinges form in non-dissipative elements (central beams of the CBF frame and central beams and columns for the dual frame) with values of plastic rotations that in some cases do not satisfy the acceptance criteria for the corresponding performance level (LS). For stiff soil ($T_C=0.5s$) plastic hinges are limited to braces for both structures. The structures with and without dampers have a similar behaviour with values of all plastic axial deformation that satisfy the acceptance criteria for LS.
- At CP with $a_{g,SLS} = 1.5 \cdot a_{g,ULS}$ the type of seismic motion greatly influences the behaviour of the structures. For soft soil ($T_C=1.6s$) the structures with dampers form plastic hinges in central beams of the CBF and central beams and columns for the dual structures. Values of plastic rotation do not satisfy the acceptance criteria for CP. The behaviour of the structures is considered unsatisfactory due to the large number of plastic hinges that form in non-dissipative elements. For stiff soil ($T_C=0.5s$) the dual structure with dampers does not have plastic hinges in central beams or columns. Plastic hinges are developed only in the braces and in the MRF beams with values of plastic axial deformation and rotation that satisfy the acceptance criteria for CP. For the CBF frame plastic hinges form only in braces with only a few exceptions when plastic rotations are recorded in central beams but with very low values.

As a conclusion this type of damper has a negative influence on the behaviour of the structures for earthquakes characterized by long corner period $T_C=1.6s$ (soft soil). Under this type of seismic motions the structures with dampers form plastic hinges in non-dissipative elements with values that exceed the

acceptance criteria for the corresponding performance levels. However this type of damper is efficient in reducing the seismic response of a building for earthquakes characterized by short corner period $T_c=0.5s$ (stiff soil) by preventing the formation of plastic hinges at SLS and reducing the permanent displacement of the structure.

4.6.2 Structures with FD3 Type Damper in the Braces

Both CBF and dual MRF+CBF structures with FD3 dampers had a similar general behaviour with small differences at certain performance levels. The behaviour of these structures differs depending on the type of seismic motion.

- For soft soil ($T_c=1.6s$) the type of FD3 structures have higher values of drift and top displacement than the "undamped" structures. At SLS and ULS the CBF structure has no plastic hinges in any elements and the dual structure forms plastic hinges only in MRF beams. At CP the behaviour of both structures with this type of damper is considered unsatisfactory due to formation of plastic hinges in central beams and several columns.
- For stiff soil ($T_c=0.5s$) the structures with FD3 dampers have lower values of drift only for SLS and higher at ULS and CP. Top displacement is higher for the structures with dampers at all levels of seismic action. No plastic hinges appear in any of the two structures with FD3 dampers regardless of the level of seismic action.

All the structures with dampers exhibited a significant increase in permanent displacement regardless of the type of seismic motion used or performance level considered.

This type of damper is efficient in reducing the seismic response of CBF and dual MRF+CBF structures for earthquakes characterized by long corner period $T_c=1.6s$ (soft soil) at SLS and ULS avoiding the formation of plastic hinges in elements.

For earthquakes characterized by short corner period $T_c=0.5s$ (stiff soil) both structures with FD3 damper remained in elastic domain, no plastic hinges being formed in any elements at any level. However, due to its high inelastic behaviour, this damper leads to high values of permanent displacement of the structure.

It should be again highlighted that these 2 types of dampers exhibit completely different hysteresis mechanisms. FD3 dampers allow for a larger ductility demand with respect to SERB dampers, while dissipating a significant amount of seismic energy due to their wider hysteretic loops. On the other hand the SERB damper prototype showed higher values of axial force due to hardening of the material which may limit the displacements for unexpected strong earthquakes but in the same time may result in larger forces transmitted to beams and columns. This damper provides excellent performance in reducing the residual displacement of the top floor and also reduces maximum displacements at SLS. It should be noted that significant values of residual displacement were recorded when using FD3 friction dampers.

5 Design Recommendations

Using the results from the numerical analyses and current design provisions from Eurocode, FEMA356 and NBCC a design procedure is proposed for each of the two damper types.

5.1 Design Provisions for Structures with FD3 Type Dampers

As basis for the design principles proposed for this type of damper Eurocode 8 seismic design provisions for concentrically braced frames are taken and adapted for this case as follows:

Design criteria:

- For friction dampers with a rectangular shape hysteretic behaviour such as FD3 damper installed in the braces, the dampers are the dissipative components while braces, beams and columns are non-dissipative.
- The diagonals will be placed in such a way as to ensure a similar load deflection of the structure, at each storey, in opposite senses, under load reversals.

Analysis:

- Beams and columns will be designed to resist gravity loads without taking into account the braces
- For V bracing system both tension and compression diagonals will be taken into account in an elastic analysis. This criteria remains valid for the use of friction dampers both dampers installed in the V braces must be taken into account.

Diagonal members:

- In frames with V bracings non-dimensional slenderness $\bar{\lambda} \leq 2.0$. This criterion no longer applies for the case with dampers. Braces are designed to remain in elastic domain with sufficient over strength to the damper installed.
- Compression diagonals shall be designed for compression resistance according to EN 1993[30]. For the case of FD dampers installed the braces under compression shall be designed for compression resistance according to EN 1993[30] at 130% maximum force in the damper (slip force).
- The connection of the diagonals to other members and to the damping device will be designed at 130% maximum force in the damper (slip force).
- To ensure a homogeneous dissipative behaviour in the braces maximum and minimum overstrength Ω does not differ by more than 25%. For the case of FD damper the overstrength will be calculated as

$$\Omega = \frac{N_{DMP}}{N_{Ed}}$$

where:

- N_{DMP} = slip force of the damper
- N_{Ed} = design axial force

Beams and Columns:

Beam, columns and braces with axial forces should meet the following requirement:

$$N_{Pl,Rd}(M_{Ed}) \geq N_{Ed,G} + \gamma_{ov} \Omega \cdot N_{Ed,E}$$

where:

$N_{Pl,Rd}(M_{Ed})$ = design buckling resistance according to EN 1993 taking into account the interaction of the buckling resistance with bending moment defined as its design values in seismic design situation

$N_{Ed,G}$ = axial force due to non seismic action

$N_{Ed,E}$ = axial force due to seismic design action

γ_{ov} = overstrength factor

Ω = minimum value of $\Omega_i = N_{DMP,i} / N_{Ed,i}$ over all dampers of the braced system; where

N_{DMP} = slip force of the damper installed in brace i

N_{Ed} = design axial force in the same brace in the seismic design situation

In addition beams in the case of V bracings shall be design to resist:

- All non-seismic actions without taking into account the braces
- The unbalanced vertical seismic action effect applied to the beam after buckling of compression diagonal. In the case of FD dampers the vertical seismic action effect is cancelled because of the symmetric behaviour of the dampers in tension and compression. Instead the beam should be designed to resist the axial force component induced by 130% of the slip force in each damper ($\gamma_{ov} = 1.3$) as shown in Fig. 5.1.

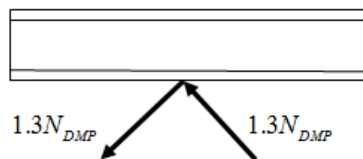


Fig. 5.1. Axial force component for beams in the case of V bracings with dampers

A discussion can be made here concerning the design of the beam in the case of V braces. The design method in which the beam is no longer designed for unbalanced vertical seismic action effect but is instead designed for axial force components corresponding to 130% of the slip force in both dampers replaces the general design for beams and columns using Ω as the minimum value of

$\Omega_i = N_{DMP,i} / N_{Ed,i}$ over all diagonal of the braced system. Furthermore Romanian Seismic Design Code P100/2006[1] recommends the use of Ω as maximum value of $\Omega_i = N_{DMP,i} / N_{Ed,i}$ over all diagonals. A small parametric study was conducted to determine the optimum method for the design of the beam in this case. Being the most direct method axial force in the beam was determined by directly applying the two components of the slip force in both braces amplified with a 1.3 coefficient. This axial force distribution was then compared to the axial force distribution obtained from the load combination that has the seismic action amplified by the factor $\gamma_{ov} \Omega$. Because the damper behaviour is similar to an ideal elasto-plastic behaviour, without strengthening, the coefficient of 1.1 was neglected and the value for the overstrength factor γ_{ov} was taken as 1.3. Ω was calculated as both minimum and maximum values of $\Omega_i = N_{DMP,i} / N_{Ed,i}$ over all diagonals. Axial force values closer to the ones obtained for the direct method were obtained by the use of the maximum values of Ω , however these values were still smaller the ones obtained by direct application of axial force components. As a conclusion to this small discussion the author recommends that the beams in the case of V braces should be designed using the axial force obtained from the pair of forces equal to 130% of the damper slip force and that columns should be designed using the maximum values of Ω_i calculated as $\Omega_i = N_{DMP,i} / N_{Ed,i}$ with an overstrength factor $\gamma_{ov} = 1.3$.

Damage limitations:

- Limitation of interstory drift is done according to EN1998-1 section 4.4.3.2[7]

Damper design:

- Damper displacement will be taken as 130% of maximum calculated displacement for CP (for example a considered earthquake which corresponds to a probability of exceedance of 2% in 50 years according to FEMA356[10]).
- All damper properties will be determined experimentally.

Based on these principles a design procedure is proposed for structures using friction dampers with rectangular hysteretic behaviour as follows:

1. Evaluation of gravity loads
 - Permanent load
 - Live load
2. Evaluation of seismic load
 - Determine the design response spectra base on the elastic response spectra characteristic to the location of the structure. The main issue here is the determination of the behaviour factor q . Because the rectangular shape hysteretic behaviour of the friction dampers is symmetrical in tension and compression, with negligible degradation, the behaviour of steel frames with this type of dampers is very similar to the behaviour of a structure with buckling restrained braces (BRB). Because the structures with BRB's have similar structural ductility to eccentrically braced frames and have the same reduction factor R in AISC 2002 [33] the behaviour factor for steel structures with BRB's can be taken equal to the behaviour factor for eccentrically braced frames from EN 1998-1[7]. This value of the behaviour factor of $q=6$ can be

adopted for steel structures with this type of friction dampers in the braces.

3. Element design at ULS in the fundamental design situation.
4. Brace design in the seismic design situation (using a behaviour factor $q=6$)
5. Evaluate damper slip load by:

$$N_{DMP} = N_{b,Rd}$$

where:

$N_{DMP,i}$ = slip force of the damper installed in brace i

$N_{Ed,i}$ = buckling resistance of brace i

6. Redesign braces at 130% slip load of damper
7. Design of beams and columns:
Columns: designed from seismic load combination containing the seismic load amplified by $\gamma_{ov}\Omega$ with Ω calculated as maximum values of $\Omega_i = N_{DMP,i}/N_{Ed,i}$ over all dampers, and $\gamma_{ov} = 1.3$
Beams: designed to resist the axial force component induced by 130% of the slip force in each damper as shown in Fig. 5.1.
8. Damage limitation: limitation of interstory drifts (EN 1998-1[7]).
Damper stiffness (until slip force is reached) should be chosen to satisfy damage limitation criteria for the structure at SLS.
9. Determination of maximum damper displacement as 130% of maximum displacement at considered earthquake at CP.
Maximum displacement (maximum drift) at CP can be calculated as:

$$d_r^{CP} = c \cdot q \cdot d_{re} \text{ (P100/2006[1])}$$

Where:

d_r^{CP} = maximum storey drift at CP

q = behaviour factor

d_{re} = maximum storey drift determined from static elastic analysis under design seismic load

c = displacement amplification coefficient that takes into account that for $T < T_C$ (T_C corner period of the response spectra) that inelastic displacement from seismic action are much larger than the elastic ones. Values for c can be calculated from:

$$1 < c = 3 - 2.5 \frac{T}{T_C} \leq 2 \text{ (P100/2006[1])}.$$

10. Prototype testing.

Damper properties should be determined experimentally.

The design criteria and design procedure proposed are aligned with design criteria for concentrically braced frames in EUROCODE 8 and contain special considerations from FEMA356 regarding structures with passive energy dissipation and from the Romanian seismic design code P100/2006.

The author strongly recommends that the performance of the dimensioned structure with dampers be determine through nonlinear time history analyses.

5.2 Design Provisions for Structures with SERB Type Dampers

The design provisions proposed for the design of structures with SERB type dampers require that the structure be designed at 3 limit states: SLS, ULS and CP. Specific provisions at each limit state will provide the designer with the dimension of structural elements and required damper parameters. For the design process the damper behaviour is considered with a simplified bilinear behaviour having two branches with stiffness $K_1 \ll K_2$. Damper properties that need to be determined and that lead to the selection of the damper itself are: (i) stiffness K_1 , (ii) displacement limit for first branch d_1 , (iii) maximum force of the damper F_{MAX} and (iv) maximum stroke of the damper d_m (Fig. 5.2).

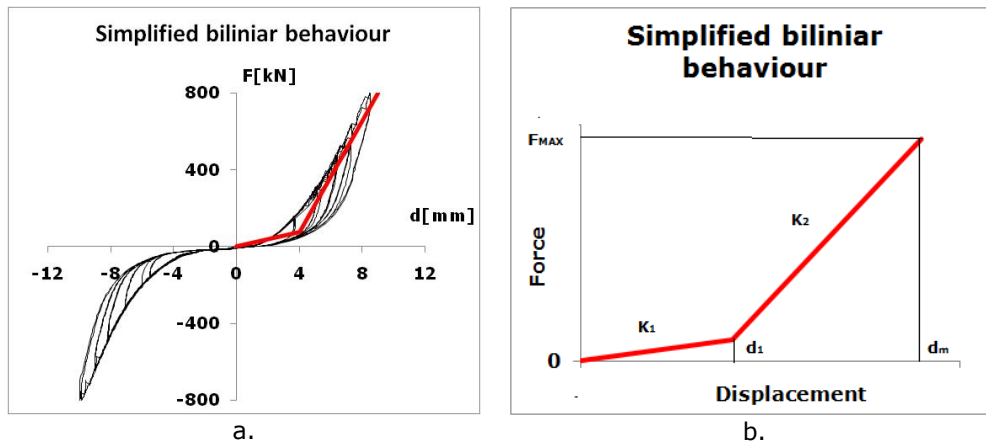


Fig. 5.2. Simplified damper behaviour: a) Example on experimental damper behaviour; b) simplified bilinear curve parameters

Design at SLS:

- Limitation of interstory drift is the main criteria for this limit state.
- Maximum displacement (maximum drift) at SLS must satisfy:

$$d_{re} \leq d_{r,a}^{SLS}$$

Where:

- $d_{r,a}^{SLS}$ = allowable drift at SLS
- d_{re} = maximum storey drift determined from static elastic analysis under design seismic load for SLS
- Values of the behaviour factor q should be taken as for an elastic structure ($q=1$).
- The design seismic load at SLS should be calculated taking into account the presence of the damper by means of viscous damping coefficient ξ .
- The structural model should include the stiffness of both the damper and the brace.
- Damper behaviour at SLS should be limited to the first branch of the simplified bilinear model as a simple linear elastic element.
- Damper effects are considered by introducing a linear elastic element in

the braces with a given stiffness and by supplemental damping ξ applied to seismic design loads (values of ξ for the damping device should be provided by the manufacturer based on stiffness and displacement of the first branch).

- Damper stiffness K_1 and displacement limit for the first branch d_1 will be determined to ensure the damper behaviour is limited to the first branch.
- It would also be recommended that values of stiffness K_1 of the damper increase the period of the structure to values beyond that of the corner period of vibration of the seismic motion ($T > T_C$). Ideally values of K_1 should be taken as minimum values that still satisfy drift condition and that also satisfy the condition $T > T_C$.

Design at ULS:

- Design of elements under design seismic action calculated with behaviour factors $q=1$ and increase in damping ξ given by the damper itself.
- The structural model should include the stiffness of both the damper and the brace.
- Stiffness of the linear elastic model of the damper should be considered as an equivalent stiffness K_{ech} (Fig. 5.5)

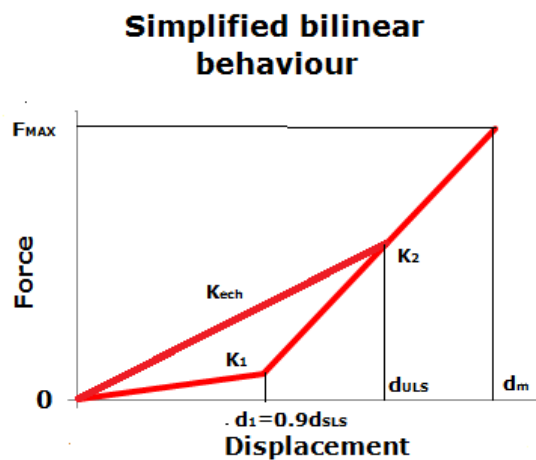


Fig. 5.3. Simplified damper behaviour at ULS

Design at CP:

Damper maximum displacement d_m will be taken as 130% of maximum calculated displacement for CP

Damper maximum force capacity F_{MAX} will be taken as 130% of maximum calculated force in the device for (FEMA356[10])

Based on these principles a design procedure is proposed for structures using SERB friction dampers with hardening branch hysteretic behaviour as follows:

1. Evaluation of gravity loads

Permanent load

Live load

2. Evaluation of seismic load

Determine the design response spectra base on the elastic response spectra characteristic to the location of the structure with behaviour factor $q=1$ and increased values of damping ξ . Values for ξ should be taken after careful consideration and if possible after consulting the manufacturer. The effect of supplemental damping is taken into account in determining the design seismic action through the values of the damping correction factor

$$\eta = \sqrt{10/(5 - \xi)} \geq 0.55 \text{ (EN1998-1[7])}$$

3. Element pre-design at ULS. This step is a predimensioning of structural elements and does not take into account the effects of the damper other then the supplemental damping included in the design seismic action.(for a first iteration values of ξ can be taken as the minimum values guaranteed for this type of damper)

4. Design at SLS. Using the element dimensions from the predimensioning stage the model of the structure must now include the damper simplified model as a linear elastic element. Design seismic action is calculated considering, $q=1$, and for a first iteration the same values of ξ as the ones used at previous step can be considered. Values of stiffness K_1 and displacement limit for the first branch d_1 will be determined from maximum drift values of $d_{re} = 0.9 \cdot d_{r,a}^{SLS}$. If possible minimum values of K_1 will be chosen to also satisfy the condition $T > T_C$. This is an iterative process as the values of ξ for the damper are dependent on parameters K_1 and d_1 .

5. Design at CP. Determination of damper maximum displacement d_m from drift and damper maximum force capacity F_{MAX} at CP.

6. Element design at ULS. Knowing all the parameters of the damper the simplified behaviour of the damper as a linear elastic element with equivalent stiffness can be computed and implemented in the model. All structural elements except damper should be designed:

$$N_{Pl,Rd}(M_{Ed}) \geq N_{Ed,G} + 1.3 \cdot N_{Ed,E}$$

where:

$N_{Pl,Rd}(M_{Ed})$ = design buckling resistance according to EN 1993 taking into account the interaction of the buckling resistance with bending moment defined as its design values in seismic design situation

$N_{Ed,G}$ = axial force in beam or column due to non seismic action

$N_{Ed,E}$ = axial force in beam or column due to seismic design action

1.3 = safety factor. The structure is considered brittle and is over designed to take into account the variability of the seismic motion.

7. Prototype testing.

Damper properties should be determined experimentally.

The author strongly recommends that the performance of the dimensioned

structure with dampers be determined through nonlinear time history analyses. It should be noted that another approach is possible for this case. In principle values of the behaviour factor could be taken $q > 1$ leading to a dissipative design method. Using higher values of q factor (for example $q = 2.5$ for CBF structures) will result in having 2 sources of energy dissipation in the structure: the damper installed in the brace and the energy dissipation provided by the ductile behaviour of the brace.

Difference in design:

- The structure is designed using $q = 2.5$.
- The braces are designed under design seismic actions
- The damper, the beams and the columns are dimensioned using capacity based design.

Taking into account the value of the behaviour factor 2.5 and that values of overstrength factor Ω will range between 2 and 2.5, no important gains in material consumption will be obtained (material consumption will vary mostly for the braces). In addition this design concept automatically implies the acceptance of degradation in the structure (braces will enter plastic domain) that can lead to supplementary repair costs. Numerical analyses presented in chapter 4 showed that this design concept has a negative influence on the behaviour of the structures for earthquakes characterized by long corner period $T_C = 1.6s$ (soft soil). Under this type of seismic motions the structures with dampers form plastic hinges in non-dissipative elements with values that exceed the acceptance criteria for the corresponding performance levels. For earthquakes characterized by short corner period $T_C = 0.5s$ (stiff soil) the damper improved the behaviour at SLS, by preventing the formation of plastic hinges, and reduced the permanent displacement of the structure. Therefore the design of the structure for the case study was made according to design methodology proposed in this sub-chapter.

5.3 Case Studies

5.3.1 Case Study for Structure with FD3 Damper

For the case study a CBF structure with the same dimensions and load considerations as the structure presented in section 4.3.1 was considered. The structure was designed following the design procedure proposed.

Loads considered:

- Permanent load: $p = 10.75kN / m$ from bay, $P = 60kN$ from secondary beams;
- Live load: $q = 3kN / m$ from bay, $Q = 36kN$ from secondary beams;
- Seismic load: design spectra for Bucharest with a corner period of $T_C = 1.6s$ (Fig. 5.4) with behaviour factor $q = 6$ (high ductility class)

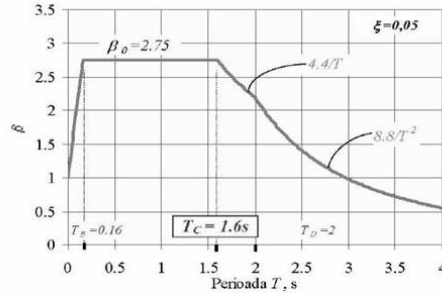


Fig. 5.4. Design spectra for Bucharest [1]

The computed mass at each level for spectral and modal analysis is $m = 113.3t$ for levels 1 through 4 and $m = 106.7t$ for the top level.

Design of elements under the fundamental load combination.

Design at ULS:

- Dissipative elements (braces) were designed at $1.0G + E + 0.4Q$. Using the resulted dimensions of the braces the damper slip load was considered as $N_{DMP} = N_{b,Rd}$ (Table 119).

where:

$N_{DMP,i}$ = slip force of the damper installed in brace i

$N_{Ed,i}$ = buckling resistance of brace i

Storey	Brace Section	$N_{b,Rd}$ [kN]	N_{DMP} [kN]
1	HEA180	523.34	530
2	HEA180	523.34	530
3	HEA160	381.885	390
4	HEA160	381.885	390
5	HEA160	159.2	160

Table 119. Selection of damper slip load

After the determination of damper slip load braces were redesigned at 130% slip load of damper.

Design of beams and columns:

Columns: designed from seismic load combination containing the seismic load amplified by $\gamma_{ov}\Omega = 2.15$ with Ω calculated as maximum values of $\Omega_i = N_{DMP,i}/N_{Ed,i}$ over all diagonals, and $\gamma_{ov} = 1.3$

Beams: designed to resist the axial force component induced by 130% of the slip force in each damper

Design at SLS:

Limitation of interstory drift and determination of damper stiffness.

Design at CP:

Determination of maximum damper displacement as 130% of maximum displacement at CP.

The resulting dimensions for the CBF structure are presented in Fig. 5.5.

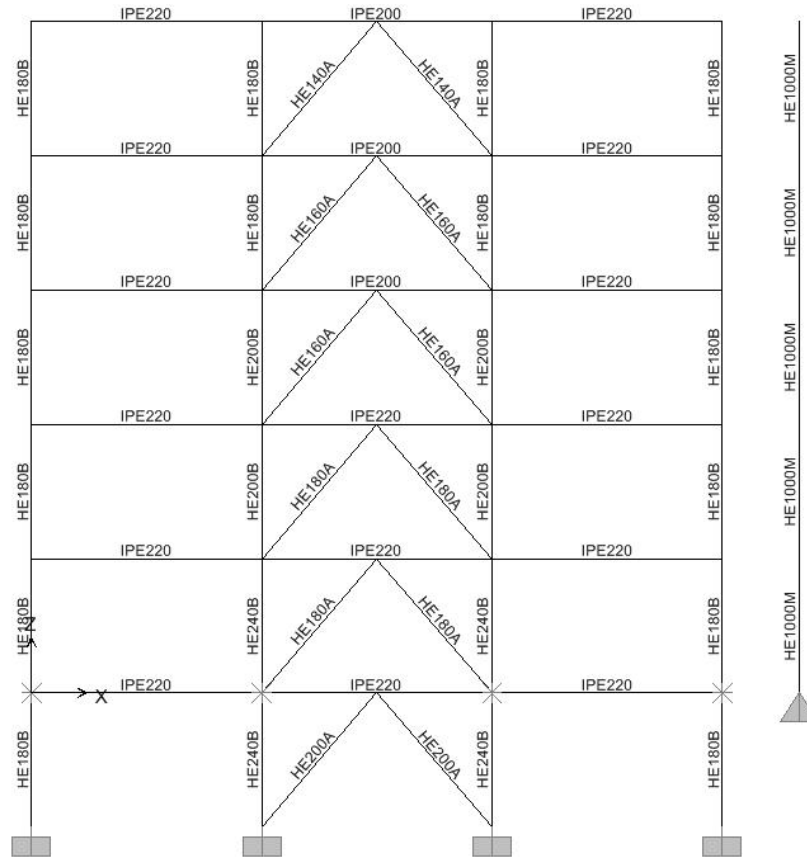


Fig. 5.5. Section dimensions for the CBF with FD3 dampers case study

5.3.2 Case Study for Structure with SERB Damper

For the case study a CBF structure with the same dimensions and load considerations as the structure presented in section 4.3.1 was considered. The structure was designed following the design procedure proposed. Seismic action was considered through equivalent lateral forces computed using lateral force method.

Loads considered:

- Permanent load: $p = 10.75 \text{ kN/m}$ from bay, $P = 60 \text{ kN}$ from secondary beams;
- Live load: $q = 3 \text{ kN/m}$ from bay, $Q = 36 \text{ kN}$ from secondary beams;
- Seismic load: equivalent lateral forces computed using lateral force method with design spectra for Bucharest with a corner period of $T_c = 1.6 \text{ s}$ (Fig. 5.4) and behaviour factor $q = 1$.

The computed mass at each level for spectral and modal analysis is

$m = 113.3t$ for levels 1 through 4 and $m = 106.7t$ for the top level.

Predesign at ULS:

- Predesign of elements using gravity actions and seismic actions introduced by means of equivalent lateral forces computed using lateral force method without considering damper with $q = 1$ and $a_g = 0.24g$.

Design at SLS:

- Structure model included damper effects by introducing linear elastic behaviour elements (links) in the braces and by recalculating design spectra with $a_{g,SLS} = 0.5 \cdot a_{g,ULS}$ and increased damping values.
- From drift limitation conditions stiffness K_1 and displacement limit for the first branch d_1 were determined. After several iterations values obtained were $K_1 = 50000 \text{ kN/m}$ and $d_1 = 11 \text{ mm}$.

Design at CP:

- Several iterations were made changing values of damper stiffness in the model to obtain maximum displacement d_m from drift and damper maximum force capacity F_{MAX} . It should be noted that damper stiffness in the linear elastic model represents equivalent stiffness of the simplified bilinear model considered for the model (see also Fig. 5.3).
- Values obtained for damper parameters were $d_m = 29.2 \text{ mm}$ and $F_{MAX} = 2280 \text{ kN}$ corresponding to a stiffness of the second branch $K_1 \approx 130000 \text{ kN/m}$.

Redesign at ULS:

- Using the considered bilinear behaviour of the damper several iterations were made varying equivalent stiffness and recalculating lateral forces at each step in the structural model that includes the damper, considering an overstrength factor of 1.3 for seismic design action.

The resulting dimensions for the CBF structure are presented in Fig. 5.6.

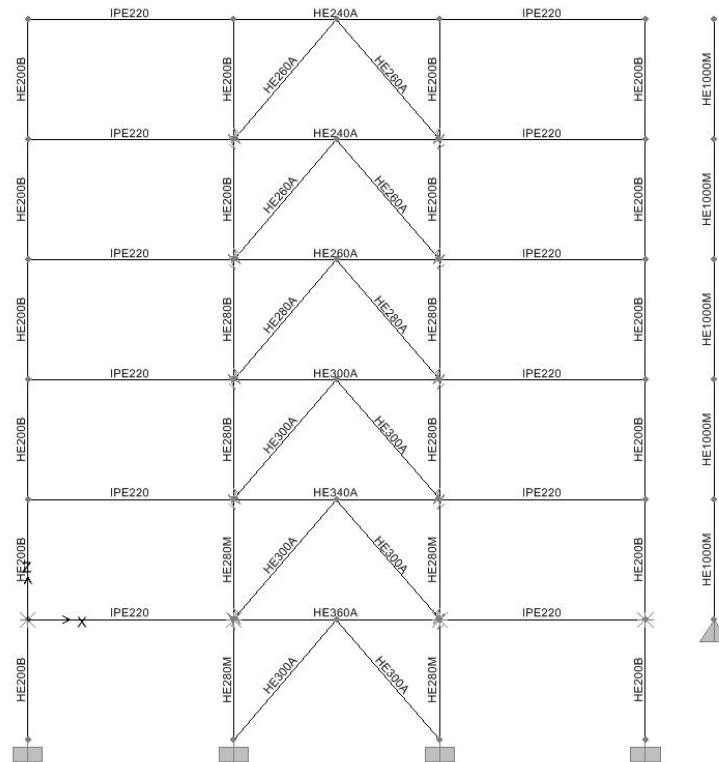


Fig. 5.6. Section dimensions for the CBF with SERB dampers case study

5.3.3 Evaluation of Seismic Performance

The performance of the structures was evaluated using nonlinear time-history analyses using (i) 3 seismic recordings characteristic to soft soil type ($T_C=1.6s$) and (ii) 3 seismic recordings characteristic to stiff soil ($T_C=0.5s$), scaled on the elastic response spectra relevant to their type. The two target spectra were scaled to the fundamental period of vibration of the analysed structure, so as to yield roughly the same design seismic forces. The results will be presented for the pair of seismic recording that generated the maximum response in the structure. The performance of the 2 structures with dampers will be compared with the structure without dampers where relevant.

5.3.3.1 Seismic recordings characteristic to soft soil ($T_C=1.6s$),

Maximum drift levels (Fig. 5.7), maximum drift at each storey (Fig. 5.8), top displacement for the structure (Fig. 5.9) and permanent displacement (Fig. 5.10) of the structures with dampers are presented for maximum seismic motion at levels corresponding to SLS, ULS and CP. The results are compared to the values obtained for the structure without dampers.

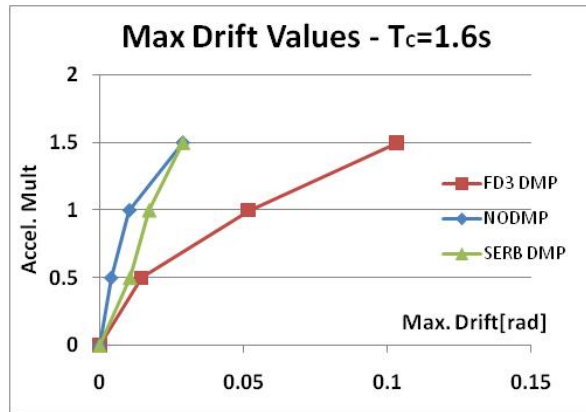


Fig. 5.7. Maximum drift values for the structures with dampers (soft soil)

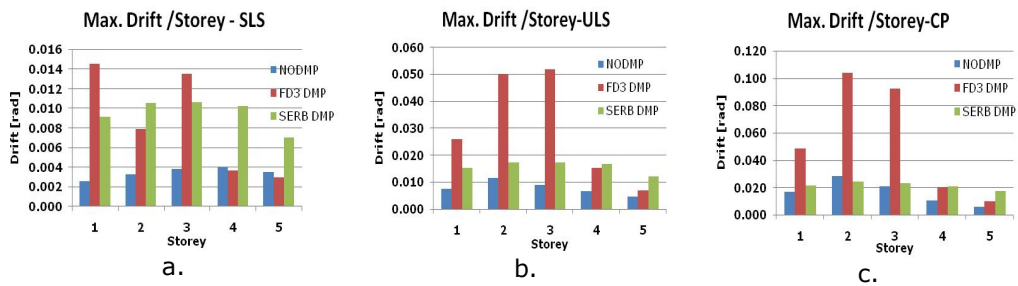


Fig. 5.8. Maximum drift values at each storey at: a) SLS; b) ULS and c) CP (soft soil)

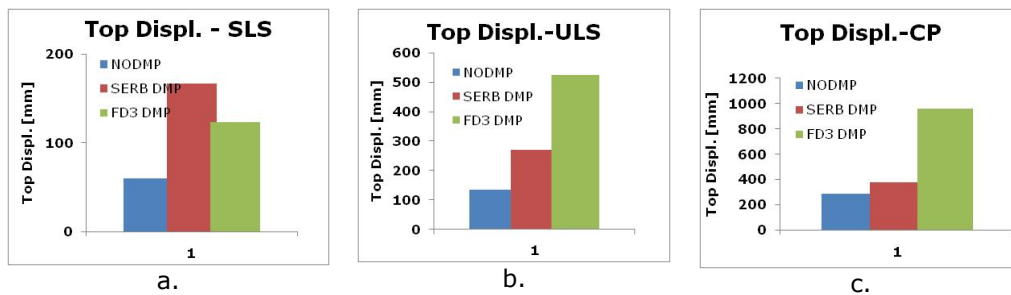


Fig. 5.9. Top displacement: a) SLS; b) ULS and c) CP (soft soil)

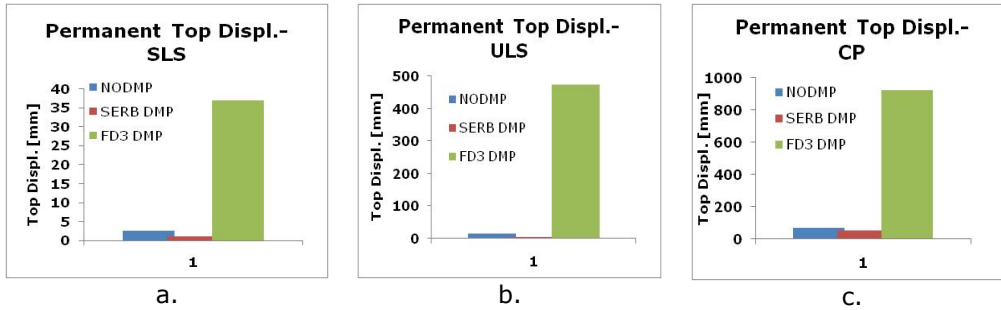
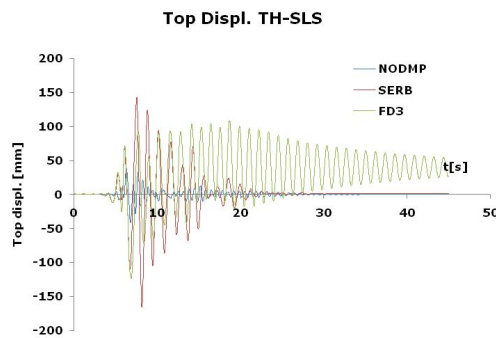
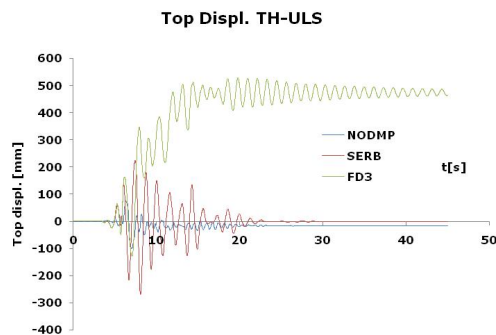


Fig. 5.10. Permanent top displacement at a) SLS; b) ULS and c) CP (soft soil)

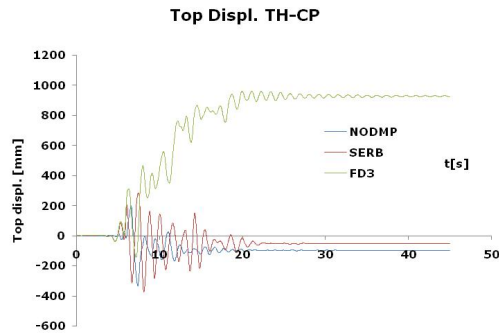
SERB dampers showed higher values of axial force in the dampers due to hardening of the behaviour curve which limits the displacements for all levels of seismic actions. For seismic recordings characteristic to soft soil ($T_C=1.6s$) the increase in flexibility of structures with SERB dampers increases values of drift and top displacement compared to the structure without dampers and will eventually lead to the appearance of plastic zones in beams and columns. This damper however, reduces drift, top displacement and residual displacements at top floor compared to the FD3 damper. It should be noted that significant values of residual displacement were recorded when using FD3 friction dampers. The distinct behaviour of the 2 dampers can be better observed in the displacement time history of the top floor (Fig. 5.11a,b,c).



a.



b.



C.

Fig. 5.11. Displacement time-history of top floor at: a) SLS; b) ULS and c) CP (soft soil)

No plastic hinges formed in any elements at SLS for both the structure with FD3 dampers and the structure with SERB dampers. At ULS only the structure with SERB dampers forms plastic hinges in central columns only of the 1 st floor (Fig. 5.12). At CP plastic hinges form in columns and several central beams (Fig. 5.13) with values of plastic rotation that exceed the acceptance criteria for the considered performance level for both types of dampers.

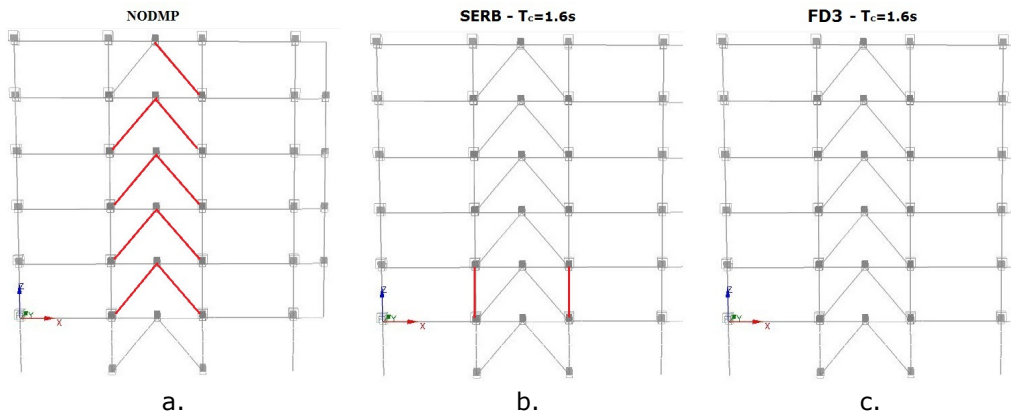


Fig. 5.12. . Plastic hinge location at ULS: a) No damper; b) SERB damper; c) FD3 damper (soft soil)

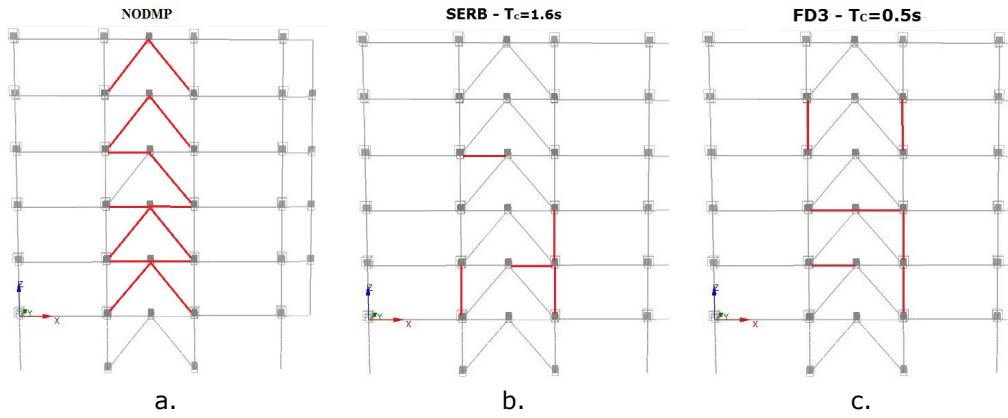


Fig. 5.13. Plastic hinge location at CP a) No damper; b) SERB damper; c) FD3 damper (soft soil)

Values of plastic rotations of central beams and columns are presented in Table 120 and Table 121.

BRACE Compr.	Plastic deformation demand-CP , mm			Plastic deformation capacity, mm CP
	LOC.	NODMP	SERB	
BR1L	2.883	NO PLASTIC DEFORMATION	NO PLASTIC DEFORMATION	31.43
BR1R	2.546			31.43
BR2L	2.727			31.43
BR2R	2.927			31.43
BR3L	1.620			27.755
BR3R	1.639			27.755
BR4L	1.477			25.046
BR4R	1.361			25.046
BR5L	0.767			19.376
BR5R	0.722			19.376
BR(storey no.)R- right brace for selected storey				
BR(storey no.)L- left brace for selected storey				

Table 120. Maximum values of plastic deformation in compression braces at CP (soft soil)

BRACE Tension.	Plastic deformation demand-CP , mm			Plastic deformation capacity, mm CP
	LOC.	NODMP	SERB	
BR1L	6.506	NO PLASTIC DEFORMATION	NO PLASTIC DEFORMATION	51.7221
BR1R	5.856			51.7221
BR2L	18.453			51.7221
BR2R	17.474			51.7221
BR3L	0.554			51.39
BR3R	0.476			51.39
BR4L	0.112			50.76
BR4R	0.268			50.76
BR5L	0.000			50.193
BR5R	0.000			50.193
BR(storey no.)R- right brace for selected storey				
BR(storey no.)L- left brace for selected storey				

Table 121. Maximum values of plastic deformation in tension braces at CP (soft soil)

Values of plastic rotations of central beams and columns are presented in Table 122 and Table 123.

BEAM LOC.	NODMP		SERB		FD3	
	Plastic rotation demand-CP, rad	Plastic rotation capacity, rad CP	Plastic rotation demand-CP, rad	Plastic rotation capacity, rad CP	Plastic rotation demand-CP, rad	Plastic rotation capacity, rad CP
CB1a	0.0146	0.0240	-	-	-	-
CB2a	0.0127	0.0238	-	-	0.110	0.0453
CB3a	-	-	0.00899	0.00611	-	-
CB4a	-	-	-	-	-	-
CB5a	-	-	-	-	-	-
CB1b	0.0230	0.0220	0.00840	0.00423	-	-
CB2b	0.0139	0.0230	-	-	-	-
CB3b	0.0023	0.0268	-	-	-	-
CB4b	-	-	-	-	-	-
CB5b	-	-	-	-	-	-
CB(storey no.)a- central beam for selected storey at end a						
CB(storey no.)b- central beam for selected storey at end b						

Table 122. Maximum values for plastic rotation at CP for central beams (soft soil)

COLUMN LOC.	NODMP		SERB		FD3	
	Plastic rotation demand-CP, rad	Plastic rotation capacity, rad CP	Plastic rotation demand-CP, rad	Plastic rotation capacity, rad CP	Plastic rotation demand-CP, rad	Plastic rotation capacity, rad CP
CC1L	NO PLASTIC ROTATION	VARIES	0.00432	0.00376	0.0239	0.00640
CC2L		VARIES	-	-	0.0295	0.00719
CC3L		VARIES	-	-	-	-
CC4L		VARIES	-	-	0.0340	0.00829
CC5L		VARIES	-	-	-	-
CC1R		VARIES	0.00814	0.00302	-	-
CC2R		VARIES	0.00211	0.00168	-	-
CC3R		VARIES	-	-	-	-
CC4R		VARIES	-	-	0.0400	0.00737
CC5R		VARIES	-	-	-	-
CC(storey no.)L- left central column for selected storey						
CC(storey no.)R- right central column for selected storey						

Table 123. Maximum values for plastic rotation at CP for central columns (stiff soil)

The numerical analyses showed that for soft soils introducing dampers in the structure can reduce the seismic response of the structure to levels up to ULS. At CP the dampers have reduced effect and careful consideration must be taken with regard to limitation of storey drifts and acceptance of degradation in the structure. It should be noted that SERB dampers have a limited effect for seismic motions characterised by long corner periods.

5.3.3.2 Seismic recordings characteristic to stiff soil ($T_c=0.5s$),

Maximum drift levels (Fig. 5.14), maximum drift at each storey (Fig. 5.15), top displacement for the structure (Fig. 5.16) and permanent displacement (Fig. 5.17) of the structures with dampers are presented for maximum seismic motion at levels corresponding to SLS, ULS and CP.

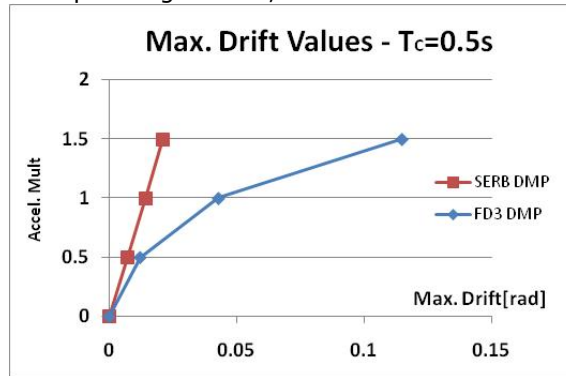


Fig. 5.14. Maximum drift values for the structures with dampers (stiff soil)

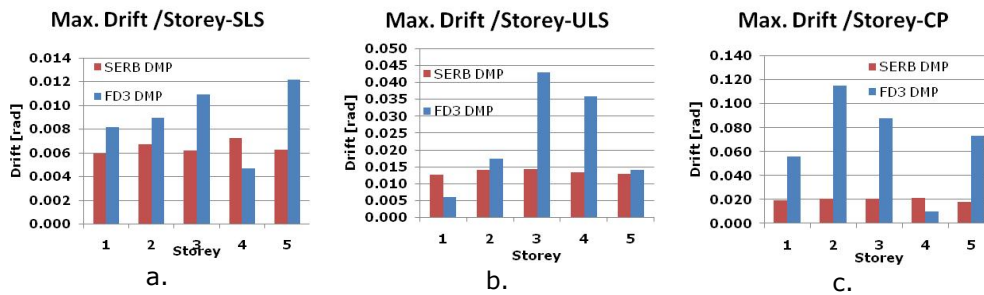


Fig. 5.15. Maximum drift values at each storey at: a) SLS; b) ULS and c) CP (stiff soil)

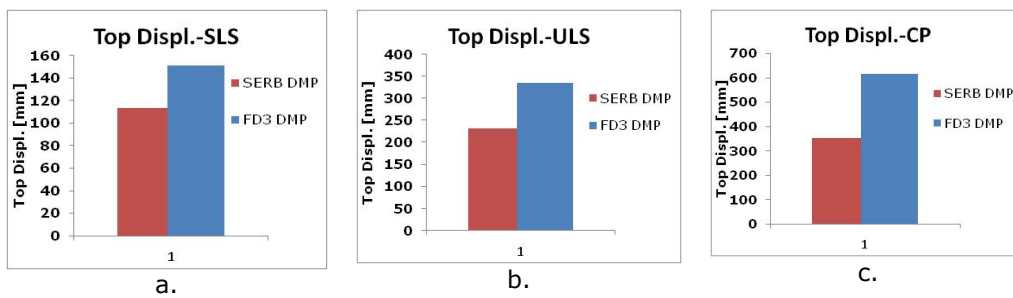


Fig. 5.16. Top displacement: a) SLS; b) ULS and c) CP (stiff soil)

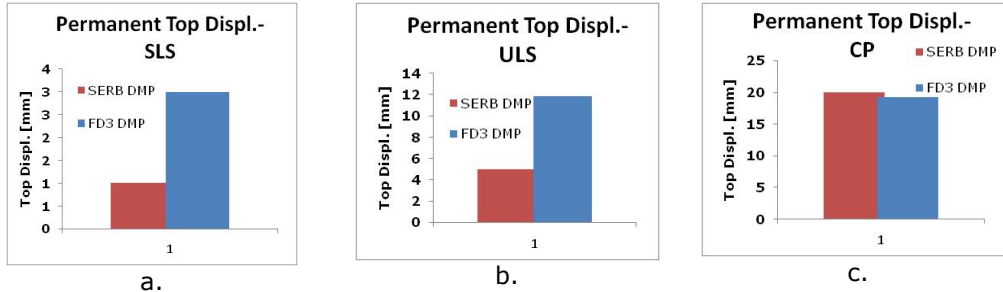
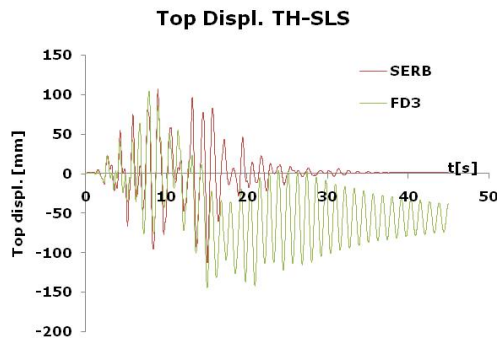
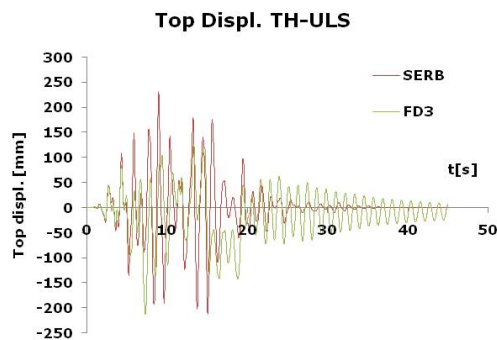


Fig. 5.17. Permanent top displacement at a) SLS; b) ULS and c) CP (stiff soil)

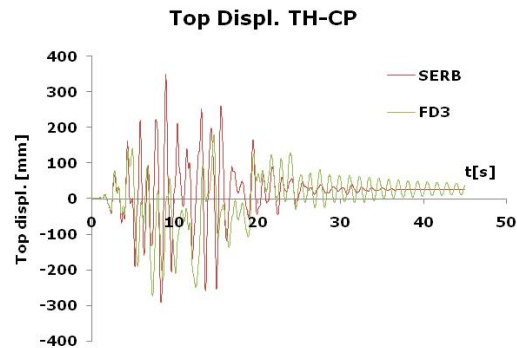
SERB dampers showed higher values of axial force in the dampers due to hardening of the behaviour curve which limits the displacements for all levels of seismic actions. This damper reduces drift, top displacement and residual displacements at top floor and provides a more uniform distribution of storey drift compared to the FD3 damper. It should be noted that values of residual displacement at CP were similar for both dampers. The distinct behaviour of the 2 dampers can be better observed in the displacement time history of the top floor (Fig. 5.18).



a.



b.



C.

Fig. 5.18. Displacement time-history of top floor at: a) SLS; b) ULS and c) CP (stiff soil)

No plastic hinges formed in any elements at SLS and ULS for both the structure with FD3 dampers and the structure with SERB dampers. At CP plastic hinges form in columns and several central beams (Fig. 5.19) with values of plastic rotation that exceed the acceptance criteria for the considered performance level.

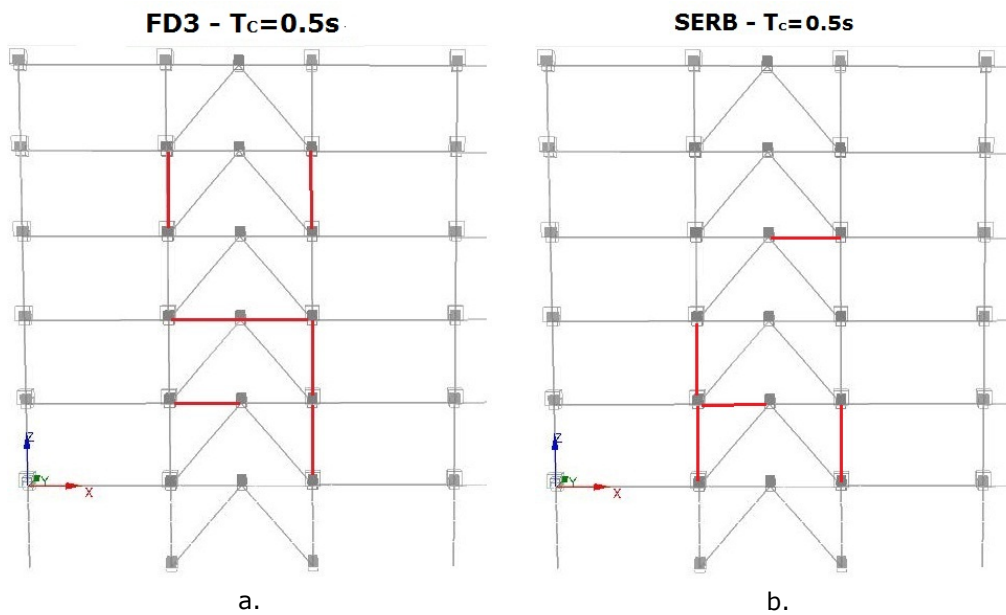


Fig. 5.19. Plastic hinge location at CP: a) structure with FD3 damper; b) structure with SERB damper (stiff soil)

Values of plastic rotations of central beams and columns are presented in Table 124, Table 125.

BEAM LOC.	FD3		SERB	
	Plastic rotation demand-CP, rad	Plastic rotation capacity, rad CP	Plastic rotation demand-CP, rad	Plastic rotation capacity, rad CP
CB1a	0.0631	0.0421	0.009819	0.00468188
CB2a	-	-	-	-
CB1b	0.0694	0.0407	-	-
CB2b	0.109	0.0573	-	-
CB3b	-	-	0.005879	0.00622892
CB(storey no.)a- central beam for selected storey at end a				
CB(storey no.)b- central beam for selected storey at end b				

Table 124. Maximum values for plastic rotation at CP for central beams (stiff soil)

COLUMN LOC.	FD3		SERB	
	Plastic rotation demand-CP, rad	Plastic rotation capacity, rad CP	Plastic rotation demand-CP, rad	Plastic rotation capacity, rad CP
CC1L	-	-	0.007178	0.0027857
CC2L	0.026510	0.00782191	0.005033	0.00181247
CC4L	0.058254	0.00783398		
CC1R	0.025084	0.00686546	0.007087	0.00341237
CC2R	0.023190	0.00841465		
CC4R	0.055007	0.00874685		
CC(storey no.)L- left central column for selected storey				
CC(storey no.)R- right central column for selected storey				

Table 125. Maximum values for plastic rotation at CP for central columns (stiff soil)

5.4 Discussion

The numerical analyses were performed to determine the seismic performance of CBF frames under 2 types of seismic motions: seismic recordings characteristic to soft soil type ($T_c=1.6s$) and (ii) seismic recordings characteristic to stiff soil ($T_c=0.5s$). The structures were designed using 3 different approaches: (i) a "classical" CBF structure without dampers designed according to EC8 provisions with a behaviour factor of $q=2.5$, (ii) a CBF structure equipped with FD3 type friction dampers in the braces designed considering the high energy dissipation of the devices through high values of the behaviour factor ($q=6$) and (iii) a CBF structure equipped with SERB type friction dampers in the braces designed to remain in elastic domain ($q=1$) and considering damper effects by reducing the design seismic action by an increased value of damping.

The design of the structure with FD3 damper centers on the similarities between the behaviour of the damper and that of a buckling restrained brace that lead to the selection of a behaviour factor of $q=6$. Damper properties are determined at SLS, ULS and CP. Beams, columns and braces are designed considering an overstrength factor of 1.3 with respect to damper capacity.

The design of the structure with SERB damper centers on designing the structural elements to remain in elastic domain ($q=1$) and considering the effects of the dampers by introducing the damper in the structural model used for design as a linear elastic element with appropriate stiffness and by considering the increase in damping in the determination of design seismic loads. For design purpose the damper behaviour is idealised by a bilinear behaviour curve. Damper properties are determined at SLS, ULS and CP. Beams, columns and braces are designed considering an overstrength factor of 1.3 with respect to damper capacity.

The structure with FD3 dampers had high values of drift and top displacement at all performance levels. Although no plastic hinges were formed at SLS and ULS this drastic increase in drift levels could mean a severe degradation of non-structural elements. This highly inelastic behaviour of the damper leads to excessive values of drift with the formation of plastic hinges in columns at CP. Significant values of residual displacement were recorded when using FD3 friction dampers.

The structures with SERB dampers showed higher values of axial force in the dampers due to hardening of the behaviour curve which limit the displacements for all levels of seismic actions having significantly lower values of drift than the structure with FD3 dampers and a more uniform distribution of drift at each floor. For seismic motions with long corner periods the damper did not manage to increase the period of vibration of the structure beyond the corner period and although designed to remain in elastic domain plastic hinges formed in the central columns of the first floor. This could be avoided by performing nonlinear TH analyses using appropriate seismic recordings with a more detailed numerical model of the damper to complete the design. It should be noted that this damper provides excellent performance in reducing the residual displacement for this type of seismic motion. For seismic recordings characteristic to stiff soil, SERB damper increases the period of vibration of the structure to values higher than that of the corner period. Drift values still lower than the ones recorded for the structure with FD3 damper and no plastic hinges were formed in any elements at SLS and ULS. At CP the structure forms plastic hinges in columns and several central beams with values of plastic rotation that no longer satisfy the acceptance criteria. A comparison of the behaviour of the structures with the two types of dampers for the two types of seismic motions considered is presented in Fig. 5.20, Fig. 5.21, Fig. 5.22, Fig. 5.23 and Fig. 5.24.

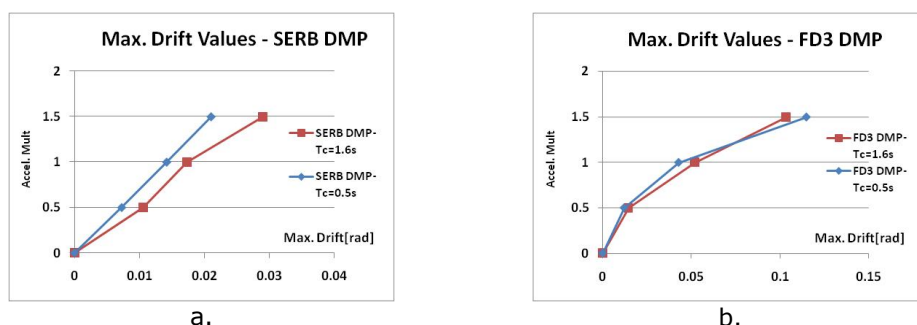


Fig. 5.20. Comparison of maximum drift values for the 2 types of seismic motions used for: a) structures with SERB damper; b) structures with FD3 damper

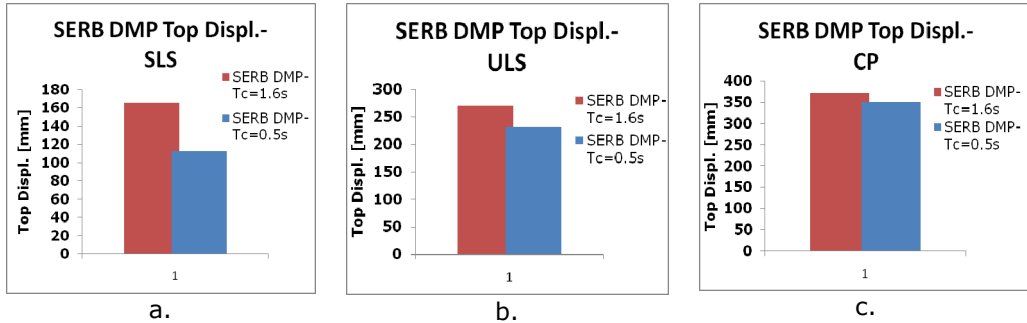


Fig. 5.21. Comparison of top displacement of structures with SERB dampers for the 2 types of seismic motions used for: a) SLS; b) ULS and c) CP

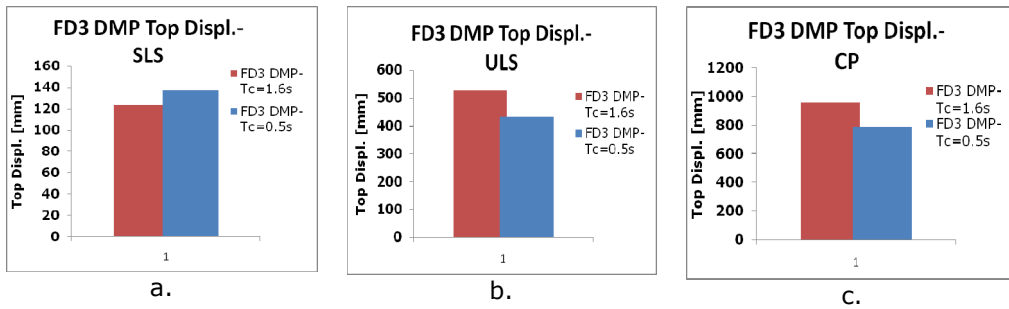


Fig. 5.22. Comparison of top displacement of structures with FD3 dampers for the 2 types of seismic motions used for: a) SLS; b) ULS and c) CP

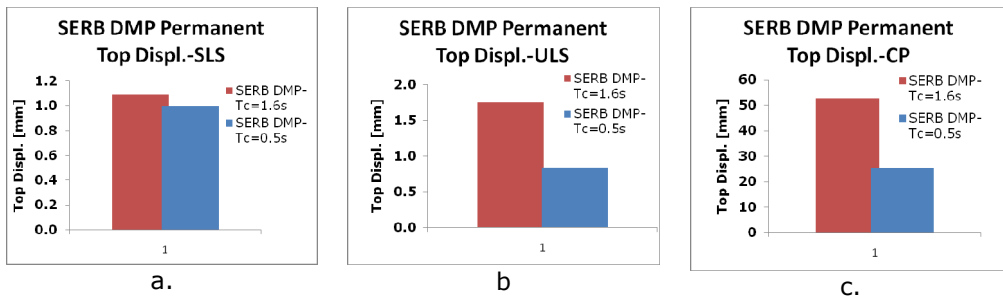


Fig. 5.23. Comparison of permanent top displacement of structures with SERB dampers for the 2 types of seismic motions used for: a) SLS; b) ULS and c) CP

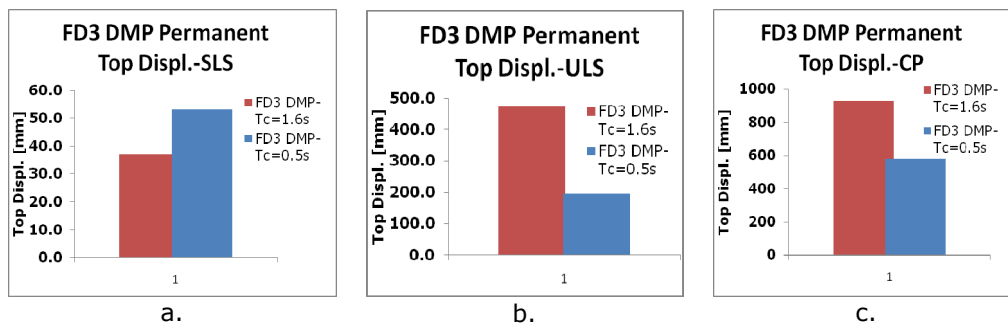


Fig. 5.24. Comparison of permanent top displacement of structures with FD3 dampers for the 2 types of seismic motions used for: a) SLS; b) ULS and c) CP

The structures with SERB dampers recorded significantly lower values of drift, top displacement and residual displacement at the top floor for seismic motions characteristic to stiff soils compared with the same quantities semi-artificial for seismic motions characteristic to soft soil type. In the case of FD3 dampers, the structure had similar values of drift for the two seismic motions with lower values at SLS and ULS for stiff soil. Top displacement values for the structure with FD3 damper vary slightly with lower values for seismic motions characteristic to stiff soils. Significantly lower values of residual top displacement were recorded for $T_c=0.5s$ for this type of damper at ULS and CP. It should be noted that the structure with FD3 dampers had higher values of top displacement and permanent top displacement for seismic motions characteristic to stiff soil compared to the values recorded for seismic motions characteristic to soft soil only at SLS.

In general both types of dampers proved to be efficient in reducing seismic action for the designed CBF structures. It is clear that both dampers have their advantages and careful consideration must be taken when selecting one type or the other. The results obtained for the two structures designed according to proposed methodologies respected the concepts of their design but showed the need of nonlinear TH analyses to better predict the behaviour of the dimensioned structures.

From an economical point of view the use of dampers in the structures reduced material consumptions for the design frames. The frame with SERB dampers had a material reduction of approximately 30% while the structure with FD3 dampers with 50%. It should be noted here that the cost reduction on steel is must be considered in conjunction with the price of the devices themselves. For example considering an approximate price of SERB damper of about 1000 euro and a price of 1.5euro/kg of steel materials the designed frame with dampers will yield roughly the same costs. It should be noted that for a more comprehensive view of structure economics concerning damper use the cost reduction of steel materials, damper price, cost of rehabilitation and/or repair in the case of a seismic event and performance increase of the structure must be carefully balanced.

6 Conclusions and Personal Contributions

6.1 Summary

In this paper the performance of concentrically braced frames with friction dampers in the bracing was analysed. Two types of concentrically braced frames were analysed: (i) simple CBF and (ii) dual CBF with 2 adjacent MRF. The structures considered were analysed using 2 sets of seismic motions recordings scaled to the design spectra: (i) semi-artificial seismic motion characteristic for soft soil type (Bucharest) and (ii) artificially generated seismic motions characteristic for stiff soil (Class B soil according to SREN1998-1[7]). The two target spectra were scaled to the fundamental period of vibration of the analysed structure, so as to yield roughly the same design seismic forces. All the analyses were made with two distinct types of dampers placed in the braces and comparing the results with the corresponding structures without dampers.

Chapter 2 presented a general overview on the characteristics of seismic motions and on current use of passive damping devices in civil engineering applications. It was shown that seismic motions with long period of vibration can be caused by soft soils and the forward directivity effect. It was pointed out that the nonlinear dynamic response of the structures can have significant variations depending on the period of vibration. This led to the choice of two types of seismic motions that were used in the analyses: (i) semi-artificial seismic motions characteristic for soft soil type (Bucharest, $T_C=1.6s$) and (ii) artificially generated seismic motions characteristic for stiff soil (Class B soil according to SREN1998-1 with $T_C=1.6s$). The overview of passive damping devices showed that the use of damping devices, in different configurations, is a modern and effective way of reducing seismic response of structures. It is pointed out that the behaviour of the damper prototype studied in this paper is different from the general current concept of passive damper. This fact correlated with current interest worldwide towards devices that reduce seismic actions provides the motivation of this thesis.

Chapter 3 presents the experimental program for SERB type damper prototypes. Experimental tests were made on two dampers with capacities of 800kN and 1500 kN to validate their hysteretic behaviour and to ensure that the devices function in the desired parameters having a symmetric behaviour in tension and compression with stable hysteretic loops. The devices were then tested using a brace with damper assembly under two different design concepts. The first concept states that the brace with damper are designed so that energy dissipation occurs in the device alone and the brace remains in elastic domain, achieved by ensuring that the brace has sufficient overstrength

in comparison with the damper. The second design concept states that the brace will enter plastic domain and both brace and damper will contribute to final response of the assembly, achieved by ensuring the overstrength of the damper compared to buckling capacity of brace. As a result of the experimental tests the hysteretic behaviours of the dampers and of the brace with damper assembly were obtained.

Chapter 4 presents the numerical program performed to determine the performance of concentrically braced structures with dampers in the braces. Based on the results from the experimental program numerical models for the damper, brace and brace with damper assembly were calibrated. Nonlinear time-history analyses were made using two sets of seismic motions recordings scaled to their respective design spectra. Three performance levels were considered for each seismic motion having ground accelerations of $a_{g,SLS} = 0.5 \cdot a_{g,ULS}$, $a_{g,ULS}$ and $a_{g,CP} = 1.5 \cdot a_{g,ULS}$ corresponding to serviceability limit state (SLS), ultimate limit state (ULS) and collapse prevention (CP). Performance based evaluation was performed using acceptance criteria for plastic axial deformation in the braces and plastic rotation for beams and columns according to FEMA356. Two types of concentrically braced frames were analysed: (i) simple CBF and (ii) dual CBF+MRF without dampers. The same structures were analysed equipped with SERB dampers and with "classic" friction damper in the braces.

Both CBF and dual MRF+CBF structures with SERB dampers had a similar behaviour. The structures with dampers were more flexible in all cases with drift levels and values of maximum top displacement higher than the ones of the structures without dampers at all performance levels under both types of seismic motions. It was shown that this type of damper has a negative influence on the behaviour of the structures for earthquakes characterized by long corner period $T_c=1.6s$ (soft soil). Under this type of seismic motions the structures with dampers form plastic hinges in non-dissipative elements with values that exceed the acceptance criteria for the corresponding performance levels. However this type of damper is efficient in reducing the seismic response of a building for earthquakes characterized by short corner period $T_c=0.5s$ (stiff soil) by preventing the formation of plastic hinges at SLS and reducing the permanent displacement of the structure.

Both CBF and dual MRF+CBF structures with FD3 dampers had a similar general behaviour with small differences at certain performance levels. It was shown that this type of damper is efficient in reducing the seismic response of CBF and dual MRF+CBF structures for earthquakes characterized by long corner period $T_c=1.6s$ (soft soil) at SLS and ULS avoiding the formation of plastic hinges in elements and completely avoids the formation of plastic zones for earthquakes characterized by short corner period $T_c=0.5s$ (stiff soil) However, due to its high inelastic behaviour, this damper leads to high values of permanent displacement of the structure.

It was shown that these 2 types of dampers exhibit completely different hysteresis mechanisms. "Classic" friction dampers allow for a larger ductility demand with respect to SERB dampers, while dissipating a significant amount of seismic energy due to their wider hysteretic loops but leads to high values of residual displacements. On the other hand the SERB damper prototype showed higher values of axial force due to hardening of the material which may limit the displacements for unexpected strong earthquakes and also reduces

residual displacements of the top floor but in the same time may result in larger forces transmitted to beams and columns.

Chapter 5 proposed design provisions for the design structures with SERB dampers and “classical” friction dampers. A design methodology is proposed for each type of damper and case studies were made following the proposed methodology.

The proposed design guidelines for structures with FD dampers follows the guidelines of EC8 for concentrically braced structures, considering the behaviour of the braces with dampers similar to that of buckling restrained braces. Damper properties are determined gradually from the design at SLS, ULS and CP.

The proposed design guidelines for structures with SERB dampers are based on a simplified bilinear behaviour model. Damper effects considered through linear elastic behaviour type elements in the model and through higher values of damping for evaluation of design seismic action. An iterative procedure is proposed to determine the required damper properties at each of the three levels of seismic action considered (SLS, ULS and CP).

For both proposed design cases it is recommended that the properties of the devices be determined experimentally and nonlinear dynamic analyses be made on the structural models that include damper models.

Both design methodologies proposed were applied for case studies on the structures with FD3 dampers and SERB dampers. The performance of the structures was evaluated using 3 pairs of seismic motions for soft soil and stiff soil. The results of the TH analyses were presented comparatively for the structures without dampers and the two structures with dampers for the pair of seismic motions that generated the maximum response.

In general, both types of dampers proved to be efficient in reducing seismic action for the designed CBF structures. It is clear that both dampers have their advantages and careful consideration must be taken when selecting one type or the other. The results obtained for the two structures dimensioned according to proposed methodologies respected the concepts of their design but showed the need of nonlinear TH analyses to better predict the behaviour of the dimensioned structures.

6.2 Personal Contributions

Based on the experimental and numerical studies performed by the author the following contributions can be highlighted:

- Concept, design and execution of an experimental program on damper prototypes and brace with damper assembly. It can be noted here that the experimental program conducted by the author is the first of its kind in our country.
- Calibration of a numerical model for the damper, brace and brace with damper assembly based on the results of the experimental study.
- Implementation of numerical models for dampers in performance based analysis of two structures under two distinct sets of seismic recordings, each equipped with two different types of dampers.

- Proposal of design principles and design methodologies for each of the two types of dampers.
- Case studies on structures designed following the proposed design methodology for each type of damper.

The experimental program, and the entire research made in these four years was in the framework of two research programs: Grantul PNCDI II „Parteneriate”, contract nr. 31.042/2007, cu titlul “ Raspunsul seismic al cadrelor multietajate cu contravantuiri centrice echipate cu disipatori prin frecare ” in contextul cerintelor de dezvoltare durabila PROACTEX and COST C26 Urban Habitat Constructions under Catastrophic Events.

During the research the results of this thesis were published and disseminated in articles, presentations and workgroups as follows:

- “Sesiunea Nationala de Comunicari Stiintifice Studentesti”, editia a VII-a, 18.04.2008, U.T. Cluj-Napoca, title: *Cladiri Metalice Dotate cu Contravantuiri Centrice Situate in Zone Seismice*, author Filip Vacarescu Norin;
- International Symposium: „Mineral Resources And Environmental Engineering”, Universitatea de Nord, Baia Mare, 2008, ISBN 978-973-1729-74-9, title: *Seismic Performance of Steel Centrally Braced Frames Equiped with Friction Dampers*, author Filip Vacarescu Norin;
- 11th WSEAS Int. Conference on Sustainability in Science Engineering (SSE '09), Timisoara, Romania, 27-29.05.2009, ISBN 978-960-474-080-2(ISI), title: *Numerical Modelling of Centrally Braced Frames Equiped With Friction Dampers in the Bracingsa*, authors Filip Vacarescu Norin, Dan Dubina;
- „Comportarea Structurilor Metalice La Actiuni Extreme” Symposion, in the framework of the XI-th edition of “Zilelor Academice Timisene”, 29.05.2009, title: *Modelarea numerica a cadrelor contravantuite centric dotate cu amortizori pe baza de frecare in contravantuiri*, authors Filip Vacarescu Norin, Dan Dubina;
- Presentation of the paper „Experimental Program to Calibrate the Hysteretic Model of a Brace-Damper System” COST C26: Urban Habitat Constructions under Catastrophic Events WG2: Earthquake resistance General Meeting, 27-28 November 2009, Aveiro, authors Norin Filip-Vacarescu, Aurel Stratan, Dan Dubina;
- 6th PhD. &DLA Symposium, University of Pecs, Pollack Mihaly Faculty of Engineering, septembrie 2010, title: BEHAVIOUR OF CENTRICALLY BRACED FRAMES WITH FRICTION DAMPERS. Filip-Vacarescu, Aurel Stratan, Dan Dubina;
- 12-th National Conference on Steel Structures, Timisoara, 26-27 Noiembrie 2010, title: Cadre metalice contravântuite centric dotate cu amortizori cu frecare., authors Filip-Vacarescu, Aurel Stratan, Dan Dubina;

- COMPDYN 2011 3rd ECCOMAS Thematic Conference on Computational Methods in Structural Dynamics and Earthquake Engineering Corfu, Greece, 25–28 May 2011, title: Behavior of Concentrically Braced Frames with Friction Dampers, authors: Filip-Vacarescu, Aurel Stratan, Dan Dubina;
- Accepted for presentation at EUROSTEEL 2011 Conference, August 31 - September 2, 2011, Budapest, Hungary, title: Behavior of Concentrically Braced Frames with Friction Dampers, authors: Filip-Vacarescu, Aurel Stratan, Dan Dubina;

The author also participated in several training programs:

- "Validation of Numerical Models" – Summer School, Weimar, Germany, 08.2008
- "Sustainability of Structures And Structural Interventions", COST C25/C26 Training School, Thessaloniki, Greece, 05.2009

The author also participated in the following research programs:

- RFCS-CT-2007-00050 „Steel Solutions for Seismic Retrofit and Upgrade of Existing Constructions“ STEELRETRO (2007-2010)
- „Robustetea structurilor in cadre metalice multietajate la actiuni extreme“, Proiect de cercetare COST C26.
- SERIES TA User Agreement JRC N° 31817, "Full-scale experimental validation of dual eccentrically braced frame with removable links (DUAREM)"

References

- [1] P100-1/2006, "Cod de proiectare seismic-Partea I – Prevederi de proiectare pentru cladiri ",Romania, 2006.
- [2] Soong, T.T., Spencer Jr, B.F.," Supplemental energy dissipation: state-of-the-art and state-of-the practice", Engineering Structures 24 243–259, 2002.
- [3] Stratan, A., "Studiul comportării clădirilor multietajate cu cadre metalice duale amplasate în zone seismice", Teza de doctorat, Universitatea POLITEHNICA din Timișoara Facultatea de Construcții și Arhitectură, Departamentul de Construcții Metalice și Mecanica Construcțiilor, 2003.
- [4] Oros, E. (2002). "Cutremurele de pământ și cercetarea seismologică – concepte, tipuri de seisme, rezultate". Prezentare la seminarul cu tema: Influența tipului de cutremur și a condițiilor locale asupra răspunsului seismic al construcțiilor, Timișoara, 6 decembrie 2002.
- [5] Stewart, J.P., Chiou, S-J., Bray, J.D., Graves, R.W., Somerville, P.G., Abrahamson, N.A.. "Ground Motion Evaluation Procedures for Performance-Based Design". PEER Report 2001/09, Pacific Earthquake Engineering Research Center, College of Engineering, University of California, Berkeley, 2001.
- [6] Chandler, A.M., Hutchinson, G.L. și Wilson, J.L.. "The use of interplate derived spectra in intraplate seismic regions". 10th World Conference of Earthquake Engineering, Balkema, Rotterdam, 1992.
- [7] EN1998-1, Eurocode 8. "Design of structures for earthquake resistance. Part 1: General rules, seismic actions and rules for buildings". Final Draft, December, CEN - European Committee for Standardization, 2003.
- [8] Whittaker, A., Hart, G., and Rojahn, C.. "Seismic Response Modification Factors". Journal of Structural Engineering, Vol.125, No.4, pp. 438-443, 1999.
- [9] NEHRP 2000 Building Seismic Safety Council, BSSC. "NEHRP Recommended Provisions for Seismic Regulations for New Buildings and Other Structures, Part 1 — Provisions and Part 2 — Commentary". Federal Emergency Management Agency, Washington D.C., 2001.
- [10] FEMA 356, "Prestandard and commentary for the seismic rehabilitation of buildings", Federal Emergency Management Agency, Washington (DC), 2000.
- [11] Elghazouli, A. Y., Málaga-Chuquitaype, C., "Consideration of seismic demand in the design of braced frames", Ernst & Sohn Verlag für Architektur und technische Wissenschaften GmbH & Co. KG, Berlin · Steel Construction 4, No. 2, 2011.
- [12] Topkaya, C.C., Kurban, C.O., "Natural periods of steel plate shear wall systems", Journal of Constructional Steel Research 65 542–551, 2009, from

www.sciencedirect.com.

[13] Alinia, M.M., Dastfan, M. "Cyclic behaviour, deformability and rigidity of stiffened steel shear panels", *Journal of Constructional Steel Research* 63 554–563, 2007, from www.sciencedirect.com.

[14] Bruneau, M., Berman, J., Lopez Garcia, D., Vian, D., "Steel Plate Shear Wall Buildings: Design Requirements and Research", NASCC, 2005.

[15] Seilie, I.F., Hooper, J.D., "Steel Plate Shear Walls: Practical Design and Construction", *Modern Steel Construction*, April, 2005.

[16] Astaneh-Asl, A., "Seismic Behavior and Design of Steel Shear Walls-SEONC Seminar", Paper Distributed and presented at the 2001 SEONC Seminar, Structural Engineers Assoc. of Northern California, November 7, 2001, San Francisco, 2001.

[17] PROHITECH, WP6 Report, *Set-up of Advanced Reversible Mixed Technologies for Seismic Protection*, edited D.Beg., P.Skuber. L.Pavlocic, University of Ljubljana Faculty of civil and geodetic engineering Slovenia

[18] Bordea, S., "Dual Frame Systems of Buckling Restrained Braces", PhD. Thesis, Universitatea POLITEHNICA din Timișoara Facultatea de Construcții și Arhitectură, Departamentul de Construcții Metalice și Mecanica Construcțiilor, 2010.

[19] Kimura, I., "The Unbonded Brace A New Alternative for Seismic Lateral Systems Steel Structure" Div., Nippon Steel Corporation Tokyo, JAPAN, (ppt. presentation), 2002.

[20] "NIPON STEEL NEWS", no.333, september 2005, (Published monthly by Public Relations Center General Administration Div. Nippon Steel Corporation, (<http://www.nsc.co.jp>))

[21] Castellano, M.G., Medeot, R., "Seismic Protection of Cultural Heritage through Shape Memory Alloy Based Devices", International Post-SMIRT Conference Seminar on Seismic Isolation, Passive Energy Dissipation and Active Control of Seismic Vibrations of Structures, Taormina, Italy, August 25-27, 1997.

[22] Song, G., Ma, N., Li H.-N., "Applications of shape memory alloys in civil structures", *Engineering Structures* 28 1266–1274, 2006, from www.sciencedirect.com.

[23] Castellano, M.G., Medeot, R., "Application of Seismic Devices to Italian Cultural Heritage Structures", Proceedings of the 7th International Seminar on Seismic Isolation, Passive Energy Dissipation and Active Control of Seismic Vibrations of Structures, Assisi, Italy, October 2-5, 2001.

[24] Arato, B.G., "Application of Innovative Antiseismic Techniques to the

Seismic Retrofit of Italian Cultural Heritage Damaged by Recent Earthquakes” Proc. Of Momentum 98, Workshop on Seismic Performance of Monument, Lisbon, 1998.

[25] Kelly, T.E., “Design Guidelines”, Holmes Consulting Group, Revision 0, July 2001, www.holmesgroup.com

[26] PALL, A., PALL, R.T., “Performance Based Evaluation using Pall Friction Dampers- an Economical Design Solution”, 13th World Conference on Earthquake Engineering, Vancouver, B.C., Canada, August 1-6, 2004.

[27] Panait, A., Șerban, V., Androne, M., Ciocan, G.A., Zamfir, M., “Metoda ȘERB - SITON pentru controlul, limitarea si amortizarea miscarilor seismice a structurilor metalice”, A X-a ediție a “ZILELOR ACADEMICE TIMIȘENE” Timișoara, “STRUCTURI METALICE AMPLASATE ÎN ZONE SEISMICE. PREOCUPARI ACTUALE” 25 mai 2007.

[28] ECCS. "Recommended Testing Procedures for Assessing the Behaviour of Structural Elements under Cyclic Loads", European Convention for Constructional Steelwork, Technical Committee 1, TWG 1.3 – Seismic Design, No.45, 1985.

[29] Programul 4 “Parteneriate in domeniile prioritare” 2007-2013, Sectiunea 1, Raportul Stiintific si Tehnic(RST), etapa de executie NR. 2.1/2009 title: “Realizarea si experimentarea unui model DTS pentru cladiri medii”, from <http://cfdp.utcb.ro>

[30] EN1993-1-1, Eurocode 3 (2003). "Design of steel structures. Part 1-1: General Rules and Rules for Buildings". CEN - European Committee for Standardization

[31] SEISMOSOFT, SEISMOSTRUCT version 5.5 build 10 Reference Manual

[32] Landolfo, R., D’Aniello, M, Portioli, F., “Simulation of inelastic cyclic behaviour of steel concentric bracings”, 14ECEE 30.08-3.09 2010, Ohrid, T3, no.1816

[33] AISC (2002). "Seismic Provisions for Structural Steel Buildings". American Institute of Steel Construction, Inc. Chicago, Illinois, USA.

Appendix A: Calibration of numerical model of brace

This appendix presents some of the parameters considered in determination of the numerical model of the brace. A parametric study for calibration of numerical model of brace was made considering brace subdivision in 2 and 4 elements and different values of bow imperfections. Table A. 1. presents considered values of imperfections applied in z directiona at corresponding values of x coordinate Fig.A.1.

Node	X [mm]	$e_x(z)$ [mm]	$e_x/2(z)$ [mm]	$e_x/3(z)$ [mm]	$e_x/4(z)$ [mm]
x1	0	0	0	0	0
x2	995.25	19.9	9.9	6.6	4.9
x3	1990.5	26.5	13.2	8.8	6.6
x4	2667.27	19.9	9.9	6.6	4.9
x5	3981	0	0	0	0

Table A. 1. Computed values of imperfection for HEA brace

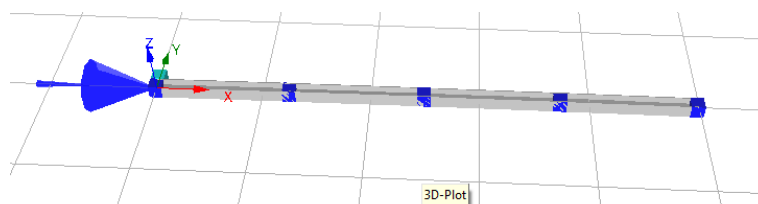


Fig.A. 1. Element local axes HEA brace model (4 elem.)

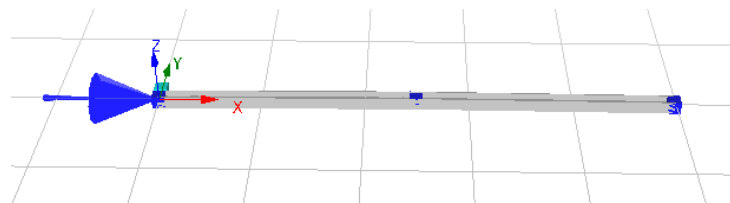


Fig.A. 2. Element local axes HEA brace model (2 elem.)

Results obtained for this parametric study are presented in Fig A.2.

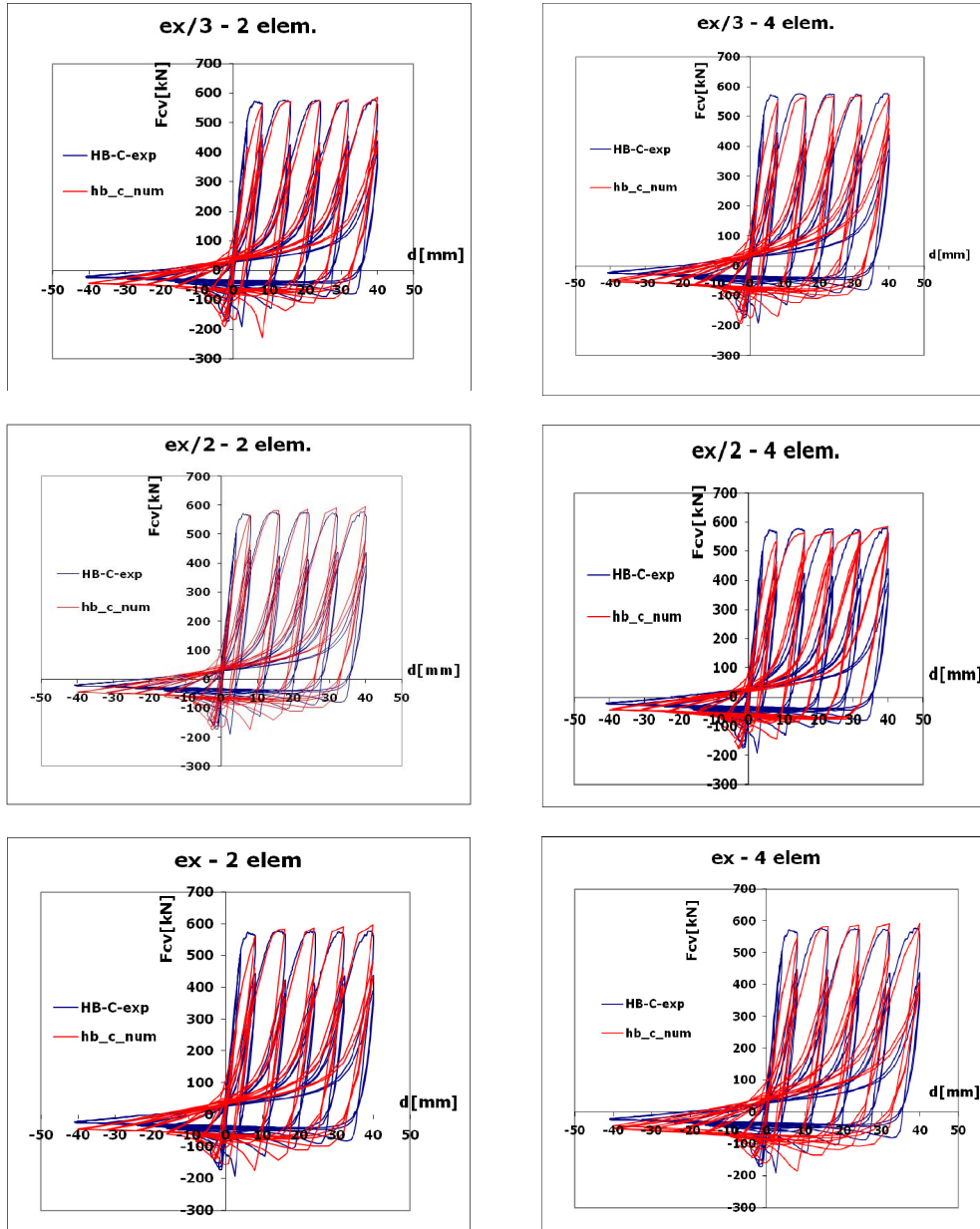


Fig.A. 3. Calibration of numerical model for HEA brace

Appendix B: Calibration of numerical model of damper

Numerical model of the damper was made using 2 link elements in parallel: a gap-hook link behaviour and a vilinear symmetric link behaviour. The selected parameters for gap-hook behaviour and bilinear-symmetric behaviour link elements (units: kN and m) are presented in Fig B.1 and Fig B.2:

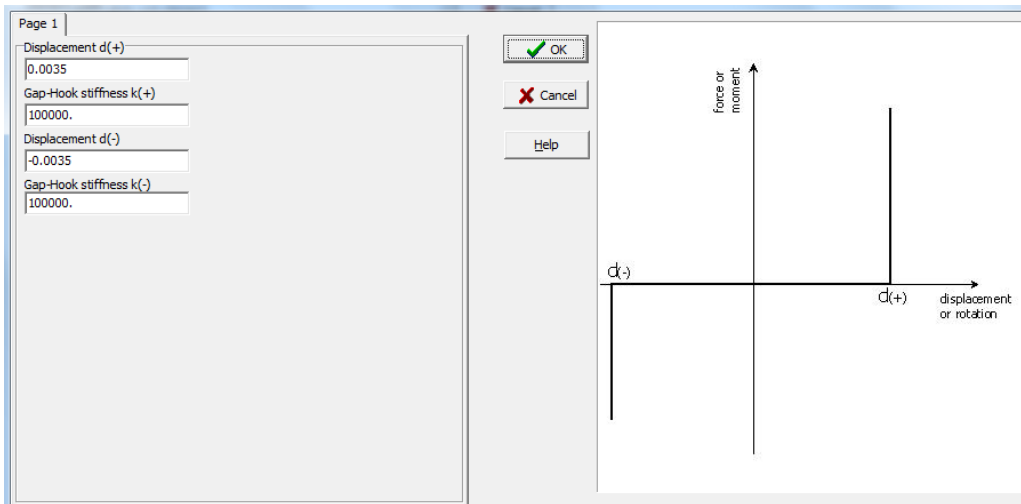


Fig.B. 1. Gap-hook parameters

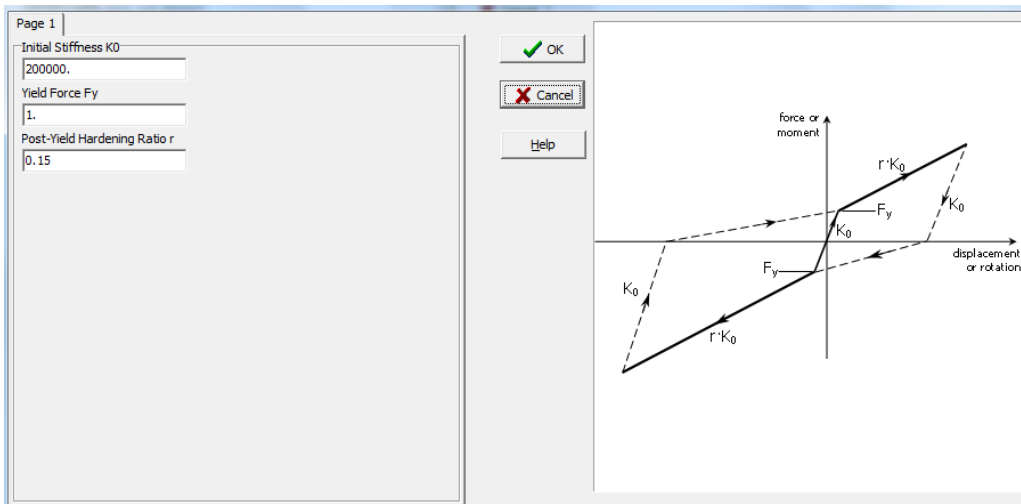


Fig.B. 2. Bilinear-symmetric parameters

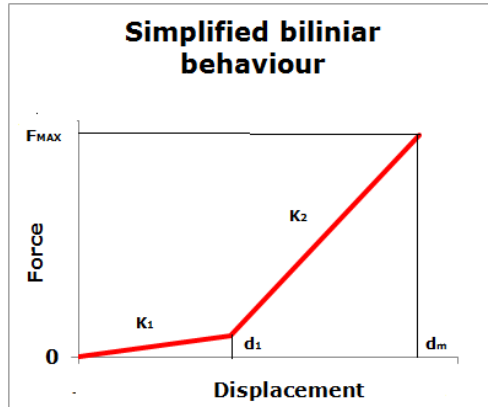


Fig.B. 3. Simplified behavior of SERB damper

Considering a idealised simplified behaviour of the SERB damper divided into two braches parameters for the two link elements are determined following a iterative procedure based on the following key points:

- d_1 = gap hook opening parameter
- K_2 = equivalent stiffness of gap-hook element + $r.K$ for bilinear symmetric element
- K_1 = equivalent stiffness of gap-hook element + bilinear symmetric element

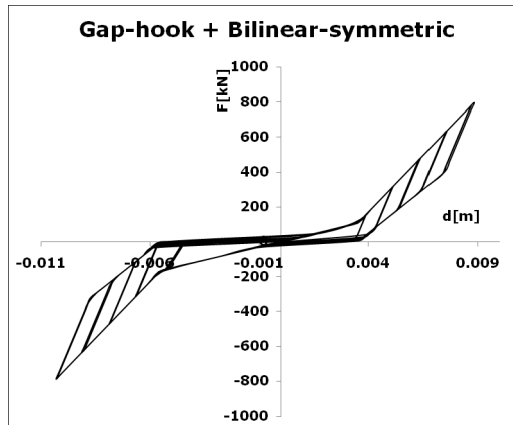


Fig.B. 4. Behavior of numerical model for damper